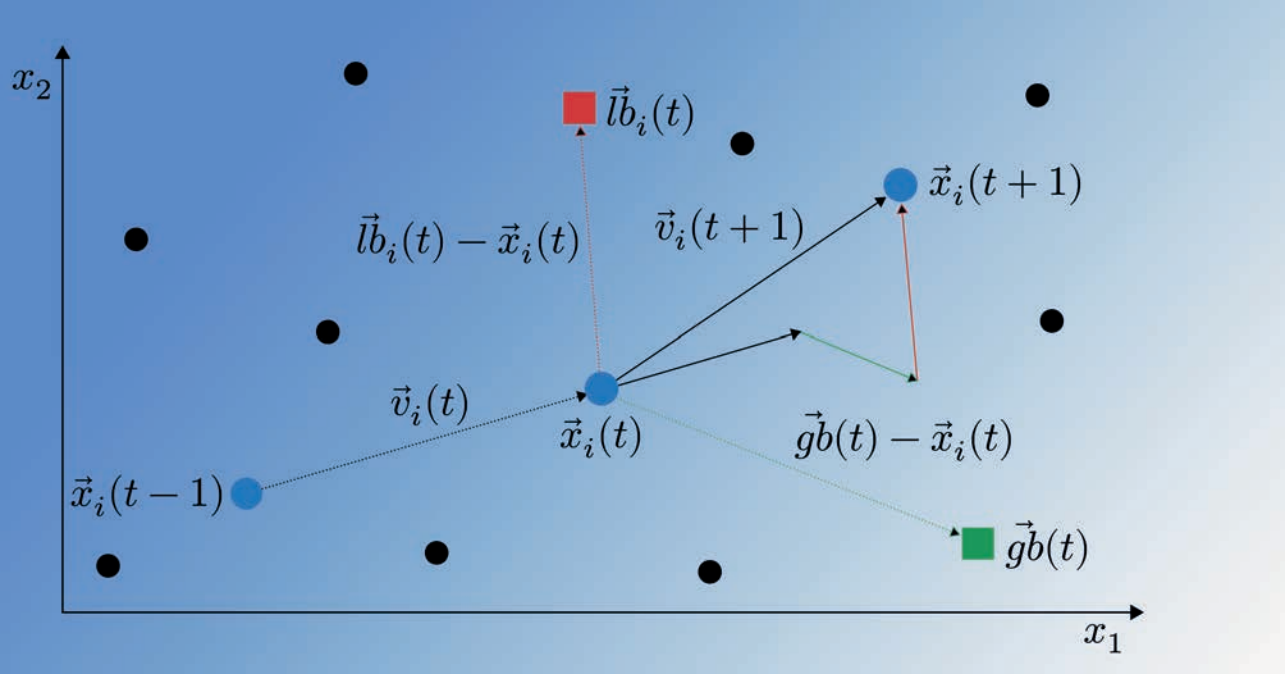

FAU Forschungen, Reihe B, Medizin, Naturwissenschaft, Technik 44

Georg Janick Meyer

Protection Concept Optimization Regarding Dynamic Security and Dependability in Multivariate Power Systems

FAU University Press

Georg Janick Meyer

Protection Concept Optimization Regarding Dynamic Security and Dependability in Multivariate Power Systems

FAU Forschungen, Reihe B
Medizin, Naturwissenschaft, Technik
Band 44

Herausgeber der Reihe:
Wissenschaftlicher Beirat der FAU University Press

Georg Janick Meyer

Protection Concept Optimization Regarding Dynamic Security and Dependability in Multivariate Power Systems

Erlangen
FAU University Press
2023

Bibliografische Information der Deutschen Nationalbibliothek:
Die Deutsche Nationalbibliothek verzeichnet diese Publikation in der Deutschen Nationalbibliografie; detaillierte bibliografische Daten sind im Internet über http://dnb.d-nb.de abrufbar.

Kontakt: Georg Janick Meyer, https://orcid.org/0000-0003-3214-1257

Bitte zitieren als
Meyer, Georg Janick. 2023. *Protection Concept Optimization Regarding Dynamic Security and Dependability in Multivariate Power Systems.* FAU Forschungen, Reihe B, Medizin, Naturwissenschaft, Technik Band 44. Erlangen: FAU University Press. DOI: 10.25593/ 978-3-96147-710-4.

Der vollständige Inhalt des Buchs ist als PDF über OPEN FAU
der Friedrich-Alexander-Universität Erlangen-Nürnberg abrufbar:
https://open.fau.de/home

Verlag und Auslieferung:
FAU University Press, Universitätsstraße 4, 91054 Erlangen

Druck: docupoint GmbH

ISBN: 978-3-96147-709-8 (Druckausgabe)
eISBN: 978-3-96147-710-4 (Online-Ausgabe)
ISSN: 2198-8102
DOI: 10.25593/ 978-3-96147-710-4

Protection Concept Optimization Regarding Dynamic Security and Dependability in Multivariate Power Systems

Schutzkonzeptoptimierung hinsichtlich dynamischer Sicherheit und Zuverlässigkeit in multivariaten Energiesystemen

Der Technischen Fakultät
der Friedrich-Alexander-Universität
Erlangen-Nürnberg

zur
Erlangung des Doktorgrades Dr.-Ing.
vorgelegt von

Georg Janick Meyer, M.Sc.
aus Hamburg

Als Dissertation genehmigt
von der Technischen Fakultät
der Friedrich-Alexander-Universität Erlangen-Nürnberg

Tag der mündlichen Prüfung:	06. Oktober 2023
Gutachter:	Prof. Dr.-Ing. Johann Jäger
	Prof. Dr.-Ing. Christian Rehtanz

Acknowledgment

This work was written during my time as a research assistant at the Institute of Electrical Energy Systems (EES) of Friedrich-Alexander-Universität Erlangen-Nürnberg (FAU) from July 2017 to June 2023 under the supervision of Prof. Dr.-Ing. Johann Jäger. He deserves my very special gratitude. His unique way of recognizing contexts and looking at them objectively, sharing and discussing findings and always putting scientific progress in the foreground of his work and thus also of his supervision were inspiring, exemplary and helpful. He always gave me the freedom to think through my own ideas and unconventional approaches, to test them, and to fail and cheer along the way. It was always a great pleasure and honor to work under him, and I hope to remain on friendly terms in the future.

I would like to thank the Federal Ministry of Education and Research (BMBF) of the Federal Republic of Germany for the funding and all participating universities, research institutions, industrial partners, non-governmental organizations, transmission and distribution system operators for the partnership and productive cooperation in the large-scale project Kopernikus ENSURE.

Prof. Dr.-Ing. Christian Rehtanz of the Technical University of Dortmund, Germany, I would like to express my appreciation for the time he invested in reviewing this work and preparing the second opinion. For chairing the examination board, I would like to thank Prof. Dr.-Ing. Matthias Luther.

I would like to sincerely thank my predecessor, project partner and friend, Dr.-Ing. Christian Romeis, for the great cooperation in the ENSURE project, his always professional advice as well as his constant support.

Maximilian Dauer was my supervisor during my student days, the overall project manager during the ENSURE project 2&3 and has been a friend and mentor for many years. I thank him for everything.

Prof. Dr.-Ing. Anatoli Wellhöfer deserves my thanks for his patience and for more than 10 years continuous support in all technical, especially simulation related, questions.

Randomness has made us colleagues and time together friends. For reviewing this work, I sincerely thank Georg Kordowich, Jonathan Löbel, and Tobias Lorz, as well as Marco Maximowitz and Stefan Schilling. For support, teamwork, exchange, discussions, and distinct rounds of table soccer, my thanks go to Dr.-Ing. Martin Biller, Dr.-Ing. Stefan Henninger, Dr.-Ing. Michael Jaworski,

David Knothe, Florian Mahr, Jonas Prometta, Jakob Schindler, and all other colleagues. I would like to thank Johanna Biegel, Christine Karl, Monika Bittan, Dr.-Ing. Gert Mehlmann and Klaus Schneider for their commitment in the areas of bureaucracy, project management and IT.

My long-time student assistants Ioannis Dimopoulos, Jean-Frédéric Vogelbacher and René Wehner as well as all other students deserve my thanks for the very pleasant, trustful and productive collaboration.

A loving thanks goes to my brothers, Niklas and Bennet, and especially to my parents, Ute and Joachim. I wish every person in this world to have parents like you. My girlfriend Isabella I want to thank for all the small miracles of everyday life, which became and become reality through her.

Erlangen, October 2023

Georg Janick Meyer

Documentation of Own Contribution

This paper is written in a monographic style. All sources used are referenced accordingly and listed in the bibliography in the order in which they are cited. A distinction is made between all publications and the author's own publications. Some of the new approaches, methods and results mentioned have already been published. This fact is referred to at the relevant points. These publications are also listed in the bibliography. In detail, these are the following chapters and publications:

- The new PSO variant presented in section 4.2 is mainly based on the approach and results of the author's master thesis. The variant was published together with the supervisor in [P37]. Other new PSO variants of chapter 4 as well as the related results from chapter 5 are unpublished.
- A fuzzy method for direct assessment of protection settings, first presented in [67] and extended in [P70] and [P71], is discussed in section 7.1. Part of the work [P71] is revisited in section 10.3.2.2 and used in a modified form. Here, the author of this work was only involved in the publications [P70] and [P71] as first author. The contributions of the co-authors were in form of consultation, programming and simulation work. The fuzzy method itself was not further investigated within the scope of this work.
- Major parts of chapter 8 are based on [P77], [P78] and [P79]. For both publications, the author of this work is first author and the only coauthor is the author's supervisor.
- The overall concept of the Protection Toolchain, which is the subject of chapter 10, is a joint result of the project Kopernikus ENSURE 1 and 2 [114]. The collaborative approach was first published in [P109], where the author of this work is first author. Further publications of the concept followed in [P110], [P111], [P112] and [P113], presented by the author of this work. Due to the modular structure, each partner had its own scope and responsibility in the process. Thus, the sections 10.2.1, 10.2.3 and 10.2.4 were mainly handled by the different partners and are therefore only briefly explained. The model presented in section 10.1 is based on preliminary work by [115] and is unpublished in its currently implemented form. The approach presented in section 10.3 is also unpublished. The results of chapter 11 and 12 are unpublished.

The supervisor of the author provided advisory support for all publications mentioned. He is therefore also corresponding co-author on all of them.

Abstract

Power systems worldwide play a key role in achieving climate goals, electrifying sectors, and connecting renewable energies. They face major challenges and are confronted with increasing changes, variable infeed and integration of new technologies. Operating and fault conditions are becoming more diverse, probabilistic, and difficult to predict.

Protection systems have the task of preventing power systems from the consequences and impacts of faults. However, protection concepts are still created by experts today and are rarely reviewed and adapted after changes. Despite the increasing volatility of grid structures, methods have hardly evolved.

The aim is therefore to digitize and fully automate the generation, parameterization, assessment and optimization of protection concepts. Protection systems shall be adjusted prior to system changes or when security vulnerabilities occur. The approach consists of six sequential steps and is called Protection Toolchain (ProToc). The tools are Typical Matching, Pre-Calculations, Algorithm Selection, Settings Calculation, Protection Security Assessment, and Optimization. The workflow relies on a comprehensive database and a generic data model to process, compute and analyze protection and simulation data. In order to adjust different protection functions of multiple protective devices of a system-wide grid section coordinately, a hybrid Binary Particle Swarm Optimization algorithm is proposed. Together with an assessment method designed for this purpose, it can generate applicable and trustworthy protection settings. To do so, the approach distances itself from traditional setting philosophies that focus on selectivity. Instead, it takes a holistic view of the power system, including all the effects of a fault and the protection system on system stability and security of supply.

The results of simulations and laboratory tests prove that the ProToc is able to set different protection function types and setting values together in an exceptionally coordinated manner. Protection systems and concepts are adapted to existing multivariate power system situations and topologies in a highly flexible way. The approach works detached from usual constraints and thus achieves maximum system and protection security also in situations where other techniques fail. Even previously unknown and unconventional strategies are developed. At the same time, the optimized setting values are closely linked to the structure used and the underlying load flow situation. The main challenge lies in the effective and precise control of the optimization process via appropriate search spaces and corresponding evaluation and penalty functions. Undoubtedly, the ProToc is still at an early stage. The novel approach, however, already shows its effectiveness, versatility and potential.

Zusammenfassung

Elektrische Energieversorgungssysteme sind Wegbereiter und Motor des Wohlstandes moderner Gesellschaften. Hierbei nehmen diese weltweit eine Schlüsselrolle zur Erreichung von Klimazielen, bei der Elektrifizierung von Sektoren und dem Anschluss von Erneuerbaren Energien ein. Die gesamte Energiesystemlandschaft steht vor großen Herausforderungen und sieht sich mit zunehmenden Veränderungen, variabler Einspeisung, Integration neuer Technologien, sowie massiven Um- und Ausbauten konfrontiert. Betriebs- und Störungszustände werden dadurch vielfältiger, probabilistischer sowie schwerer vorhersehbar und unterscheidbar.

Schutzsysteme haben die Aufgabe, Störungen bestmöglich zu erkennen, abzuschalten und das System vor Folgen und Auswirkungen zu schützen. Schutzkonzepte werden jedoch bis heute von Fachexperten in enger Abstimmung mit der vorliegenden Netztopologie und auf Basis von bereits existierenden Schutzschemata erstellt. Trotz der zukünftig zunehmenden Flexibilität und Volatilität der Netzstrukturen haben sich die Methoden kaum weiterentwickelt und gestalten sich arbeitsintensiv und aufwendig. Darüber hinaus findet eine Überprüfung der Schutzsicherheit nach erfolgten Änderungen am Energiesystem nur selten statt.

Ziel und Pflicht ist es daher, die Prozesse der Schutzkonzepterstellung, Parametrierung, Bewertung und Optimierung zu digitalisieren und vollständig zu automatisieren. Schutzsysteme müssen vor geplanten Netzveränderungen oder bei Feststellung von Sicherheitslücken umgehend an neu vorliegende Bedingungen adaptiert werden. Der in dieser Arbeit vorgestellte Lösungsansatz besteht aus sechs verschiedenen, aufeinander aufbauenden Arbeitsschritten und trägt den Namen Protection Toolchain (ProToc). Nacheinander werden die interoperablen Tools Typical Matching, Pre-Calculations, Algorithm Selection, Setting Calculation, Protection Security Assessment und Optimization durchlaufen. Dabei setzt der Arbeitsablauf auf eine umfassende Datenbasis aus Primär- und Sekundärdaten sowie ein eigenes generisches Datenmodell zur Verarbeitung, Berechnung und Analyse von Schutz- und Simulationsdaten. Die Vorgehensweise kann sowohl zum Erstellen von ganzen Schutzkonzepten sowie zur Bewertung und Optimierung von bestehenden Schutzkoordinationen eingesetzt werden.

Um verschiedene Schutzfunktionen mehrerer Schutzgeräte eines systemweiten Netzabschnittes aufeinander abgestimmt und zusammenhängend einstellen zu können, wird ein neuer, hybrider Binary Particle Swarm Optimization (BPSO) Algorithmus vorgeschlagen. In Zusammenarbeit mit einer dafür

speziell konzipierten Bewertungsmethode können so verwendbare und verlässliche Schutzeinstellungen vollautomatisiert ermittelt werden. Dabei nimmt der Ansatz Abstand von traditionellen Einstellphilosophien, die den Fokus rein auf Selektivität legen. Ziel ist es vielmehr, das Energiesystem ganzheitlich zu betrachten und alle Auswirkungen eines Fehlers und des Schutzsystems auf die Systemstabilität und die Versorgungszuverlässigkeit mit einzubeziehen und zu bewerten. Nur so ist ein optimaler Kompromiss aus dynamischer Sicherheit und Zuverlässigkeit möglich. Darüber hinaus kann auch der zeitliche Verlauf einer Fehlerklärung berücksichtigt und Unselektvititäten gegeneinander abgewogen werden.

Die Ergebnisse von Simulationen und praktischen Tests im Echtzeitlabor beweisen, dass die ProToc unabhängig der vorliegenden Topologie und Netzart in der Lage ist, verschiedene Schutzfunktionsarten und Einstellwerte gemeinsam und präzise aufeinander abgestimmt zu parametrieren. Schutzsysteme und Konzepte werden hoch flexibel an vorliegende, multivariate Netzsituationen optimiert. Die Vorgehensweise arbeitet losgelöst von üblichen Beschränkungen und erzielt so selbst in Situationen, wo andere Techniken versagen, maximale Sicherheit. Dabei werden auch bisher unbekannte und unkonventionelle Lösungsstrategien erarbeitet, die es unter anderem ermöglichen, bereits vorhandenen und verbauten Schutzgeräte effizienter und wirkungsvoller einzusetzen. Die größte Herausforderung liegt dabei in einer effektiven und präzisen Steuerung des Optimierungsprozesses über geeignete Suchräume und entsprechende Bewertungs- und Straffunktionen. Zweifelsohne befindet sich die ProToc noch in einem frühen Entwicklungsstadium. Sie beweist jedoch schon heute, dass sie einen erheblichen Mehrwert zur nachhaltigen Entlastung von Netzbetreibern und aufgrund ihrer Effektivität und Vielseitigkeit zur Aufrechterhaltung der Netz- und Schutzsicherheit leisten kann.

Contents

The only constant in live is change.

Heraclitus of Ephesus
Greek philosopher
ca. 500 BCE

1 Introduction

1.1 Background & Motivation

The electrical power supply system can be described as the largest technical system worldwide, which also places it among the most complex systems in the world. It extends across national borders, connects continents with each other, and is a pioneer and driver of the prosperity of modern societies.
As a network, it comprises operating resources for power generation, transmission, distribution and consumption. This includes thermal power plants, Renewable Energy Sources (RES), transformers, transmission lines, substations, and the loads to be supplied. These include industries, companies, hospitals, infrastructures, schools, government buildings, households and many other important consumers. Maintaining a high level of security of supply goes hand in hand with a high level of reliability of supply and is of paramount importance.

However, political, societal, economic, technical and regulatory requirements are constantly increasing, making the maintenance and operation of power systems more complex and challenging. Additionally, we as mankind, as guests of this world, have the common task to massively reduce the emission of greenhouse gases and to live a climate as well as resource neutral life. The populations of the industrialized nations in particular must become aware of their social responsibility. There is a kind of *noblesse oblige* to rethink fundamentally, to act energetically, to protect and preserve the environment

purposefully, so that future generations can lead a dignified and livable life on this planet.

RES and the energy system take on a key role in meeting these challenges. Electrical energy is a universally applicable, excellently transmittable and well controllable energy source of highest quality. It enables a wide range of sectors such as transport, heat and industry to be supplied without fossil primary energy sources, while maintaining a high level of efficiency. However, for this to succeed, a massive increase and expansion of RES is required in addition to the continuous electrification of all sectors. Only the use of green and thus CO_2-free electricity will ultimately lead to the necessary decarbonization and a cost-effective and independent energy supply.

To achieve this, the electrical energy system must also be modified and expanded accordingly. In many places, the necessary transformation process has already begun, although the speed and intensity must increase significantly. The high degree of change required and the variability of RES, as well as new consumers such as charging stations and heat pumps, require new approaches, grid topologies and technologies. The operation and behavior of transmission and distribution systems must remain controllable, and emerging load and fault situations must be considered, detected, and the latter disconnected via protection systems. However, this is where traditional methods of protection concept design and parameterization reach their limits.

Regular review and, if necessary, optimization of protection concepts, protective devices and protection settings are necessary to maintain long-term protection security in changing power systems. At the same time, the maintenance, inspection and parameterization effort increases with the currently growing number of required protective devices. Nowadays, the decision whether to make such an adjustment depends primarily on the foreseeable consequences, if it is not made. However, there is also a lack of suitable tools that can determine and evaluate the effects of unselective or delayed fault tripping on the basis of concrete factors.

Therefore, new, comprehensive, systemic, and holistic approaches are needed that combine the tried and true with new automated tools to address the variety of possible fault scenarios and provide solutions. Traditional techniques will sooner or later start to fail and deliver results of insufficient quality. The management of multivariate power system states requires the use of equally variable tools. Therefore, the goal is to digitize, flexibilize and automate the protection concept generation, assessment and optimization. For this reason, this work proposes and describes in detail the use of global optimization, a

specially developed assessment method, and the simultaneous simulation and consideration of protection security and dynamic system stability.

Last but not least, it may be mentioned that every transformation process is difficult at first. Obstacles must be overcome, courage and perseverance must be shown in the face of the unexpected and inconveniences. But the benefits for each of us, as well as for our nature and wildlife, lie at the end of this path.

1.2 Key Challenges

In order to generate, assess and optimize protection concepts in a fully automated, reliable and trustworthy way, the following challenges have to be overcome.

A global optimization method is needed that...

- is independent of the size, type and topology of the power system to be optimized as well as of the structure and design of the protection system. This is the only way to optimize future, unconventional and multivariate structures without having to adapt the optimization method each time.
- can flexibly handle any number of protective devices, protective functions and setting values to be optimized, and can process both real numbers such as reactance values and binary numbers for the activation or deactivation of protective functions.
- is efficient, secure, and provides consistent results throughout so that the generated protection settings can meet applicability, plausibility, and reliability requirements.

A protection assessment method is needed that...

- is applicable regardless of the selected power system type, voltage level, and existing generating units and loads, and is not based on the current characteristics of the system under study.
- bridges the gap between protection analysis and dynamic studies in the context of fault simulations in order to capture the mutual effects and dependencies and to evaluate them accordingly.
- does not focus on how a fault is cleared, but evaluates the quality of how well a protection system contributes to securing and maintaining overall stability as well as security of supply. Only then is it possible to compare and prioritize unselective and delayed fault tripping.

- maps a fitness landscape that efficiently guides an optimization method and thus leads to improved as well as correct protection settings. Thus, a change in the protection system or the setting values must also lead to a change in the assessment.

A concept as well as the implementation of a toolchain is required, which...

- sensibly structures, efficiently organizes and holistically combines a system of different tools for automated protection concept generation, assessment and optimization, taking into account all boundary conditions.
- provides a data management with corresponding interfaces to simulation programs, databases and other tools, so that all necessary primary and secondary data can be considered and necessary analyses as well as protection calculations can be carried out.

1.3 Structure & Design

This work is divided into three main parts based on the challenges identified. Each part contains an introductory theory section, a description of the respective challenges, and the presentation and discussion of new solutions. The main parts are as shown in Figure 1.

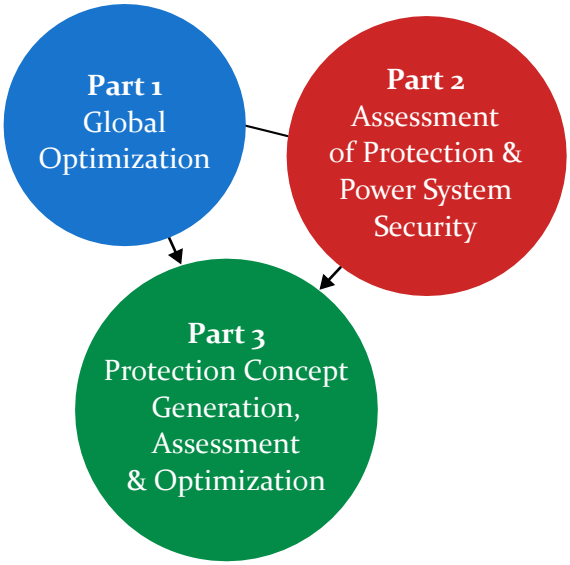

Figure 1: This work is divided into three main parts, with Part 1 and Part 2 brought together in Part 3.

Part I - *Global Optimization*
The parameterization of a system-wide protection system is a complex task and thus an optimization problem to be solved. The first part of chapter 2 therefore deals with the general mathematical modeling and the properties of optimization problems. Based on this, the presentation and overview of different available optimization methods follows. It is described how manifold and diverse the methods are and in which way they can be classified and categorized. It is shown that metaheuristics in particular, as problem-independent methods, can be used universally and efficiently to solve a wide variety of highly complex problems. In contrast to exact algorithms, metaheuristics do not require a priori information about the problem to be solved and do not depend on the existence of concrete mathematical properties.
Therefore, in the following chapter 3, the Particle Swarm Optimization (PSO) method is selected as a swarm-based metaheuristic and described in detail. Then, the Binary Particle Swarm Optimization (BPSO) variant is presented, which is specifically designed for solving binary optimization problems.
Building on this, more advanced, hybrid and self-adaptive PSO variants are presented in chapter 4. These all aim to solve problems faster, more accurately, and more efficiently. Also presented here are new BPSO variants specifically designed for simultaneous optimization of real and binary protection settings.
The first main part ends with chapter 5 and a large benchmark of all available PSO methods.

Part II- *Assessment of Protection & Power System Security*
The second part starts with chapter 6 and a basic explanation, description and definition of the most important protection and stability terms. Building on this, the following chapter 7 presents the currently most common security assessment systems for evaluating dynamic stability and protection security. In each case, the differences, strengths, and weaknesses of the systems are highlighted, and it is explained why they are not suitable for optimizing protection concepts using metaheuristics.
In the last and most comprehensive chapter, the new assessment method developed specifically for optimization is presented and described. This envisages evaluating protection systems from a whole-system perspective and evaluating both the protection behavior and the impact on system stability and security of supply. Therefore, new indices and evaluation techniques are required, which are explained and described one after the other. The second part ends with a description of the structure of the final overall assessment value, which can be returned as Fitness Value (FV) to an optimization method.

Part III - *Protection Concept Generation, Assessment & Optimization*
In the last and third part, the two previous parts are merged and applied. The first part starts with chapter 9 and the expected changes in the power system landscape. This highlights the challenges that will be faced in protection design and coordination in the future. An explanation of the basic operation of distance and overcurrent protection functions follows. A variety of examples are used to discuss the difficulty of coordination in respect to various negative impacts. The chapter ends with a description of the state of the art in protection design and makes it clear that this will not be sufficient in the future to maintain the protection and security of the power system.
As a solution approach, a chain of different tools for automated protection concept generation, assessment and optimization is proposed in the subsequent chapter 10. Within this chain, a generic data model performs the function of data storage and distribution as well as providing computational and analytical functions. The structure, classes, and connectivity of the objects are described in detail. This is followed by a description of the concept of protection concept generation and the tools available for this purpose. The chapter ends with a description of the implemented, merged and realized tools for the assessment and optimization. Simulation and hardware setups, models used, adjustable values that can be optimized, and the automated generation of search spaces for the optimization process are explained.
This is seamlessly followed by chapter 11, in which the previously presented toolchain is brought to bear. A distribution and a transmission system are used to describe in detail where the strengths and weaknesses of the toolchain lie. It is explained which protection settings the optimization leads to for different framework conditions and which potential the system offers, especially for unconventional structures. The simulation and evaluation results are analyzed and discussed together with the detected transient effects.
In the last chapter 12 of the third part, various fault scenarios and detected phenomena are investigated for plausibility in the real-time laboratory with real protection devices. For this purpose, the setting values optimized in the previous chapter are applied to the real devices and the behavior is compared with that of the generic devices from the simulation.

Part I

Global Optimization

For since the fabric of the universe is most perfect and the work of a most wise creator, nothing at all takes place in the universe in which some rule of maximum or minimum does not appear.

Leonhard Euler
Swiss mathematician and physicist
* 1707, + 1783

2 Introduction & Taxonomy

Especially in sports, there are a multitude of tournaments, competitions and leagues in which the best athlete or team is regularly determined and crowned. What child doesn't dream at some point of winning gold at the Olympics, becoming soccer world champion or winning the Super Bowl? The goal of achieving the best possible, in other words the optimum, under given conditions is a natural human endeavor. This can be observed not only in sports, but also in economics, industry, art, society and science.

The term optimization is widely used and has different connotations for many people. Therefore, this chapter first explains the basics of mathematical modeling and optimization. Then, the various requirements and challenges of optimization problems as well as the optimization methods available for solving them are discussed. Finally, the heuristic optimization algorithm PSO used in the remainder of this thesis is presented in detail.

2.1 Mathematical Modeling & Programming

Optimization has become an integral part of modern mathematics and has produced a wide variety of approaches, techniques and methods. It can be understood as a process that attempts to solve complex problems in the best possible and efficient way by adapting a system. In this context, the question of the optimal solution to a problem often leads to disputes, because the optimal solution is usually the best compromise among different solutions. Therefore, in order to avoid disputes, a clear objective and a concrete definition of all framework conditions and assumptions are required in advance. However, these have the disadvantage that a complex, real-world problem must be simplified and broken down to a mathematical model. This process is called *mathematical modeling* and was described by the Dutch mathematician S. W. Rienstra as follows [1]:

> Mathematically modeling is describing a real-world problem in a mathematical way by what is called a model, such that it becomes possible to deploy mathematical tools for its solution. The model should be based on first principle and elementary relations and it should be accurate enough to have reasonable claims to predict both quantitative and qualitative aspects of the original problem. The accuracy of the description should be limited in order that the model not be unnecessarily complex.

Modeling a mathematical model is therefore a creative process, whereby the model can be freely designed to a certain extent. In this regard, it takes a crucial role in applied mathematics and modern engineering sciences, as these cannot be applied to a real-world problem without modeling. Figure 2 shows a simple schematic representation of the modeling process, which is recognized in the general literature. At the beginning, there exists a real problem to be solved or investigated. In a first step, this problem is simplified and only the necessary and applicable relationships are defined. Subsequently, this problem is transformed into a mathematical model under consideration of all defined basic conditions, the restrictions and constraints. It should be noted that for this purpose there are no automata that can transform real problems quickly and easily. Rather, it is the main task of an engineer to work out a correct and appropriate translation of the technical conditions into the mathematical model. Once the problem to be solved has been modeled, it is the task of mathematical programming to determine optimal solutions for the problem. Nowadays, computer-aided methods are mainly used to solve the model analytically or numerically. If the methods consist of more complex algorithms, which among other things cope with large amounts of data, the

term *scientifing computing* is also applied. Higher programming languages such as C++, C# or Java are often used for this purpose, or commercial programs or simulation packages such as MatLab are relied upon. The engineer's task is then again to interpret the resulting outcomes and to check their usability with respect to the real problem. Especially when running pure numerical simulations, it is useful if the engineer has already anticipated the solutions. The determined solutions applied to the real problem should lead to usable, plausible and acceptable results. This circumstance illustrates once again the importance of modeling the real problem as detailed and correct as possible. If an inappropriate model is used, even optimal solutions would only be transferable to the associated real problem to a limited extent or not at all. [2]–[4]

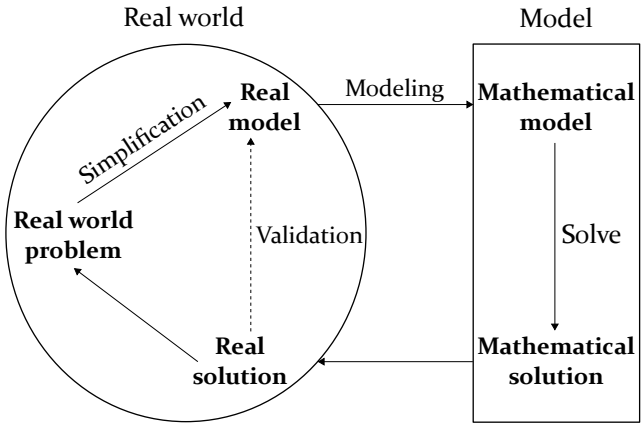

Figure 2: Schematic representation of the mathematical modeling process.

2.2 Objective Functions

Not every mathematically described optimization problem necessarily has one or more optimal solutions. This depends on the defined framework conditions. If these contradict each other, no optimal solution exists. If all determined solutions are equal and therefore none is better than the other, depending on the objective none or many optimal solutions exist. In order to solve this dilemma and to be able to compare different results of a modeled problem, the so-called *objective function* or *fitness function* according to (1) is introduced. These can be used to determine which solution is superior to another. An objective function is to be designed in such a way that it must be either maximized (profit) or minimized (cost). Figure 3 schematically

represents a one-dimensional objective function $f(x)$ with different local and global extrema. For the task of minimizing an objective function, an optimization problem $P_{\min}$ according to (2) with constraints $h(x)$ and $g(x)$ is obtained.

$$f : X \to \mathbb{R}, \quad x \mapsto f(x) \tag{1}$$

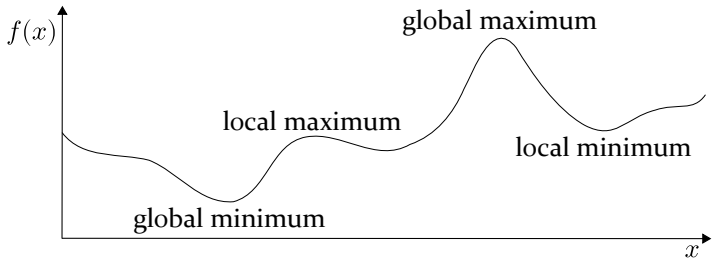

Figure 3: Graph of an objective function with local and global extrema.

$$P_{\min} \; : \; \min f(x) \quad s.t.^{1} \quad x \in X,\; h(x) = 0,\; g(x) \leq 0 \tag{2}$$

A solution $x^* \in X$ is called optimal for a problem P if no solution $x \in X$ yields a better FV. Subsequently, with respect to the minimization task, the inequality given by (3) holds and the optimal function value is obtained from (4).

$$f(x^*) \leq f(x) \quad \forall x \in X \tag{3}$$

$$f_{\min}(x) = \min_{x \in X} f(x) \tag{4}$$

The domain X is called *decision space*, *solution space* or *search space* and can represent any kind of elements like integers, real numbers, lists, plans, etc. It is selected depending on the problem to be solved and mathematical model. According to the decision space X, the variables or solutions x to be optimized are also called *decision variables*. The goal of any optimization procedure is to determine the best possible decision variables x^* from the set X considering the set of all objective functions F of a modeled problem in the shortest possible time interval. F consists of $m = |F|$ objective functions f_j, each representing a criterion to be optimized, and is given by formula (5). In a global optimization, all optimal solutions are sought in the entire decision

space X. In contrast, in a local optimization only the optima related to a subset of X are searched.

$$F = \{f_j : X \to \mathbb{R},\ 0 < j \leq m\} \tag{5}$$

In real engineering applications it can be assumed that X is at most a subset of the finite-dimensional Euclidean space $\mathbb{R}^n$. It follows that all solutions $x \in X \subseteq \mathbb{R}^n$ represent points in the n-dimensional space. Therefore, in the following of this work, they are often referred as solution points $\vec{x}$ or just points as well as the optimal point and not the optimal solution. Finally, Figure 2 can be extended in Figure 4 to include the scope of optimization methods and fitness functions.

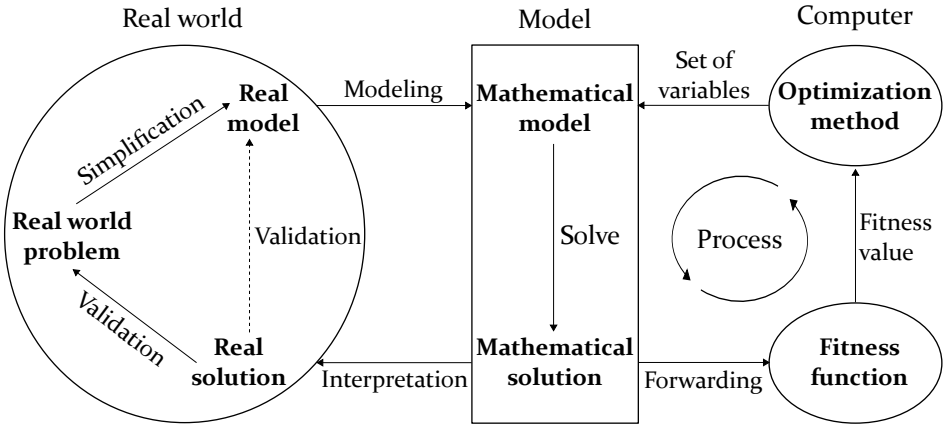

Figure 4: Schematic representation of the mathematical modeling and optimization process with fitness functions.

2.3 Optimization Methods & Classification

Figuratively speaking, the selection of optimization methods is like a box full of different Lego bricks, which are both similar, but also clearly different from each other, and with each year more bricks and thus methods are added. In the relevant literature, there are various approaches to categorize and classify optimization methods, depending on their focus. The goal of this section is to give a short and concise overview of the differences and most important features in order to create an understanding of when and under which conditions an algorithm can be used. For more in-depth information around the enormous variety of local and global optimization methods, the following literature is recommended for the interested reader: [3], [5]–[10]. A

historical review of various taxonomies of optimization techniques over the past decades, which attempt to address and organize the broad field, can be found in [11].

The simplest and oldest global optimization method in the world is the testing of all possibilities to obtain the optimal point of an optimization problem. This method is also known as the *brute-force* method. For more complex systems, it quickly reaches the limits of computing capacity, even with today's modern computers. The circumstance can be explained well by the example of the most well-known combination problem the Traveling Salesman Problem (TSP). The problem is that n cities are given on a map. The merchant has to cross all cities one after the other exactly once and finally return to the place of origin. The optimization problem is to find out which is the shortest route. Figure 5 visualizes the problem as a graph. For a TSP, there are exactly $(n-1)!$ possibilities to travel to each city successively, if the starting point is fixed. For a small TSP with four cities there are 6 possible routes. With 6 cities there would be 120 possibilities, with 10 cities 362,880 with 14 cities there would be 6,227,020,800 $\sim$ 6.23 trillion variants and with 25 cities the possible number of routes would be approx. 6.2×10^{23} or 620 sextillion. Assuming that today's supercomputers operate at 100 petaFLOPS, which corresponds to 100×10^{15} floating point operations per second, and computing a route costs n operations, computing all routes for 25 cities would take almost 5 years. This example illustrates that computing all possible routes is far too computationally and time consuming. Nevertheless, in order to be able to determine the optimal point of a complex problem, there are numerous, different optimization methods that are best suited for certain types of problems. In order to be able to select the right algorithm, it is crucial to identify the characteristics of a problem and then select the appropriate optimization method for it. The main criteria are the number of objective functions to be optimized simultaneously, the definition of the decision space, the constraints of an optimization problem, and the design and hence complexity of the landscape of objective functions. According to these main categories, which are shown in Figure 6, optimization methods can be grouped, described and subdivided depending on their functionality and thus suitability for the problem.

2.3.1 Number of Objectives

Depending on the number m of objective functions f_j of the set F to be optimized, optimization problems are divided into single- and multi-objective functions. While in single-objective problems there is only one objective function, in multi-objective problems there are at least two functions. Thus, in

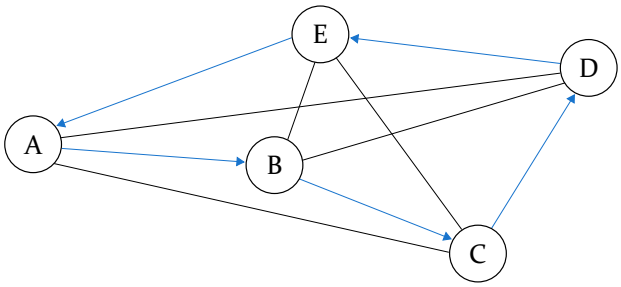

Figure 5: Traveling Salesman Problem with five cities.

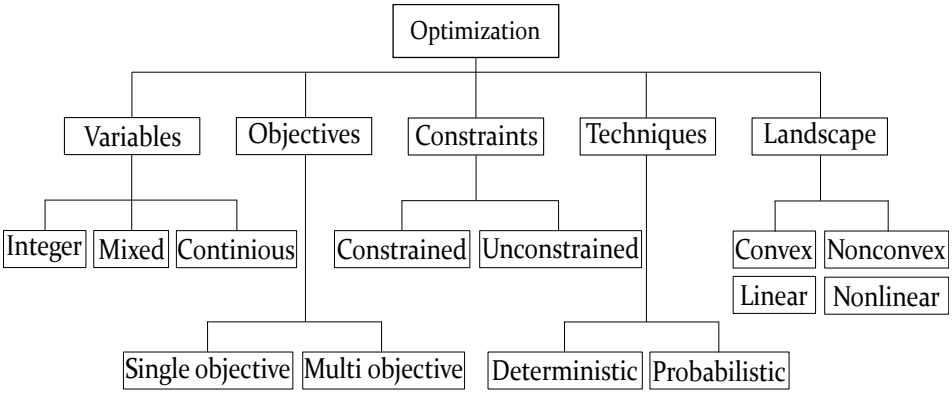

Figure 6: Classification categories of optimization methods.

multi-objective problems, an optimization algorithm has to find a compromise between the often conflicting objective functions. Another difficulty is that not only one single optimal point exists, but a whole set of points, which can be called optimal, form the solution of a multi-objective problem. In the following, the issue will be illustrated by an example.

At the beginning of the development process for an electric car, many different requirements and wishes can be formulated. For example, the car should be able to be manufactured and sold at low cost, but also have a long range, offer as much comfort and space as possible, have good acceleration, be secure, be easy to steer, etc. All these objectives can be formulated as objective functions f_j of the decision variables x_i. The latter then represent the materials used, the size and shape of the components, technical and dynamic properties, or the choice of engine and tires. Depending on how the input values are chosen, the electric car ends up having different characteristics and thus results in the objective functions. Figure 7 graphically represents the multi-objective optimization problem and the relationship between input and objective variables. The

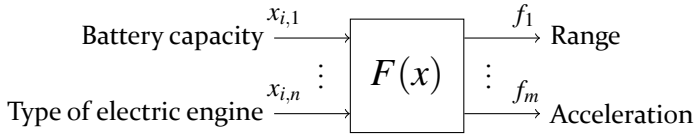

Figure 7: Multi-objective optimization problem consisting of n input variables and m objective functions.

optimization of multi-objective problems leads to no single point x, but to many different solution points x_i, which form the *Pareto set* and are thus considered *Pareto-optimal*. The definition of Pareto-optimal is closely related to the definition of *Pareto-dominance*. Thus, a solution x_1 dominates another solution x_2 if x_1 is better than x_2 in at least one objective function and at the same time is not worse than x_2 in all other objective functions. A solution $x^* \in X$ is said to be Pareto-optimal if it is not dominated by any other solution x in the decision space X. The set of Pareto-optimal solutions X^* is also called *Pareto front*. Whether the full Pareto-optimal set or a single optimal point should be the desired outcome of an optimization problem ultimately depends on the user and the set of objective functions. Optimizing a Pareto front requires special techniques, which is why not all optimization methods are able to solve multi-objective optimization problems. Moreover, this requires more computation time and requires to select a solution from the Pareto front at the end of the optimization. This can be disadvantageous, but at the same time it is an additional degree of freedom that can be used. [5], [6]

One approach to transform multi-objective optimization problems into single-objective problems is the *weighted sums* method. Here, the weighted sum $g(x)$ is formed from all objective functions f_j according to formula (6). Each objective function is multiplied by an associated weighting value w_j, which reflects the importance of the function f_j relative to the other functions. In this way, a multi-objective problem can be reduced to a single-objective problem. However, the weighted sums method requires that the qualitative results of the different objective functions can be offset relative to each other.

$$g(x) = \sum_{j=1}^{m} w_j f_j(x) = \sum_{\forall f_j \in F} w_j f_j(x) \tag{6}$$

2.3.2 Type of Variables

When creating a suitable objective function for a problem, the first step is to define the variables to be optimized. Both the number and the respective value ranges of the variables have a significant influence on the complexity of the objective function. In chapter 2.2 it was already explained that in real applications the decision space X is at most a subset of the real numbers $\mathbb{R}$. If for an optimization problem $x \in X \subseteq \mathbb{R}$ holds, then it is called *continuous or real-parameter optimization*.
In *discrete* or *binary optimization*, in turn, the decision space X is a finite or countably infinite set, respectively. Hence, many problems exist in which the decision variables may take either only integers $x \in X \subseteq \mathbb{Z}$ or natural numbers $x \in X \subseteq \mathbb{N}$. These problems are also called Integer Programming (IP) methods. For pure binary problems, the decision space is even restricted to the set $\mathbb{B} = \{0, 1\}$ and these are referred to as *0/1-IP methods*.
If the decision variables of a problem should be part of different sets and thus continuous and discrete variables exist simultaneously, this is called a Mixed Integer Programming (MIP) model.

2.3.3 Constraints

There are few real-world applications that are not subject to constraints at all. Constraints limit the valid decision space X and can therefore also be called bounds. Like objective functions, constraints can be formulated in terms of linear or nonlinear equations $h(x)$ or inequalities $g(x)$, as is the case with (2). Figure 8 represents the relation of constrained decision space and the corresponding target space. The solution point x of the decision is transferred to the objective space via the set $F(x)$ of objective functions.

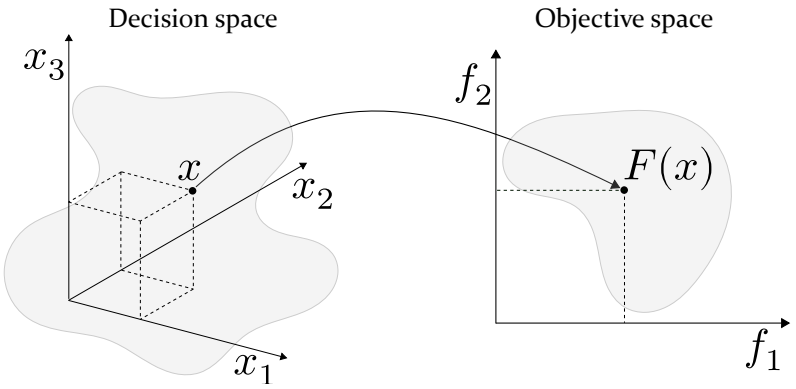

Figure 8: Representation of a restricted decision space and the associated objective space.

One way to deal with constraints is to discard invalid points and ignore them in the further course of the optimization. However, this requires that the valid decision space is large enough to prevent the search from stagnating early. Moreover, the information that would possibly result from the discarded points would be lost. Another option is to include constraints as another objective function, but this would expand a single-objective optimization problem into a multi-objective problem. One of the most popular options is likely to use penalty functions. These are combined with the actual objective function in such a way that an invalid solution point leads to worse results than an admissible point. There are virtually no limits to the design of the implementation of this method. For example, the penalty functions can be formulated dynamically and thus as a function of the number of iterations, or they can change adaptively as the optimization proceeds. Since not all optimization methods are able to deal with constraints, they can also be distinguished according to this. [3], [5]

With reference to the example already mentioned, the development process of an electric car, a necessary constraint would be the limitation of the material thickness of the body. Thus, a negative body thickness or a thickness of zero would not make sense. An upper limit on the thickness of the body can, in turn, help an optimization algorithm to arrive at an optimal solution more quickly and in a more targeted manner.

2.3.4 Fitness Landscape

The notion of *landscape* as a metaphor for describing complex interrelationships has gained acceptance in many areas of mathematics and science. The pre-visualization of pleasant terrains up to stony mountain landscapes makes it possible to make the most diverse properties graspable and imaginable. In the field of optimization, the term *fitness landscape* is mainly used to characterize objective functions and to compare them with each other. Also, the progress of an optimization process can be understood as an adaptive hike through the landscape over hills and valleys, where the goal is to find the deepest valley. Various properties of fitness landscapes and thus characterizing attributes have already been introduced in the previous sections. For example, the decision variables used can be continuous, discrete, or mixed. Moreover, a distinction is made between objective functions free of constraints and those subject to them. Another important property is the issue of convexity. A set $X \subset \mathbb{R}^n$ is called convex if (7) is true. Graphically, this means that a connecting line between any two points from X is completely contained in X, as shown in Figure 9. A function $f : X \to \mathbb{R}$ is also convex on the convex set X if (8)

holds, and strictly convex if (9) holds. The function graph of f then passes below each of its secants and is continuous, making any local minimum also a global minimum. Figure 10 illustrates the matter. This fact simplifies an optimization problem, since once an optimal point is found, the optimization is finished. An optimization problem is said to be convex if both the objective functions, constraints and the set of admissible points are convex. In addition, for strictly convex optimization problems, there is at most one optimal point, which further simplifies the optimization. It should be noted, however, that a convex function does not necessarily have an optimum point. For example, the function $f(x) = exp(x)$ is strictly convex, but has no extreme point. Only when the decision space X is bounded does an optimal point x^* exist on the boundary of X. [7], [12]

$$tx + (1-t)y \in X \quad s.t. \quad \forall x, y \in X,\ \forall t \in [0,1] \tag{7}$$

$$f(tx + (1-t)y) \leq tf(x) + (1-t)f(y) \quad s.t. \quad \forall x, y \in X,\ t \in [0,1] \tag{8}$$

$$f(tx + (1-t)y) < tf(x) + (1-t)f(y) \quad s.t. \quad \forall x, y \in X,\ x \neq y,\ t \in [0,1] \tag{9}$$

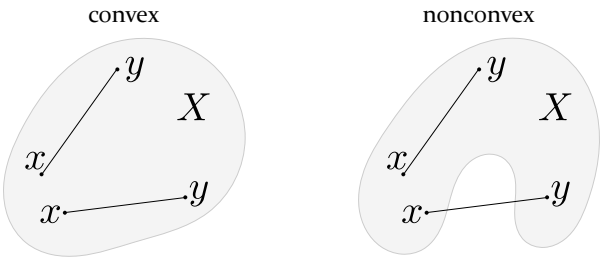

Figure 9: Convexity of sets in $\mathbb{R}^2$.

2.3.5 Taxonomy

As already mentioned in the introduction of this section, there are many different optimization methods for solving different problems. A good overview is provided by Figure 11, which represents a taxonomy of different optimization

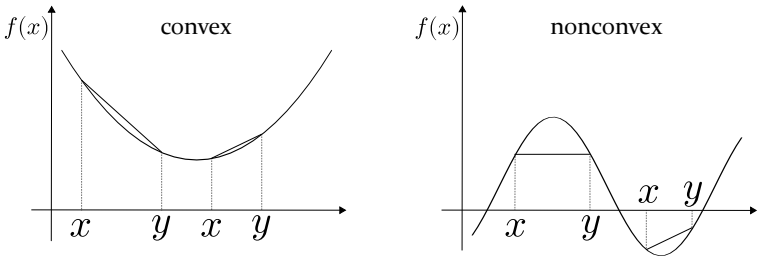

Figure 10: Convexity of functions in $\mathbb{R}^2$.

methods tailored for this work. On the left side are the main optimization methods: exact methods, heuristics, and metaheuristics. On the right side is the field of Artificial Intelligence (AI), which has seen a great growth, especially in the past years. On the one hand, this can be attributed to the greatly increased computing power of high-performance computers and the enormous storage and usage possibilities of data volumes. On the other hand, the algorithms AlphaGo and AlphaZero of the subsidiary DeepMind Technologies of Alphabet Inc. were able to defeat the world's best chess programs and Go players several times and gained worldwide attention. The algorithms are based on Reinforcement Learning (RL) approaches and combine techniques from Machine Learning (ML) especially Deep Learning (DL) with heuristics such as Monte Carlo-Tree Search (MCT) from the field of optimization. Also, many powerful and efficient optimization methods take advantage of and combine the strengths of different fields of mathematics and computer science, as will be shown throughout this work.
However, an interesting aspect to consider when designing and selecting an optimization procedure is the No Free Lunch (NFL) theorem for optimization published by David H. Wolpert and William G. Macready in 1997 [13]. This states that an optimization method that performs particularly well on one class of problems must underperform on the remaining optimization problems. Therefore, there is no optimization method that performs on average better than all other methods with respect to all possible problems. Even an optimization method based purely on randomness offers the same performance as any other method when measured across all types of problems.

However, concrete, real problems are only a small part of the theoretically existing totality of possible problems of the universe. The NFL theorem assumes a uniform distribution of all problems, giving unrealistically high importance to random, unstructured and therefore meaningless problems. As a result, it can be assumed that *free lunches* may occur after all, and thus some methods give better results than others for certain classes of problems.

However, the NFL theorem ties this circumstance to the condition that each optimization method must be adapted to the structure of the problem to be optimized in order to perform above average. This can be done already during the development of the method, before the start of the optimization when selecting suitable parameters or during the optimization process by monitoring and adapting parameters. Another conclusion of the NFL theorem is that the use of a priori information about a problem to be optimized can lead to a significant performance increase and this information should be used in the design and selection of the optimization method. Exact methods, in particular, take advantage of this fact. [11], [14]

2.3.5.1 Exact Algorithms

Exact optimization methods are a subcategory of deterministic methods. Deterministic means in this case that in each execution step of the optimization there is only at most one further possible step to continue. Otherwise, the optimization is finished. Deterministic and exact methods do not use random numbers or randomness based principles to decide what to do next. They are mainly used when the problem to be solved has concrete mathematical properties such as convexity, continuity, differentiability, linearity, etc. and thus complete a priori information about the optimization problem is available. They take advantage of these properties and apply strategies directly adapted to the problem in order to solve it as efficiently as possible. Another advantage of exact methods is that they guarantee finding the global optimum of a problem with a predictable amount of resources, such as Function Evaluations (FES) or computation time, within a predefined tolerance. For this purpose, larger problems are often broken down into smaller subproblems and solved separately. [11]

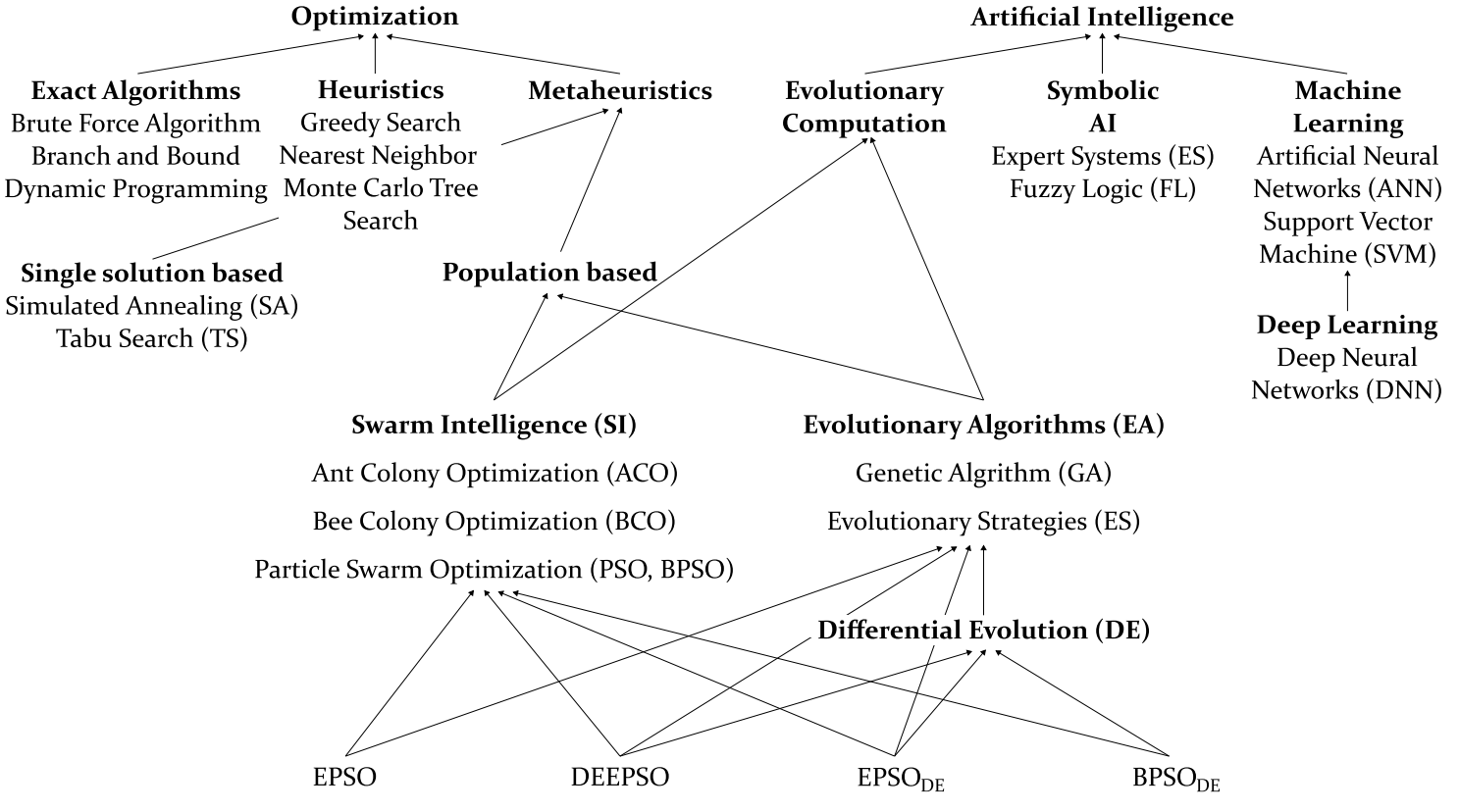

Figure 11: Taxonomy of optimization algorithms, which can be assigned to Global Optimization and Artificial Intelligence.

2.3.5.2 Heuristics and Metaheuristics

Heuristics are approximate methods and techniques that allow to decide which solution point of an optimization problem should be investigated next. They cannot guarantee the finding of a global optimum, but they can speed up the search process significantly. They are widely used in modern computer-aided optimization because they are versatile and can be applied broadly to problems of all kinds. They are based on the principle of trial and error to systematically improve and increase the return value of an objective function to be achieved. In doing so, they often use stochastic elements to efficiently explore the decision space, which is usually referred to as the search space S in heuristics. However, heuristics are problem-dependent and must be adapted to the problem to be solved.

Metaheuristics, on the other hand, are problem-independent, higher-order methods that can be used universally to solve optimization problems. They select, generate, or combine heuristic methods to be able to determine solutions even without insight into the structure of a problem. Such optimization problems, where little to no a priori information about the objective function is available, are also referred to as *black-box* problems, as graphically illustrated in Figure 12. At this point, the question can now be raised to what extent metaheuristics can be able to solve optimization problems efficiently at all, if the NFL theorem contradicts this in principle. And indeed, there is no universal best optimization algorithm. However, this is neither sought nor needed especially by engineers who want to optimize concrete problems. The NFL theorem makes clear that the use of problem-specific information leads to a significant increase in performance, which does not seem to exist especially for black-box problems. But appearances are deceptive. Our world follows basic physical laws and thus gives it a usable structure at the same time. Even if these laws are not known in detail, it can be assumed that the fitness landscapes of real problems are also subject to these laws and thus also have usable structures. Therefore, the idea of optimizing black-box problems is not to solve problems without structure, but to take advantage of the presence of the unknown structure. [15], [16]

Metaheuristics are often inspired by nature and pick up natural phenomena (biological evolution, social behavior of swarms) or physical processes (configuration of atoms). They mainly make use of information obtained from the fitness landscape during the optimization process to solve a problem efficiently. Thus, insights from visited points are used to decide which solution points to investigate next. Depending on the particular search strategy, this involves exploring new points throughout the search space while investigating

promising areas in more detail. These two competing goals are also referred to as exploration and exploitation.

Exploration (learning) describes searching broadly to discover good regions within a fitness landscape. The goal is to explore the area as broadly as possible and not get stuck on individual optima. Figuratively speaking, it is about discovering all the elevations of the fitness landscape to make certain that the greatest mountain is among them. Exploitation (optimal decisions), on the other hand, aims to explore individual areas in great detail. Elevations, for instance, need to be examined to see if they are just smaller, local hills or possibly the biggest mountain in the landscape. The weighting between exploration and exploitation and keeping the balance is the task of the method. To do this, most metaheuristics draw on knowledge gained during the search process to increase efficiency. Thus, useful information is stored, which is then taken into account in subsequent decisions about which point to visit next. The goal is always not to get stuck on local optima and to determine the global optimum as accurately as possible.

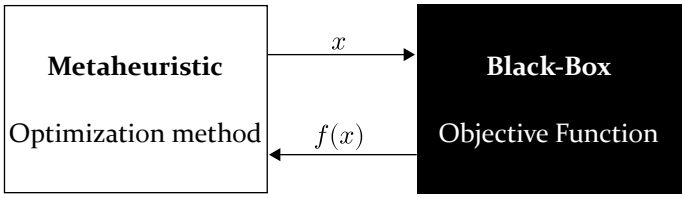

Figure 12: Sketch of a Black-Box objective function to be optimized by a metaheuristic optimization method.

Metaheuristics can be divided into two categories. Methods based on single solutions start with a single starting point and then move forward step by step, each with a next solution point. In doing so, they form a trajectory as they progress, which is why the methods are often referred to as trajectory methods. In contrast to this are population-based methods. These start with many different solution points distributed in the search space. From there, several solution points are always explored, evaluated and stored in the following steps. Depending on the optimization method, different population-based operators are then used, which use the collected information to determine the next solution points. Swarm-based approaches, which are grouped under the category of Swarm Intelligence (SI), have been particularly successful in recent decades. These are usually based on processes that occur in nature and take advantage of the coordinated behavior of birds, fish, or insects. Another successful and well-known category is Evolutionary Algorithm (EA), whose

functioning is inspired by the evolution of natural organisms. Both methods therefore also belong to the category of Evolutionary Computation (EC), which in turn is a subfield of AI.

Evolutionary Algorithm EAs use biologically inspired mechanisms and survival of the fittest to improve during an optimization process. A population of solution points or individuals evolves under selection pressure, resulting in better FV through natural selection. The main flowchart looks similar for all EAs. Initially, a new population of solution points is generated in the search space. This is often done using random-based methods. Each solution point is evaluated and thus has a FV, which means that the quality of each point is known and all solution points can be compared with each other. Via the respective method of EA, new solution points are then generated or new descendants are reproduced in a next iteration. In the field of EAs therefore also the term generations is used. Mostly techniques based on mutation and recombination are used. The new solution points are evaluated and then a selection process is used to determine which solution points or parents are retained and are thus available for the generation of new solution points (new individuals) of the next generation. These are then finally subjected to variation and the process is repeated.

EAs are robust and flexibly applicable metaheuristics that can be adapted to a problem to be solved by many mechanisms. They are suitable for multimodal, multicriteria, and dynamic problems and have been successfully applied to a large number of real-world problems. A disadvantage is often the high number of FES needed for convergence. [10], [11]

Differential Evolution Differential Evolution (DE) is a subcategory of Evolutionary Strategy (ES) and thus belongs to EAs. It was first introduced in 1997 for minimizing nonlinear and non-differentiable continuous functions with real-valued parameters and thus belongs to the newer optimization methods. Unlike many EAs, in DE the number of solution points used and thus the size of the population used does not change during the optimization process. The key novelty of DE lays in the procedure of generating new solution points. These are formed by adding the weighted difference of two randomly selected solution points to a third point. This procedure can be seen as a mutation process of the method. If the newly generated solution point has a better FV than a selected comparison point, it replaces it. Depending on the particular exact method, the best solution point that is newly generated after each iteration is explicitly included in the search process. DE methods are generally considered to be relatively fast, robust and accurate. Main

advantages are the easy applicability and simplicity of the algorithm as well as the calculation in floating point format with high accuracy. [6], [17]

Swarm Intelligence Animals living in swarms, such as insects, fish or birds, coordinate their common direction of movement, swimming or flight in order to escape hunters, find new feeding grounds or adapt to changing environmental conditions. Flocks of birds, for example, fly in V formations to minimize drag during their long flight and thereby conserve energy. Although the individuals of flocks are not highly intelligent creatures, they are still able to exchange information and communicate with each other through simple actions and reactions in order to solve tasks in cooperation. The movement of all the individuals creates a complex movement pattern of the entire swarm, where the disadvantage of the simple abilities of each individual is compensated by the large number and the parallelism achieved through this. The environment is included and used as an external memory. Many aspects of the collective activities are self-organized, functioning without central control. In this way, the individuals of a swarm can also teach each others when finding food, thus increasing the chances of survival for the swarm as a whole. This principle of social exchange, collective and coordinated trade of the whole swarm is called SI. [18], [19]

The concept of SI originated in the field of AI and was first used in connection with the work of cellular robotic systems in 1989 [20]. The authors were concerned with the interactions of simple, self-organized robots, which they described as mechanical automata capable of both mechanical and informational behavior. They used the term SI as a new buzzword, for a particular class of robot swarms. These swarms, however, were more like an artificial, constructing system that attempts to use patterns or some sort of ordered structure to organize itself. In biology, however, swarms are seen more as pattern analyzers. Biological swarms are able to figure out on their own what is the best way to do something. They use ordered patterns to do this, which is a characteristic of intelligence [20], [21]. In the context of this approach, a publication appeared in 1999 entitled *Swarm Intelligence: From Natural to Artificial Systems* [22], in which the authors of the Santa Fe Institute in New Mexico significantly expanded the term, which had been used rather restrictively until then. Among other things, they defined as SI any attempt to develop algorithms or distributed problem-solving devices inspired by the collective behavior of insect colonies and other animal societies. They also referred to the emergent collective intelligence of groups of simple agents as SI. In the same year, one of the authors published the Ant Colony Optimization (ACO) method, which became the best-known optimization method based

on the behavior of ants. It is based on the observation that ants can find the shortest path from the nest to a goal, avoiding obstacles [23].

In 2001, the inventors of the PSO described in the next chapter 3 published a book entitled *Swarm Intelligence* [19]. They agreed in principle with the definition of SI described by the Santa Fe Institute authors, but objected that they were not talking about agents. In their view, the global behavior of a swarm is largely determined by the local interactions of the individuals or particles in a swarm. In a system of agents, the behavior is rather a sum of the contributions of the individual agents.

A swarm can therefore be described as a large number of loosely structured particles interacting with each other. For example, swarms of birds, bees, and fish represent swarms, where the individual particles are birds, bees, or fish. However, traffic can also be referred to as a swarm of cars. Crowds are a swarm of people, an immune system is a swarm of cells and molecules. Here, the term swarm always suggests physical movements of the individual particles in a three-dimensional space. However, it is true that a swarm can also exist in a high-dimensional, cognitive space where collisions of particles are not a problem. [19]

Evidence that social interaction between particles, and thus direct application of SI, is capable of solving complex tasks is provided by the PSO optimization method described next.

Even dumb dots on a computer screen are able to figure out extremely hard problems, just by remembering their own experiences and being influenced by the experiences of others.

Book - Swarm Intelligence
by James Kennedy, Russel C. Eberhart and Yuhui Shi
published 2001

3 Particle Swarm Optimization

Nature often serves as a source of inspiration for people to develop new approaches. While researching topics in AI and creating a computer model to describe the social behavior of swarms, electrical engineer and biotechnologist R. Eberhart and social psychologist J. Kennedy published their first version of the PSO optimization method in 1995 in their paper *A New Optimizer Using Particle Swarm Theory* [24]. They use the method to train an Artificial Neural Networks (ANN), which was designed to estimate the state of charge of a battery pack for electric vehicles, and optimize the weights. Compared to conventional *backpropagation*, this took them only a fraction of the time and they recognized the power of the new method.

It uses two different social learning methods, which living creatures also use to improve themselves and their environment. Firstly, PSO taps into the ability to learn from personal experience, which is called *Individual Learning*. Secondly, living beings can learn from the experiences of others through knowledge transmission, which is referred to as *Cultural Transmission*. The method requires little computational power and memory due to its simple mathematical operations, and is one of the population-based metaheuristics that use techniques from SI. [19], [25]

3.1 Original PSO

In the following, the structure and the operation of the original method are described. Here D denotes the number of dimensions and thus the variables

to be optimized. A swarm consists of n particles, where each i-th particle has a position vector according to (10) in the decision space X and a velocity vector according to (11) at the time of iteration t.

$$\vec{x}_i(t) = (x_{i,1}(t), x_{i,2}(t), x_{i,d}(t)..., x_{i,D}(t)) \tag{10}$$

$$\vec{v}_i(t) = (v_{i,1}(t), v_{i,2}(t), v_{i,d}(t)..., v_D(t)) \tag{11}$$

3.1.1 Initialization

At the beginning of the optimization process, all particles in the multidimensional decision space are randomly distributed and the positions are evaluated. The particle with the best FV of all particles in the swarm is designated as *global best particle* and the associated position vector $\vec{gb}(t)$ is communicated to all particles in the swarm. In addition, the current position of each individual particle is stored as the *local best solution* $\vec{lb}_i(t)$ of each particle, respectively, since it is also the only solution point at that time. Later in the optimization, $\vec{lb}_i(t)$ and $\vec{gb}(t)$ are then updated only when better local or global solution points are found. Finally, an arbitrary initial velocity vector is generated at random for each particle, which is needed for the following movement equation.

3.1.2 Particle Movement

Each particle is moved once per iteration step by adding a new velocity vector $\vec{v}(t+1)$ to a new position point $\vec{x}(t+1)$ and thus to a new solution point. The movement equation to generate the new velocity vector is obtained for each particle i according to (12) and the new position vector subsequently according to (13).

$$\vec{v}_i(t+1) = w_1 \cdot \vec{v}_i(t) + w_2 \cdot r_1 \cdot (\vec{lb}_i(t) - \vec{x}_i(t)) + w_3 \cdot r_2 \cdot (\vec{gb}(t) - \vec{x}_i(t)) \tag{12}$$

$$\vec{x}_i(t+1) = \vec{x}_i(t) + \vec{v}_i(t+1) \tag{13}$$

The movement equation is composed of three different parts, where the factors w_1, w_2 and w_3 are weighting values in order to incorporate the individual terms to different extents. The variables r_1 and r_2 are uniformly distributed random

variables in the range of 0 to 1 and are determined anew for each dimension of each particle. The proportions can be described as follows:

- $\boldsymbol{w_1 \cdot \vec{v}_i(t)}$ represents the inertia of the movement equation. This hinders the trajectory of the particle from changing abruptly, and the particle maintains its previous direction of motion proportionally. It also prevents early convergence of all particles.
- $\boldsymbol{w_2 \cdot r_1 \cdot (\vec{lb}_i(t) - \vec{x}_i(t))}$ represents the memory or cognitive part of the equation in which each particle always moves toward its personal best position. The term reflects the individual learning of each particle.
- $\boldsymbol{w_3 \cdot r_2 \cdot (\vec{gb}(t) - \vec{x}_i(t))}$ is the cooperation or social part of the equation, whereby all particles move toward the global best position of the swarm at the current time step. This accounts for the influence of knowledge sharing among all particles and thus the ability to learn from the experience of other particles.

Figure 13 graphically represents the locomotion of a particle over the three different movement terms during the iteration time step $t + 1$ in a two-dimensional decision space.

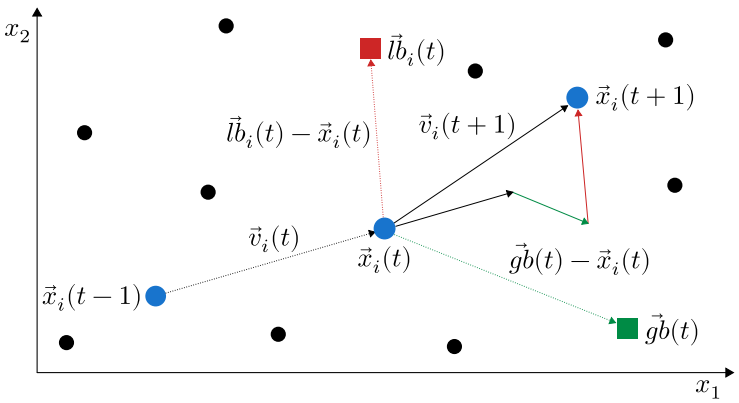

Figure 13: Composition of the PSO motion vector in two-dimensional space.

If the given number of iterations or a previously defined target value has not been reached, after (12) and (13) all particles are changed again with each iteration and moved to new positions. If the optimization process is successful, all particles will end up near the optimum of the optimization problem. Figure 14 exemplifies the positions of all particles after initialization (a) and at the end of the optimization method (b). The complete optimization process can be traced using the pseudocode of Algorithm 1.

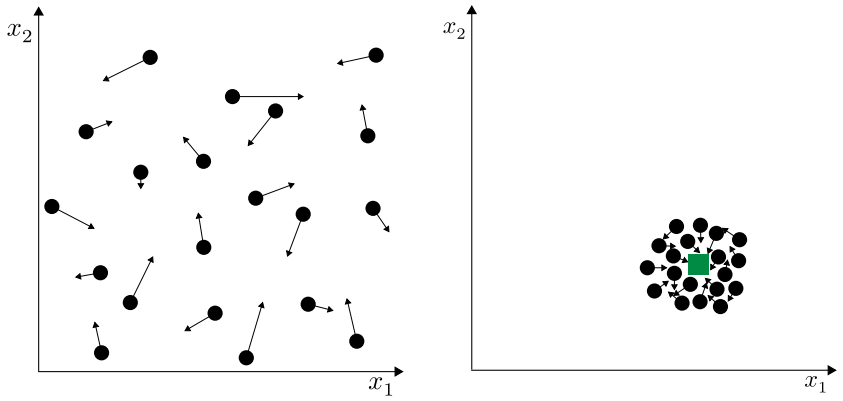

a) Start b) End

Figure 14: Distribution of particles in the decision space at the beginning (a) and end (b) of a PSO.

Algorithm 1 Sequence of the PSO optimization method with minimization

for $i = 1 : N$ **do**
    Initialize particle i
    $\vec{lb}_i(t) = f(\vec{x}_i(t))$
    if $\vec{lb}_i(t) < \vec{gb}(t)$ **then**
        $\vec{gb}(t) = \vec{lb}_i(t)$
    end if
end for
while Maximum iterations or minimum error criteria are not reached **do**
    $\vec{gb}(t+1) = \vec{gb}(t)$
    for $i = 1 : N$ **do**
        for $d = 1 : D$ **do**
            Calculate $\vec{v}_{i,d}(t+1)$
            Calculate $\vec{x}_{i,d}(t+1)$
        end for
        if $f(\vec{x}_i(t+1)) < f(\vec{lb}_i(t))$ **then**
            $\vec{lb}_i(t+1) = \vec{x}_i(t+1)$
            if $f(\vec{lb}_i(t+1)) < f(\vec{gb}(t+1))$ **then**
                $\vec{gb}(t+1) = \vec{lb}_i(t+1)$
            end if
        end if
    end for
end while

3.1.3 Influence of the Weighting Values

The weighting value w_1 is called the inertia factor and has the greatest influence on the course of the optimization. It can either have a constant value or be dynamically adjusted in the course of the simulation. The inertia factor can be used to adjust the global exploration within the search space, as larger values lead to higher particle velocities and lower directional changes. This increases the probability of leaving local optima and finding the global optimum. However, local fine tuning is more likely to be enabled by a smaller inertia factor.

The acceleration coefficients w_2 (*cognitive weighting factor*) and w_3 (*social weighting factor*) control the influence of the individual and global best position, respectively, on the calculation of the new velocity vector. They do not have to be equal, but this usually leads to a good balance of individual and social learning. Both factors often have to be empirically adapted to the problem to be optimized. Small values limit the speed of the particle and the influence of inertia increases. Choosing values that are too large can cause the particles to converge prematurely.

In the literature, the following combinations have given good results under a wide variety of conditions:

- $w_1 = 0.72984$, $w_2 = w_3 = 1.49445$ [19], [26]
- $w_1 = 0.72984$, $w_2 = w_3 = 2.0$ [19]
- $w_1 = [0.4; 0.9]$ linear decreasing, $w_1 = w_2 = 1.494$ [19], [27]
- $w_1 = [0.4; 0.9]$ linear decreasing, $w_1 = w_2 = 2.0$ [19], [28]

Problem-dependent parameterization is one of the major drawbacks of the original PSO method. It is costly and has to be finely tuned to the problem to be optimized. Also, a linear decrease of the inertia factor only leads to good results with an appropriate choice of iterations. Otherwise, the influence of the inertia factor may be eliminated too early and the particles get stuck at local optima. The Evolutionary Particle Swarm Optimization (EPSO) method presented in the following section introduces new techniques to overcome these drawbacks.

3.2 Evolutionary PSO

EPSO is a hybrid optimization method that combines the concept of PSO with techniques from EA and was first proposed by V. Miranda and N. Fonseca presented in 2002 [29]. EPSO, like PSO, resorts to a particle swarm for

exploring the search space. The basic techniques of independent learning and social exchange among individual particles are also retained. Additionally, an evolution-based method is used, which causes the weighting vectors of the movement equation to evolve and adapt independently. The basic scheme of EPSO is as follows:

- **Replication:** Each particle is replicated or cloned r-times before moving.
- **Mutation:** All weighting factors of the cloned particles are mutated.
- **Reproduction:** Each particle generates a new offspring using the particle movement equation.
- **Evaluation:** The FV of all offsprings is calculated.
- **Selection:** By a selection process, only the best offspring of each ancestor survives.

The movement vector of the EPSO method thus results modified for each particle i according to (14) and is shown graphically in Figure 13 with a replication of $r = 1$ including mutation. The subsequent calculation of the new particle position remains identical according to (13). In contrast to the movement equation of the original PSO method, mutated and particle-related weighting vectors ($\vec{w}_{1i}^*$, $\vec{w}_{2i}^*$ and $\vec{w}_{3i}^*$) are applied in the EPSO method. These ensure that even with the same particle position $\vec{x}_i(t)$, local best position $\vec{lb}_i(t)$, and global best position $\vec{gb}^*(t)$, the recalculated movement vector $\vec{v}_i(t+1)$ takes a different position for all replicated particles. The factors are mutated using either a normally distributed or log-normally distributed random variable with mean zero and variance one according to (15) or (16). [29]–[31]

$$\begin{aligned}\vec{v}_i(t+1) = \vec{w}_{1i}^*(t) \cdot \vec{v}_i(t) + \vec{w}_{2i}^*(t) \cdot (\vec{lb}_i(t) - \vec{x}_i(t)) \\ + \vec{w}_{3i}^*(t) \cdot (\vec{gb}^*(t) - \vec{x}_i(t)) \cdot \vec{P}_i\end{aligned} \tag{14}$$

$$\vec{w}_i^*(t) = \vec{w}_i^*(t-1) + \tau \cdot N(0,1) \tag{15}$$

$$\vec{w}_i^*(t) = \vec{w}_i^*(t-1) \cdot [LogN(0,1)]^{\tau} \tag{16}$$

Stochastic mutation of the weighting vectors results in a different movement vector for each replicated particle, so that all particles end up in different positions per iteration. The subsequent selection ensures on the one hand that only the best particle survives and that the swarm develops optimally, and on the other hand that the weighting vectors adapt themselves to the

conditions of the optimization problem. Since the weighting vectors are mutated again with each iteration, they may evolve in one direction or towards a certain value in the long run. For example, over a period of time, if larger and larger values in the weighting vectors lead to better solutions, the values will increase and thus support the optimization process. The same is true for consistently smaller values. Especially at the end of the optimization, when the amounts of the memory and cooperation terms are decreasing due to the convergence of the particles, a constant high inertia value can ensure that the particles do not converge too early and thus the optimization progresses. Conversely, it is also possible that for the final fine tuning, the velocity is kept constant in the lower range in order to obtain an exact solution. This self-adaptation of the weighting vectors is a major advantage of EPSO over the original PSO method. The learning parameter τ, which can be set externally, can be used to adjust the amplitude of the respective mutation. Large values lead to a stronger change of the weighting vectors while smaller values lead to a higher probability of obtaining similar values as before.

In addition to the weighting vectors, the position of the global optimum $\vec{gb}^{\,*}(t)$ is also changed. The particles are supposed to move towards the position of the best particle at the iteration time step t, but since this point has already been found, the area around it is also supposed to be explored by slightly adjusting the position. This is to increase the probability of finding the global optimum. The modified position $\vec{gb}^{\,*}(t)$ is calculated using (17) or (18). The latter introduces the *noise vector* $\vec{w}_{4i}^{*}(t)$, which is also mutated via (16). Therefore, a more targeted change is possible via (18), which is why this method is used.

$$\vec{gb}^{\,*}(t) = \vec{gb}^{\,*}(t-1) + \tau' \cdot N(0,1) \tag{17}$$

$$\vec{gb}^{\,*}(t) = \vec{gb}^{\,*}(t-1) + \vec{w}_{4i}^{*}(t) \cdot N(0,1) \tag{18}$$

The communication vector $\vec{P}_i$, which is multiplied by the cooperation term $(\vec{gb}^{\,*}(t) - \vec{x}_i(t))$, was not introduced in EPSO until the publication of the subsequent Differential Evolutionary Particle Swarm Optimization (DEEPSO) method. It creates a stochastic communication topology between individual particles in the swarm. Each dimension of $\vec{P}$ is set to value one with the communication probability p and zero with $(1-p)$. This means that a particle in that dimension will move toward the best position only with the probability p. With $p = 1$ the best position is always used in all dimensions and with $p = 0$ in no dimension at all. Therefore, the communication vector can be used to significantly influence how social exchanges within particles in the swarm are

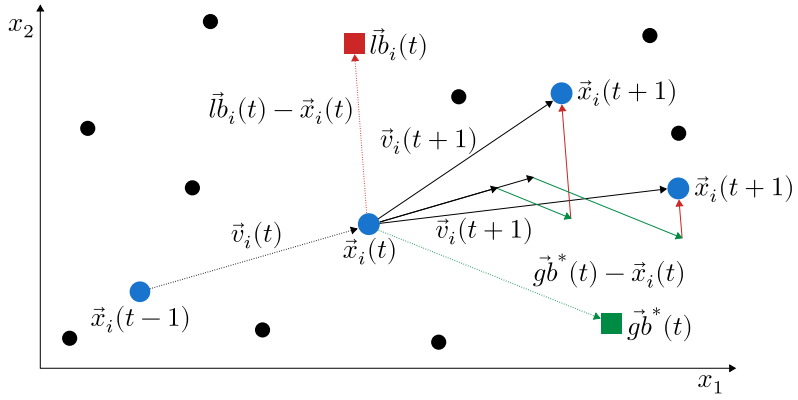

Figure 15: Composition of the EPSO motion vector in two-dimensional space.

shaped and how quickly they converge. If the global optimum is easy to find, a high value for the communication probability lends itself to minimizing the runtime of the algorithm. For complex optimization problems, smaller values are often appropriate to prevent early convergence of the particles and to better explore the search space.

In the following, another PSO variant is presented, which is similar to the EPSO method, but still makes use of techniques from DE.

3.3 Differential Evolutionary PSO

DEEPSO is a hybrid optimization method that combines the concepts of EPSO and DE and was first presented in 2013 as an extension of EPSO in [31]. DE is based on the principle of generating new solution points via a weighted difference from other solution points. This idea is taken up by DEEPSO, which integrates the method into the particle movement equation. Thus, the memory term is modified such that each particle moves towards the position of a third particle $\vec{x}_r$ to be determined, rather than towards its best position found so far. The memory term is therefore modified to another cooperation term. The movement equation results from (19) for the task of minimization.

$$\vec{v}_i(t+1) = \begin{cases} \vec{w}^*_{1i}(t) \cdot \vec{v}_i(t) & \\ +\vec{w}^*_{2i}(t) \cdot (\vec{x}_r(t) - \vec{x}_i(t)) & f(\vec{x}_r(t)) \leq f(\vec{x}_i(t)) \\ +\vec{w}^*_{3i}(t) \cdot (\vec{gb}^*(t) - \vec{x}_i(t)) \cdot \vec{P}_i & \\ & \\ \vec{w}^*_{1i}(t) \cdot \vec{v}_i(t) & \\ +\vec{w}^*_{2i}(t) \cdot (\vec{x}_i(t) - \vec{x}_r(t)) & f(\vec{x}_i(t)) < f(\vec{x}_r(t)) \\ +\vec{w}^*_{3i}(t) \cdot (\vec{gb}^*(t) - \vec{x}_i(t)) \cdot \vec{P}_i & \end{cases} \tag{19}$$

The selection of the particle x_r has a great influence on the movement equation and thus on the complete course of the optimization method. Here the authors from [31] presented a total of four variants.

1. **DEEPSO-Sg:** One particle is randomly selected from the set of all particles in the swarm of the same generation Sg.
2. **DEEPSO-Sg-rnd:** The same principle applies as in DEEPSO-Sg, whereby a randomly new particle is determined for each dimension. Thus, at the end, $\vec{x}_r$ represents an imaginary particle composed of different positions.
3. **DEEPSO-Pb:** One particle is randomly selected from the set of historically best positions Pb found so far during the optimization process. The size of the set must be determined in advance.
4. **DEEPSO-Pb-rnd:** The same principle applies as for DEEPSO-Pb, with a randomly new particle being determined for each dimension.

Which of the variants is preferable cannot be determined arbitrarily and depends on the problem to be optimized. In [31], DEEPSO-Pb-rnd is considered the most successful variant. In [32], on the other hand, it performs particularly poorly and the DEEPSO-Sg-rnd variant shows superiority both in the test functions used and in the real power applications presented.

In the following, the binary version of the PSO algorithm published by the PSO inventors is presented, which is preferable especially for binary optimization problems.

3.4 Binary PSO

In 1997, two years after the publication of the original PSO method, R. Eberhart and J. Kennedy published a discrete binary version of their optimization

method [33]. They realized that the original PSO method is only partially suitable for solving discrete problems, which primarily involve a large number of decisions such as *yes* or *no*, *true* or *false*, resp. *with* or *without* have to be made.

3.4.1 Particle Movement

In discrete problems, where the valid search space S is restricted to a binary space $\mathbb{B} = \{0, 1\}$, the individual particles cannot fly over optimal points and search around them as they do in discrete space. Rather, the particles are located in the corners of a hypercube and can only move their position by flipping one or more bits in order to reach closer or more distant corners of the cube. The velocity of each particle is thus given by the number of bits flipped per iteration. If no bit is changed, the velocity is zero. If all bits are flipped, the particle velocity reaches the theoretical maximum. The Hamming distance is used for the calculation. This is a measure of the randomness of strings and calculates the number of different places for bits with the same length, as is the case with the particle position. This allows the basic form of the velocity equation of PSO to be preserved and results in (20) for the BPSO method, where $\vec{x}_i(t)$, $\vec{lb}_i(t)$ and $\vec{gb}(t)$ represent integers in 0,1. The difference then lies in the interpretation of the calculated velocity. In the BPSO method, this does not represent a measure of the speed of a particle in a particular direction, but describes a probability with which the particle will change its bit position. If the velocity vector is positive and large, the probability that the bit will take a value of one increases. If the velocity vector is negative, the probability that the bit will change to a zero increases. If the velocity is zero, then there is a 50 % probability that the bit will change to a zero or one. To determine the probability, a sigmoid function is used as a transformation function according to (21) and is shown in Figure 16. The position calculation for BPSO is then obtained using (22), where $rand()$ is a random number of a uniform distribution in the interval [0.0, 1.0] for each dimension. [33]

$$\begin{aligned}\vec{v}_i(t+1) &= w_1 \cdot \vec{v}_i(t) + w_2 \cdot r_1 \cdot (\vec{lb}_i(t) - \vec{x}_i(t)) + w_3 \cdot r_2 \cdot (\vec{gb}(t) - \vec{x}_i(t)) \\ &= \begin{cases} \vec{v}_{max} & \vec{v}_i(t+1) > \vec{v}_{max} \\ -\vec{v}_{max} & \vec{v}_i(t+1) < -\vec{v}_{max} \end{cases}\end{aligned} \tag{20}$$

$$S(\vec{v}_i(t+1)) = \frac{1}{1 + e^{-\vec{v}_i(t+1)}} \tag{21}$$

$$\vec{x}_i(t+1) = \begin{cases} 1 & S(\vec{v}_i(t+1)) > rand() \\ 0 & \text{otherwise} \end{cases} \tag{22}$$

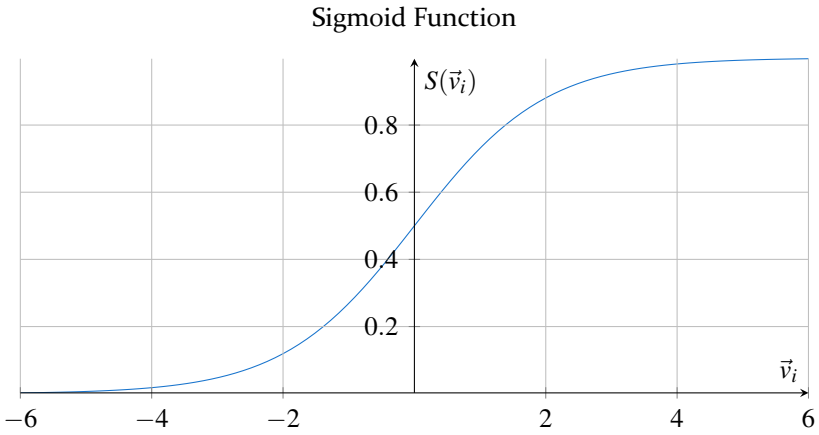

Figure 16: Representation of the sigmoid function according to (21) for the transformation of the velocity vector $\vec{v}_{i,d}$ into the probability range [0,1].

A decisive influence on the performance of BPSO is the maximum allowed speed $\vec{v}_{max}$. This ensures that the velocity cannot achieve an amount that is too large and that after the transformation by the sigmoid function the probability of a bit change does not come too close to 0 % or 100 %, respectively. Thus, there always remains a certain degree of probability that a bit will be flipped again. In practice, a value of ±4 [19] or ±6 [33], [34] has proven to be effective, which means that a minimum residual probability of 1.8 % or 0.25 %, respectively, is preserved. As with PSO, the choice of weighting vectors w_1, w_2, and w_3 plays an important role in BPSO. In the original 1997 version, w_1 was set to the value of one. The factors w_2 and w_3 for the memory as well as cooperation term were set to an equal value. According to [19], it holds for PSO as well as for BPSO that $w_2 = w_3 = 2.0$ leads to good results.

3.4.2 Optimizing Real Numbers

However, the BPSO method is not only suitable for discrete binary optimization problems. Continuous problems with decimal numbers can also be optimized by converting the latter to the standard binary system.

3.4.2.1 Division Method

Integers can be converted simply with the division method as shown in Sample 1 for the conversion of the decimal number 34. The value is divided by two and the remainder is noted until the equivalent binary number is obtained. The back calculation is possible according to Sample 23.

Sample 1

$$
\begin{aligned}
34/2 &= 17 && -> \textit{ rest } 0\\
17/2 &= 8 && -> \textit{ rest } 1\\
8/2 &= 4 && -> \textit{ rest } 0\\
4/2 &= 2 && -> \textit{ rest } 0\\
2/2 &= 1 && -> \textit{ rest } 0\\
1/2 &= 0 && -> \textit{ rest } 1\\
34_{10} &= 100010_2
\end{aligned}
$$

$$1 \cdot 2^5 + 0 \cdot 2^4 + 0 \cdot 2^3 + 0 \cdot 2^2 + 1 \cdot 2^1 + 0 \cdot 2^0 = 34_{10} \tag{23}$$

The conversion of decimal numbers is more problematic. Up to the decimal point, the division method can be used. Subsequently, the multiplication method as shown in Sample 2 for the conversion of the number 34.6875 is used. The calculation is finished as soon as the result reaches one. However, this is a major disadvantage of the method, since even the conversion of simple decimal numbers such as 0.1 can never end in a one and can thus become excessively long depending on the precision.

Sample 2

$$
\begin{aligned}
34.6875_{10} &= 34_{10} + 0.6875_{10}\\
0.6875 \cdot 2 &= 1.375 && -> \textit{ take } 1\\
0.375 \cdot 2 &= 0.75 && -> \textit{ take } 0\\
0.75 \cdot 2 &= 1.5 && -> \textit{ take } 1\\
0.5 \cdot 2 &= 1 && -> \textit{ take } 1\\
34.6875_{10} &= 100010.1011_2
\end{aligned}
$$

3.4.2.2 IEEE 754 Standard

A solution is provided by the *IEEE 754 standard* (*IEEE Standard for Floating-Point Arithmetic*) [35], which specifies exact methods for operations, conversions, and roundings. The standard defines fixed lengths and divides a bit sequence into sign s, exponent e, and significand m sections. A decimal number is then described by the expression $s \cdot m \cdot 2^e$ in binary. Advantages lie in the wide spreading, the uniform system and directly usable libraries for most programming languages. Disadvantages are however on the one hand the sign bit, the general structure and the minimum length of 32 bit, which is needed even for simple accuracy. When using a sign bit, a change from 0 to 1 would cause the decimal number to immediately change sign from + to -. Thus, a minimal change in the sign bit in the position bit of a particle would result in large changes in the decimal number under some circumstances. The use of a sign bit should therefore be avoided. Furthermore, the length of the bit sequence used has an influence on the duration of an optimization process. The length of the bit position should therefore always be only as long as necessary to achieve the required accuracy. The structure also poses a problem because the Hamming distance does not increase evenly with the decimal numbers. This is also true for the standard binary system. For example, the number 7_{10} corresponds to 0111_2 in the binary system and to 0100001111+21·0 according to the IEEE 754 single precision standard. The 8_{10} is a 1000_2 in the binary system and a 0100000010000+21·0 according to IEEE 754. Numerically increasing the 7_{10} by one to 8_{10} results in a *Hamming cliff* in both binary representations. It gives a Hamming distance of four, which is thus significantly larger than the numerical change in the decimal number. Such a *cliff* is difficult to overcome for optimization methods, since many bits must be suitably changed simultaneously.

3.4.2.3 Gray Code

A solution to the problem, which is also used in this work, is the *Reflected Gray code* also called *Reflected Binary Code* or only *Gray Code*. This is a special binary and continuous code, where two consecutive binary numbers always differ in only one bit. The name goes back to the physicist, Frank Gray, who published the code in his first U.S. patent in 1953. With (24) a standard binary number can be converted into Gray code. The length of the binary number and the whole left bit remain unchanged. Starting with the second bit from the left, the corresponding bit G_j results at the j-th position of the Gray code. B_j is the j-th bit at the position of the standard binary number and B_{j-1} is the previous bit. The XOR function returns a zero if the adjacent bits are the same

or a one if they differ. Table 1 illustrates the difference between the standard binary system and the Gray code. [19], [36]

$$G_i = XOR(B_j, Bj - 1) \tag{24}$$

Table 1: Comparison of decimal numbers in standard binary and Gray Code. Between the numbers 7 and 8 a hamming-cliff occurs in the binary code.

Decimal	Binary Code	Gray Code
0	0000	0000
1	0001	0001
2	0010	0011
3	0011	0010
4	0100	0110
5	0101	0111
6	0110	0101
7	**0111**	**0100**
8	**1000**	**1100**
9	1001	1101
10	1010	1111
11	1011	1110
12	1100	1010
13	1101	1011
14	1110	1001
15	1111	1000

3.4.2.4 Procedure in this Work

To avoid the problem of the precision of decimal numbers in the binary system, all binary optimization methods in this work calculate exclusively with integers. For this purpose, the necessary precision of decimal places must be defined for each dimension before starting the optimization process. Afterwards each decimal number can be converted into an integer by multiplication of the necessary power of ten and then finally into the binary system and into the Gray code. This step must be recalculated before returning the variable to

the fitness function. Similar principle is also used to avoid the necessity of a sign bit. Thus, each admissible search space can be dynamically shifted so that the lowest limit is always at zero. This bypasses negative numbers within the optimization steps. At the end, the numbers only have to be calculated back into the actual search space. Via (25), the necessary bit length of each dimension can be calculated for each variable x depending on the allowed lower limit $x_{\min}$ and the upper limit $x_{\max}$. rf is the *resolution factor* of the dimension and discretizes the search space into rf long steps. $log_2()$ is the logarithm to base 2 and the bracket expression $\lfloor\rfloor$ stands for the floor function $floor()$. This returns the largest integer less than or equal to the number inside the parenthesis. For the optimization of a variable x an accuracy of three decimal places shall be valid as an example. This results in an rf of 0.001. The valid search space is defined from $x_{\min} = -100$ to $x_{max} = 100$. The necessary bit length n_b then consist of only 18 bit.

$$n_b = \lfloor log_2(\frac{x_{\max} - x_{\min}}{rf})\rfloor + 1 \tag{25}$$

Finally, the Sample 3 shows the various conversion steps from decimal numbers of individual dimensions through the defined search space to the resulting and composite binary position vector in Gray code of a particle.

Sample 3 *Let* $f(x) = x_1^2 + x_2^2 + x_3^2$ *with* $x_{\min} = -5.12$, $x_{\max} = 5.12$ *resulting in* $rf = 0.01$ *and* $n_{i,b} = 11$.

Steps	**Variable**	x_1	x_2	x_3
1	Decimal value	-5.12	0.0	5.12
2	Shifted decimal	0	512	1024
3	Standard binary	00000000000	01000000000	10000000000
4	Gray Code	00000000000	01100000000	11000000000
Final	Position Bit	000000000000110000000011000000000		

The tools and technologies we have developed are really the first few drops of water in the vast ocean of what AI can do.

Fei-Fei Li
American computer scientist
* 1976

4 Advanced PSO-Variants & Techniques

In this chapter, advanced and adapted PSO optimization methods are presented. These rely on the basic techniques of PSO, EPSO, DEEPSO and BPSO, but combine them in a new way to solve optimization problems faster, more accurately and more applicable.

4.1 Differential Evolutionary PSO-Sg(LB)-rnd

The DEEPSO-Sg(LB)-rnd method is another DEEPSO variant. The movement equation according to (19) remains unchanged. The third particle $\vec{x}_r$ to be selected is also chosen randomly from the current set of all particles in the swarm. Subsequently, however, the best position $\vec{lb}_i(t)$ found so far for the selected particle is used. This principle is applied anew for each dimension of the movement equation, so that $\vec{x}_r$ is an imaginary particle consisting of all best local positions of all particles found so far. The method is thus similar to the EPSO algorithm, but differs in that a particle moves not only toward its own best position so far, but toward the best positions so far of all particles in the swarm. This type of application thus represents a novel mixture of memory and cooperation terms. The communication part comes from the fact that the information about the local best positions is made available to the whole swarm. The memory part results from the fact that the local best positions have to be stored and remembered. Thus, there is stronger communication within the swarm than with EPSO, which should lead to better exploitation while searching. Disadvantages could be an earlier convergence

of particles and thus getting stuck at local optima. Compared to the classical DEEPSO-Sg-rnd variant, the performance should be significantly improved since the particles no longer move towards an imaginary position consisting of the current positions of all particles in the swarm. The current positions do not represent particularly good positions to move towards. Furthermore, in classical DEEPSO-Sg-rnd the movement of the particles towards each other is too focused, which usually results in early convergence.

Another method, which also makes use of the best local positions of all particles, is the following one.

4.2 Evolutionary PSO with Differential Evolution

The Evolutionary PSO with Differential Evolution (EPSO_{DE}) method is a combination of EPSO and DEEPSO, but fundamentally changes the nature of the social exchange of particles in the swarm and thus the design of the cooperation term. In all PSO methods introduced so far, knowledge sharing in the swarm takes place via the communication of the best found position $\vec{gb}(t)$ of a particle. All particles move proportionally toward this position. However, this approach is not necessarily true for swarm animals. In fact, depending on the size of the swarm, it seems impossible for all individuals to learn simultaneously from the best individual in the swarm, regardless of their current position. Rather, knowledge transfer within the swarm occurs across all individuals. If one fish from a large-numbered shoal finds a feeding site, it will not be able to communicate this information immediately to all fish. The information is first picked up by the neighboring fish, which then react to it and subsequently pass the information on as well. This is also true for flocks of birds, colonies of bees or ants. Therefore, the cooperation term in EPSO_{DE} is modified so that not all particles move towards the global best position of the swarm, but towards the local best positions of all particles. This principle has already been presented in the DEEPSO-Sg(LB)-rnd method, but is now used in EPSO_{DE} at the position of the cooperation term. Thus, the particles move with probability p toward an imaginary particle $\vec{lb}_{rnd}(t)$, which is randomly composed of the components of all local best positions. The movement equation is obtained for each particle according to (26). The method was first published in [P37].

$$\begin{aligned}\vec{v}_i(t+1) = \vec{w}^*_{1i}(t) \cdot \vec{v}_i(t) + \vec{w}^*_{2i}(t) \cdot (\vec{lb}_i(t) - \vec{x}_i(t)) \\ + \vec{w}^*_{3i}(t) \cdot (\vec{lb}_{rnd,i}(t) - \vec{x}_i(t)) \cdot \vec{P}_i\end{aligned} \tag{26}$$

A variation of EPSO_{DE} is the $\text{EPSO}_{\text{DE}}2$ method. This uses the cooperation probability p in a new way, so that it becomes possible to use the global best position $\vec{gb}(t)$ and the imaginary position $\vec{lb}_{rnd}(t)$ composed of the local best positions simultaneously. Depending on the ratio of p to a uniformly distributed random number $rnd()$ in [0,1], which is recalculated for each dimension, the calculation of the velocity vector is adjusted. If p is greater than or equal to $rnd()$, the movement equation remains identical to EPSO_{DE}. However, if p is smaller the cooperation term does not simply become zero, but according to (27) the global best position of the swarm $\vec{gb}(t)$ is used. This creates a new method of communication of the particles in the swarm and thus a new stochastic communication topology that takes advantage of the strengths of both methods. The particles can both learn from the best particle directly, but also use the slower knowledge transmission via the local best positions. Setting p to zero results in the classical EPSO method. If p is one, then only the EPSO_{DE} method is used. For all values in between, the result is a hybrid method that never forgoes the influence of a cooperation term to enable the best possible performance.

$$\vec{v}_i(t+1) = \begin{cases} \vec{w}^*_{1i}(t) \cdot \vec{v}_i(t) \\ +\vec{w}^*_{2i}(t) \cdot (\vec{lb}_i(t) - \vec{x}_i(t)) & p \geq rnd() \\ +\vec{w}^*_{3i}(t) \cdot (\vec{lb}_{rnd,i}(t) - \vec{x}_i(t)) \\ \\ \vec{w}^*_{1i}(t) \cdot \vec{v}_i(t) \\ +\vec{w}^*_{2i}(t) \cdot (\vec{lb}_i(t) - \vec{x}_i(t)) & p < rnd() \\ +\vec{w}^*_{3i}(t) \cdot (\vec{gb}(t) - \vec{x}_i(t)) \end{cases} \tag{27}$$

In the following, the way of using the differential part of EPSO_{DE} is transferred to the BPSO method.

4.3 Binary PSO with Differential Evolution

In the Binary PSO with Differential Evolution (BPSO_{DE}) method, the classical BPSO algorithm is extended by a differential part in the movement equation. Here, the basic principle of EPSO_{DE} is taken up, but the differential method is integrated into the binary plane. While in the non-binary methods the difference of two decimal numbers of one dimension is used in the velocity equation, in the binary methods the difference of two binary places is used, where each decimal number can be represented by n_b binary numbers. The same principle applies to the composition of the imaginary particle $\vec{lb}_{rnd}(t)$.

For each binary digit of each dimension, a new particle is randomly chosen. This creates more mixing in the generation of the random vector $\vec{lb}_{rnd}(t)$, resulting in a more uniform distribution of information within the swarm at each iteration t. Only for the case $n_b = 1$ would there be no change in the composition of $\vec{lb}_{rnd}(t)$ compared to EPSO_{DE}. The movement equation of BPSO_{DE} is given by (28), with the same velocity constraint as for (20). In addition, there is also the cooperation factor P to control the communication topology.

$$\begin{aligned}\vec{v}_i(t+1) = w_1 \cdot \vec{v}_i(t) + w_2 \cdot r_1 \cdot (\vec{lb}_i(t) - \vec{x}_i(t)) \\ + w_3 \cdot r_2 \cdot (\vec{lb}_{rnd,i}(t) - \vec{x}_i(t)) \cdot \vec{P}_i\end{aligned} \tag{28}$$

Based on the $\text{EPSO}_{\text{DE}}2$ method, the $\text{BPSO}_{\text{DE}}2$ method is introduced. This takes advantage of the possibility of knowledge transfer in the swarm about the global best as well as the composite imaginary particles alike. The movement equation is given by (29) while keeping the velocity constraint.

$$\vec{v}_i(t+1) = \begin{cases} w_1 \cdot \vec{v}_i(t) & \\ +w_2 \cdot r_1 \cdot (\vec{lb}_i(t) - \vec{x}_i(t)) & p \geq rnd() \\ +w_3 \cdot r_2 \cdot (\vec{lb}_{rnd,i}(t) - \vec{x}_i(t)) & \\ & \\ w_1 \cdot \vec{v}_i(t) & \\ +w_2 \cdot r_1 \cdot (\vec{lb}_i(t) - \vec{x}_i(t)) & p < rnd() \\ +w_3 \cdot r_2 \cdot (\vec{gb}(t) - \vec{x}_i(t)) & \end{cases} \tag{29}$$

Many extensions of PSO resort to mutation and selection as a strong tool to make the methods or the weighting vectors adapt themselves. However, this always carries the risk that wrong conclusions are drawn during optimization and that the vectors evolve in a bad direction in the long run. In addition, suitable bounds for the mutating weighting vectors must always be defined. This topic is explained in detail in section 4.5. Therefore, the adjustment effort remains high even when mutation is used. In the BPSO_{DE} method, the evolutionary part is intentionally omitted. In exchange, the method can use twice as many iterations with the same number of FES, since no particle clones have to be evaluated. In contrast, there is the following EPSO_{DE} method, which reintroduces the evolutionary part and is thus a complete fusion of EPSO_{DE} and BPSO.

4.4 Evolutionary Binary PSO with Differential Evolution

As the last new hybrid PSO version, Evolutionary Binary PSO with Differential Evolution ($EBPSO_{DE}$) results in a fusion of all previously introduced distinctive optimization components. $EBPSO_{DE}$ builds on the basic procedure of $BPSO_{DE}$ and adds an evolutionary part to it, as known from EPSO, $EPSO_{DE}$ and DEEPSO. The movement equation is given by (30) and for the variant $EBPSO_{DE}2$ by (31).

$$\begin{aligned}\vec{v}_i(t+1) = \vec{w}^*_{1i}(t) \cdot \vec{v}_i(t) + \vec{w}^*_{2i}(t) \cdot (\vec{lb}_i(t) - \vec{x}_i(t)) \\ + \vec{w}^*_{3i}(t) \cdot (\vec{lb}_{rnd,i}(t) - \vec{x}_i(t)) \cdot \vec{P}_i\end{aligned} \tag{30}$$

$$\vec{v}_i(t+1) = \begin{cases} \vec{w}^*_{1i}(t) \cdot \vec{v}_i(t) & \\ +\vec{w}^*_{2i}(t) \cdot (\vec{lb}_i(t) - \vec{x}_i(t)) & p \geq rnd() \\ +\vec{w}^*_{3i}(t) \cdot (\vec{lb}_{rnd,i}(t) - \vec{x}_i(t)) & \\ & \\ \vec{w}^*_{1i}(t) \cdot \vec{v}_i(t) & \\ +\vec{w}^*_{2i}(t) \cdot (\vec{lb}_i(t) - \vec{x}_i(t)) & p < rnd() \\ +\vec{w}^*_{3i}(t) \cdot (\vec{gb}(t) - \vec{x}_i(t)) & \end{cases} \tag{31}$$

4.5 Use of the Weighting Vectors

A crucial influence on the movement equation of the evolutionary PSO variants and thus on the particle behavior and the overall performance of the optimization are the mutating weighting vectors $\vec{w}^*_1$ - $\vec{w}^*_4$. These can be held constant, be particle dependent, but also be mutated anew in each dimension or even for each bit, providing new values. The goal is for them to adapt themselves to the problem to be optimized during optimization, thus bypassing the need for time-consuming parameterization in advance. However, it is necessary to specify how and when the mutation should take place before starting the optimization. In [29], the authors refer to the weighting vectors mentioned here as particle dependent weighting factors or strategic parameters. This suggests that the factors are the same for all dimensions. In [31], the authors refer to these as simple parameters or weights and define them as diagonal matrices.

Since in the further course of the work the optimization methods shall be used to optimally adjust different setting values in the field of power system protection coordination, this means that the individual dimensions of the

particles represent different parameters with different sets of values with different sized search spaces. Therefore, the notion of particle dependent weighting vector is deliberately used in this work, so that each particle and each dimension has its own value to be mutated. Thus, it is possible that the corresponding value $\vec{w}^*_{1i,1}$ of x_1 variable is already decreasing, while the value $\vec{w}^*_{1i,2}$ of x_2 still remains at a high level to reach the optimal point faster. The values of the weighting vectors $\vec{w}^*_{1i}$ and $\vec{w}^*_{2i}$ are therefore mutated individually for each dimension for the calculation of the movement equation.

This also applies to all generated particle clones, so that no value is kept constant. This provides a higher degree of evolvability and adaptation, which helps to ensure that fewer particles get stuck at local optima. Thus, the weighting vectors of two particles at the same location can mutate differently. For example, one value could increase and the other decrease. It would also be possible for one value to increase slightly and the other to increase greatly. Depending on which particle leads to a better fitness value after execution of the movement, the mutated factors are maintained. Own analyses have shown that keeping the present values of the weighting vectors of the non-cloned particles is disadvantageous.

The weighting vectors $\vec{w}^*_3$ and $\vec{w}^*_4$ of the cooperation term are treated differently. Since a particle usually moves toward another particle only with the cooperation probability p in each dimension depending on the movement equation, many values of the weighting vectors do not apply when $\vec{P}_i = 0$. In the subsequent evaluation and selection, only the best particle ultimately survives, but it cannot be determined holistically whether the individually mutated values of the weighting vectors led to good or worse positions if they were not used at all. This would result in the values of $\vec{w}^*_3$ and $\vec{w}^*_4$ evolving in a partially random manner, which would hinder the progress of the optimization process. Therefore, in the following, both $\vec{w}^*_3$ and $\vec{w}^*_4$ use the same particle dependent value in all dimensions, which is thus mutated only once per iteration and particle.

The EBPSO_{DE} method would allow even more individual use of weighting values on bit level. Here, each bit could receive its own mutable value. However, a similar problem as with the cooperation term arises. Only a composite bit string of several bits represents a corresponding decimal number, which then leads to better or worse results in the evaluation. A conclusion on the differently mutated values of the individual bits is not possible. Therefore, the individual values cannot develop reasonably and would hinder the optimization process. Subsequently, no change is made to the EBPSO_{DE} method either.

The mutation of the weight values of $\vec{w}_1^*$, $\vec{w}_2^*$ and $\vec{w}_3^*$ takes place exclusively according to formula (16) in the further course of the work, which has some advantages. In this multiplicative version, the probability of a value being multiplied by a number greater than one is the same as the probability of being multiplied by a number less than one. The change is more uniform over the entire range of values and has a more adaptive character. In addition, the unfavorable case of a weighting value taking on negative values or a value of zero cannot occur. The additive form of (15) has the disadvantage that the weighting values can evolve to be worse. If a weighting value is at a value of 1.0 and now a value of 0.2 is added via mutation, then this has less strong effects than if the value was previously at 0.2. In the latter case, the value is directly doubled, even if the difference in amount is the same. For the mutation of $\vec{w}_4^*$, (18) is used, which allows more flexibility than (17).

To ensure that all values of all weighting vectors do not become too large or small, whereby they would either effectively eliminate or over-influence every term in the movement equation, fixed limits are used for all values. Eliminating the inertial part would lead to early convergence of the particle with others. Subsequently, the search space cannot be searched as well. Too much weighting of inertia causes a particle to strongly adhere to its movement direction and the velocity to remain very high. This means that optimal points cannot be examined more closely. The same happens if the cognitive and social parts become too small. Too much weighting of the latter two parts can result in both early convergence and random wandering through the search space. Unfavorable weighting values may occur if the normal distribution from (16) and (18) yields values greater than or less than one too many times in succession. Moreover, while the weighting values are self-adjusting, the evolution is based on a simple selection process per iteration. Therefore, rapid improvements in particular have a large impact on the evolution of the values. The long-term development and finding the global optimum is not the main focus. For this reason, all weighting values are kept within an optimal range of values using limits to be defined.

It is a capital mistake to theorize before one has data. Insensibly one begins to twist facts to suit theories, instead of theories to suit facts.

Sir Arthur Ignatius Conan Doyle
British writer and physician
* 1859 + 1930

5 Proof of Performance & Comparison

The PSO variants presented in the last chapter are applied in this chapter and their suitability regarding the optimization of problems is proven. Furthermore, it is determined which method achieves particularly good results for which functions and difficulty levels and thus achieves a higher performance than other methods on average. The goal is to determine the best method for coordinating the power system protection, which will be covered in chapter 11 because, on the one hand, the global optimum will be an unknown value and, on the other hand, an evaluation of the fitness function will cost considerably more computational effort. In addition, depending on the power system to be optimized, the fitness function used and all the framework conditions that depend on it, a new fitness landscape always results. Therefore, the overcoming of different challenges and constraints shall be investigated for all methods.

Since, according to the NFL theorem, no universal optimization algorithm can exist, the problem class to be solved must be defined in advance, for which the various PSO variants are designed and thus specified to ensure an efficient search and transferability to power system protection coordination. Understanding, formulating, and properly aligning an algorithm is probably the most important aspect of developing metaheuristics. In the further course of this work, the optimization of power system protection refers to single-objective, nonconvex, multidimensional problems with restricted search space and, depending on the variables used, pure real parameter or mixed parameter problems. For these types of problems, numerous test functions exist in the

literature that have a known global minimum and can be used to evaluate performance. They are often named after the respective inventors and differ in their properties in order to be able to examine the search and convergence behavior as well as the reliability and efficiency. Often problematic, however, is the fact that there is no standardized and generally accepted process protocol. Many new optimization methods are therefore tested with the help of their respective empirical studies, which are based on classical test functions, but differ with respect to further framework conditions. For example, many authors use their own subsets of functions, a self-defined number of repetitions, function calls and dimensions, and different value ranges. This makes a later comparison difficult. To solve the problem, a set of different test functions along with constraints was predefined by experts for the *Special Session on Real-Parameter Optimization* at the IEEE Congress on Evolutionary Computation (CEC) in 2005 [38]. Optimization methods can be evaluated equally and systematically using these, since the size of the problems, the initialization scheme, termination criteria, etc. are defined uniformly for all methods. All functions are designed to be scalable and are evaluated at different times or passing iterations. Since then, new sets of functions for performance evaluation of multi-objective optimization, global optimization of large scales, or computationally intensive numerical optimization have been repeatedly presented in the run-up to the CEC. In this work, various test functions of the CEC 2005 (Special Session on Real-Parameter Optimization) and 2008 (Competition on Large Scale Global Optimization) test suite, which are described in detail in chapter 5.2 are used. Before that, however, the main properties and hence difficulties of fitness landscapes are described.

5.1 Characterisitics of Test Functions

Test functions can be categorized and distinguished on the basis of various characteristics. The most important three properties are modality, separability and dimensionality. These properties are described in the following. [16], [39]

5.1.1 Modality

The modality *M* describes the presence of difficult-to-interpret optima that manifest as peaks in the fitness landscape. These peaks form local and global optima and complicate the exploration process. In particular, they occur frequently in simulation-based problems such as the power system protection coordination. There is a risk that an optimization method stagnates at these local optima and thus does not effectively search the feature landscape. Multimodal functions with many optima are therefore among the most difficult problems for many optimization methods. However, problems with a flat

fitness landscape can also be difficult to solve if the flatness does not provide sufficient information to guide the search process to the global optimum. A function with more than one local optimum is called multimodal. In turn, functions that have only one valley and one global minimum when minimized or one mountain and one global maximum when maximized are termed unimodal. Unimodal functions can usually be solved much easier.

5.1.2 Separability

The separability Se expresses the property whether the individual dimensions of the function are independent of each other and therefore separable, or whether they depend on each other and therefore are not separable. If a function is completely separable, each variable can be optimized independently of the others. Functions of this type are generally easier to optimize. In the case of functions that are only partially separable or not separable at all, the individual variables influence each other and the degree of difficulty increases. The coordination of the power system protection is a non-separable optimization problem, because all setting values of all protective devices affect and influence each other. Both unimodal and multimodal functions can be separable and non-separable.

5.1.3 Dimensionality

The dimensionality D indicates the number of dimensions of a problem. If the number increases, then the search space to be examined increases exponentially and thus also the fitness landscape. While with few dimensions it is still possible to search the entire search space to a large extent, this becomes increasingly difficult or impossible with increasing dimensionality. Therefore, functions with few dimensions are easier to optimize than high dimensional ones.

5.2 Used Test Functions

To investigate the performance and subsequent comparison of all PSO variants, four real-parameter test functions that are part of the CEC 2005 and CEC 2008 test suites and one purely discrete binary test function are used in the following: Shifted Sphere's function, shifted Rosenbrock's function, shifted Griewank's function, shifted Rastrigin's function and OneMax function.

The functions differ in distinctive features in order to be able to test different fitness landscapes and degrees of difficulty. This covers a wide range in order to find out which method, on average, performs best and is therefore most

suitable for coordinating power system protection in the further course of this work. All five functions are designed to be scalable and shifted compared to the original function. This is achieved via a bias f_{bias} to be added to the actual function. Different biases for different test functions of a test suite ensure that optimization algorithms are not designed to always achieve a specific target value or the in principle known global optimum $f(\vec{x}^*)$. Otherwise, the methods would already know during the optimization process whether they have arrived at the optimum or not. For official competitions this is therefore necessary, so that no participant can cheat. However, the bias has no influence on the difficulty of the function itself. For reasons of clarity, the bias is set to 1.0 for all functions in this work, which also means that the global optimum is 1.0.

Via a *shift* $\vec{o}$ the point of the global optimum $\vec{x}^*$ is shifted and thus redefined. In principle, almost all test functions used for optimization have their optimal point at (0,0,...,0) or (1,1,...,1) for reasons of clarity and to be able to work better with the optimization methods themselves. Over different shifts these points can be modified, so that during competitions optimization methods do not categorically visit the known optimal points immediately. The shift itself has no influence on the difficulty level, unless the optimization methods have been intentionally adapted to take advantage of this prior knowledge. For the optimization methods it does not matter which solution values have to be achieved in the single dimensions as long as they are within the allowed search range S. The structure of all functions including bias and shift can be taken from (32).

$$f(\vec{x}) = g(\vec{z}) + f_{\text{bias}} \quad \text{with} \quad \vec{z} = \vec{x} - \vec{o} \quad \text{and} \quad \vec{x} = [x_1, x_2, \cdots, x_D] \tag{32}$$

A summarized overview of all features of all test functions used in the following is shown in Table 2. These are described in detail in the further course.

5.2.1 Shifted Sphere's Function

The shifted sphere function is one of the simplest functions for testing optimization methods. It is a scalable, shifted, convex, separable and unimodal function belonging to the family of quadratic functions. It has an optimal point at $\vec{x}^* = \vec{o} = [o_1, o_2, \cdots, o_D] = [1, 1, \cdots, 1]$. As bias, $f_{\text{bias}} = 1.0$ is used

Table 2: Properties and comparison of the used real-parameter and discrete test functions. Legend: u=unimodal, m=multimodal, s=separable, ns=non-separable.

	Shifted Sphere	Shifted Rosenbrock	Shifted Griewank	Shifted Rastrigin	OneMax
M	u	m	m	m	u
Se	s	ns	ns	s	s
D	50	30	30	30	1000
S	$[-100; 100]^D$	$[-100; 100]^D$	$[0; 600]^D$	$[-5; 5]^D$	$[0,1]^D$
$\vec{o}$	[1,1...,1]	[1,1...,1]	[100,100...,100]	[1,1...,1]	/
$\vec{x}^*$	[1,1...,1]	[2,2...,2]	[100,100...,100]	[1,1...,1]	[0,0...,0]
$f(\vec{x}^*)$	1.0	1.0	1.0	1.0	1
rf	0.01	0.01	0.1	0.001	1

with $D = 50$ dimensions. The function is defined according to (33) and shown in Figure 17 as the original function.

$$\begin{aligned} f(\vec{x}) &= \sum_{i=1}^{D} z_i^2 + f_{\text{bias}} \\ S &= [-100, 100]^D \\ f(\vec{x}^*) &= 1.0 \end{aligned} \tag{33}$$

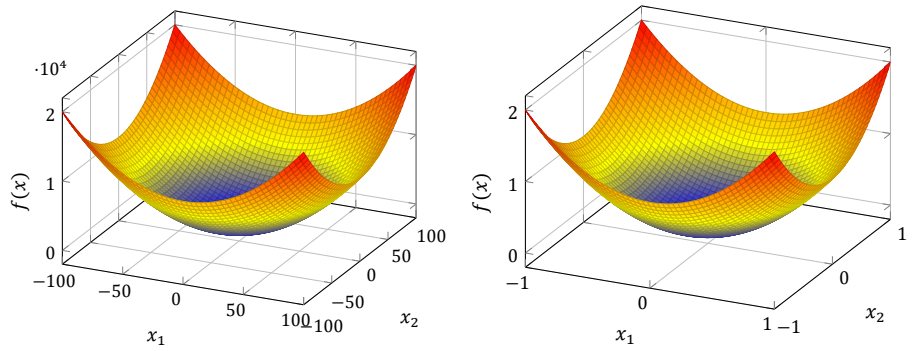

(a) Search space [-100,100]

(b) Search space [-1,1]

Figure 17: Two dimensional plot of the Sphere's function with different search spaces.

5.2.2 Shifted Rosenbrock's Function

The shifted Rosenbrock's function is a scalable, shifted, non-convex, non-separable and multimodal function, also called *banana function*. The global minimum lies in a long, narrow, parabolically shaped, shallow valley. Finding the valley itself is easy for most optimization methods, but discovering the minimum point within the valley is a complex problem. The function has an optimal point at a shift of $\vec{o} = [o_1, o_2, \cdots, o_D] = [1, 1, \cdots, 1]$, giving an optimal point at $\vec{x}^* = [2, 2, \cdots, 2]$. The bias used is $f_{\text{bias}} = 1.0$ with $D = 30$ dimensions. The function is defined according to (34) and shown in Figure 18 as the original function.

$$\begin{aligned} f(\vec{x}) &= \sum_{i=1}^{n-1} (100(z_i^2 - z_{i+1})^2 + (1 - z_i)^2) + f_{\text{bias}} \\ S &= [-100, 100]^D \\ f(\vec{x}^*) &= 2.0 \end{aligned} \tag{34}$$

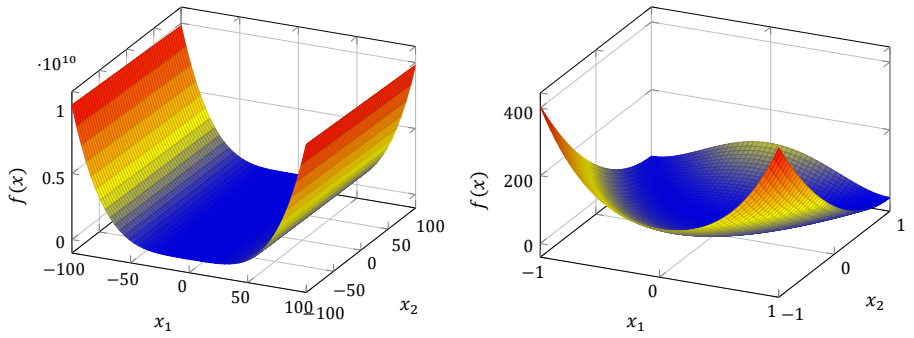

(a) Search space [-100,100] (b) Search space [-1,1]

Figure 18: Two dimensional plot of the Rosenbrock's function with different search spaces.

5.2.3 Shifted Griewank's Function

The shifted Griewank function is a scalable, shifted, nonconvex, nonseparable, and multimodal function that has many uniformly distributed local minima and is similar to the shifted Rastrigin function. A special property of the function is that the number of local minima increases as the number of dimensions increases. On the one hand, this can increase the difficulty, but at the same time it can decrease it, because the minima move closer together, so that an optimization method can find it easier to leave them again. The

search space is set to [0,600] and thus asymmetrical to the zero point. This is untypical for test functions, but it better reflects reality with respect to the coordination of the protection system, since protection settings are basically defined positively. The function has an optimal point at the edge of the search range at $\vec{x}^* = \vec{o} = [o_1, o_2, \cdots, o_D] = [100, 100, \cdots, 100]$. The shift is chosen large enough to push the optimal point far enough away from the zero point so that no optimization method can exploit this circumstance. The bias used is $f_{\text{bias}} = 1.0$ with $D = 30$ dimensions. The function thus follows (35) and is shown as the original function in Figure 19.

$$\begin{aligned} f(\vec{x}) &= 1 + \frac{1}{4000}\sum_{i=1}^{D} z_i^2 - \prod_{i=1}^{D} cos(\frac{z_i}{\sqrt{i}}) + f_{\text{bias}} \\ S &= [0, 600]^D \\ f(\vec{x}^*) &= 1.0 \end{aligned} \tag{35}$$

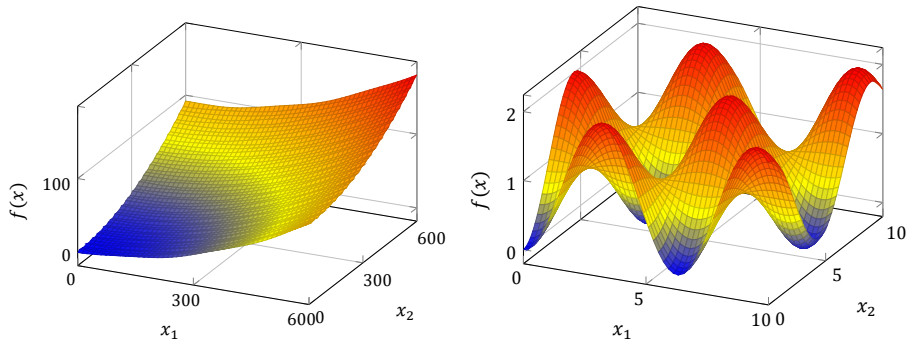

(a) Search space [0,600] (b) Search space [0,10]

Figure 19: Two dimensional plot of the Griewank's function with different search spaces.

5.2.4 Shifted Rastrigin's Function

The shifted Rastrigin's function is a scalable, shifted, non-convex, separable and highly multimodal function. The global minimum is hard to find due to the large number of local, equally distributed and deep minima. It has an optimal point at $\vec{x}^* = \vec{o} = [o_1, o_2, \cdots, o_D] = [1, 1, \cdots, 1]$. As bias, $f_{\text{bias}} = 1.0$ is

used with $D = 30$ dimensions. The function is defined according to (36) and shown in Figure 20 as the original function.

$$f(\vec{x}) = \sum_{i=1}^{D} (z_i^2 - 10cos(2\pi z_i) + 10) + f_{\text{bias}}$$
$$S = [-5, 5]^D \tag{36}$$
$$f(\vec{x}^*) = 1.0$$

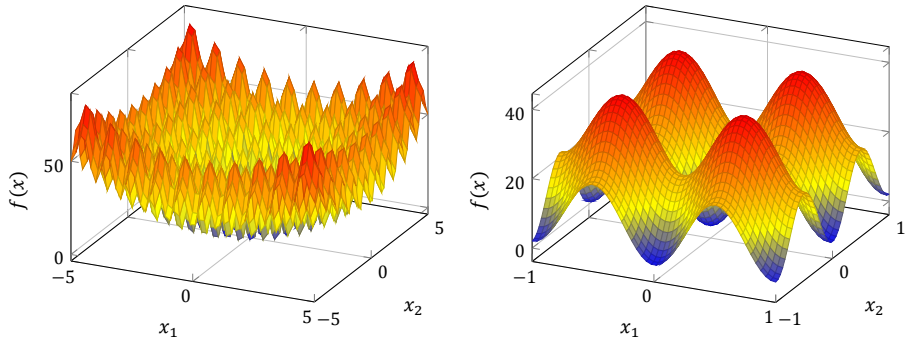

(a) Search space [-5,5] (b) Search space [-1,1]

Figure 20: Two dimensional plot of the Rastrigin's function with different search spaces.

However, since in the area of protection coordination not only real parameters but also binary setting values occur, such as activation of a power swing blocking function, a load sector or an out-of-step function, a purely binary test function is used in the following to investigate the ability of all optimization methods to solve such problems as well.

5.2.5 OneMax Function

The OneMax function is a scalable, convex, separable and unimodal function which simply adds up the number of all bits and thus looks easy to optimize. The search range corresponds with $S = \{0, 1\}^D$ only to the binary numbers 0 and 1. The number of dimensions D is set to a high value of 1000, which means that the binary methods have to optimize more than twice as many bits compared to the previous discrete test functions. The bias corresponds to

$f_{\text{bias}} = 1.0$. The function has an optimal point at $\vec{x}^* = [0, 0, \cdots, 0]$, which is defined according to (37) and shown in Figure 21.

$$\begin{aligned} f(\vec{x}) &= \sum_{i=1}^{D} z_i + f_{\text{bias}} \\ S &= \{0, 1\}^D \\ f(\vec{x}^*) &= [0, 0, \cdots, 0] \end{aligned} \tag{37}$$

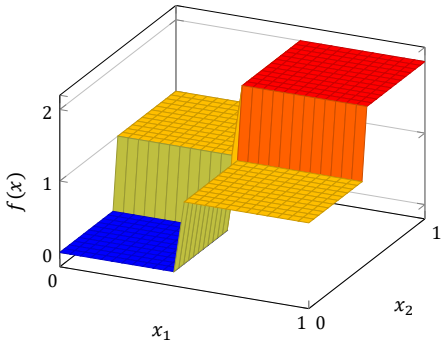

Figure 21: Two dimensional plot of the OneMax function.

After all real and binary test functions are presented, the framework of the investigations is explained in the following.

5.3 Experimental Setup

To ensure that the results are highly transparent and reproducible, all selected settings, additional functions, parameters and test conditions are described in this section.

5.3.1 Selection of Optimization Methods

All optimization methods presented in the previous chapters are used and examined. A special case is the DEEPSO method, since different variants are available for selection. In [31], DEEPSO-Pb-rnd is considered the most successful variant. Contradictory, in [32] this method is considered to be the worst choice, and DEEPSO-Sg-rnd should be selected. Own investigations confirm that the DEEPSO method is strongly problem dependent and therefore the variants and parameters have to be adapted. Universally across all test

functions the new variant DEEPSO-Sg(LB)-rnd from section 4.1 performed best, which is why it is used as the sole DEEPSO method in the following.

5.3.2 Target Formulation

First of all, the question shall be clarified, how to determine, whether an optimization method is considered good or bad and which characteristics are important for the optimization. Metaheuristics are usually computationally less demanding, so their computations play only a minor role compared to the evaluation of the fitness function. Therefore, in the following, the computational and thus temporal effort of an optimization is expressed exclusively by the required number of FES. This has the advantage that it does not matter what kind of calculations the fitness function performs, since only the number of calls is decisive.

Thus, two main criteria can then be used to evaluate the performance of optimization methods. On the one hand the best achieved FV and on the other hand the required FES. Both criteria can only be considered together and in context with each other. The goal of an optimization run can be defined in two different ways depending on the two criteria. On the one hand, the achievement of a best possible FV within a defined number of FES can be the goal. On the other hand, a target value can also be formulated in advance, which is to be achieved in as few FES as possible. Depending on the specification, optimization methods can then be compared with each other. The latter method is particularly useful if the target to be achieved is known and it is to be found out with which method this can be determined in the shortest time. In real-world problems, however, the global optimum is usually unknown, making it difficult to specify an exact target value. The limiting factor in real applications is usually the computational effort of the fitness function, so that the maximum should be extracted in a given number of FES. This method is also used in the competitions of the CEC. Depending on the used functions, dimensions and search spaces, a maximum number of FES is given. The number varies from competition to competition. This work is based on the progress protocol of the CEC2005. In it a maximum number of FES of $1e3 \cdot D$, $1e4 \cdot D$, $1e5 \cdot D$, resulting in 3E4, 3E5 and 3E6 FES for 30 dimensions, is specified. This number of maximum FES is used to evaluate all optimizer procedures at all test functions.

5.3.3 Number of Executions

Since all optimization methods are metaheuristics that use randomness-based techniques, all optimization runs are performed 25 times in direct succession, such as in CEC2005. Then, the average of all runs is computed. Each run is terminated when the maximum number of FES is reached.

5.3.4 Rounding of Decision Variables

In order to use the different BPSO methods, a resolution factor rf is defined for each test function in Table 2 as described in chapter 3.4.2. This allows the binary strings to be converted to real numbers with a certain precision. To ensure that the same conditions and requirements apply to all methods and thus also to the continuous PSO methods, their decision variables are rounded using the floor function before being passed to the respective fitness function according to (38). Thus, the methods continue to calculate internally with real numbers of greater precision, only the passed values are adjusted. This method is also reasonable as long as variables of real problems can usually be defined in advance with a sufficient accuracy. This also applies to the setting parameters of the power system protection coordination. For the OneMax function, an rf of one for a search range of [0,1] together with (38) causes all values smaller than 0.5 to be rounded down to zero and all others to be rounded up to one. This also allows the continuous PSO variants, to optimize the discrete test function.

$$x_i = \lfloor \frac{x_i}{rf} + 0.5 \rfloor \cdot rf \tag{38}$$

5.3.5 Parmeter Tuning

A suitable parameterization is crucial for a performant and successful optimization. To achieve the best possible performance, the available tuning options must be individually explored and adapted for each fitness function. The process of finding the right parameters is time-consuming and complex, since it is almost exclusively a trial-and-error process and different parameters influence each other, which exponentially increases the number of possible parameter setups. A direct comparison of results as well as the use of parameters from the literature is usually difficult, since parameter specifications are often missing, test functions differ, they have been modified or other framework conditions have been used. Since a function evaluation of the presented test functions costs only a fraction of the time of the later fitness function of the power system protection coordination, mainly setups are to be used, which

achieve good results over all functions, so that these can then be used in the further course of this work. Thus, the goal is explicitly not to determine the best possible modification of each PSO variant per test function. This would mean a parameter tuning per test function, which means that in the end it is not clear which method with which settings should be used for the later, very computationally intensive assessment of the protection coordination.

All parameters used in all optimization methods can be found in the respective Tables 3 to 11. The parameterization is based on own results as well as findings from the literature and will be explained in detail in the following.

Table 3: Parameter settings of the PSO and BPSO methods.

	PSO-1	PSO-2	BPSO-1	BPSO-2
$\vec{w}_1$	-	0.729	-	1.0
$w_{1,\max}$	0.9	-	0.9	-
$w_{1,\min}$	0.4	-	0.4	-
$\vec{w}_2$, $\vec{w}_3$	2.0	1.49445	2.0	1.5
V_{max}, $V_{\min}$	-	-	±4	

Table 4: Parameter settings of the EPSO methods.

	EPSO-1	EPSO-2	EPSO-3	EPSO-4
p	0.2	0.5	0.75	0.9
$\vec{w}^*_{1,\text{init}}$	0.5			
$\vec{w}^*_{2,\text{init}}$, $\vec{w}^*_{3,\text{init}}$	1.0			
$\vec{w}^*_{4,\text{init}}$	rf for real-parameter and 0.001 for discrete			
$w_{1,\max}$, $w_{2,\max}$, $w_{3,\max}$	1.0			
$w_{1,\min}$, $w_{2,\min}$, $w_{3,\min}$	0.25			
$w_{4,\max}$	$2.0 \cdot \vec{w}^*_{4,\text{init}}$			
$w_{4,\min}$	$0.5 \cdot \vec{w}^*_{4,\text{init}}$			

Table 5: Parameter settings of the DEEPSO methods.

	DEEPSO-1	DEEPSO-2	DEEPSO-3	DEEPSO-4
p	0.2	0.5	0.75	0.9
$\vec{w}^*_{1,\text{init}}$	0.5			
$\vec{w}^*_{2,\text{init}}$, $\vec{w}^*_{3,\text{init}}$	0.3			
$\vec{w}^*_{4,\text{init}}$	rf for real-parameter and 0.001 for discrete			
$w_{1,\max}$	1.0			
$w_{1,\min}$	0.25			
$w_{2,\max}$, $w_{3,\max}$	0.6			
$w_{2,\min}$, $w_{3,\min}$	0.2			
$w_{4,\max}$	$2.0 \cdot \vec{w}^*_{4,\text{init}}$			
$w_{4,\min}$	$0.5 \cdot \vec{w}^*_{4,\text{init}}$			

Table 6: Parameter settings of the EPSO_{DE} methods.

	EPSO_{DE}-1	EPSO_{DE}-2	EPSO_{DE}-3	EPSO_{DE}-4
p	0.2	0.5	0.75	0.9
$\vec{w}^*_{1,\text{init}}$, $\vec{w}^*_{2,\text{init}}$, $\vec{w}^*_{3,\text{init}}$	0.5			
$w_{1,\max}$, $w_{2,\max}$, $w_{3,\max}$	1.0			
$w_{1,\min}$, $w_{2,\min}$, $w_{3,\min}$	0.25			

Table 7: Parameter settings of the $\text{EPSO}_{\text{DE}}2$ methods.

	$\text{EPSO}_{\text{DE}}2$-1	$\text{EPSO}_{\text{DE}}2$-2	$\text{EPSO}_{\text{DE}}2$-3	$\text{EPSO}_{\text{DE}}2$-4
p	0.1	0.2	0.5	0.75
$\vec{w}^*_{1,\text{init}}$, $\vec{w}^*_{2,\text{init}}$, $\vec{w}^*_{3,\text{init}}$	0.5			
$w_{1,\max}$, $w_{2,\max}$, $w_{3,\max}$	1.0			
$w_{1,\min}$, $w_{2,\min}$, $w_{3,\min}$	0.25			

Table 8: Parameter settings of the BPSO_{DE} methods.

	BPSO_{DE}-1	BPSO_{DE}-2	BPSO_{DE}-3	BPSO_{DE}-4
p	0.2	0.5	0.75	0.9
$\vec{w}_1$	1.0			
$\vec{w}_2$, $\vec{w}_3$	2.0			
$V_{\max}$, $V_{\min}$	±6			

Table 9: Parameter settings of the BPSO_{DE}2 methods.

	BPSO_{DE}2-1	BPSO_{DE}2-2	BPSO_{DE}2-3	BPSO_{DE}2-4
p	0.1	0.2	0.5	0.75
$\vec{w}_1$	1.0			
$\vec{w}_2$, $\vec{w}_3$	2.0			
$V_{\max}$, $V_{\min}$	±6			

Table 10: Parameter settings of the EBPSO_{DE} methods.

	EBPSO_{DE}-1	EBPSO_{DE}-2	EBPSO_{DE}-3	EBPSO_{DE}-4
p	0.2	0.5	0.75	0.9
$\vec{w}^*_{1,\text{init}}$, $\vec{w}^*_{2,\text{init}}$, $\vec{w}^*_{3,\text{init}}$	1.0			
$w_{1,\max}$, $w_{1,\min}$	1.0			
$w_{2,\max}$, $w_{3,\max}$	2.0			
$w_{2,\min}$, $w_{3,\min}$	0.5			

Table 11: Parameter settings of the EBPSO_{DE}2 methods.

	EBPSO_{DE}2-1	EBPSO_{DE}2-2	EBPSO_{DE}2-3	EBPSO_{DE}2-4
p	0.1	0.2	0.5	0.75
$\vec{w}^*_{1,\text{init}}$, $\vec{w}^*_{2,\text{init}}$, $\vec{w}^*_{3,\text{init}}$	1.0			
$w_{1,\max}$, $w_{1,\min}$	1.0			
$w_{2,\max}$, $w_{3,\max}$	2.0			
$w_{2,\min}$, $w_{3,\min}$	0.5			

5.3.5.1 Number of Particles

A first parameter to choose is the number of used particles n that make up a swarm. Thus, a larger number can lead to an increase in performance. More particles are able to search the fitness landscape better in parallel and collect more information about the fitness function per iteration step. However, performance can also decrease, of course, because more particles per iteration step also require a higher number of function calls. With a fixed maximum number of FES, this in turn means that the method is terminated after fewer iterations. The number of particles is chosen based on the difficulty of the problem, the available number of FES, the number of dimensions to be optimized and the specific method used. In general, it is recommended to choose a particle number between 20 and 60, with 30 to 50 particles being the most commonly used. Although it is advantageous to adapt the particle number to the conditions, it nevertheless plays a rather minor role. In this work, the particle number is set to $n = 30$ for all test functions. [19], [29], [40], [41]

5.3.5.2 Position Limits

The admissible search space S must be defined in advance for each variable of the fitness function. Thus, for each variable exists a lower $S_{i,\min}$ and an upper $S_{i,\max}$ admissible limit. For a particle moving in the D-dimensional space of the fitness function, this means that it must not exceed these limits in any dimension, otherwise it would leave the allowable search space. If it occurs that the addition of a new velocity vector causes a particle to exceed a position limit in one dimension, various methods can be used to correct the problem and improve performance. The simplest method, which is also used in this work, is to set that particle in the dimension back to the allowable limit. An alternative would be to move the particle back into the search space by the amount it left the search space. This method is particularly effective when the global optimum lies in the middle of the search space. However, this is rarely the case in real-world problems and, more importantly, it cannot be known in advance. Just for many test functions, this circumstance is often true. Another method is to allow the particle to exceed the limits of the search space, but not evaluate this in the fitness function and give it a bad return value instead.

5.3.5.3 Velocity Limits

At each iteration, all particles move towards a new position determined by the velocity vector. The calculation of the velocity vectors is based on stochastic techniques and depends on the previous velocity. To prevent the velocity vector from becoming too large, so that particles would only move from one

end of the search space to the other, it is recommended to limit the velocity. For some fitness functions, it may be advantageous to greatly reduce the maximum allowed velocity $V_{\max}$ so that particles search the search space slowly and steadily. For other functions, however, this can be disadvantageous if it prevents local optima from being bypassed or exited and significantly increases the required number of FES. For this work, the particle velocity is constrained only slightly by (39). This allows a particle to cross the entire search space in one iteration, but does not increase the velocity any further. Basically, this kind of limitation should almost never be needed during the optimization process anyway, if the optimization method including its particles works efficiently, since the convergence of all particles is a mathematical property of the methods.

$$\begin{aligned} V_{\max} &= S_{max} - S_{\min} \\ V_{\min} &= -1 \cdot V_{\max} \end{aligned} \tag{39}$$

A special characteristic is the velocity limitation in the BPSO methods. Here, the velocity vector is not used directly to move the particle, but is transformed into a probability of a bit change via a sigmoid function. A velocity constraint must be used to ensure that a residual probability of a bit change is always preserved. In this work, a V_{max} or $V_{\min}$ of four is used, leaving a residual probability of 1.8 %. Good results have been obtained with this in the past [19]. For BPSO_{DE}, $\text{BPSO}_{\text{DE}}2$, EBPSO_{DE}, and $\text{EBPSO}_{\text{DE}}2$, a velocity limit of ±6 is used, leaving a residual probability of 0.25 %.

5.3.5.4 Weighting Vectors

The weighting vectors $\vec{w}_1$ - $\vec{w}_4$ have a decisive influence on the movement equation and thus on the particle behavior and the overall performance of the optimization. In order to achieve optimal performance, they must be adapted to the problem being optimized. There are numerous different combinations of setups in the literature that have achieved good results under a variety of conditions.

There are two common methods to test for the PSO method. One is to keep the inertia vector $\vec{w}_1$ constant and the other is to decrease it linearly with increasing iteration number in the range $\vec{w}_{1,\max}$ to $\vec{w}_{1,\min}$. The methods are listed in Table 3 as *PSO-1* and *PSO-2*.

In the evolutionary methods, the weighting vectors are mutated at each iteration and therefore have an adaptive nature due to subsequent selection. This allows the vectors to adapt to the problem itself over time. However, this

requires that enough better points are found during the optimization process for the adaptation to work effectively. The values for the weighting vectors used in this paper are based on own experiments and results from the literature. For a reliable optimization it is also necessary to formulate sufficient bounds for the values of the weighting vectors, which must not be exceeded or fallen short of. Although the weighting vectors are partially self-adjusting, they must be kept within a reasonable and efficient range of values. If the values are too small, local optima cannot be left and the optimization process gets stuck. Values that are too large cause particles to converge too quickly or change position too radically. When the defined limits are exceeded, various methods can then be used to bring the values back into the acceptable range. Since the publications of EPSO and DEEPSO lack data on values and techniques, results based on own investigations are used. For $\vec{w}_1^*$, a dynamic limit according to (40) is used. This has the advantage that inertia values that are too small or too large are more quickly returned to the optimal range and thus local optima can be overcome more easily. For $\vec{w}_2^*$, $\vec{w}_3^*$ and $\vec{w}_4^*$ static limits are used according to (41). This allows for even better matching and partitioning of the cognitive and social components. All weighting values and bounds used in this work are listed in the Tables 4, 6, 7, 8, 9, 10, and 11 for the different methods. Problem-dependent settings that lead to even better results overall have been omitted with respect to the power system protection coordination.

$$\vec{w}_{ij}^* = \begin{cases} w_{i,\max} - (\vec{w}_{ij}^* - w_{i,\max}) & \vec{w}_{ij}^* > w_{i,\max} \\ w_{i,\min} + (w_{i,\min} - \vec{w}_{ij}^*) & \vec{w}_{ij}^* < w_{i,\min} \\ \vec{w}_{ij}^* & \text{otherwise} \end{cases} \tag{40}$$

$$\vec{w}_{ij}^* = \begin{cases} w_{i,\max} & \vec{w}_{ij}^* > w_{i,\max} \\ w_{i,\min} & \vec{w}_{ij}^* < w_{i,\min} \\ \vec{w}_{ij}^* & \text{otherwise} \end{cases} \tag{41}$$

5.3.5.5 Mutation Rate

A small mutation rate τ leads to a slower development of the weighting vectors. The consequence is a slower optimization progress, if particularly large or small values and thus speeds are necessary in the moment of the optimization. However, the weighting vectors can adapt to this over iteration steps. The situation is different if the mutation rate is set too high. Here it can happen that the weighting vectors become too large or too small too quickly and have to be restricted beyond the defined limits. The consequence is that

no real adaptation and thus no targeted modification and development of the weighting vectors can take place due to the mutation, since they rather jump back and forth and the optimization process gets stuck. Therefore, large values should be chosen with caution and be suitable for the fitness function. A mutation rate of $\tau = 0.5$ has proven to be a good compromise and effective value for a wide variety of problems, and is used for all evolutionary methods.

5.3.5.6 Communication Factor

The communication factor p has a decisive influence on the communication vector $\vec{P}$ and thus on the communication structure of the different methods. For the already published methods PSO, EPSO, DEEPSO and EPSO_{DE}, different values have led to good as well as bad results under different conditions. The communication factor p has a decisive influence on the communication vector $\vec{P}$ and thus on the overall communication structure of the different methods. Compared to all presented parameters, it probably has the greatest influence on the course of the optimization process. In the case of the previously published methods EPSO, DEEPSO and EPSO_{DE}, different values of p have thereby led to both good and bad results in different situations. Thus, unfortunately, a generally applicable setting rule cannot be formulated. In particular, for the new methods $\text{EPSO}_{\text{DE}}2$, $\text{BPSO}_{\text{DE}}2$ and $\text{EBPSO}_{\text{DE}}2$, p determines the influence of the best position found. To test a variety of values, four values are used for EPSO, DEEPSO, EPSO_{DE}, $\text{EPSO}_{\text{DE}}2$, BPSO_{DE}, $\text{BPSO}_{\text{DE}}2$, EBPSO_{DE}, and $\text{EBPSO}_{\text{DE}}2$. Nomenclature and parameterization of the methods can be taken from the tables presented before.

5.3.6 Results

The FV of all used optimization methods for the shifted sphere function according to 3E3, 3E4 and 3E5 FES, averaged over all 25 runs, are listed in the Appendix under A in Table 19. For better overview and evaluation, the values as well as the corresponding methods are sorted according to the overall performance achieved from the smallest (best) to the largest (worst), depending on the number of FES indicated. This principle of presentation and evaluation is also used at the CEC competitions. The results for the shifted Rosenbrock function can be seen in Table 20, for the shifted Griewank function in Table 21, for the shifted Rastrigin function in Table 22, and for the OneMax function in Table 23. The corresponding graphs showing the detailed optimization process of each method for each test function at a given number of FES can also be found in the Appendix at A after the respective tables. In this way, the entire optimization process can be traced back.

In order to be able to make a better statement about which method or methods have performed best and are suitable for the optimization of the power system protection coordination, a more precise evaluation of the results is required. At the CEC 2005 a success rate was introduced for this purpose. This puts the number of successful runs in relation to the total number. Therefore a target value is formulated in advance for each test function, which must be reached for a valid success. However, the use of target values is not free of bias, as it accommodates some methods and others not. This type of evaluation was therefore abandoned in subsequent years. The evaluation in the following competitions is based solely on the achieved FV or the degree of deviation from the optimal point at different FES, functions and dimensions. To what extent results have been further evaluated is not always disclosed and also differs from contest to contest. The possibilities here are numerous. Mean and median values can be calculated and accounted for at different points in time. A special point allocation depending on the ranking order can be used or the complexity of the test functions as well as the effort of parameterization of the optimization methods can be taken into account. [38], [42]–[44]

In this work, an objectivity-oriented evaluation procedure is used to compare all PSO variants with each other. First of all, each variant receives a rank for each test function with a given number of maximum FES depending on the average FV achieved. With 36 different PSO variants, there are thus also 36 ranks to be assigned. If the average best FV of two or more optimization methods is equal, then all methods receive the same rank of higher standing. Here, an accuracy of 10^{-10} was kept, even if this is not shown in the tables mentioned before. Next, average rankings for all optimization methods are determined from the different rankings. Table 12 lists the average ranks achieved by each method for 3E3, 3E4 and 3E5 FES across all test functions, as well as the average rank across all FES. Table 13 lists the averaged ranks when optimizing the real-parameter functions and Table 14 for the OneMax function. Highlighted are the 3 best results in each case. In darker gray, the best FES result is highlighted, while second and third place are marked in light gray. Should the PSO variant occupy a first place, the method is highlighted. This gives a solid picture of which optimization method performs best for which given number of FES, for which type of test function, and which methods give the best results on average across all test functions and FES.

The results show that the optimization methods perform differently depending on the maximum allowed number of FES and optimized test function. It is clear that the methods PSO, DEEPSO and BPSO underperform and do not occupy any of the first ranks. Therefore, these do not represent good methods

Table 12: Overview of all optimization results of all PSO variants for the real-parameter and discrete test functions at different FES.

Method	Average	3E3 FES	3E4 FES	3E5 FES
PSO-1	33.8	30.6	35.4	35.4
PSO-2	29.4	20.4	33.4	34.4
EPSO-1	16.1	20.4	14.0	13.8
EPSO-2	14.2	12.6	13.6	16.4
EPSO-3	13.7	10.8	12.6	17.8
EPSO-4	14.1	12.6	12.2	17.4
DEEPSO-1	18.5	13.6	22.4	19.6
DEEPSO-2	19.6	15.8	20.6	22.4
DEEPSO-3	19.3	14.6	21.0	22.4
DEEPSO-4	18.9	15.0	20.8	20.8
$EPSO_{DE}$-1	21.0	24.4	20.6	18.0
$EPSO_{DE}$-2	22.3	16.6	24.6	25.8
$EPSO_{DE}$-3	22.0	12.6	25.4	28.0
$EPSO_{DE}$-4	21.5	**8.0**	27.0	29.6
$EPSO_{DE}$2-1	19.6	10.6	22.8	25.4
$EPSO_{DE}$2-2	17.3	9.2	19.8	23.0
$EPSO_{DE}$2-3	15.5	**6.4**	16.2	24.0
$EPSO_{DE}$2-4	16.5	**5.6**	19.2	24.8
BPSO-1	35.5	36.0	35.4	35.2
BPSO-2	19.7	9.4	23.0	26.8
$EBPSO_{DE}$-1	21.2	31.8	24.6	7.2
$EBPSO_{DE}$-2	18.4	24.6	19.6	11.0
$EBPSO_{DE}$-3	15.9	21.4	13.8	12.4
$EBPSO_{DE}$-4	16.1	20.2	10.8	17.2
$EBPSO_{DE}$2-1	21.0	35.0	26.8	**1.2**
$EBPSO_{DE}$2-2	21.4	32.8	24.6	6.8
$EBPSO_{DE}$2-3	18.2	25.0	18.6	11.0
$EBPSO_{DE}$2-4	17.5	21.4	14.2	17.0
$BPSO_{DE}$-1	13.1	26.0	10.6	2.6
$BPSO_{DE}$-2	10.4	16.4	6.2	8.6
$BPSO_{DE}$-3	**9.4**	11.2	**5.8**	11.2
$BPSO_{DE}$-4	**8.1**	9.0	**4.6**	10.6
$BPSO_{DE}$2-1	17.9	31.4	21.4	**1.0**
$BPSO_{DE}$2-2	13.2	26.2	10.8	**2.6**
$BPSO_{DE}$2-3	11.5	17.2	6.4	10.8
$BPSO_{DE}$2-4	**8.9**	11.2	**5.2**	10.2

Table 13: Overview of all optimization results of all PSO variants for the real-parameter test functions at different FES.

Method	Average	3E3 FES	3E4 FES	3E5 FES
PSO-1	33.4	29.8	35.3	35.3
PSO-2	28.3	17.5	33.3	34.3
EPSO-1	13.8	19.0	9.5	13.0
EPSO-2	11.6	9.8	9.3	15.8
EPSO-3	**10.8**	7.3	8.5	16.8
EPSO-4	**10.8**	8.5	8.5	15.5
DEEPSO-1	18.4	12.0	23.3	20.0
DEEPSO-2	19.3	15.3	20.5	22.3
DEEPSO-3	18.4	13.5	19.8	22.0
DEEPSO-4	17.2	13.5	18.5	19.5
$EPSO_{DE}$-1	20.3	22.3	21.3	17.5
$EPSO_{DE}$-2	21.9	15.3	25.8	24.8
$EPSO_{DE}$-3	21.6	11.5	26.0	27.3
$EPSO_{DE}$-4	21.3	7.3	27.5	29.0
$EPSO_{DE}$2-1	16.8	**6.5**	20.3	23.5
$EPSO_{DE}$2-2	15.1	**5.8**	17.8	21.8
$EPSO_{DE}$2-3	14.5	**4.5**	14.3	24.8
$EPSO_{DE}$2-4	15.8	**4.5**	18.5	24.3
BPSO-1	35.7	36.0	35.5	35.5
BPSO-2	20.5	10.8	24.5	26.3
$EBPSO_{DE}$-1	22.9	32.8	27.3	8.8
$EBPSO_{DE}$-2	20.8	27.5	21.5	13.5
$EBPSO_{DE}$-3	18.3	24.8	15.0	15.3
$EBPSO_{DE}$-4	17.6	23.5	11.5	17.8
$EBPSO_{DE}$2-1	21.9	35.0	29.5	**1.3**
$EBPSO_{DE}$2-2	22.8	33.3	27.0	8.3
$EBPSO_{DE}$2-3	20.8	28.3	20.5	13.5
$EBPSO_{DE}$2-4	19.0	24.5	15.3	17.3
$BPSO_{DE}$-1	14.4	28.8	11.5	3.0
$BPSO_{DE}$-2	12.4	19.3	7.5	10.5
$BPSO_{DE}$-3	11.4	13.5	**7.0**	13.8
$BPSO_{DE}$-4	**9.8**	11.0	**5.5**	13.0
$BPSO_{DE}$2-1	18.8	31.8	23.5	**1.0**
$BPSO_{DE}$2-2	14.6	28.8	12.0	**3.0**
$BPSO_{DE}$2-3	13.7	20.0	7.8	13.3
$BPSO_{DE}$2-4	**10.7**	13.3	**6.3**	12.5

Table 14: Total overview of all optimization results of all PSO variants for the OneMax test function at different FES.

Method	Average	3E3 FES	3E4 FES	3E5 FES
PSO-1	35.3	34.0	36.0	36.0
PSO-2	33.7	32.0	34.0	35.0
EPSO-1	25.0	26.0	32.0	17.0
EPSO-2	24.7	24.0	31.0	19.0
EPSO-3	25.3	25.0	29.0	22.0
EPSO-4	27.0	29.0	27.0	25.0
DEEPSO-1	19.0	20.0	19.0	18.0
DEEPSO-2	20.7	18.0	21.0	23.0
DEEPSO-3	23.0	19.0	26.0	24.0
DEEPSO-4	25.7	21.0	30.0	26.0
$EPSO_{DE}$-1	23.7	33.0	18.0	20.0
$EPSO_{DE}$-2	24.0	22.0	20.0	30.0
$EPSO_{DE}$-3	23.7	17.0	23.0	31.0
$EPSO_{DE}$-4	22.7	11.0	25.0	32.0
$EPSO_{DE}$2-1	31.0	27.0	33.0	33.0
$EPSO_{DE}$2-2	26.3	23.0	28.0	28.0
$EPSO_{DE}$2-3	19.7	14.0	24.0	21.0
$EPSO_{DE}$2-4	19.7	10.0	22.0	27.0
BPSO-1	35.0	36.0	35.0	34.0
BPSO-2	16.7	4.0	17.0	29.0
$EBPSO_{DE}$-1	14.3	28.0	14.0	**1.0**
$EBPSO_{DE}$-2	8.7	13.0	12.0	**1.0**
$EBPSO_{DE}$-3	6.0	8.0	9.0	**1.0**
$EBPSO_{DE}$-4	10.0	7.0	8.0	**15.0**
$EBPSO_{DE}$2-1	17.3	35.0	16.0	**1.0**
$EBPSO_{DE}$2-2	15.7	31.0	15.0	**1.0**
$EBPSO_{DE}$2-3	8.0	12.0	11.0	**1.0**
$EBPSO_{DE}$2-4	11.7	9.0	10.0	**16.0**
$BPSO_{DE}$-1	7.7	15.0	7.0	**1.0**
$BPSO_{DE}$-2	2.3	5.0	**1.0**	**1.0**
$BPSO_{DE}$-3	**1.3**	**2.0**	**1.0**	**1.0**
$BPSO_{DE}$-4	**1.0**	**1.0**	**1.0**	**1.0**
$BPSO_{DE}$2-1	14.7	30.0	13.0	**1.0**
$BPSO_{DE}$2-2	7.7	16.0	6.0	**1.0**
$BPSO_{DE}$2-3	2.7	6.0	**1.0**	**1.0**
$BPSO_{DE}$2-4	**1.7**	**3.0**	**1.0**	**1.0**

for optimizing the power system protection coordination. The following methods emerge as the winners of the different categories:

Average over all functions and FES:	$BPSO_{DE}$-4
Average over all real-parameter functions and FES:	$BPSO_{DE}$-4
Discrete OneMax function with all FES:	$BPSO_{DE}$-4
Average over all functions with 3E3 FES:	$EPSO_{DE}$2-4
Average over all real-parameter functions with 3E3 FES:	$EPSO_{DE}$2-4
Discrete OneMax function with 3E3 FES:	$BPSO_{DE}$-4
Average over all functions with 3E4 FES:	$BPSO_{DE}$-4
Average over all real-parameter functions with 3E4 FES:	$BPSO_{DE}$-4
Discrete OneMax function with 3E4 FES FES:	$BPSO_{DE}$-4
	and 4 more
Average over all functions with 3E5 FES:	$BPSO_{DE}$2-1
Average over all real-parameter functions with 3E5 FES:	$BPSO_{DE}$2-1
Discrete OneMax function with 3E5 FES:	$BPSO_{DE}$2-1
	and 14 more

Conclusion

The overall winner of the optimization benchmark is the $BPSO_{DE}$-4 method, which performs best on average across all test functions and FES. While this statement is scientifically interesting, it plays a minor role for real-world applications of power system protection coordination. This is because for this application it is known in advance whether the function to be optimized is purely continuous, purely discrete or mixed. In addition, a maximum number of FES must be specified for a practical implementation, since the global optimum is completely unknown.

Using 3E3 FES, the $EPSO_{DE}$2-4 method gives the best results. Only for the discrete OneMax function the $BPSO_{DE}$-4 method achieves better results again. Depending on the computational effort required for the power system protection coordination and the time available for it, the $EPSO_{DE}$2-4 or $BPSO_{DE}$-4 method is best suited to achieve a result with as little FES as possible.

If 3E4 FES are used, then the $BPSO_{DE}$-4 method ranks first everywhere. When optimizing the OneMax function, the $BPSO_{DE}$-2, $BPSO_{DE}$-3, $BPSO_{DE}$2-3, and $BPSO_{DE}$2-4 methods perform equally well. However, the corresponding plots of Figure 109 and Figure 110 show that $BPSO_{DE}$-4 found the global optimum fastest by a small margin. Thus, if at least 3E4 FES can be used for optimization, then $BPSO_{DE}$-4 should be used.

If it is possible to use 3E5 FES, then the $BPSO_{DE}$2-1 method delivers the best result unerringly. For all functions, $BPSO_{DE}$2-1 was always in first place at the end of the optimization process. Although this is at the expense of good performance and thus speed with fewer FES available, it ultimately delivers very good results. For the OneMax function, 14 other variants also reached the global optimum. The fastest in this run was the $BPSO_{DE}$2 method.

Part II

Assessment of Protection & Power System Security

If terms are not correct, one cannot speak smoothly and reasonably, and if one cannot speak smoothly and reasonably, affairs cannot be managed successfully.

Konfuzius
Chinese philosopher
ca. * 551 BC, + 479 BC

6 Protection Requirements, Criteria & Terms

Some terms are explained first so that there is clarity about their use and the differences between them.

6.1 Power Supply

6.1.1 Security of Supply

Security of Supply (SoS) describes the long-term securing of sufficient generation, conversion, transmission and distribution of electrical energy. This includes the provision of appropriate primary energy resources, ensuring sufficient maintenance of all operating equipment and ensuring the technical feasibility of transmission and distribution. Together with environmental compatibility and economic efficiency, it forms an equal-ranking objective of energy policy, thus forming a triangle of goals [45]. The term is often used differently in different contexts and differs depending on the adopting perspective of the user (generator, consumer, distributor).

6.1.2 Quality of Supply

Quality of Supply (QoS) includes the sub-areas Reliability of Supply (RoS), voltage quality, frequency quality and service quality. RoS describes the suitability of an electricity supply system to fulfill its supply task under specified conditions during a specified period of time without interruptions or disturbances. In inverse proportion to this is the concept of supply continuity, which describes the permanent and thus uninterrupted supply of electrical energy to all customers. The latter is often measured and compared in minutes or hours of undelivered electrical energy per year. An interruption occurs when the voltage at the consumer's connection node drops to an amount below 1 % of the nominal voltage and continues for 3 min. Voltage collapse is referred to when the voltage drops to 10 % to 60 % of the nominal voltage for less than 1 min [46]. Voltage and frequency quality describe the quality of the voltage and frequency, respectively, arriving at the consumer. Service quality, in turn, is a non-technical criterion and assesses the relationship and all associated services between network operators and customers.

The RoS is thus a decisive pillar of the QoS and necessary to ensure the SoS in the long term. High RoS requires high power system security and protection security, both of which are mutually dependent.

6.2 Power Systems

Electrical power systems are highly complex, technical systems that are among the largest in the world. They can be described as a set of many different interconnected components that together perform the tasks of energy conversion, storage, transport and consumption. In its entirety, the power system can be viewed as an independent system with its own state and interfaces to the outside world. The components can be divided into the basic categories of primary and secondary equipment. The primary equipment covers the components necessary for directly fulfilling the tasks defined above. Secondary equipment, on the other hand, includes all components that are required to ensure operation. This includes all measuring, control, communication and protection systems. The greatest external influence is exerted by people in the form of control center operators and by the market in the form of electricity trading. Laws, standards and regulations define the necessary rules and framework conditions for all stakeholders.

6.2.1 Power System Security

Power system security, or simply system security, is a term to characterize the degree of risk that faults and other types of unpredictable events will cause interruptions in the supply to customers. It thus expresses the robustness of the system to withstand imminent disturbances.
Existing operating conditions and the probability of potential faults thus affect power system security. The former are increasingly influenced by the integration and the resulting volatile feed-in of renewable energies. In addition, the n-1 criterion and the existing protection security play a major role in the event of a fault. In the past years, operating and fault conditions have become more and more similar, so both power system security and protection security are becoming increasingly important. In addition, system security is closely linked to the concept of system stability. [47], [48]

6.2.2 Power System Stability

Power system stability describes the ability of an electric power system to continuously maintain an intact and synchronous operation of all operating devices as well as a state of equilibrium after a physical disturbance or fault, with most system variables bounded. Thus, it is the most important factor in maintaining power system security. The interaction of all the interconnected primary and secondary equipment of the power system is a high-order multi-dimensional process, whose overall response is composed of the individual responses of all the devices involved. However, depending on the current operating conditions, the topology of the power system, the type of disturbance, the control behavior of feeders and loads, and the behavior of the protection system, there may be a persistent imbalance in the system, which in turn may lead to various forms of instability. [47], [48]

Figure 22 shows the effects of a fault on the system state and thus on the system stability by means of three different, colored courses, which in turn can be divided into three different time periods. First, the power system is in a state prior to a fault, which usually corresponds to a stable and fault-free operating state. Then, with the occurrence of a fault, the pre-fault state changes to a faulty and dangerous state. A strong reaction of the system occurs, and depending on their physical nature, both the primary and secondary equipment reacts according to their predetermined algorithms. This fault period lasts until the faulted section has been completely isolated from the rest of the system by protective device tripping, or until the fault extinguishes itself. This is followed by the post-fault period. In this period, the stability is still at risk and it is necessary to return to an old or new stable operating point and to

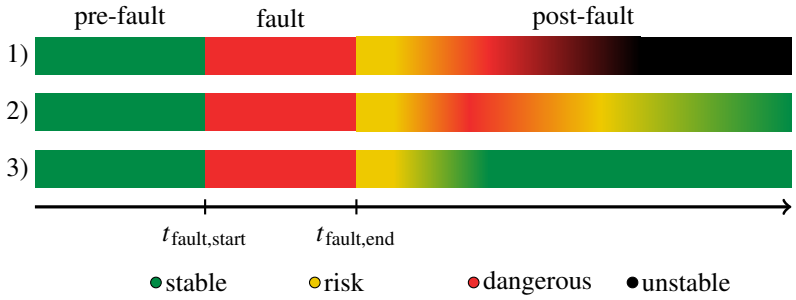

Figure 22: Subdivision of the temporal course of a fault into the three periods pre-fault, fault and post-fault, as well as presentation of three different developments of power system stability after fault clearing.

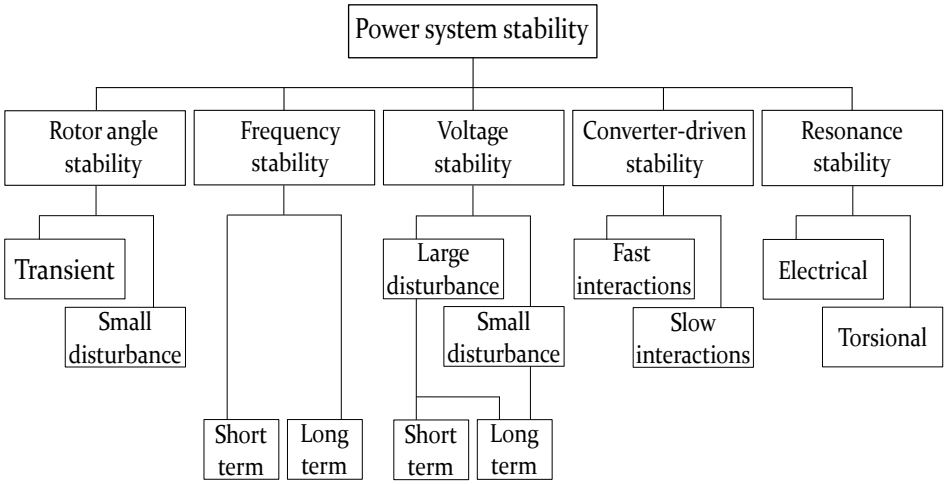

Figure 23: Overview of the main criteria of power system stability. Based on [49].

avoid an unstable state in any case. The latter is often the result of further unintentional protection tripping, which can eventually lead to a blackout.

To make the concept of power system stability more tangible and understandable, it is usually divided into the main categories of rotor angle stability, frequency stability, and voltage stability. [47], [48] Due to the significant increase of devices with power electronic converter interface such as wind energy and photovoltaic systems, Flexible AC Transmission Systems (FACTS) and High Voltage Direct Current (HVDC) systems as well as storages and loads with power converters, the concept of stability has recently been extended to include the criteria of resonance stability and converter controlled stability [49]. Figure 23 graphically represents the different types of system stability.

The impact of various disturbances, dynamic events and controllers can be roughly divided into four temporal ranges. In the nanosecond to millisecond time range, wave phenomena mainly have an impact. In the range of microseconds to one second, electromagnetic phenomena take place. In the time range from milliseconds to minutes, electromechanical phenomena dominate, and in the range from seconds to hours, mainly thermodynamic phenomena have an effect. Electromechanical effects can be further divided into short-term (a few seconds) and long-term (a few minutes) events, which mainly affect voltage and frequency stability.

In the area of voltage and rotor angle stability, a distinction can be made between small and large or transient disturbances. Small disturbances are disturbances for which the system dynamics can still be calculated with linearized equations. These include disturbances that result in very slow changes over time. Examples would be the failure of a line that is only lightly loaded or the slow and continuous increase of a load. In contrast, large or transient disturbances cause a sudden and significant change in the power system, require the action of protection systems, and have a critical impact on system stability.

Converter-driven stability can be divided into fast and slow interactions. The subdivision is based on the frequency of the phenomena that occur. Phenomena with a high frequency in the range of 10 Hz to 100 Hz, possibly kHz, belong to fast interactions. Phenomena with frequencies of 10 Hz and less belong to slow interactions.

Resonance stability is divided into torsional and purely electrical resonance. In the first case, resonant oscillations occur with the drive train of a turbine generator. In the second case, the electrical characteristics of a generator are involved. [49], [50]

6.2.2.1 Rotor Angle Stability

The active power delivered by a synchronous machine to the power system depends on the amplitude of the rotor and stator voltage and the difference angle of the two voltage phasors, the so-called rotor angle. The same principle applies in general to the transmission of active power between two nodes in an AC system. This always requires a voltage angle difference between the respective voltage phasors, which rotate at the same frequency in steady state. [51]
In the event of the occurrence of a large disturbance such as a short circuit, this strongly excites the entire power system including all connected synchronous machines and brings them out of their state of equilibrium. The rotor angle

stability, for large disturbances also called transient stability, is the then necessary ability of all synchronous machines to maintain synchronism. It occurs immediately after, in some cases even during, the actual fault and is a first indicator of whether the power system remains stable. Crucial for rotor angle stability is the balance between electromagnetic and mechanical torque of the individual machines. In steady state, the two correspond to each other and the speed of each machine remains constant. If the equilibrium is disturbed, an imbalance occurs and thus the rotor speeds increases or decreases. If the rotor speed of one machine increases relative to the other machines, the angular position of the rotor shifts forward. The resulting angular difference then ensures that the faster-turning machine supplies a greater proportion of the load, which counteracts the speed and angular difference. However, the relationship between angle and transmitted power is not linear. Beyond a certain limit, which in static stability corresponds to an angular difference of 90°, the increase in angular difference is accompanied by a decrease in active power transmitted, so that the angular distance increases continuously. In the case of rotor angle stability, larger angles than 90° can also be achieved due to the flux linkage of the stator and rotor windings and the inertia of the turbine set. This implies that there is a certain inherent flexibility and reserve in the system.
Machine instability follows when the power system is unable to absorb the kinetic energy of the synchronous machine, causing it to decelerate. [47], [52] In addition, electromechanical transients often occur between individual synchronous machines or coherent groups as a result of angle differences, which then run synchronously among themselves but not to the entire system. The resulting power swings can then lead to unintentional tripping of protective devices [53].

In power systems of the future, which will have a significantly higher penetration of infeeds via power converters and, in return, fewer or even eventually no rotating machines at all, the overall inertia of the power system will decrease, whereby the relevance of the rotor angle stability as a characterizing criterion will initially increase in the transition phase and eventually disappear. The displacement of synchronous generation by converter interfaced generation and the associated decrease in physical inertia leads to a change in the damping characteristics of the overall system. This in turn results in changing electromechanical transients and power oscillations and could be accompanied by a decrease in rotor angular stability. Concrete effects are currently the subject of research and depend mainly on the control and location of the power converter interfaced generation as well as the power system design and the type of disturbance [49].

6.2.2.2 Frequency Stability

A frequency deviation is the result of an imbalance between generated and consumed active power in the system. All devices that generate and consume active power therefore influence the frequency. When there is a shortfall in the generation of active power, the frequency decreases, while it increases when there is a surplus of active power. Grid operators are tasked with maintaining frequency within a narrow band around the nominal frequency at all times. Frequency stability is defined as the ability to keep the frequency as constant as possible after the occurrence of a disturbance, thus maintaining the balance between generation and load in the system [47]. It is a fundamental requirement for a stable power system. When a large disturbance occurs, it usually results in high frequency excursions, but also affects power flow, voltage, and rotor angle stability. All electrical equipment connected to the system responds physically and/or in terms of its control to frequency changes. [47]

When a synchronous machine loses synchronism with the power system, its frequency continuously increases until the overfrequency protection shuts it down. As a result, the system loses generating power, which in turn must be provided from reserves. Otherwise, loads must be disconnected by load shedding to restore balance. Small generating units are more vulnerable than the large rotating masses of the larger power plants. In turn, the disconnection of generating units and loads can have a significant impact on voltage, further affecting the balance between generation and consumption. As a result, other protective functions may be triggered, causing the system to break down into subsystems. Within the subsystems, further frequency stability problems may then occur due to a lack of generation and/or load. Therefore, for effective frequency stability studies, it is important to include and simulate protective devices, generator protection, and load shedding functions. [47], [52], [53]

Unlike synchronous machines, converter interfaced generation units have no physical inertia. In power systems with increasing feed-in from power converters, this fact has a negative impact on frequency stability in the presence of large disturbances such as short circuits. The low inertia makes faster frequency excursions and earlier instabilities more likely. Nonetheless, generating units coupled to power converters can make a faster contribution to primary control than synchronous machines via dedicated controls, since the response time is mainly determined by the electronic devices and not by mechanical systems such as the turbine. This has a positive effect on frequency stability. However, the cost of maintaining sufficient reserves is economically

more expensive, since the power electronic components must be oversized and storage must be installed to accommodate them. [49]

6.2.2.3 Voltage Stability

Voltage plays a central role in the transmission of electrical power. Alongside frequency, it is another characteristic of the QoS of the power system and must always be kept within a certain band. Voltage stability is therefore understood as the ability to keep the voltage as constant as possible at all nodes of the system [47]. In contrast to frequency, voltage can vary more locally, i.e. from node to node. It is largely determined by the transmission capability of the equipment in the system and is less oriented to the balance between generation and load. Therefore, the amount of transmitted reactive power also has a greater influence on voltage stability than that of active power. If there is an increase in reactive power demand that cannot be met locally, it must be transmitted from further away, causing the voltage to drop even more. This effect can be amplified by the behavior of various loads should they then have an increased reactive power demand due to the lower voltage. In the case of a steady voltage drop, the maximum transmission capacity of the grid is reached at some point and a voltage collapse, i.e. loss of voltage stability, is the consequence. [52], [54]

In conclusion, it can be said that the voltage stability focuses on the magnitudes of the different voltage phasors of all grid nodes. The frequency stability in turn depends on the angular velocities of all voltage phasors and the rotor angle stability is based on the voltage angle differences of the respective phasors.

6.2.2.4 Converter-driven Stability

The control and thus response behavior of generating units with power converters differs fundamentally from the behavior of classic synchronous machines. Depending on the design of the power converter as well as the filters applied, the specified operating behavior, the control mode used and the suitability for grid parallel operation, power converters can be classified and exhibit different dynamic behavior [55]. A key feature of power converter systems is the significantly faster control, which is also accompanied by a significantly faster overall behavior. This can lead to stability problems when control systems of different systems such as converter interfaced generation units, HVDC or FACTS interact rapidly with power system components or other power electronic equipment. In addition, high-frequency switching of power electronic components can cause harmonic oscillations and hence resonances. These effects, with frequencies typically ranging from hundreds to several kilohertz,

are categorized as fast-interactions. This contrasts with slow-interactions phenomena, which typically have 10 Hz and less, and are characterized by slow interactions of power electronic components with other components of the power system. An example would be the classical interaction with the electromechanics of synchronous generators. [49]

6.2.2.5 Resonance Stability

In general, resonance is the amplified oscillation with higher amplitude of an oscillating element or system when it is periodically excited from the outside. Depending on the damping, the excitation occurs at a frequency equal to or close to the natural frequency of the system, which is referred to as harmonic resonance. Should a system be excited via nonlinear oscillations, subharmonic resonance occurs. The excitation frequency that leads to resonance is the resonant frequency. In the electrical power system, excitations of various kinds can cause equipment or components to exchange energy periodically, resulting in resonance if damping is inadequate. The consequences are increases in voltage, current and torque. If threshold values are exceeded, the system is resonance unstable. [49] According to [49], the new term resonance stability includes subsynchronous resonances, which can be divided into the categories torsional and electrical. Here, either the drive train of a turbine generator or the electrical characteristics of a generator with a series compensation oscillate in the system. In the former, the electrical energy system and a turbine generator exchange large amounts of energy at one of the natural frequencies of the mechanical shaft of the drive train of a turbine generator. In other forms, energy exchange occurs with rapidly regulated systems such as HVDC and FACTS, and with power system stabilizers (PSS) regulated machines. In the case of the latter, only doubly-fed asynchronous machines seem to be affected, since they are induction generators directly connected to the grid.

6.2.2.6 Summary

In summary, an energy system is only considered sufficiently stable if all stability criteria are stable in themselves. However, these are all interrelated and influence each other. A concrete separation and separate consideration is hardly possible. Nevertheless, all problems and instabilities express themselves at some point in the voltage magnitudes, frequency, and the respective rotor or transmission angles of the system. These are the fundamental characteristics of electrical power systems. In order to prevent instabilities caused by oscillations, a good layout and design of the components to be connected and the controls used are required above all, as well as system studies that identify

problems beforehand. When considering the concept of stability, the size, complexity and diversity of the power system becomes apparent. Maintaining stability is a major challenge. In the event of disturbances, the protection system must take action to protect the stability as well as the security of the system.

6.3 Protection Systems

A protection system is a system consisting of one or more technical devices that is used to detect faults in the power system and isolate the affected components by opening breakers. The goal is to minimize the effects of a fault so that the rest of the system remains stable and continues to run. The devices used for this purpose are special protective devices or intelligent electronic and thus programmable protective devices that receive measurement data via interfaces and can communicate with each other and the environment.

6.3.1 Protection Reliability

Protection reliability describes the probability that a protection system will always operate correctly. This means that it reacts correctly both in normal operation and during the event of faults, which means that it also correctly does not react when this is required. The most important and decisive criteria for this are security and dependability. [56]

6.3.2 Protection Security

Protection security expresses the degree of probability that a protection system will not react when faults for which it is not responsible are present. It thus describes the quality that there are no unnecessary trips under all operating conditions and faults caused by the protection system. Thus, security is a subset of reliability and is closely related to the concept of selectivity. [56]

6.3.3 Protection Dependability

Protection dependability expresses the degree of probability that a protection system will respond when faults, for which it is responsible, are present. It thus describes the quality that all faults, for which the protection system is partly responsible, will be isolated. [56]

6.3.4 Protection Selectivity

Selectivity describes the ability of all protective devices involved in the clearing of a fault to react in such a way that as few components as possible are disconnected from the power system in the event of a fault. This is intended to minimize the effects of a fault. A distinction can be made between absolute and relative selectivity. Absolute selectivity is achieved by protection systems that are specially designed for a component or a specific protection zone. This includes, among other things, differential protection. Relative selectivity is achieved by coordinating different protective devices. In this case, different devices react to one and the same fault, but the use of different protection functions such as the overcurrent protection or the impedance protection and their settings ensure that the overall behavior of the protection system is selective. Furthermore, via suitable protection coordination, back-up functionality can be provided to ensure that both security and dependability requirements are met. However, there is often a fine line between the two criteria, as they place conflicting demands on the setting values. [56], [57]

6.3.5 Protection Sensitivity

Sensitivity describes the sensibility of a protection system to recognize a fault as such via the incoming measured values. In this respect, digital relays are much more sensitive than earlier electromechanical devices. However, there are faults such as high-impedance ground faults that still pose a challenge. [58]

6.3.6 Fault Clearing Time

Fault clearing time is the time that elapses between the occurrence of a fault and its complete isolation from the rest of the power system.

6.3.7 Fault Tripping Time

The fault tripping time is the time that elapses until all current paths to the fault are completely disconnected and thus currentless. In the case of distributed generation units, a fault may already be isolated from the power system, but the generation unit's system protection switches off later.

What we do today determines what the world will look like tomorrow.

Marie Ebner von Eschenbach
Moravian-Austrian writer
* 1830, + 1916

7 Security Assessment Systems

In order to be able to determine, calculate and quantify the security of both power and protection systems in the course of increasingly progressive changes in the power system landscape, automated security analysis systems, which can also be referred to as tools, have become increasingly popular. In recent decades, two systems in particular have stood out. One is the Dynamic Security Assessment (DSA) system, which assesses power system security based on stability during transient disturbances [48], [59]–[64], and secondly, the Protection Security Assessment (PSA) system, which assesses the security of a protection system based on its selective behavior during short circuits [57], [65]–[69]. Both systems are presented below.

7.1 Protection Security Assessment

PSA systems have meanwhile already become part of some simulation and analysis software and are listed there, for example, under the names *Protection Analysis* (PSS©Sincal by Siemens AG) or *Protection Audit* (PowerFactory by DIgSILENT GmbH). All systems share the common basic principle of assessing and identifying potential weaknesses in the protection system or in protection coordination. To do this, the tools use a variety of quasi-stationary short-circuit current calculations simulated at a predefined distance on each path within the system. This type of approach is also called simulation of a *running fault*. The type of fault as well as the amount of fault resistance, failing protective devices or failing breakers can usually be set as well. Within each fault simulation the response of the protection system to the fault is simulated. After each trip of a protective device and thus opening of a breaker,

the short-circuit simulation is recalculated and continued under the changed topology. The process is repeated until all reactions have been completed. At the end, the respective fault clearing time and the concrete pickup and tripping behavior of all protective devices in the power system are obtained for each fault. Finally, the evaluation is carried out for each simulated fault using established indices. The focus is primarily on the tripping behavior of all protective devices involved. In this way, selective fault clearings, under- and over-functions as well as no fault clearings can be quickly identified and graphically displayed in tabular form. PSA systems thus assess the security and dependability of a protection system, relying mainly on selectivity criteria.

Conducted PSA-studies, in which different power system configurations and situations are checked, currently take place exclusively offline, so that the results are not directly used further for the assessment of a currently present overall system state. This could change in the future, as the operational state and fault state become closer together, making it more difficult to clearly separate them in all situations. Thus, the results from PSA-studies gain importance, which could perspectively also lead to measures like a direct adaptation of the present protection system. What is not yet available, however, is an automated optimization of protection coordination based on PSA results.

In [68], the possibility of improving power system protection as a whole based on deterministic optimization methods is investigated. In a first step, the theoretical obligation to trip on a fault is first determined for each protective device. A distinction is made between the responsibility as main or backup protection. In a second step, mathematical equations and inequalities are established to test the suitability, adjustability and boundedness of the protection system. The adjustability consisting of measurement range and selectivity analysis is given special attention. Non-convex, mixed-integer and non-linear optimization problems arise, which cannot be solved deterministically without simplifications and constraints.
Independently and decoupled from the optimization approach, an PSA-based method with extended indices is also presented. For this, [68] introduces the three top quality assessment indices *q_protection*, *q_system* and *q_overall*. These are derived from the evaluation indices *fault recovery status*, *fault recovery time*, *line failure*, *additional line failure*, *load failure*, *additional load failure*, and *cost*. Each fault is evaluated according to these indices, and the results are then proportionally assigned to the respective main indices using a self-determined weighting matrix and the Analytical Hierarchy Process (AHP) method. The calculation of an overall return value is omitted in favor of ordered boxplots resulting for each fault simulation and main index. The

specific evaluation functions can be found in [68].
Furthermore, [68] establishes another scheme for direct assessment of all protective devices using the device-dependent quality factor *q_ied*. For this purpose, the indices *dependability*, *security* and *tripping times* are used, which in turn result from the evaluation of the pickup and tripping behavior of all protective devices in the power system. They offset the number of trips of each protection device with the number of simulated faults inside and outside the respective protection zone of each protection device. In addition, the number of simulated faults with overfunction and the total number of simulated faults are used. In this way, the evaluation of a protective device is not based solely on the evaluation of a single fault, but incorporates the results of all simulated faults. According to [52], this sum can also be called a *fault package* with *nF* faults.

A method first presented in [67] and extended in [P70] and [P71] for direct assessment of the protection settings of all protective devices present in the power system is not based on evaluation of protection reactions, but uses fuzzyfication to classify the quality of each setting value of all devices into the fuzzy sets *q_dependability* and *q_security*. Fuzzy sets allow a graded assignment of elements to sets, extending the otherwise binary classification in favor of a degree of membership. The quality of each protection setting is thus expressed based on a degree of membership in both criteria. A final arithmetic averaging of all fuzzy sets leads to an optimizable fitness function, which thus computes and returns a quality index or fitness value. In [P37] and [P71], the methodology was used to automatically determine new protection settings for all protective devices present in the power system simultaneously via an PSO method. This reveals the strength of the methodology, as the assessment requires no or only a few simulations and is thus not very computationally intensive. The results obtained showed good outcome and were checked for plausibility in [P71] using the classical PSA methodology of the simulation program PSS©Sincal. However, a shortcoming of the approach remains that an optimal assessment of the fuzzy methodology does not have to correspond to an optimal protection behavior. The best possible compromise of the fuzzy sets *q_dependability* and *q_security* does not necessarily lead to the desired tripping behavior, which is why a result of the fuzzy methodology must always be checked and optimized in another way in case of weaknesses.

An important aspect that PSA systems have neglected so far is the fact that the power system must return to a stable operating state after fault clearing. Due to the often historically separate consideration of protection systems and dynamic phenomena, this was mostly neglected and could not be simulated by

the almost exclusively used quasi-stationary short-circuit current calculations. However, large disturbances in the past years have shown that selective fault clearing does not necessarily lead to a return to a stable operating point. Influences such as electromechanical transients or re-adjusting load currents can lead to further undesirable and cascading trips after the actual fault, affecting grid stability. [72]–[74]

The DSA systems presented below are used to assess the security of the power system based on dynamic stability after the occurrence of faults.

7.2 Dynamic Security Assessment

Under the umbrella term DSA, a variety of different implementation types can be found. They all aim at assessing the security of the power system before and after a disturbance occurs and at classifying the effects of an event. The focus here is on severe events or failures that may occur in certain system states and threaten the security of the power system. The ultimate goal is to verify the dynamic response of all primary elements and controllers to ensure that the overall system remains stable and that any balancing events that occur subside. The power system should always be at a stable operating point and return to one after displacement. [48], [63]

For a complete examination of security, all operating criteria must be analyzed before and after a disturbance. This includes the thermal load of all system elements as well as the stability of the power system, which can be quantified in the form of the various stability criteria. The simulations and calculations required for this are technically challenging and usually require considerable computing effort. Depending on the application purpose, the available time and the necessary effort for the investigations, the DSA system is therefore used as an offline or online tool. Both tools pursue the same goals and can be used to identify critical operating points and work around them during system operation. Offline analyses are mainly performed by system and operations planning. During system operation, online analyses are used by power system operators to check the current power system situation in real time. For this purpose, the existing topology as well as the load flow, which can be derived from snapshots of the actual system state, is used as a starting point for the subsequent analyses. [61], [63], [75]

[63] and [64] present specific indices used to assess system stability. These are also likely to be used to a large extent in the Siemens AG model-based DSA tool called SIGUARD©DSA. The tool can be used both online in the control room and offline in operations planning. The indices are designed to assess

system stability as well as dynamic performance using RMS simulations in the time domain. They are based on the evaluation of occurred rotor angles, frequencies, voltages, load flows, failures and utilization of resources. Nine evaluation indices are used in [63] to form the overall stability index *q_stability* and another three evaluation indices are used to form the final security index *q_security*, which are merged at the end via a multilevel fuzzy inference system. The evaluation indices *frequency gradient*, *maximum frequency deviation* and *frequency recovery time* evaluate the frequencies at nodes where generator units feed in. The *quasi stationary voltage*, *dynamic voltage* and *voltage ride through* indices evaluate the voltage at specific nodes with respect to previously defined allowable voltage limits. The *angle* index results from the maximum rotor angular deflection occurred with respect to a previously defined allowable angle. The *line power flow* and *transformer power flow* indices evaluate the utilization of lines and transformers. The *load shedding* index offsets the lost load against the total load. The *small signal stability* index is used to evaluate the small signal stability and the *energy margin* index is used for the energy margin. The concrete evaluation functions of the indices can be found in [63] and [64].

From the point of view of the protection system, however, the design of many indices is problematic because they are designed in such a way that no protection system is or can be active during the dynamic simulations. Thus, often only the worst point that occurred or the largest deviation that occurred at a location in the system is used to evaluate and thus calculate the respective index. Thus, mainly the effects of the first disturbance are evaluated. The subsequent course with further potential reactions of the protection system can only be recorded if cascading false trips lead to an even worse situation than the actual disturbance. Otherwise, the effects by the protection system in the post-fault cannot be captured. This issue can be well explained by the widely known and used Rate of Change of Frequency (ROCOF) index (df/dt) or Frequency Gradient Index (FGI) from [63] and [64]. Both indices are a measure to describe the inertia of a system. Depending on the initial ROCOF in response to an event, both indices attempt to describe the dynamic security of the system. However, the actual rate of frequency change from the occurrence of the disturbance, through the clearing, to the return to a stable operating point does not matter. This means that unintentional false tripping, necessary disconnections of generators or loads, and other interactions between primary and secondary resources as well as a possible division of the system into subsystems are not evaluated. This requires an evaluation of the time course. The mere rate of change as the initial response to a disturbance event is not sufficient. Another disadvantage of evaluating

only by the worst point is that a trip by protective devices immediately results in a poor evaluation for some indices. In this context, the disconnection of an out-of-step generator, the separation into two subsystems, the shedding of a load, or the unselective tripping of a protective device that isolates nodes from voltage, are not always to be equated with an instability or a serious event. Furthermore, the size of the power system under investigation is lost if the worst result alone determines the evaluation. In this context, large, meshed power systems are much more robust than small ones, and local deviations have less impact on the rest of the system. Many indices also base their relative evaluation on reference points at which protective devices would trigger. If this point is reached, only no protective device triggers in the simulation, so it is also not possible to understand how the dynamic stability would have developed. For this purpose, the corresponding index is set to its worst value. However, it cannot be determined in this way whether, for example, the disconnection of a generation unit would really lead a stability problem. This approach is particularly disadvantageous in the course of the energy transition and the associated disconnection of large power plants in favor of many smaller, distributed generation units. Last but not least, many indices only evaluate the operating point at the end of the simulation. The path that led there plays no role in these.

A first attempt to combine PSA and DSA in a tool that considers the behavior of protection systems during dynamic fault simulations is presented next.

7.3 Dynamic Protection Security Assessment

An initial approach to merging PSA and DSA in one tool was presented for the first time in [52] in the form of an Dynamic Protection Security Assessment (DPSA) tool. The focus here is on the assessment of the protection system in dynamic simulations and on the effects of further and thus non-selective protection tripping in the post-fault period caused by electromechanical interactions. DPSA thus extends classical DSA simulations by the level of the protection system, so that possible critical cascades and islanding can be detected. Due to the high computational complexity of the simulations, DPSA has initially been presented as a pure offline tool. The evaluation indices used aim to evaluate the behavior of the protection at the relay level and in the overall system and to identify weak points. Unlike DSA, the course of system stability does not play a role. [52]

Similar to the PSA tool from [68], different levels and main rating indices are used in the assessment. The goal is to create different ranking lists to quickly identify critical cases and protective devices. Thus, similar to the PSA system,

a running fault is simulated. All individual faults of the running fault, where protection settings, infeed and topology remain the same, are combined into one fault package.

The protection behavior in a fault event is evaluated using the three indices *behaviour pattern*, *security factor*, and an optional *no pickup* and summarized using a fuzzy inference system to form the *q_relay security* index. The *behaviour pattern* index thereby evaluates the number of pickups with subsequent fallback of all protective devices that have occurred on a fault. The degree of deterioration is set by an exponential function. The *security factor* index evaluates the duration of a trajectory within the zone characteristic of distance protection relays. Should an unintentional trip occur, both indices take the worst value. The *no pickup* index again evaluates for non-pickedup distance protection devices, the distance of the measured impedance trajectory to the outer zone boundary as well as its direction of movement and duration of stay near the zone. The final result is a ranking of all protective devices within a fault package. [52] The *q_relay security* index thus increasingly aims at evaluating the risk of unintentional tripping. Especially strong electromechanical interactions lead to a worse evaluation, but also enlarged zone characteristics have a disadvantageous effect in this kind of evaluation.

The five indices *trip occurrence*, *trip period*, *pickup occurance*, *pickup period* and *load power* are used to evaluate the effects of a fault. These are finally combined via an intermediate level to form the *q_contingency* index. The *trip occurence* and *trip period* indices evaluate the number and time period of unwanted trips in relation to the worst value in the fault package. The *pickup occurence* and *pickup period* indices evaluate the number and time period of pickups in relation to the fault package, and the *load power* index evaluates the load failure at the end of the simulation. [52] The advantage of the relative evaluation to the fault package is that outliers can be well identified via the ranking of all faults. However, the fact that an improvement of the worst fault in the fault package leads to a change of the relative reference for all faults is problematic, which means that all ratings tend to be worse. The final evaluation values therefore hardly allow any conclusion as to how difficult a fault really was. Especially if all faults in the fault package rank well, the relative reference is misleading.

The protection behavior in a fault package is evaluated via the *q_protection relay* index, which in turn is composed of the five indices *protection relay trip occurrence*, *weighted trip time*, *protection relay pickup occurrence*, *weighted pickup time* and *protection relay load power*. The goal is to rank all protective devices in the fault package. The *protection relay trip occurrence* index eval-

uates the number of unselective trips of the protective device related to the worst value of a protective device within the fault package. The *weighted trip time* index includes all faults where the protective device to be evaluated has tripped and there have been at least two trips separated in time. The time at which the protective device tripped is evaluated in relation to the first and last trip that resulted from the fault. The index is obtained as the worst value obtained by the device in all faults. The *protection relay pickup occurrence* index evaluates the number of pickups of the protective device relative to the largest number of pickups in the fault package. The *weighted pickup time* index is similar to the *weighted trip time* index, referring only to the pickup. The last index *protection relay load power* evaluates the participation of a protective device in a non-selective fault clearing with simultaneous load failure. For calculation, the failing load for each protective device is summed up and related to the worst value within the fault package. [52] The procedure provides a ranked list of all protective devices relative to all running faults in the power system. This allows the protection engineer to easily identify problematic protective devices. The problem of relative reference has already been discussed. Therefore, a final rating value does not exist for DPSA.

To improve the protection system, the use of inference mechanisms is proposed in [52]. These use a knowledge base as well as stored rules to suggest improvements based on the input data. The general approach is to compare the results of two sets of cases. If all boundary conditions are kept the same and only the protection setting is changed, conclusions about the better setting values can be drawn by comparison. In the interaction of dynamics and protection, this procedure was a novelty. However, with many existing protective devices in the system, the process is enormously time-consuming or can only be carried out in a generalized form, so that, for example, the third zone is reduced or increased for all distance protection devices. Individual adjustments for each device are almost impossible to achieve. A simple comparison can also be problematic if it is not clearly evident which fault package is clearly better and compromises have to be accepted.

DPSA's assessment does not focus on the stability of the power system. The security of the system is identified solely on the basis of the various indices, the majority of which evaluate the risk and behavior of all protective devices. For identifying cascading trips that severely compromise power system security, the system appears to be well suited. However, to realistically rank the impact of one or more unselective trips, time-delayed selective trips, or protective device failures in terms of power system security, it would also require an assessment of dynamic stability.

You can never solve problems with the same mindset that created them.

Albert Einstein
German physicist
* 1879, + 1955

8 Guiding Protection Security Assessment for Optimization

The previous chapter 7 describes in detail the current status as well as strengths and weaknesses of existing security assessment systems and their capabilities to consider protection systems in analyses. What all systems have in common is the lack of an effective mechanism that independently and automatically develops proposals for improving power system and protection security based on the respective systems.

The aim of this chapter is to develop a clear assessment system for protection coordination in multivariate power systems based on the basic concept of PSA, which can be used in the future to improve protection systems in a fully automated, reliable and efficient way via optimization methods. For this purpose, this must meet the following challenges:

- Representation of a fitness landscape that has, if possible, no or only a few local optima and only one global optimum. It should guide the optimization method during the optimization process and lead to improved and correct protection settings for all selected protective devices of the power system.
- Return a single overall assessment value that is conclusively composed and traceable. Relative references should be used only with respect to power system size. Otherwise, effects of one disturbance should always result in the same return value, independent of the assessment results of other disturbances.

- A change in the protection system or the setting values utilized by the protective devices should also lead to a change in the overall assessment, which means that no plateaus are formed within the fitness landscape. When using different indices, this means that a change in one index, will also lead to a change in the overall value. A subdivision into ranges or categories with the same return value is to be refrained from. Otherwise, a clear feedback for the optimization method is missing.
- The assessment system should be usable regardless of the selected power system type, voltage level, and existing generating units as well as loads, and should not be based on specifics of the particular system under study. Special features should be simulated and the assessment should be structured as generically and comprehensively as possible to allow the analysis of multivariate system states as well as all existing protective devices and protection functions.

To address these challenges, a new approach is needed, which has been published in [P76], [P77] and [P78]. It foresees to consider the performance of a protection system from a total system perspective and to focus on the actual main objective of the protection. As defined in chapter 6.3, a protection system should minimize the effects of disturbances and unwanted events so that the rest of the system can continue to operate as stably as possible. The new approach is therefore based on the simple as well as tangible assumption that a best possible protection system on the one hand isolates a fault, but on the other hand also leaves and keeps the rest of the power system in a best possible stable state after a fault. Thus, the focus should no longer be on the type of fault clearing, but on the quality of how well a protection system contributes to securing and maintaining the overall stability as well as the quality of supply. To this end, new assessment indices need to be designed that can qualitatively capture the impact and consequences of a disturbance on the overall system despite triggering protective devices. Previous indices that relied solely on traditional protection criteria such as security and dependability are no longer sufficient. While these still provide protection engineers with important information about where and which protective devices are not responding as expected based on classical coordination, they are not capable of assessing the various impacts on the power system. For example, they cannot capture the consequences of different non-selective or delayed fault clearings, making it impossible to compare and prioritize these fault cases. The new assessment approach must focus on the system state. All stability criteria from 6.2.2 express themselves via the voltages and currents present in the system. Therefore, these must be analyzed, evaluated, and combined

in such a way that a fitness function is created that provides a return value suitable for an optimization method. It must become clear which protection settings obtained lead to better overall system states so that a protection system can be improved in a fully automated, reliable and efficient manner. The goal here is not to measure the risk of instability or to accurately classify the stability of different power system states. More importantly, an improvement of the fitness value also represents an improvement of the overall system state in reality. The extent to which the results can be translated into a linguistic rating system such as "good", "at risk" or "unstable" is of secondary importance. The assessment system must meet the following challenges for this:

- Consistent and coherent evaluation of all primary and secondary system responses and their impact on power system stability and quality of supply during the fault and post-fault periods.
- Consideration of various protective responses that could range from selective fault clearing to cascading tripping, as well as load and generation disconnections and the resulting possible partial and islanding with different frequencies, centers of inertia, and voltages.
- Distinguishing the effects of different disturbance types, locations, and durations, which in turn lead to different assessment results and thus fitness values, so that they can be compared and put into context. This allows an optimization method to make trade-offs.

The following chapters introduce the indices of the new assessment approach. These can be divided into four different categories: dynamic stability, supply reliability, protection security and guiding penalty.

8.1 Dynamic Stability

The stability indices are based on the evaluation of amplitude, angular frequency and angular difference of different voltage phasors resulting from simulations, in order to evaluate the stability of the power system. For this purpose, it is necessary to evaluate the different courses of the signals in a coherent and consistent way, despite protection trips, control interventions, load disconnections and other measures.
Coherent in this context means that the evaluation is not logically contradictory. This implies that the various evaluation steps build on each other, are interconnected, and that the entire evaluation chain is traceable. For example, a specific disturbance event, such as a three-phase short circuit with an exact length at a defined location in an unaltered power system, must always lead to the same evaluation result. In addition, it is important to capture

and account for events in the post-fault period. An initial disturbance event may not initially have much effect on the stability of the system. However, a later false trip of a protective device can lead to serious, negative effects on stability. Therefore, the complete course of a signal must be evaluated in a comprehensible way and must be included in the final result.
At the same time, the evaluation must be consistent. This means that it is free of contradictions and without gaps. Applied to signal courses, this means that dips, oscillations, undershoots or overshoots of limit values, the transition or the return to certain states are included and plausibly combined and evaluated. The evaluations of individual criteria must not conflict with each other, but must be able to stand side by side. For this purpose, it is also necessary to analyze the courses of events as a whole. The basis for this is the evaluation by windows explained in the following.

8.1.1 Window Evaluation

The Window Evaluation (WE) is used to correctly detect and evaluate various temporal events located in the signal curves to be analyzed. It was first introduced in [P78] and [P79]. Similar to the Short-Time Fourier Transform (STFT) and the Wavelet Transform (WT), WE passes different analysis windows stepwise over a signal to be transformed in order to extract certain features from the signal. In the STFT, a Fourier transform is performed within the windows. In the WT, oscillating and mean-free window functions, called wavelets, are used to compute the convolution integral as the wavelets are shifted. The WE method now makes use of elements of the STFT and the WT. Different rectangular window functions $g_w(t)$ of different length with a height of one are used, which are called *time windows* in the following and are also shifted over the signal $f(t)$ to be evaluated. A height of one is used because a prerequisite of the WE is that the best value of the signal to be evaluated is one and the worst value to be assumed is zero. While shifting the time window, the convolution integral between the time signal $f(t)$ to be examined and the respective w-th window $g_w(t)$ is now formed according to (42). Convolution of the functions $f(\lambda)$ and $g_w(t-\lambda)$ calculates the common area for every displacement of the functions, yielding the overlapping area at time t in each case. The process is thus a nonlinear transformation. Using multiple time windows nW with different lengths results in multiple transformed signals $h_w(t)$, thus extracting different information from $f(t)$. Narrow windows allow to capture mainly short-term, strong events. In turn, as the width of the windows increases, phenomena of longer duration can be considered. The time period considered $[t_s,\ t_e]$ depends on the simulations previously performed, which lead to the signals $f(t)$ to be evaluated, and the temporal

section to be evaluated. Since all simulations always start at $t = 0$ and end at $t = t_{sim}$, the maximum period under consideration lies in the interval [0, t_{sim}] with the condition $0 \leq t_s \leq t_e \leq t_{sim}$. Depending on the time period under consideration, only the fault period or the post-fault period can also be included in the evaluation.

$$\begin{aligned} h_w(t) &= f(t) * g_w(t) \\ &= \int_{t_s}^{t_e} f(\lambda) g_w(t-\lambda) d\lambda \end{aligned} \tag{42}$$

In order to evaluate a simulated time signal $x(t)$ using the WE method, the signal must first be normalized and transformed into the value range [0, 1] according to (43). Subsequently, the signal is linearized over the range of values [X_{min} , X_{max}] to be defined beforehand using (44), which finally leads to the signal $f(x)$ that can be further used for the WE method. The different transformation steps are shown in Figure 24 using an exemplary voltage time signal as $x(t)$.

$$f_{01}(t) = \begin{cases} x(t) & x(t) \leq 1 \\ 1 - (x(t) - 1)\dfrac{1 - X_{\text{min}}}{X_{\text{max}} - 1} & x(t) > 1 \end{cases} \tag{43}$$

$$f(t) = \begin{cases} 0 & f_{01}(t) < X_{\text{min}} \\ \dfrac{f_{01}(t) - X_{\text{min}}}{1 - X_{\text{min}}} & \text{otherwise} \end{cases} \tag{44}$$

Finally, in order to calculate the resulting evaluation and thus return value from all univariate signals $h_w(t)$, an averaging of the minimum values is performed according to (45). Since it is established via nomination that one is the best and zero is the worst value of the signal under investigation, a minimum function can be used to capture and extract the worst state that occurred in each case. The most negative effects of an incident disturbance event, including all subsequent reactions in different time ranges, are determined via the windows of different widths. The method is thus independent of the type and duration of a disturbance as well as the timing of further reactions.

$$WE_{\text{min}}(x(t)) = \frac{1}{nW} \sum_{w=1}^{nW} \min_{t \in [t_s, t_e]} [h_w(t)] \tag{45}$$

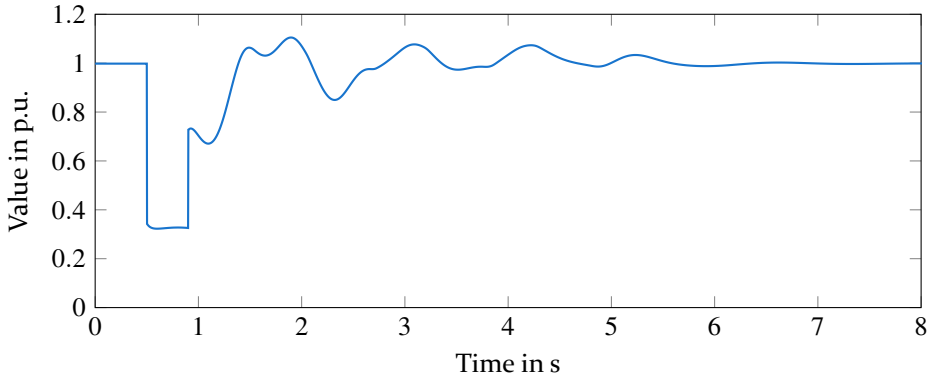

(a) Original time signal $x(t)$

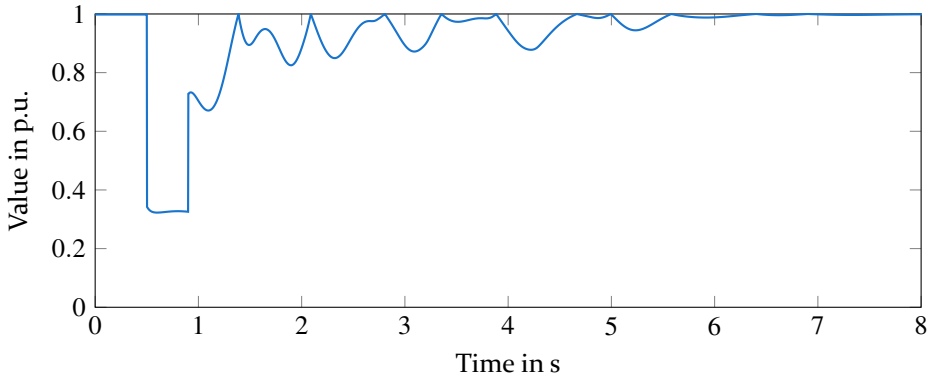

(b) Transformed signal $f_{01}(t)$

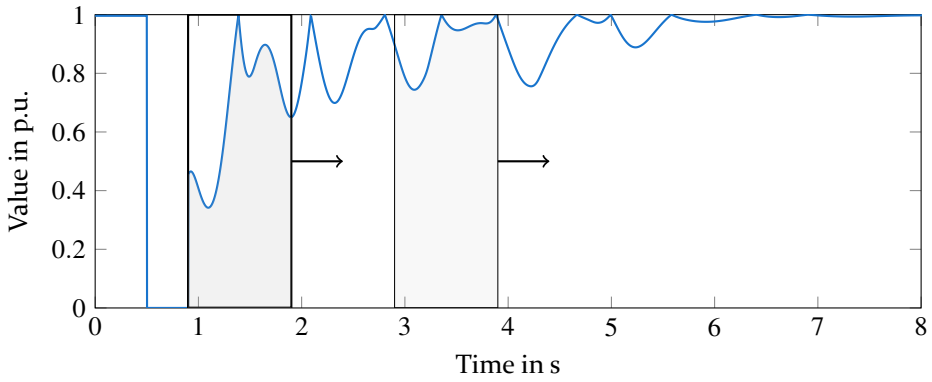

(c) Linerized and transformed signal $f(t)$

Figure 24: Graphical illustration of the Window Evaluation. The signal to be evaluated $x(t)$ is first normalized and then linearized leading to $f(t)$. After that, the convolution integral between $f(t)$ and different time windows can be calculated.

In the following, the new indices, which among other things use the WE method to evaluate voltage, rotor angle and frequency curves are presented.

8.1.2 Voltage Funnel Index

The Voltage Funnel Index (VFI) quantifies the size of a voltage funnel developing over time and is defined by (46). It thus represents a measure of the spread of a voltage dip within the whole power system caused by a disturbance or other events. In this respect, it is a quantitative evaluation parameter that includes the voltages $u_i(t)$ of all nodes of the system nN. The evaluation basis are the limits $U_{\min}$ and $U_{\max}$ to be defined. Within these limits, the voltage $u_i(t)$ of i-th node is considered acceptable. Outside the limits, the voltage band is considered violated and the evaluation value $EV_i(t)$ takes the value zero. The index is the average of all individual node ratings from the start time point t_s to the end time point t_e. It ranges from one for the case that no violation of the voltage band occurs to zero for the case that the voltage at all nodes violates the voltage band during the entire period under consideration.

$$\begin{aligned} \mathrm{VFI} &= \frac{1}{nN}\sum_{i=1}^{nN}\frac{1}{T}\int_{t_s}^{t_e} EV_{\mathrm{VFI},i}(t)\,dt \\ EV_{\mathrm{VFI},i}(t) &= \begin{cases} 1 & U_{\min} \le u_i(t) \le U_{\max} \\ 0 & \text{otherwise} \end{cases} \end{aligned} \tag{46}$$

8.1.3 Voltage Quality Index

The Voltage Quality Index (VQI), which was firstly introduced in [P78], is responsible for the qualitative evaluation of the voltage in the power system. It is intended to quantify the specific magnitude and duration of voltage dips and their recoveries at key nodes in the power system. It also includes longer lasting deviations and disconnections due to short circuits, switching operations or non-selective protection tripping. For this purpose, it evaluates the temporal voltage curves $u_i(t)$ of all load and generation nodes as well as all nodes with more than two connections to other nodes of the power system nVN. The evaluation function used is the WE method according to (47). All nodes that belong to the respective affected protection zone in case of a disturbance are excluded from the evaluation. These must and will be disconnected from the rest of the system even in the case of a plain selective fault clearing, whereby an evaluation would falsify the result in terms of voltage stability. For the use of the WE, after (43) and (44), the lower and upper limits

$U_{\min}$ and $U_{\max}$ have to be defined. These can be set individually for each node and for each time window depending on the system topology and applicable regulations and laws. In addition, it is possible to implement different voltage stability requirements for short-term and long-term voltage deviations. All used nodes are weighted depending on their number of connections nc_i to other nodes. Load and generation nodes have the same weighting as the nodes with the largest number of connections in the system. The sum of all weights describes nc_{total}. The index is obtained as the average value of all evaluated node voltages in the period t_s to t_e.

$$\text{VQI} = \frac{1}{nc_{\text{total}}} \sum_{i=1}^{nVN} nc_i \cdot WE_{\min}(u_i(t)) \tag{47}$$

8.1.4 Frequency Deviation Index

The Frequency Deviation Index (FDI) quantitatively evaluates according to (48) the frequency deviation of all feeder nodes nGN over time in the power system. It is thus a measure of the active power balance in the system and measures the ability of all connected generating units to maintain the system frequency in a defined frequency band despite a disturbance event. If a generating unit disconnects from the grid during an event for protection reasons, the frequency of the node is no longer included in the evaluation from the time of disconnection, since the generating unit no longer contributes to maintaining the system frequency. As a basis for the evaluation, the limits $F_{\min}$ and $F_{\max}$ are to be defined. Within these limits, the frequency $f_i(t)$ of the i-th node is considered acceptable. Outside the bounds, the frequency band is violated and the evaluation value $EV_i(t)$ takes the value zero. The index is the average of all node ratings from the start time t_s to the end time t_e. It ranges from one for the case when no violation of the frequency band occurs to zero for the case when the frequency violates the frequency band at all generating nodes during the considered time period.

$$\begin{aligned} \text{FDI} &= \frac{1}{nGN} \sum_{i=1}^{nGN} \frac{1}{T} \int_{t_s}^{t_e} EV_{\text{FDI},i}(t)dt \\ EV_{\text{FDI},i}(t) &= \begin{cases} 1 & F_{\min} \leq f_i(t) \leq F_{\max} \\ 0 & \text{otherwise} \end{cases} \end{aligned} \tag{48}$$

8.1.5 Frequency Quality Index

The Frequency Quality Index (VQI), which was firstly introduced in [P78], is responsible for the qualitative evaluation of frequency deviations in the power system. It is intended to quantify the specific magnitude, duration and recovery time of a deviation at all voltage generating nodes of the system nGN. This includes rotating generators but also converters in grid-forming operation. The temporal frequency curves $f_i(t)$ are evaluated by using the WE method according to (49). For the use of the WE, after (43) and (44), the lower and upper limits $F_{\min}$ and $F_{\max}$ have to be defined. These can be set individually for each generating unit and for each time window depending on the type of unit and regularities. Protection-related evaluations such as the maximum frequency deviation at which a generating unit would trip do not need to be taken into account, since the frequency protection is simulated as well. If a generating unit disconnects from the grid for protection reasons, the frequency of the node is no longer included in the evaluation from the time of disconnection, since the generating unit no longer contributes to frequency stability. The VQI thus evaluates the effectiveness of the primary and secondary control of the system as well as the ability of all generation units to keep the frequency as stable as possible. All nodes used are weighted proportionally of their power input S_i measured to the total generation of the system S_{total}. The index is obtained as the average value of all evaluated node frequencies in the period t_s to t_e.

$$\mathrm{FQI} = \frac{1}{S_{total}} \sum_{i=1}^{nGN} S_i \cdot WE_{\min}(f_i(t)) \tag{49}$$

8.1.6 Angle Deviation Index

The time characteristic of the rotor angle represents the basis for the stability consideration of synchronous generators. The Angle Deviation Index (ADI) quantitatively evaluates the rotor angles respectively the rotor angle differences of all synchronous generators in the power system. For this purpose, a suitable reference point is required for which the angle differences can be calculated in each case and evaluated on the basis of these. Various indices have already been presented in the literature for evaluating rotor angles. The Transient Severity or Transient Stability Index (TSI) according to (50) uses the largest angular difference $\Delta\delta_{\max}(t)$ between two machines defined by (51) for the

evaluation of the rotor angular stability. Here nG is the total number of generators in the system. [80]–[83]

$$\mathrm{TSI}(t) = \frac{360 - \Delta\delta_{\max}(t)}{360 + \Delta\delta_{\max}(t)} \tag{50}$$

$$\Delta\delta_{\max}(t) = \max \mid \delta_i(t) - \delta_j(t) \mid \quad \forall i, j \in 1, 2, ..nG \tag{51}$$

A variation of the TSI is the $\mathrm{TSI}_{\mathrm{COI}}$, which evaluates the maximum angular difference according to (52) to the center of inertia δ_{COI} defined by (53) and (54). Where nG refers to the number of generators in the system, M_i represents the moment of inertia of the i-th machine, M_{total} is the sum of all moment of inertias and K is the trajectory constant with a value between 120° and 360° [84].

$$\mathrm{TSI}_{\mathrm{COI}}(t) = \frac{K - \Delta\delta_{i,\mathrm{COI}}(t)}{K + \Delta\delta_{i,\mathrm{COI}}(t)} \tag{52}$$

$$\Delta\delta_{i,\mathrm{COI}}(t) = \mid \delta_i(t) - \delta_{\mathrm{COI}}(t) \mid \quad \forall i \in 1, 2, ..nG \tag{53}$$

$$\delta_{\mathrm{COI}}(t) = \frac{1}{M_{\mathrm{total}}} \sum_{i=1}^{nG} M_i \delta_i(t) \tag{54}$$

Depending on the exact intent and usage goal, the TSI and $\mathrm{TSI}_{\mathrm{COI}}$ can then be evaluated either at certain points in time, such as immediately or after a few cycles after the fault tripping, or at the end of the simulation time. However, both have disadvantages. Evaluating too early would not include renewed deterioration of rotor angular stability caused by false tripping of protective devices due to power swings. Applied at the end of the simulation, the most critical state that occurred would be lost, since the system can improve significantly again by the end of the simulation. Alternatively, a minimum evaluation of the TSI curve would be possible, in which the worst occurring state is extracted over time. In this case, however, the information about the extent to which the system has improved is lost. To solve this issue, the ADI is introduced with 55. Since protection trips can split the grid into subsystems, the ADI considers all electrically interconnected machine groups

nGR separately. This makes it possible to suitably evaluate even different subsystems that may have formed as a result of protection tripping. When synchronous generators are tripped by protective functions, they no longer have any connection to the power system and thus to other generators. In that case, they then also no longer have any influence on the transient stability of the system, which is why they are only included in the evaluation until the time they are disconnected. However, this can also have a positive effect. Should a trip from an out-of-step generator occur, the index would improve again as a result. Thus, for each j-th group of machines of a subsystem, a separate COI_j is calculated from the total number of machines $nGGR$ in each group. The rotor angles of all interconnected synchronous machines at time t are included. Finally, for each i-th machine within the group, the difference angle $\Delta\delta_{j,i,\mathrm{COI}}(t)$ is calculated according to (53). The limit angle $A_{\max}$ must be defined as the basis for the evaluation. If $\Delta\delta_{j,i,\mathrm{COI}}(t)$ is smaller than $A_{\max}$, the rotor angle difference is considered acceptable. For larger angle differences, the security margin is considered violated and the evaluation value $EV_{j,i}(t)$ takes the value zero. The index is the average of all single machine evaluations of a group and finally the average of all subsystems from the start time t_s to the end time t_e. It ranges from one for the case where no violation of the security margin occurs to zero for the case where all machines have an angle difference greater than $A_{\max}$ to their COI_j during the entire period under consideration. The ADI thus quantifies the temporal rotor angle difference and indirectly also the angle reserves of all machines of the system.

$$\begin{aligned} \mathrm{AFI} &= \frac{1}{nGR}\sum_{j=1}^{nGR}\frac{1}{nGGR}\sum_{i=1}^{nGGR}\frac{1}{T}\int_{t_\mathrm{s}}^{t_\mathrm{e}} EV_{\mathrm{AFI},j,i}(t)\,dt \\ EV_{\mathrm{AFI},j,i}(t) &= \begin{cases} 1 & \Delta\delta_{j,i,\mathrm{COI}}(t) \le A_{\max} \\ 0 & \text{otherwise} \end{cases} \end{aligned} \tag{55}$$

8.1.7 Angle Quality Index

The Angle Quality Index (AQI) is proposed for the qualitative evaluation of all rotor angle deviations in the power system. It considers the exact rotor angle curves $\delta_i(t)$ of all connected generators and relates them to the respective inertia M_i of each machine. The basis is the Integral Square Generator Angle Index (ISGA), also known as Rotor Oscillation Index (ROI), known from the

literature, according to (56) [82], [85]. Here nG is the number of all machines in the system and M_{total} is the sum of all moments of inertia.

$$\begin{aligned} \text{ISGA} &= \frac{1}{T}\int_0^T M\delta 2(t)dt \\ M\delta 2(t) &= \sum_{i=1}^{nG}\frac{M_i}{M_{\text{total}}}\Delta\delta_{i,\text{COI}}(t)^2 \end{aligned} \tag{56}$$

The AQI, first introduced in [P78], is used to qualitatively evaluate the severity of stable and unstable transient events. It is an extension of the ROI and, like the ADI, allows the evaluation and hence formation of subsystems by protection trips. It is defined by (57), where nGR is the number of coherent machine groups and $nGGR$ is the number of machines within each group of each subsystem. If a generator is completely disconnected from the system by protection trips, then it will not be included in the various calculations from the time it is disconnected. While the ISGA forms the integral over the entire simulation period via the expression $M\delta 2(t)$ and thus calculates the time average weighted squared deviation of each generator to the center of inertia, the AQI uses the WE method and $x(t) = M\delta 2(t)$ an even more accurate evaluation technique. One difference from the other applications of the WE method here is that a maximum function rather than a minimum function is used at the end to extract the worst state for each window section. However, as usual, $x(t)$ must be converted to the value range [0,1] beforehand. For this purpose, the normalized value angle difference $\Delta\delta_{i,\text{COI},01}(t)$ is used before to calculate $M\delta 2(t)$ instead of $\Delta\delta_{i,\text{COI}}(t)$ according to 58. The upper limit $A_{\max}$ to be defined can be chosen individually, but should be less than or equal to 120°. $A_{\min}$ is clearly defined with 0° deviation.

$$\text{AQI} = 1 - \frac{1}{nG}\sum_{i=1}^{nGR} nGGR \cdot WE_{\max}(M\delta 2_i(t)) \tag{57}$$

$$\Delta\delta_{i,\text{COI},01}(t) = \begin{cases} \frac{\Delta\delta_{i,\text{COI}}(t)}{A_{\max}} & \Delta\delta_{i,\text{COI}}(t) \le X_{\max} \\ 1 & \text{otherwise} \end{cases} \tag{58}$$

8.1.8 Dynamic Stability Index

The Dynamic Stability Index (DSI) is calculated according to (59) as the average of all introduced stability indices of voltage, frequency and angle in the post-fault period. Thus, any improvement or deterioration of one of the indices also leads to a direct improvement or deterioration of the DSI, which gives it the necessary feedback to an optimization method. An individual weighting of the different indices is not necessary, since all indices are already sufficiently normalized via the maximum and minimum limits used and adapted to the legal as well as technical regulations. Only the post-fault period is considered, so that the dynamic stability is always evaluated under the same conditions and comparability between all faults is given. Faults of different duration will of course affect the post-fault period. However, a longer lasting fault does not necessarily lead to worse stability afterwards.

$$\mathrm{DSI} = \frac{1}{6}(\mathrm{VFI} + \mathrm{VQI} + \mathrm{FDI} + \mathrm{FQI} + \mathrm{AFI} + \mathrm{AQI}) \tag{59}$$

8.2 Supply Reliability

Maintaining overall system stability during and after a fault is an important aspect of ensuring reliability of supply and also allows the severity of faults to be measured. But the stability criterion alone is not sufficient to serve as the sole yardstick for the design of a protection system. The actual supply task as well as economic aspects and risk factors must also be taken into account so that the results of an optimization based on a guiding assessment are within the scope of a reasonable and, above all, applicable solution. In the following, the necessary indices of reliability of supply are presented, which together form the Supply Reliability Index (SRI).

8.2.1 Load Loss Index

The main task of a power supply system is to continuously provide the connected loads and thus customers with electrical energy. Disconnection of this for the sake of system stability or other criteria should only occur in extreme exceptions, which is why this criterion is of particular importance. If a short circuit occurs in the power system, the affected protection zone must be disconnected from the rest of the system. In this case, it cannot be avoided that loads are also disconnected. This circumstance is a matter of grid planning and not of the evaluation of the protection coordination, which takes place chronologically afterwards. However, further load disconnections due to, for example, unselective protection tripping should be avoided in any case.

The Load Loss Index (LLI) according to (60) evaluates additional and thus avoidable load disconnections. Here, S_{total} is the apparent power of all loads nLO still connected at the end of the simulation outside the protection zone affected by the fault. S_i is the nominal apparent power of the respective i-th load still connected. The LLI ranges from one for the case where no load at all has been disconnected unnecessarily to zero for the case where all loads in the system are no longer supplied. It is an index calculated entirely at the end of the post-fault period and therefore at the end of the simulation. A weighting of the various loads occurs via the amount of their nominal apparent power. This also determines how severe an unnecessary disconnection of a load is. Furthermore, this forms the basis for an optimization procedure to decide whether a load disconnection is justified in favor of other criteria.

$$\mathrm{LLI} = \frac{1}{S_{\mathrm{r},total}} \sum_{i=1}^{nLO} S_{\mathrm{r},i} \tag{60}$$

8.2.2 Fault Current Index

The goal to obtain as short fault durations as possible cannot always be ensured, especially if protective devices have to be coordinated with each other via time staggering. The question therefore arises as to when a short circuit may last longer and when it is better to clear it as quickly as possible. The most important criterion here is that the stability of the system is maintained, which is already covered by the proposed stability criteria. Otherwise, the decisive factor is how high the short-circuit current is and what damage it will cause, if it is not cleared in time. The damage can range from non-existent, to shortened lifetime, to excessive stretching of the conductor lines and thus danger to people and nature as well as destruction. Therefore, the Fault Current Index (FCI) evaluates the thermal short-circuit current capability of all lines and cables in the grid, taking into account the material property as well as the length and duration of the short-circuit current. Design basis is the 1 s short-time current density $S_{th,1s,r}$ according to (61) with the temperature coefficient α_{20}, the start temperature ϑ_s, the maximum allowed end temperature ϑ_e and the variable for the material property MP according to (62) with the specific heat capacity c, the density ρ and the specific conductivity κ_{20} of the respective line [86].

$$S_{\mathrm{th,1s,r}} = \sqrt{MP \cdot \ln \frac{1 + \alpha_{20}(\vartheta_e - 20\,^{\circ}\mathrm{C})}{1 + \alpha_{20}(\vartheta_s - 20\,^{\circ}\mathrm{C})}} \tag{61}$$

$$MP = \frac{c \cdot \rho \cdot \kappa_{20}}{\alpha_{20}} \tag{62}$$

The FCI is calculated via the ratio of the actually existing 1 s short-time current density $S_{\mathrm{th,1s}}$ to the 1 s rated short-time current density $S_{\mathrm{th,1s,r}}$ of the respective line according to (63). $S_{\mathrm{th,1s}}$ can be calculated using the equivalent thermal short-circuit current I_{th} and the cross-sectional area A according to (64). Here T_{f} is the fault duration, which ranges from the time of fault inception $t_{\mathrm{f,s}}$ to complete isolation of the fault from the rest of the system $t_{\mathrm{f,e}}$. The equivalent thermal short-circuit current is given by (65). The FCI is therefore a pure criterion of the fault period and evaluates the fault current flowing through all lines of the power system at fault time. It is as good as one for the case when the fault current seen by all lines is low and short, and takes the value zero in case all design short-time current densities are exceeded.

$$\mathrm{FCI} = \frac{1}{nL} \sum_{i=1}^{nL} 1 - \frac{S_{\mathrm{th,1s}}}{S_{\mathrm{th,1s,r}}} \tag{63}$$

$$S_{\mathrm{th,1s}} = \sqrt{\frac{I_{\mathrm{th}}^2 T_{\mathrm{f}}}{A}} \tag{64}$$

$$I_{\mathrm{th}}^2 T_{\mathrm{f}} = \int_{t_{\mathrm{f,s}}}^{t_{\mathrm{f,e}}} i^2(t) dt \tag{65}$$

8.2.3 Grid Loading Index

Every disconnection of a faulty area is accompanied by a change in the topology, which results in a new load flow in the power system. As a result, there is a new load flow in the power system, which generally leads to a higher load on the transmitting equipment, since the electrical energy is distributed over fewer components. This reduces the reserves of transmission capacity, which in turn reduces the robustness of the system against further faults and disturbances. In addition, further violations of equipment limits and subsequent tripping by protective devices can occur, which would further worsen the load flow. To prevent this, power systems are operated in a (n-1) secure manner, if possible,

to prevent chain reactions from the outset. Since the system stability may be acceptable in the post-fault period, but the load flow and thus the utilization of the equipment in the steady state may be at risk, the Grid Loading Index (GLI) to (66) is introduced to evaluate the transition range from just harmless to dangerously high system load. Here nL is the number of all lines in the power system except those that are part of the faulted protection zone. Up to the selectable current limit I_{lim}, $EV_i(t)$ gives a value of one for the time-dependent current $i_i(t)$. Beyond that, the value decreases linearly to a value of zero for $i_i(t) = I_n$. The GLI therefore takes a value of one for the case when the currents of all lines are less than I_{lim} in the time period considered, and zero for the case when all currents of all lines are greater than or equal to the current limit. Therefore, the utilization ratio of each line is evaluated as a function of the current with respect to its rated current and the current limit to be selected. The GLI thus evaluates the remaining transmission reserve as well as the risk of thermal overloads.

$$\begin{aligned} \text{GLI} &= \frac{1}{nL} \sum_{i=1}^{nL} \frac{1}{T} \int_{t_s}^{t_e} EV_{\text{GLI},i}(t)dt \\ EV_{\text{GLI},i}(t) &= \begin{cases} 1 & i_i(t) \leqslant I_{\text{lim}} \\ 0 & i_i(t) \geqslant I_n \\ 1 - \dfrac{i_i(t) - I_{\text{lim}}}{1 - I_{\text{lim}}} & \text{otherwise} \end{cases} \end{aligned} \tag{66}$$

8.2.4 Supply Reliability Index

The SRI is calculated according to (67) as the multiplication of all the supply reliability indices. Thus, any improvement or deterioration in any of the indices also leads to a direct improvement or deterioration in the SRI. Multiplication is used so that the deterioration of one index cannot be offset by the improvement of another. For example, unnecessary load loss must always lead to a deterioration in supply reliability.

$$\text{SRI} = \text{LLI} \cdot \text{FCI} \cdot \text{GLI} \tag{67}$$

8.3 Protection Security Index

For the protection engineer, selectivity is traditionally the benchmark of any protection assessment, since if complete selectivity is achieved for all faults, no more equipment than necessary is ever disconnected, thus minimizing the impact on the power system. In addition, the evaluation of selectivity

provides important information on where a protective device is likely to behave incorrectly and where there are still gaps in the protection coordination. In order to be able to evaluate the selectivity automatically, the responsibility of each protective device for a fault must be defined in advance, from which in turn the desired protective response can be derived. Thus, after taking into account all boundary conditions, there is either a trip command, trip prohibition or neutral expectation for a fault for each protective device. The starting point for the analysis are the protection zones that arise in the power system. These define contiguous devices that must be coherently isolated from the rest of the system in the event of a fault within the zone in order to achieve selective fault tripping. The protection zones are defined by the circuit breakers in the system and the associated protective devices. Based on this, different levels of responsibility can be defined for all protective devices in the system. These specify which devices should respond in sequence to a fault and disconnect it by opening the circuit breaker.

- Primary responsibility lies with all protective devices in the protection zone directly affected by a fault.
- Secondarily responsible for a fault are all protective devices of the directly adjacent protection zone.
- Tertiary responsibility applies to all protective devices located in the second adjacent protection zone to the fault location.

In this respect, a protective device is only responsible if the device is able and intended to detect and isolate the fault at all due to one of its protective functions. For example, direction-dependent functions and settings must be included. Also, responsibility only exists if there is an electrical connection from the rest of the power supply system via the circuit breaker to the fault location. Otherwise, from the point of view of selectivity, tripping is not necessary and there is neither a tripping requirement nor a tripping prohibition. If it should happen that the isolation of the fault results in a separate island system, then the analysis must be carried out from the point of view of both systems.

Based on the definition of the responsibility of each protective device, the desired protective response can be defined. Three scenarios must be distinguished here:

- There is no protective device which has higher priority for the fault: trip requirement.

- There is a protective device which has higher priority for the fault: trip prohibition.
- A protective device exists which has higher priority for the fault, but this device or the associated circuit breaker fails: tripping requirement.

A failure of a protective device or the circuit breaker only exists if they do not or cannot trip despite being responsible in case of a fault. Delayed tripping is to be evaluated separately from selectivity. The Protection Security Index (PSI) after (68) finally evaluates the selectivity of fault clearing based on the actually occurred compared to the determined protection response in dynamic simulations. Here, the following definition applies to the terms:

- Selective: All and only protective devices with tripping requirement have tripped.
- Overfunction: More protective devices than those with tripping requirement have tripped.
- Underfunction: Not all protective devices with tripping requirement have tripped, but the fault was isolated by other devices.
- No fault clearing: Fault was not isolated from the rest of the power system.

$$\mathrm{PSI} = \begin{cases} 1.0 & \text{Selective} \\ 0.7 & \text{Overfunction} \\ 0.4 & \text{Underunction} \\ 0.0 & \text{No fault clearing} \end{cases} \tag{68}$$

8.4 Guiding Penalty Index

All evaluation indices presented so far evaluate the reaction of the energy and protection system to a fault and are designed to quantify improvements using concrete values. The Guiding Penalty Index (GPI) has a different task. It is designed to account for conditions and risks that cannot be directly quantified. For example, in protective devices, various protective functions such as the pendulum swing blocking or the load sector can be additionally activated to block unselective tripping in special situations. However, such functions should only be used, if the functions are really needed and thus create added value. This is because activation always involves the risk that situations may arise, where the protective device tripping is incorrectly blocked and a device thus fails despite the tripping requirement. Such a risk is difficult to quantify,

especially since all eventualities can never be simulated in detail. The GPI is therefore implemented as a penalty function after (69) and evaluates the activation of further functions that represent a potential risk. Here nAF is the number of additional functions activated and $nAAF$ is the number of all functions that can be activated. The weighting factor w_{GPI} can be used to set the maximum penalty for activating all and thus one additional activatable function. This factor is to be selected in such a way that the resulting penalty value due to the activation of a function is significantly smaller than the improvements in power system and protection security measured via the other indices. It is thus to be selected as a function of the number of protective functions that can be activated and the total number of fault simulations per fault package. In the further course of this work, a value of 10E5 is used. The GPI thus has a purely guiding task during an optimization process. In relation to the other indices, it plays only a minor role in terms of magnitude, but this is sufficient for a deactivation of additional functions without added value to lead to a better result than if the functions are activated. This includes the risk of unnecessary function activations in the overall system, which is difficult to quantify.

$$\mathrm{GPI} = 1 - \frac{1}{w_{\mathrm{GPI}}} \frac{nAF}{nAAF} \tag{69}$$

8.5 Fitness Value & Visualization

After each change of the decision variables $\vec{x}$ to be optimized, an optimization method needs a return of the fitness function in order to develop the next solution based on it. Here, according to section 2.3.1, two basic types can be distinguished.

In single-objective optimization problems, there is only one objective function $f(x)$ to be optimized, so that the return corresponds to a single value, the FV of the objective function. In multi-objective problems, there are multiple functions f_j to be optimized simultaneously with the same decision variables. Therefore, there exists not only one solution point but a solution set, where the individual solution points perform differently in the respective functions. Here, a solution point $\vec{x}^*$ is considered to be Pareto-optimal if no other solution point can be found that leads to better results in one of the objective functions without simultaneously leading to worse results in the other functions. The set of Pareto-optimal solution points is then the Pareto-optimal set X^* and the solution of the optimization procedure. [5], [6]

The functions introduced in chapter 8 for the assessment of the protection coordination represent first of all a multi-objective optimization problem and could be optimized in parallel. A central problem, however, is that from the resulting Pareto-optimal set X^*, a solution $\vec{x}^*$ to be used has to be chosen in the end. For this task, different methods exist in principle with individual advantages and disadvantages. In the context of this work a different way is chosen and the weighted sums method according to (6) already introduced in chapter 2.3.1 is used to form a single-objective optimization problem from the multi-objective one. This has the advantages that an optimization run leads directly to a single solution and less computational time is needed. It is accepted that the result is not necessarily Pareto-optimal. Since all evaluation functions are already normalized to the same range of values [0,1], the weighted sums method can be used directly, yielding the final fitness function of the PSA power system protection coordination $PSA(\vec{x})$ according to (70). Here, nF represents the number of all faults simulated at a defined distance on each defined path within the system. The FV is thus calculated as the average value of all individual fault evaluations $EV_{\mathrm{PSA},i}$ of a run. The weighting factor $w \in [0,1]$ can be used to set a favored weighting between the new guiding assessment and the classical selectivity assessment. The GPI is multiplied by the result once at the end of a run. The best PSA result is thus obtained with a one and the worst with a zero. In order to minimize the function like the test functions from chapter 5.2, the function $1 - PSA(\vec{x})$ is used for optimization.

$$\begin{aligned} PSA(\vec{x}) &= \mathrm{GPI} \cdot \frac{1}{nF} \sum_{i=1}^{nF} EV_{\mathrm{PSA},i} \\ EV_{\mathrm{PSA},i} &= w \cdot \mathrm{DSI}_i \cdot \mathrm{SRI}_i + (1 - w) \cdot \mathrm{PSI}_i \end{aligned} \tag{70}$$

For a manual evaluation and analysis of potential error sources, all fault results of a run are displayed in a clear PSA matrix with color fields according to the scheme of Figure 25. This is obtained for each run of the PSA fitness function and thus provides a good overview of the performance of the protection system. Here, the left, vertical axis shows the respective protection zones with the paths, on which the faults are simulated. On the right, vertical axis, the respective failing protective devices of the fault sequence are listed. On the upper horizontal axis, the exact fault position can be taken as a percentage of the respective path. This results in a color field for each simulated fault including boundary conditions according to the evaluation value. In addition, it is possible to draw a PSA result matrix exclusively with the results of every single index. Thus, a classical PSA matrix can be created using only the PSI

index. The mapping between the evaluation value or the value of the respective index and the corresponding color is shown in Figure 26.

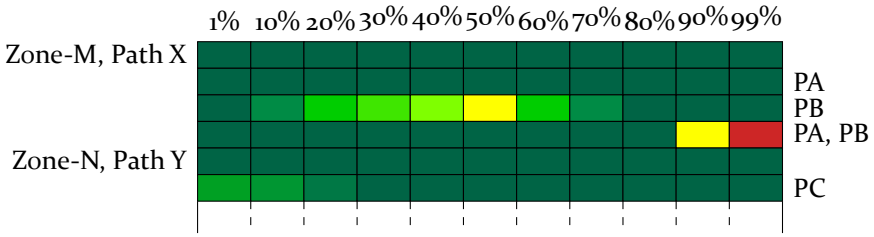

Figure 25: Schematic structure of the PSA result matrix. On the left side, the respective paths are listed. The failing protective devices are listed on the right. At the top, the respective fault location is shown as a percentage of the path.

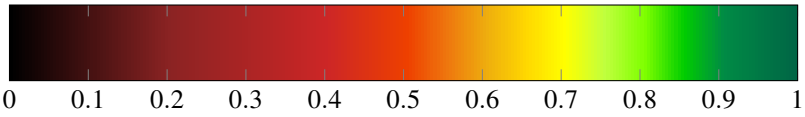

Figure 26: Overview of the assignment between result value and corresponding color.

A result value of zero with a coloring in black represents the worst possible result and a value of one and a coloring in dark green represents the best possible result. The color transitions from green to yellow to red and finally black are fluent, so that every small improvement or deterioration results in a new color. In this way, all faults as well as different PSA runs can be compared visually in an optimal way.

Part III

Protection Concept Generation, Assessment & Optimization

We need diversity of thought in the world to face the new challenges.

Tim Berners-Lee
English computer scientist
and inventor of the World
Wide Web
* 1955

9 Introduction & Challenges of Protection Coordination

9.1 Upcoming Changes in the Power System Landscape

In its *Sixth Assessment Report*, the Intergovernmental Panel on Climate Change (IPCC) warns urgently of the enormous risks and foreseeable consequences of increasing global warming [87]. Energy systems worldwide are confronted with the challenge of advancing the integration of RES and steadily expanding it over the next years and decades. The goal of all countries must be to massively reduce greenhouse gas emissions and to substitute traditional power plants that burn fossil fuels with wind turbines, solar, biogas, hydroelectric and geothermal plants. In addition, many areas such as industry and transport are to be electrified and supplied with electricity from RES in the future. All of this is already having an impact and will have an even greater impact on existing power system structures, system operation, and fault conditions that occur. In this context, the following changes also influence the mode of action of protection systems and protective devices and must be taken into account today and in the future when generating and reviewing protection concepts:

- A large part of all RES is and will be connected to the distribution system, i.e. on the medium and low voltage level. The same applies to the increasing number of prosumers participating in the market. This increases the energy exchange via the distribution systems, which are already reaching their technical limits in many places. Since these were often designed and built in the past as pure load grids, a unidirectional load flow as well as a steady drop in the voltage profile from the busbar to the consumer has been assumed. The feed-in behavior of RES is much more variable than that of conventional power plants, depending on wind, sun, season, etc. Grid planning and system management are therefore confronted with significantly fluctuating generation, a high diversity of grid operating states, and bidirectional and volatile load flows. Also, overloads of operating equipment as well as violation of the voltage band may occur. These circumstances increase the variety of possible fault scenarios that protection systems must handle. [55], [88], [89]
- Growing power grids, hybrid grid structures and changing topologies increase the interactions between transmission and distribution systems. This circumstance, together with the high number of connected RES, leads to decreasing short-circuit currents in some places, but also to increasing short-circuit currents in other places in the event of faults. In many situations, the protection criterion current alone will no longer be sufficient to reliably detect and trip fault conditions. With increasing short-circuit currents, the relevance of a short fault clearing time also increases. In addition, the number of protective devices required is increasing, which must be taken into account and configured in protection concepts. Increasing feed-in from small generators and decreasing feed-in from large rotating machines leads to greater transient reactions in the event of deviations in the overall system. Especially in distribution systems, where many of the RES are connected, dynamics will increase and time constants will decrease. [90], [91]
- The proportion of feeders with power converters is increasing, which means that the variety and complexity of control options is also steadily growing. As a result, system behavior in the event of a fault is becoming more variable and unpredictable. The fault currents of converters are mainly determined by the control system and no longer by physical relationships. Unlike synchronous machines, converter-coupled feeders also have no physical or inherent inertia. This can have a negative impact on the frequency stability of the system in the event of a fault. Low

inertia makes faster frequency excursions, and thus earlier instabilities, more likely. Nonetheless, RES with converter connection via dedicated controllers can also make a fast contribution to primary control as long as sufficient feed-in reserves are available. This would have a positive impact on frequency stability. [49], [55], [91]

- A more decentralized energy supply is often also accompanied by a greater geographical imbalance between generation and load. As a result, electricity must be transported over greater distances, which places an additional burden on the power system. In addition, bottlenecks occur more quickly after disconnections, which can lead to stability problems and electromechanical transients in the transmission system. [52], [90]
- In order to increase the transmission capacity of existing power systems, temporarily higher system loads can be used in combination with curative measures. These situations must be considered during the design of protection concepts to avoid unselective and unintended protection trips during operation. [92]

With the knowledge of the already deployed and still upcoming changes in the power system landscape, the negative effects of different impacts on protection systems are compactly described in the following. For this purpose, the two most common protection functions with backup functionality are presented first: Distance protection and overcurrent protection. If the explanations are not detailed enough, the relevant literature on protection systems, protective devices and protection coordination is recommended at this point: [55], [89], [93]–[96].

9.2 Protection Function Principles & Coordination

9.2.1 Distance Protection Function (21)

The distance or impedance protection principle is a universal short-circuit protection function. It is based on the evaluation of measured input signals of short-circuit voltage and current at installation location A in order to calculate the resulting loop impedances to fault F according to (71).

$$\underline{Z}_{\mathrm{AF,meas.}} = \frac{\underline{U}_{\mathrm{AF,meas.}}}{\underline{I}_{\mathrm{AF,meas.}}} \tag{71}$$

This can then be compared with the known impedances of the surrounding equipment to determine the distance of the protective device to the fault and

thus the fault location in the system. However, the resulting reactance part $X_{\mathrm{AF,meas.}}$ is usually used for this purpose, since the resistance part $R_{\mathrm{AF,meas.}}$ also contains the unknown fault resistance R_{F}. If the fault is located in a protection zone for which the protective device is primarily responsible, it should trip without delay. Since the measured input signals, however, always have a certain fuzziness and measurement deviations can occur due to various phenomena, which are described in more detail in section 9.3, the first tripping zone or trip stage is set short to the end of the protection zone in order to avoid a violation of selectivity. The time-delayed second tripping zone is used to protect the rest of the own protection zone. This is set to extend above its own zone with a correspondingly higher trip impedance. The time delay is on the order of 10 to 25 cycles of the fundamental frequency to allow sufficient time for command and process time of the upstream protective device, switching time of the circuit breaker, and arc extinction time. The third as well as further following tripping stages serve as reserve zones and are to ensure that in case of failure of other protective devices and/or the associated circuit breakers, a fault is nevertheless detected and isolated. For this purpose, all tripping stages of all protective devices must be coordinated with each other so that no unselective tripping occurs, but at the same time faults are always tripped. Protection coordination therefore has the task of dealing with the conflicting demands of security and dependability. This is correspondingly complicated due to the many determining factors such as power system topology and transformer data, infeed conditions, load conditions and fault resistances.

Therefore, different strategies and philosophies exist to achieve a suitable initial parameterization. The *IEEE Guide for Protective Relay Applications to Transmission Lines (C37.113)* [58] suggests settings based on (72) for non-pilot (no communication) applications in meshed systems. Figure 27 shows the corresponding grading applied to an example structure where various long sections follow a first section. Each section is protected by a protective device with distance protection function and three set tripping zones. The corresponding delay times as well as the resulting reactance setting values are plotted. The power is supplied from one source to the busbar A. It can be seen that Zone3 of protective device PA overlaps with Zone3 of PB1. This circumstance would lead to an overfunction only in case of failure of protective device PC and a corresponding fault on section CD. The setting rule thus focuses on selectivity and in return accepts higher tripping times. Thus, faults on section BE are not cleared by PA until Zone3 if protective device PB2 fails. These are typical challenges of protection coordination. In [93], protection settings according to (73) for branched radial systems and according to (74) for meshed systems are proposed as starting point. Additionally, two different

strategies can be used in the generation of an initial parameterization [93]. On the one hand, to achieve absolute selectivity, intermediate infeeds, as presented in chapter 9.3.2, can be neglected and the corresponding shorter impedance can be calculated for parallel connections. On the other hand, intermediate infeeds can also be taken into account and parallel connections can be disregarded in order to achieve shorter overall tripping times. All this illustrates the complexity and variety of setting options. Regardless of the rule selected at the beginning, all settings of all protection functions must always be individually adapted to the respective situation. [55], [58], [93]

$$\begin{aligned} X_1 &= 0.9X_{\text{AB,min}} \\ X_2 &= 1.2X_{\text{AB,max}} \\ X_3 &= X_{\text{AB,max}} + X_{\text{next,max}} \end{aligned} \tag{72}$$

$$\begin{aligned} X_1 &= 0.9X_{\text{AB,min}} \\ X_2 &= 0.9(X_{\text{AB}} + 0.9X_{\text{next}})_{\text{min}} \\ X_3 &= 0.9(X_{\text{AB}} + 0.9(X_{\text{next}} + 0.9X_{\text{next-next}}))_{\text{min}} \end{aligned} \tag{73}$$

$$\begin{aligned} X_1 &= 0.9X_{\text{AB,min}} \\ X_2 &= X_{\text{AB,max}} + 0.5X_{\text{next,min}} \\ X_3 &= 1.1X_{\text{AB,max}} + X_{\text{next,max}} \end{aligned} \tag{74}$$

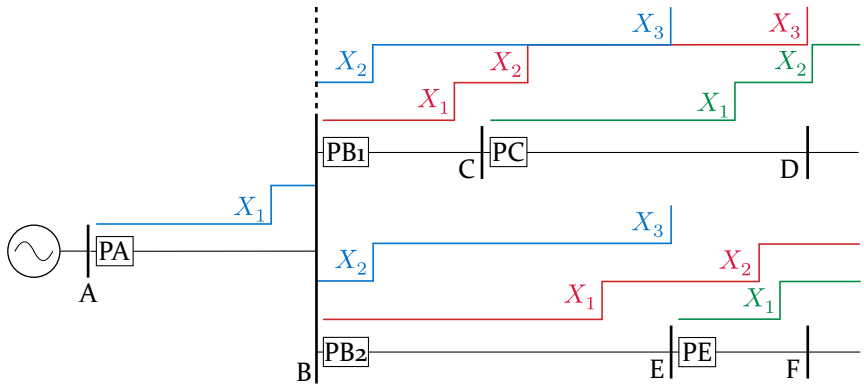

Figure 27: Distance protection function: Grading chart based on (72) for the case that two sections of different length follow a first one.

The settings of the resistance values R_1, R_2 and R_3 are set to distinguish between fault case and normal condition and are composed of the ohmic part of the equipment as well as a possible additional fault resistance R_F. Here, the settings must be large enough so that even high-impedance faults can be detected, but at the same time the R-range must not limit the load current. The fault resistance is composed of the arc resistance for phase-phase faults and a possible mast resistance for phase-earth faults. The former varies with the applied short-circuit voltage and the flowing current. If ground faults with 100 Ω and more are to be expected, additional ground fault protective devices should be used. [93]

9.2.2 Overcurrent Protection Function (50/51)

Overcurrent is the most commonly used protection function. It is used as the main and backup protection in transmission and distribution systems to detect short circuits. Here, a distinction can be made between two main types with differently designed tripping characteristics. On the one hand, there are overcurrent functions whose delay time is independent of the current level (50), and functions where the delay time depends directly on the measured current level (51). In the case of the former, a distinction is still made between two different designs. So there is the Instantaneous Overcurrent (IOC), where no delay time is used at all. But there is also the Definite-Time Overcurrent (DTOC), where tripping occurs only after a defined time. In this case, several stages can be used simultaneously in one protective device, so that tripping is graded for different currents. In contrast, the Inverse-Time Overcurrent (ITOC) (51) uses an inverse tripping characteristic in which the measured current is converted directly into a corresponding delay time via an inverse characteristic. If the protective device additionally evaluates and uses the direction of the flowing fault current, the ANSI code designation (67) is added, and a directional overcurrent function results. This is in contrast to the undirectional overcurrent function. When setting the parameters of the overcurrent protection function, care must be taken to ensure that no tripping occurs during normal operation. Therefore, the lowest tripping level must be selected so that it is still above the highest load current that occurs. At the same time, it should be possible to detect and isolate all short-circuit conditions in the relevant protection zone, which is why the level must be so low that the minimum flowing short-circuit current also leads to tripping. In order to achieve location-dependent selectivity, the various tripping characteristics of all downstream devices must be coordinated with each other. A distinction can be made between current and time grading. The former can only be used if there is a sufficiently high impedance between the protective devices to be

coordinated so that the short-circuit currents differ significantly depending on the fault location. Time grading is therefore more commonly used. Here, the closer a protective device is to a source, the more time-delayed it trips in a branch. This is done because, in proximity, all protective devices in a branch measure the same short-circuit current in the event of a fault. So that the fault can be cleared selectively, tripping is time-staggered towards the source. If the fault is isolated, the protective devices that have not tripped fall back accordingly. However, the problem arises here that the closer the faults are to a source, the later they are tripped. At the same time, the short-circuit current increases in the direction of the source.

Typical setting values for the two-stage DTOC are shown in (75). Here $I_{>>}$ is the high current stage that trips after the shorter delay time $t_{>>}$, and $I_{>}$ is the low current or reserve stage that outputs a trip signal after $t_{>}$ has elapsed. Figure 28 shows the matching tripping characteristics in the presence of a simple stub. [55], [89], [96]

$$\begin{aligned} I_{>>} &= (2.0\ldots5.0)I_{\mathrm{N}} \\ I_{>} &= (1.1\ldots2.0)I_{\mathrm{N}} \end{aligned} \tag{75}$$

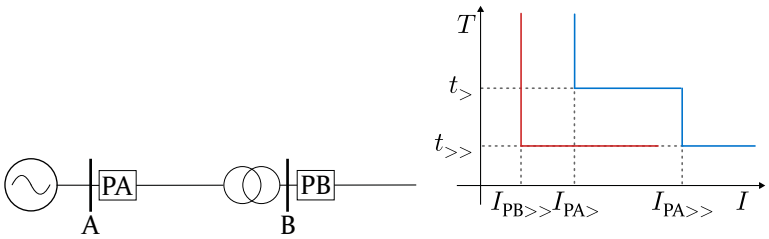

Figure 28: DTOC protection function: Grading chart for a branch section.

9.3 Adverse Effects on Protection Functions

The coordination of all protective devices including their functions is additionally complicated by numerous influencing variables. In particular, the accuracy of measurement of the distance protection function is negatively effected by a wide variety of factors. Figure 29 shows a simple power system section with the three protective devices PA, PB and PC as well as two feeders at busbars A and C. In addition, there are three switches S1, S2 and S3. For clarity, all resistances are initially assumed to be zero and the reactance of the lines are the same. The phase position of all feeders in the short-circuit case

are the same and therefore negligible. Detailed calculation steps on voltages and reactances are listed in the Appendix B. The effects of five different switch positions in case of short circuits on the lower lines AB and BC are considered in the following.

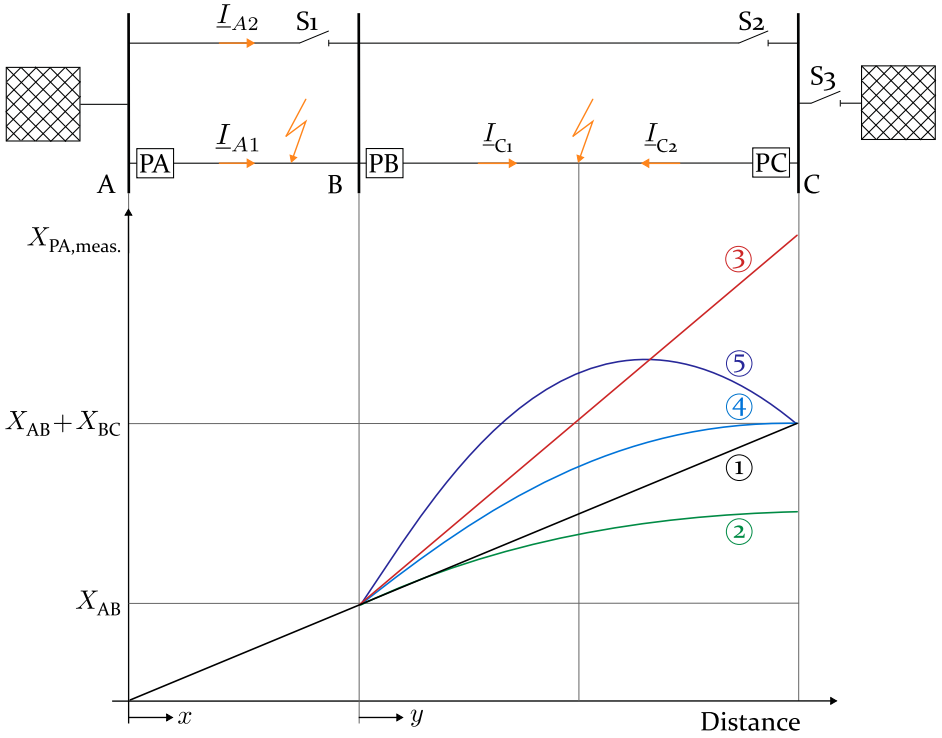

Figure 29: Influence of various effects caused by different switching states of S1, S2 and S3 on the measured reactance of protective device PA. Based on [93].

9.3.1 Topological Effect

1) S1, S2, S3 open All three switches are initially open. Thus, in the event of a fault on line sections AB and BC, only feeder A provides a short-circuit current contribution. The flowing fault current I_A is measured completely by the protective device PA. There is no intermediate infeed, no infeed from the opposite end and the resulting current path is a continuous line section. PA therefore measures the exact fault reactance X_{AF} according to (76). For the set case that the distributed reactance in p.u. X'_{AB} is equal to the distributed

reactance X'_{BC}, a linear measurement of the reactance over the distance x as well as y results.

$$X_{\mathrm{PA,meas.}} = \begin{cases} x \cdot X'_{\mathrm{AB}} & \text{fault on section AB} \\ X_{\mathrm{AB}} + y \cdot X'_{\mathrm{BC}} & \text{fault on section BC} \end{cases} \tag{76}$$

2) S1 open, S2 closed, S3 open The S2 switch is now closed. This results in a parallel line for section BC from the point of view of the protective device PA to busbar B. Proportionally to the impedances, the short-circuit current I_{A} is now divided between the two branches. The voltage at busbar A can thus be calculated according to (89), which gives the measured reactance of PA according to (77). This is now lower due to the parallel line. If the fault is applied directly to busbar C ($y = 1$), the reactance of the complete parallel line BC is measured, which then corresponds to half of the single line. Parallel lines must therefore be taken into account when generating and parameterizing protection concepts in order to avoid unselectivities.

$$X_{\mathrm{PA,meas.}} = \frac{U_{\mathrm{A}}}{I_{\mathrm{A}}} = X_{\mathrm{AB}} + X_{\mathrm{BC}}(y - 0.5y^2) \tag{77}$$

9.3.2 Intermediate Infeed Effect

An increasingly common problem in the context of decentrally distributed RES, which are often connected directly to the system without major adjustments to the existing protection system, is the intermediate infeed effect. This occurs whenever a fault current is injected somewhere between the installation location of a protective device and the fault location and additionally flows onto the fault location. This part of the fault current is then not measured by the protective device, resulting in measurement deviations.

3) S1 closed, S2 open, S3 open The switch S1 is now closed and the switch S2 is opened again. This results in a parallel line from busbar A to B. In the event of a fault on line sections AB or BC, the fault current I_{A} from source A is now divided between the two shares I_{A1} and I_{A2}, whereby only the former is measured by PA. If the fault is on line section BC, then I_{A1} corresponds exactly to half of the total current with $I_{\mathrm{A1}} = 0.5I_{\mathrm{A}}$. At busbar B, both currents flow together and through line BC to fault location F. Both currents therefore provide a voltage drop along section BF. The protective device PA measures the resulting higher voltage according to (91) at busbar A but only half of the current leading to it. This results in a measured reactance according to (78), where PA measures an overall too large reactance and therefore sees the fault

further away. The effect of the intermediate infeed is larger the larger the ratio of the intermediate injected current on the fault path to the measured current of the protective device is. Also, this increases with the impedance lying between the location of the intermediate injection and the fault location.

$$X_{\text{PA,meas.}} = X_{\text{AB}} + 2yX_{\text{BC}} \tag{78}$$

4) S1 closed, S2 closed, S3 open The switches S1 and S2 are now closed. Thus, a parallel line is created between busbars A and B, and between B and C. Thus, case 4 combines the two previous cases 2 and 3. The voltage at busbar A results according to (93) and the measured reactance of PA according to (79). Parallel line effect and intermediate infeed effect thus counteract each other, resulting in a steady increase of the reactance measurement over the section BC, although not linear. As in case 1, the largest reactance is measured at busbar C with $X_{\text{AB}} + X_{\text{BC}}$.

$$X_{\text{PA,meas.}} = X_{\text{AB}} + X_{\text{BC}}(2y - y^2) \tag{79}$$

5) S1 closed, S2 closed, S3 closed All three breakers are closed now. This means that in the event of a fault, the short-circuit current I_{C} from the source at busbar C is additionally fed to the fault. In terms of magnitude, it is assumed be twice as large as the short-circuit current from source A. Depending on the fault location, part of the current I_{C1} thus flows via the upper line of the parallel line BC via busbar B onto the fault, thus providing an additional voltage drop and an additional intermediate infeed effect. The voltage measured by PA at the busbar A thus depends on the fault location and the currents I_{A} as well as I_{C}. The measured reactance is given by (80). The result therefore depends on the ratio of I_{C} to I_{A}. As a particularity, it results that the maximum of measured reactance is located on the section and no longer at the end of the section BC. Since neither the supply of synchronous machines nor RES is necessarily constant over the entire fault duration, variable short-circuit currents and the associated dynamic intermediate infeed effect must also be expected. Also, protection tripping or disconnections may cause an intermediate infeed to drop out during the fault, causing the measured short-circuit impedance to change abruptly. Therefore, the type of infeed, connection requirements,

controls, power system topology and existing protection settings must be taken into account when configuring protective devices.

$$\begin{aligned} X_{\text{PA,meas.}} &= X_{\text{AB}} + X_{\text{BC}} \left((2y - y^2) + \frac{I_{\text{C}}}{I_{\text{A}}} \cdot (y - y^2) \right) \\ &= X_{\text{AB}} + X_{\text{BC}} (4y - 3y^2) \end{aligned} \tag{80}$$

9.3.3 Fault Resistance & Phase Angle

Up to now, the fault resistance R_{F} was always assumed to be zero. Figure 30 is now used to show the influence of an existing fault resistance on reactance and resistance measurement of PA. In the following, two different cases are considered.

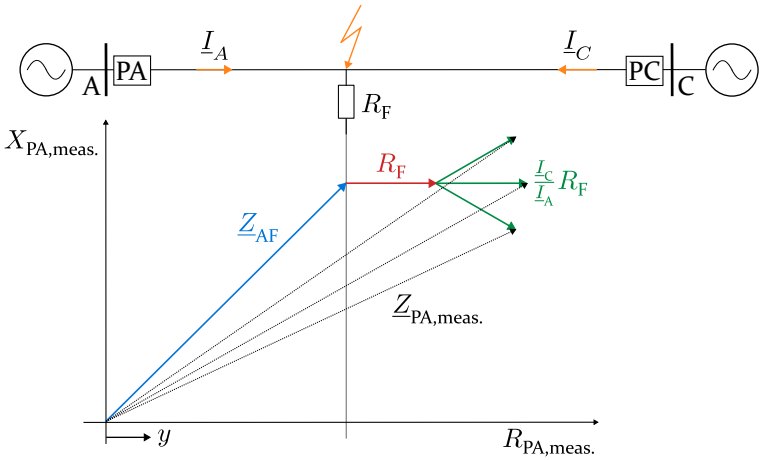

Figure 30: Influence of the fault resistance R_{F} in combination with different phase angles of two infeeds on the measured resistance and reactance of protective device PA. Based on [93].

Source Currents in Phase At first, it remains valid that the feeders A and C are in phase, which means that there is no load transmission via the line AC. Also, the sources and line impedances have almost the same short circuit angle. Thus, the short-circuit currents $\underline{I}_{\text{A}}$ and $\underline{I}_{\text{C}}$ also have the same phase and their ratio is purely real. The measured reactance $X_{\text{PA,meas.}}$ is not affected by this and measures the correct fault impedance X_{AF} in the fault condition. The resistance measurement of PA $R_{\text{PA,meas.}}$ increases by the additional applied fault resistance R_{F} as well as the additional amount of $I_{\text{C}}/I_{\text{A}} \cdot R_{\text{F}}$ caused by the opposing infeed. The complete measured impedance of PA is obtained

according to (81). Due to possible fault resistances, a sufficient R-range must therefore always be ensured.

$$\underline{Z}_{\text{PA,meas.}} = yX_{\text{AC}} + R_{\text{F}} + \frac{\underline{I}_{\text{C}}}{\underline{I}_{\text{A}}} \cdot R_{\text{F}} \tag{81}$$

Different Phase Angles Especially feeders located further away from load centers are connected to the power system via longer transmission lines. Power transmission then requires a significant angular offset of the two voltage phasors at the start and end of the line. Therefore, it should now be valid that the short-circuit currents fed in the event of a fault also have different angles. This leads to the fact that the quotient of $\underline{I}_{\text{C}}/\underline{I}_{\text{A}}$ is no longer purely real and the unmeasured short-circuit current from the opposite end leads to a voltage drop across R_{F} with different angle. PA thus measures the fault resistance as impedance rather than pure resistance. The voltage angle of the power sending side thereby leads the angle of the receiving side by an angle ϑ. Accordingly, the impedance phasor $\underline{I}_{\text{C}}/\underline{I}_{\text{A}} \cdot R_{\text{F}}$ is measured tilted downward on the power emitting side and upward on the receiving side. The corresponding measurement deviation $X_{\text{PA,dev}}$ of PA is given by (82). This results in a distance protection function measuring a fault reactance that is too small on the current sending side and a fault reactance that is too large on the current receiving side. In the first case, the protective device therefore tends to overreach, while in the second it tends to underreach. When setting the parameters for distance protection functions, the transmission angle and possible fault resistances must therefore be taken into account.

$$X_{\text{PA,dev}} = \frac{I_{\text{C}}}{I_{\text{A}}} \cdot R_{\text{F}} \cdot \sin(\vartheta) \tag{82}$$

9.3.4 Transient Stability & Power Swings

Until now, the voltage phase angles of all feeding generation units were assumed to be constant during and after a fault. However, if a short circuit or other major dynamic event occurs, this leads to an immediate response of the overall system, with all primary and secondary equipment involved interacting with each other. [51] Thus, an abrupt change in the power system impedance leads to an instantaneous change in all voltage phasors, creating a new load flow in the system. [97] As a result, synchronous machines experience an increase or decrease in rotor angle respectively power angle, which in turn results in a change in the machine's electrical output that can be dissipated. For the steady state, the corresponding dissipated active and reactive power

of a non-salient pole machine is obtained according to (83) with the help of the stator voltage U_s, the rotor excitation voltage U_r, the synchronous reactance X_d, and the rotor angle δ, neglecting the winding resistances ($R << X$). The resulting voltage change across the stator must then be counteracted by controlling the rotor excitation voltage $\underline{U}_r$ and current $\underline{I}_r$. [51] For a detailed consideration of the temporal processes of a synchronous machine as well as the resulting subtransient, transient and steady-state current in response to a short-circuit, reference is made at this point to the good literature: [51], [54], [55], [86], [98]. For understanding the processes and control of power converters, the following source is recommended: [55].

$$\begin{aligned} P &= \frac{U_s U_r}{X_d} \sin(\delta) \\ Q &= \frac{U_s U_r}{X_d} \cos(\delta) - \frac{U_s^2}{X_d} \end{aligned} \tag{83}$$

Depending on the type and location of an event that has occurred, as well as the existing operating point, the rotor of a synchronous machine is accelerated or unloaded as a reaction, which brings the machine out of its state of equilibrium. Acceleration occurs when the input drive power exceeds the output electrical power, which is often the case when a short circuit occurs in the system as the stator voltage drops in the phases. After disconnection of the short circuit, the machine must then be returned to a stable operating point and unloaded so that it does not slip and lose its synchronism with the power system. The latter happens when the rotor angle becomes too large and the electrical power that can be dissipated exceeds its maximum and starts to decrease again. Without sufficient reduction of the drive power, the machine would continue to accelerate until it is finally disconnected by the generator protection system. However, situations can also occur in which a machine has hardly fed any active power into the grid prior to a short circuit and then feeds a higher current when the fault starts, thereby delivering more electrical power than is supplied via the drive in terms of mechanical power. As a result, and if the drive power generally falls below the electrical power required by the grid, the rotational speed of the rotor decreases. In both cases, after such speed and rotor angle changes, electromechanical transients can occur in the system, in which different individual machines or even entire coherent generator groups oscillate against each other. These then exchange power with one another, which varies in magnitude and direction. This happens because both individual machines and machine groups can have different frequencies and thus time-varying rotor angles, which in turn leads to time-varying voltage

phase angles in the system. Due to angle changes, unwanted and uncontrolled power flows occur, which are referred to as power swings, power oscillations or pendulum swings and are usually in the single-digit hertz range. Voltage and speed control and power swing damping devices then have the task of re-establishing a steady-state condition with a new steady-state load flow. If this does not succeed and a power swing continues to swing up, it is said to be unstable, which then eventually leads to protective device tripping and disconnections of generators, with which the power system begins to fall apart. In turn, the stable power swing exists, which experiences sufficient damping and thus has a decaying character. [51], [52], [55]

Generation units fed via power converters, especially if they are grid-forming controlled, can also be involved in power swings. This can occur especially when a grid-forming power converter is coupled to a strong system via a small impedance. When virtual inertia is provided and controlled, frequency control reserve and behavior of a power converter are linked in the same way as for a synchronous machine. This results in a grid supporting but also analogous behavior to the synchronous machine, thus increasing the risk of participation in a power swing. [55]

Transient events can also occur even during a fault, for example during a short circuit. This is especially more likely in the case of different existing inertias of the respective generating units, since these then show a different, dynamic behavior. [55]

In Figure 31, two synchronous machines G1 and G2 are connected to each other via a transmission line. The protective devices PA and PB with distance protection function are located on busbars A and B respectively. The voltage phasors $\underline{U}_{G1}, \underline{U}_{A}, \underline{U}_{B}$ and $\underline{U}_{G2}$ are drawn above the associated busbars. The impedance diagram of PA with three tripping zones as well as the line characteristic from G1 to G2 is shown below. In addition, the initially measured load point with $R > X$ together with the power angle ϑ between $\underline{U}_{G1}$ and $\underline{U}_{G2}$ is drawn. If there is now an abrupt change in the system impedance and, as a result, time-varying voltage angles at G1 and G2, then the power angle ϑ also changes. This results in a varying voltage drop along the transmission line G1G2, which in turn causes a transient current. The resulting impedance trajectory between the generators G1 and G2 is measured by PA.

For better understanding, Figure 32 shall serve here, which shows the voltage drop along the transmission line G1G2 with phase opposition of the generator voltages. This represents an unstable condition where the intersection of the voltage drop curve with the impedance line $\underline{Z}_{total}$ marks the Electrical Center

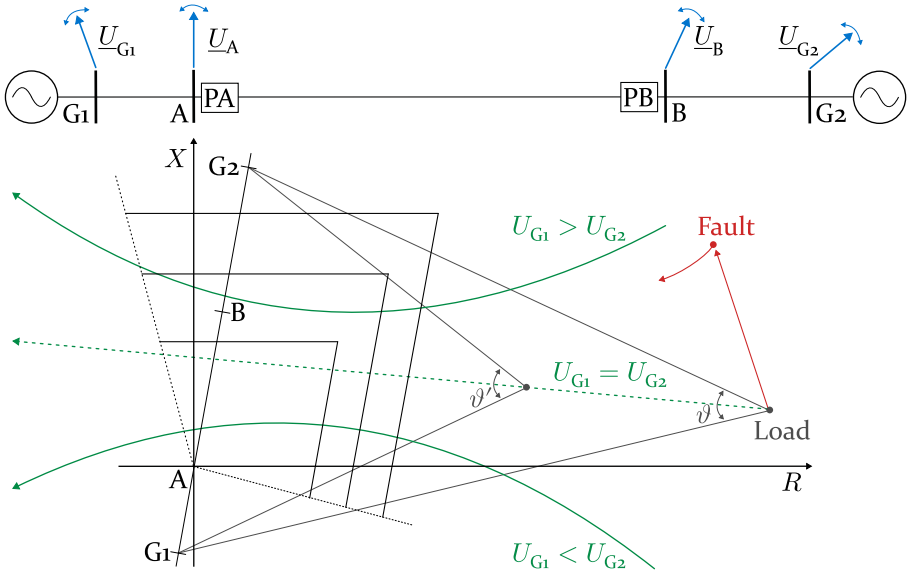

Figure 31: Representation of different impedance trajectories from the point of view of protective device PA in the impedance plane during transient events and power swings between synchronous machines G1 and G2. Based on [93].

(EC). At this point the voltage is zero. The center of the impedance line $\underline{Z}_{\text{total}}$ in turn is marked by the Impedance Center (IC) and is located exactly at half of the total impedance $\underline{Z}_{\text{total}}$. While the IC is fixed, the EC varies with the magnitude ratio of the voltage phasors of G1 and G2 at a power angle of 180°. Here, the EC is to the left of the IC if the voltage magnitude of G1 is less than that of G2 ($U_{G1} < U_{G2}$), and to the right if the voltage magnitude of G1 is greater than G2 ($U_{G1} > U_{G2}$). If the magnitudes are exactly equal ($U_{G1} = U_{G2}$), then IC and EC fall together. The EC here marks the center of the power swing of the example system.

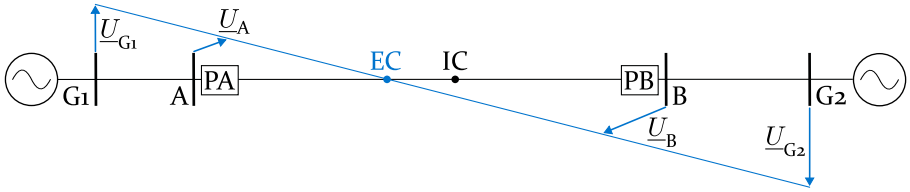

Figure 32: Curve of the voltage drop in an example system with voltage phasors of synchronous machines G1 and G2 in phase opposition. The electrical center (EC) and the impedance center (IC) are drawn.

In Figure 31 the voltage phasors of G1 and G2 are not yet unstable and in phase opposition, but they drift apart. This changes the power angle from ϑ to ϑ'. Similar to Figure 32, this causes PA to measure a lower voltage and at the same time a higher current. As a result, the measured impedance decreases and the impedance trajectory moves toward the tripping characteristic of PA. If the voltage magnitudes of G1 and G2 are equal, the impedance trajectory describes a straight line. If the voltage magnitudes are different, but the ratio of them is constant, an elliptic curve is formed. The extent to which an impedance trajectory enters into a tripping characteristic of a distance protection function in the case of transient events and power swings depends not only on the voltage phasors but also on the impedances in between. In the example shown in Figure 31, the source reactances between G1 and A and G2 and B are approximately equal to and less than the line impedance AB. Thus, the EC is on the AB section. If the source reactance should be significantly larger in relation to the line impedance, the EC can also be within the source reactance when the generator slips through, thus achieving a power angle of 180°. The voltage at the connected node then dips less as a function of the voltage magnitudes and impedances. Whether an impedance trajectory traverses a complete straight line from beginning to end, or a full circle, or performs oscillatory (semicircular) motions depends on the strength and stability of a power swing. From a distance protection point of view, an unstable power swing is often inferred when the impedance trajectory intersects the imaginary axis and thus travels through from one side to the other.

Also, a movement of the impedance trajectory can already occur during a short circuit that is still present. This effect occurs at points in the power system where the inertia of connected generating units differs significantly from each other. The excitation of the short-circuit causes rotating machines to accelerate or decelerate to different degrees, and thus to change the power angle already during the fault. The behavior of power converter fed generating units depends on the control mode used. [55]

In unfavorable cases, the measured impedance trajectory can enter the tripping zones of the distance protection both during and after a fault due to electromechanical transients. It is not readily apparent to the distance protection function whether this is a real fault condition or not. If the delay time of the corresponding tripping zone expires and the impedance trajectory is still within the tripping characteristic, the distance protection function trips unselectively. Especially for Zone1, where the delay time is usually very small, rapid tripping occurs when the tripping zone boundary is exceeded. To prevent

unselective tripping due to power swings and other transient events, the distance protection function can be extended by a Power-Swing Blocking (PSB) function. This detects power swing frequencies up to 7 Hz for unbalanced and up to 12 Hz for balanced conditions and blocks tripping of the respective zones depending on the settings. However, in the event of power swings, it can also be beneficial to have protective devices tripping at certain points in the system and splitting the system there to contain the power swing. Therefore, a general activation of the PSB function is not always advantageous. Therefore, with the Out-of-Step (OOS) detection function, it is possible to release the blocking of the PSB function in case of unstable power fluctuations. [55], [99]

9.4 State of the Art Protection Concept Generation

The previous chapter has shown how technically complex the task of protection coordination is and how many influencing factors and conditions must be considered simultaneously. In addition, regulatory requirements, structural features of the system, customer wishes and costs must be taken into account. Furthermore, in addition to the actual main protection, backup protection must always be provided, which uses a different protection principle.

In today's practice, protection concepts are generated by experts on the basis of many years of experience. As a starting point, they use predefined standard protection packages known as *Typical Protection Schemes*, which have been developed and collected over the past decades. Companies, transmission and distribution system operators can now refer to a library of standardized templates to find and select suitable protection schemes for different applications. Each typical takes up a dedicated power system topology with an equipment to be protected, including boundary conditions and a predefined protection concept. The latter in turn consists of protective devices, circuit breakers, transformers, main and backup protection functions as well as other possible devices and communication systems. Examples of typicals are stub lines with single-end infeed, double lines with intermediate infeed, short overhead lines with infeed from both ends or parallel incoming transformer infeeds. [100], [101]

After the basic protection concept has been established, the protection coordination and parameterization of all protection functions follows in close coordination with the existing grid structure. With the partial help of table lists with various setting regulations and short-circuit simulation programs, settings can be determined based on the available grid data. [93], [102] The first step in this process is to select a suitable pickup method for each protection function that can clearly distinguish a fault condition from a normal condition.

This is usually not necessary when using current differential protection (87), which compares the measured currents at all feeders of the equipment to be protected for fault detection. This requires the use of communication hardware, for which there must also be a fallback level for failure by using another protection function. For the distance and overcurrent method, there are several options to choose from. The appropriate pickup method depends on the individual case. Criteria to consider include the resulting short-circuit currents, the corresponding voltages and angles, the present neutral point treatment, and possible switching and load conditions of the system. In general, it is advisable to use the same principle for one system so that the coordination of all protective devices is clearer and thus easier. [103] The coordination and parameterization of all protective devices is then carried out, taking into account the fault clearing time to be complied with. This is usually based on guidelines, applicable recommendations and experience and depends on the voltage level, the expected short-circuit currents and the presumed dynamic effects. Often, a fixed grading time of 300 ms is used for digital devices. The setting rules used, some of which are presented in chapter 9.2 with (72), (73), (74) and (75), like the pickup method, also depend on numerous influencing factors and require individual adaptation to the existing conditions. The entire workflow is rarely automated, which is why the design of a protection concept is labor-intensive and requires a lot of expertise. [93], [100], [101], [103]

A review of the main and backup protection for various fault types, fault resistances and system states can then be carried out by using simulation and analysis programs, in which the protection system and its responses can also be simulated. PSA systems, whose functionality as well as advantages and disadvantages are described in detail in chapter 7.1, are particularly suitable for this purpose and automatically test the protection behavior via numerous quasi-stationary short-circuit current simulations. What these systems lack, however, is information on which protection settings would be more appropriate when problems and gaps in protection system behavior are identified. While numerous methods have been published to improve protection coordination of distance and/or overcurrent protection functions, a system-wide and holistic approach that equally considers protection and system responses is missing [104]–[108].

The upcoming changes in the power supply landscape described at the beginning of this chapter 9 make it increasingly necessary to regularly review and adjust protection concepts and settings to ensure the reliability of the protection system. It is true that the connection of individual RES, for example,

leads only to small local changes. However, when added up, changes quickly occur that threaten security of supply, as load and fault situations arise that were not previously taken into account when the protection concept was initially drawn up. However, since the verification and subsequent adaptation of setting values is complex and time-consuming, conventional approaches and methods of protection concept design and verification are reaching the limits of practical applicability. In addition, there is an increasing shortage of protection engineers who can address the issues. Therefore, new, flexible, and adaptable tools are needed to avoid hindering the integration of RES and the electrification of the transportation and heating sectors. In the following chapter, such a new approach for the automated generation, assessment and optimization of protection concepts is presented, which quantitatively and qualitatively addresses the great potential of dynamic simulation.

Bad programmers worry about code. Good programmers worry about data structures and their relationships.

Linus Torvald
* 1969

10 Protection Toolchain

The Protection Toolchain (ProToc), described in this chapter, is an automated and digital system of various interlocking tools for protection concept generation, assessment and optimization. The basic idea and main goal is to make the protection concept generation process holistic, digital and automated to cope with future multivariable grid structures and fault situations. It is a generalized approach designed to flexibly handle changes in the system and provide robust solutions. For this purpose, the generated and adapted protection concepts must meet the requirements of comprehensibility, verifiability, security and reliability.

The ProToc was developed collaboratively by various partners as part of the *Kopernikus ENSURE* project funded by the German Federal Ministry of Education and Research (BMBF). A first design concept was published in 2019 within [P109]. This was followed by further publications in [P110], [P111], [P112] and [P113]. The overall goal of the Kopernikus project is to develop a holistic concept for a RES based energy supply of Germany for the year 2050, showing different solution paths for the transformation process. ENSURE, as one of four subprojects, has the task of researching new grid structures, analyzing future use cases, increasing the flexibility of the power supply system, advancing grid automation, and ensuring power system security in the face of all expected changes. New devices and technologies need to be embedded into the system, the different sectors more closely interconnected, and efficiency be increased. All of this increases the complexity of the overall system, which must be managed. [114]

The ProToc consists altogether of six individual, modular tools that allow a high degree of flexibility and adaptability to existing framework conditions. Executed one after the other, they result in a continuous workflow for the generation of a system-wide, digital protection system. Each tool can also be used individually and thus independently of the others. On the one hand, this enables an automation process in partial steps and, on the other hand, each tool can thus also be used outside the workflow. In addition, the individual development of each tool is easier. The six tools and thus process steps of ProToc are:

- Typical Matching
- Pre-Calculations
- Algorithm Selection
- Setting Calculation
- Protection Security Assessment
- Optimization

The application area of the ProToc can be divided into two main areas. On the one hand, it can be used to generate new protection concepts. On the other hand, it is designed to evaluate initial or existing protection concepts and to improve them based on the results. In perspective, the ProToc can be extended to an online-capable assistance system for control room environments, so that existing protection systems in the field can be routinely reviewed and, if necessary, directly adapted to changed conditions.

Data handling between the individual tools of the ProToc is based on the object-oriented structure of the Generic Data Model (GDM), which is described in the following section 10.1. The GDM represents a simple way, designed for protection assessment, to structure primary and secondary data as well as simulation and result data. An initial concept was presented in [115]. The data format, in which the data to be exchanged is stored, is freely selectable. The ProToc uses JavaScript Objective Notation (JSON) as a compact and flexible data exchange format. This is a common and slim format that is easily readable by both humans and machines. It is programming language independent and is already used in many modern applications.

10.1 Generic Data Model

Data management is an important factor in the automated exchange, processing and allocation of data. It is responsible for capturing all necessary data,

processing it correctly, storing it securely, and making it available to other applications efficiently. In addition, it should be able to record, merge and validate data from different sources.

Implemented in an object-oriented language, the GDM is a simple, abstract and generic data management system specifically designed to handle primary and secondary power system data. It is flexible and applicable independently of proprietary applications and simulation programs. At the same time, however, the GDM also builds a bridge to other tools and simulation programs in order to make them usable in an easy and automated way. In addition, it enables simple data processing and the execution of analysis and calculation functions tailored to protection assessment. In this context, automation is a challenge, especially in the case of complex structures in the power system, since all eventualities have to be covered. The GDM creates a suitable and usable abstraction level for this purpose via an effective and targeted reduction of the level of detail. It is hereby based on principles of graph theory, the Common Information Model (CIM) and the theoretical work of [115]. It has been practically implemented in the programming language C# in the past years and continuously developed, modified and adapted to current requirements. The GDM has a compact and efficient data structure, which is also used for data exchange within the ProToc due to its flexibility and extensibility. In the following, first the most important terms of graph theory and then the CIM are explained.

10.1.1 Graph Theory

The term *graph* originates from theoretical computer science and forms the basis for many network-like structures. In addition to being used for utility supply systems, graphs are also used in social media, transportation models, molecular connections, or route planning [4]. Figure 5 from chapter 2.3, for example, shows a simple graph related to the well-known TSP combination problem with different cities. A graph can be defined in general terms as a structure consisting of a finite set of nodes and edges. Nodes, which are also called vertices, represent objects and are often represented by points in a graph. Edges, on the other hand, are links or connecting objects between exactly two vertices and are represented by lines. [7] The CIM presented in the following is based, among other things, on theoretical principles of a graph.

10.1.2 Common Information Model

The semantic, object-oriented CIM has become a large standard model with defined interfaces describing various resources of the power system via objects, classes, attributes, etc. Areas covered are power generation, transmission and distribution, as well as power market and communications. It is maintained by the TC57 Technical Committee of International Electrotechnical Commission (IEC) and published under the *IEC 61970-301* norm. [116]. The CIM is now supported by many applications and systems as an interoperable data format. To describe all classes and attributes as well as their relationships and properties, the CIM uses the Unified Model Language (UML). This is a universal and standardized modeling language used for the design, visualization, and documentation of software systems [117]. It is described in more detail in the following section 10.1.3 and is used subsequently to describe the GDM.

However, the advantages of wide coverage and detailed description of resources in CIM are at the same time the greatest disadvantages of the model. Thus, a corresponding description of a power systems in CIM is usually complex. For example, to describe the system topology, the *node-breaker-model* is used, which attempts to accurately describe the real, physical conditions of all topology components. Switches, such as circuit breakers or disconnectors, and their states are taken into account exactly in the model. Like all other electrically conductive components, these are connected to each other via *topology nodes* and *terminals* respectively. Topology nodes describe impedance-free connection points. Terminals, in turn, are entities that connect topology nodes and real existing conductive components. In terms of a graph, all electrically conductive components such as transmission lines or transformers as well as electrical nodes such as joints or busbars represent vertices or nodes of the graph in the CIM. Topology nodes and terminals in turn together form the edges connecting the vertices. The advantage of this is that component and switch configurations can be easily visualized and described in detail, and thus correspond well with the real structures. The node-breaker-model is therefore also used in real-time simulations and real-time evaluations. However, a disadvantage is that a system described in the CIM turns out to be large and bulky, making it harder to handle. [115], [116], [118]

Another drawback of the CIM is the currently very limited scope for concretely representing protective devices and protective functions. With the classes *ProtectionEquipment*, *CurrentRelay* and *SynchrocheckRelay*, only three different options for description are available. The class *ProtectionEquipment* represents a protective device in general. The class *CurrentRelay* allows the definition of overcurrent protective devices and the class SynchrocheckRelay

allows the implementation of *Synchro-check* devices, which are designed for controlled interconnection of two circuits by measuring frequency, phase angle and voltage. [116] Thus, a large part of important protection functions are missing, which cannot be neglected for a comprehensive protection concept generation, assessment, and optimization. In addition, nowadays different protective functions can be used simultaneously on modern protective devices, so that a separate consideration of the physical device and the protection functions running on it makes sense.

10.1.3 Unified Model Language

The UML in the latest version 2.5.1 from 2017 can be described as a standardized modeling language for the design, modeling and visualization of software engineering systems, processes and workflows [117]. It enables specification in a unified and understandable notation and is the result of unifying several previous modeling languages [119]. UML is currently maintained by the Object Management Group (OMG), an international and non-profit consortium, and in collaboration with the International Organization for Standardization (ISO) is now also an ISO standard for system modeling [115]. It represents a comprehensive and flexible way to map and describe various aspects, interrelationships, and properties. However, it is not a method but descriptive language, so the result is always dependent on the creator. Code, data, structures, behaviors, dependencies and interactions can be described by simple understandable graphical and textual notation elements. This simplifies the development and also enables the exchange with less software-savvy users. With UML diagrams, it is often not important to show all the details of a system in depth. Rather, the focus is on creating understanding and clarity. The use of UML in the CIM is a good example of this. Furthermore, the UML promotes the interoperability of applications, since interfaces can be described easily and efficiently. In the UML there are different types of diagrams depending on the field of application. For the description of the structural layout of the GDM the static class diagram is sufficient, which represents the static view of a program design. It represents individual classes as well as their elements and the relations of the classes among themselves. Above all inheritances, interfaces and associations can be shown and recognized well. Here classes are represented as rectangle with three ranges. At the top is the name of the class. In the center the class attributes and below the operations of the class are listed. From this information it becomes clear, which characteristics an object of this class possesses and which functions it makes available. The relations of the classes among themselves are represented in each case by different lines and symbols. For example, a bidirectional connection is represented by a

simple line and means that two classes are closely connected and objects can store each other. If the connection is directional, then this is represented via a simple additional arrow. A detailed description of all relationships can be found in the official OMG documentation [117]. The most important relationship in the following is the generalization relationship between two classes inheriting from each other. Thus, a superclass represents a generalized form from which a subclass can inherit and thus then represents a more specialized form of the superclass. An example of this can be found in Figure 33, which will be described in more detail later, where a line in generalized form is a connection element and even more generalized a primary element. [117], [119], [120]

10.1.4 Classes & Connectivtiy

In addition to the node-breaker-model, there is also the *node-branch-model* in representation of power systems, which is a more abstract model and describes the physical conditions of the topology at a given time. It is mainly used for online as well as offline system analysis, load flow calculation and grid planning and can be derived from the node-breaker-model by evaluating the topology and switch positions. It is also based on the theoretical principles of a graph, but implements them differently. In the classic node-branch-model, a branch corresponds to an electrical connection between two nodes. Examples would be transmission lines, cables, transformers, or even entire HVDC-systems. The node in the node-branch model, in turn, corresponds to an electrical node such as a joint, busbar, or an entire substation, but it can also represent a load, generator, or FACTS system. The degree of resolution of individual elements and resources depends on the particular use case and the model accuracy used. An IEC standard corresponding to the CIM for a node-branch-model does not currently exist, but many proprietary simulation programs are based on this model. [115], [118], [121] This is partly because the way the system topology can be translated into a graph makes it easy to set up the vectors and matrices often used by simulation programs, such as the admittance matrix. Calculations can thus be performed efficiently. [68], [115] However, the disadvantage remains that all proprietary programs use their own data format, which is adapted to the specific requirements of the respective program.

The GDM takes a new approach here, but also builds on the node-branch-model and the theoretical principles of a graph. Thus, resources of the power system are represented as objects, with a clear separation between electrical nodes, primary elements and secondary elements. In the GDM, all resources that have a decisive influence on the generation, transmission or consumption

of electrical energy fall under the class *PrimaryElement*. These must be considered and included in simulation programs due to their influence during the execution of analysis functions, such as power flow, dynamics, transient stability or short circuit. These include, for example, synchronous machines and RES for power injection, transmission lines, cables and transformers for power transport, and loads that absorb electrical energy. Figures 33 and 34 respectively show class diagrams of the parent class *PrimaryElement* for electrically connecting as well as electrical energy feeding and drawing primary elements.

Secondary elements, in turn, include all resources used for measuring, monitoring and protecting. Therefore, Current Transformer (CT) and Voltage Transformer (VT) and protective devices fall under the *SecondaryElement* class. To simplify the model, the definition of separate switches is omitted, as is usual for the *Bus-Branch model*. Here, the installation location of a protective device, identifies the installation location of a circuit breaker connected in reality. Figure 35 shows the UML class diagram of the *SecondaryElement* class.

The focus of the GDM is on a detailed and efficient description and simultaneous separation of protective devices, protection functions and settings. These are all represented by their own individual classes. Figure 36 shows the corresponding UML class diagram. Here, a protective device in the GDM is also referred to as an Intelligent Electronic Device (IED). However, the term IED is not clearly defined. But it can be described as a multipurpose electronic device with several processors and functions, typically intended to control, monitor or protect components [122]. This is accompanied by a corresponding ability to measure, receive and transmit external data. Thus, each protective device or IED has not only one but a whole list of functions or protection functions assigned to the device. Each function is defined by a unique string *TypeIdent* and the respective class type. Currently there are 11 different protection functions available in the GDM such as the distance protection function, overcurrent protection function, overvoltage function or PSB function. Each function in turn has a list of essential setting values. Thus, each setting value in the GDM is represented by its own object, which is generalized an object of the parent class *IEDSetting*. So there are classes for the setting value X_1 of a distance protection function, the corresponding delay time T_1 or the activation or deactivation of the first tripping zone. Depending on their value, the setting values are divided into the three classes *IEDSettingBinary*, *IEDSettingInt* and *IEDSettingDouble*. This approach allows a generic and at the same time detailed description and handling of all protec-

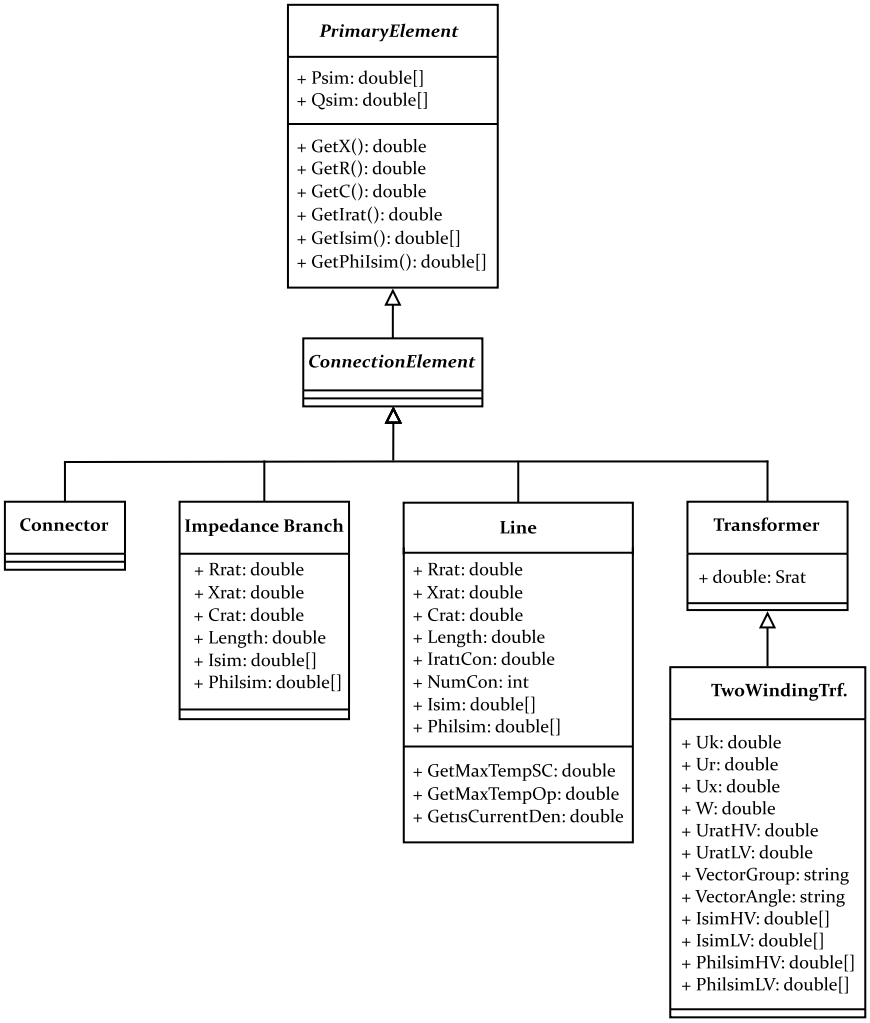

Figure 33: GDM UML class diagram of electrically connecting primary elements.

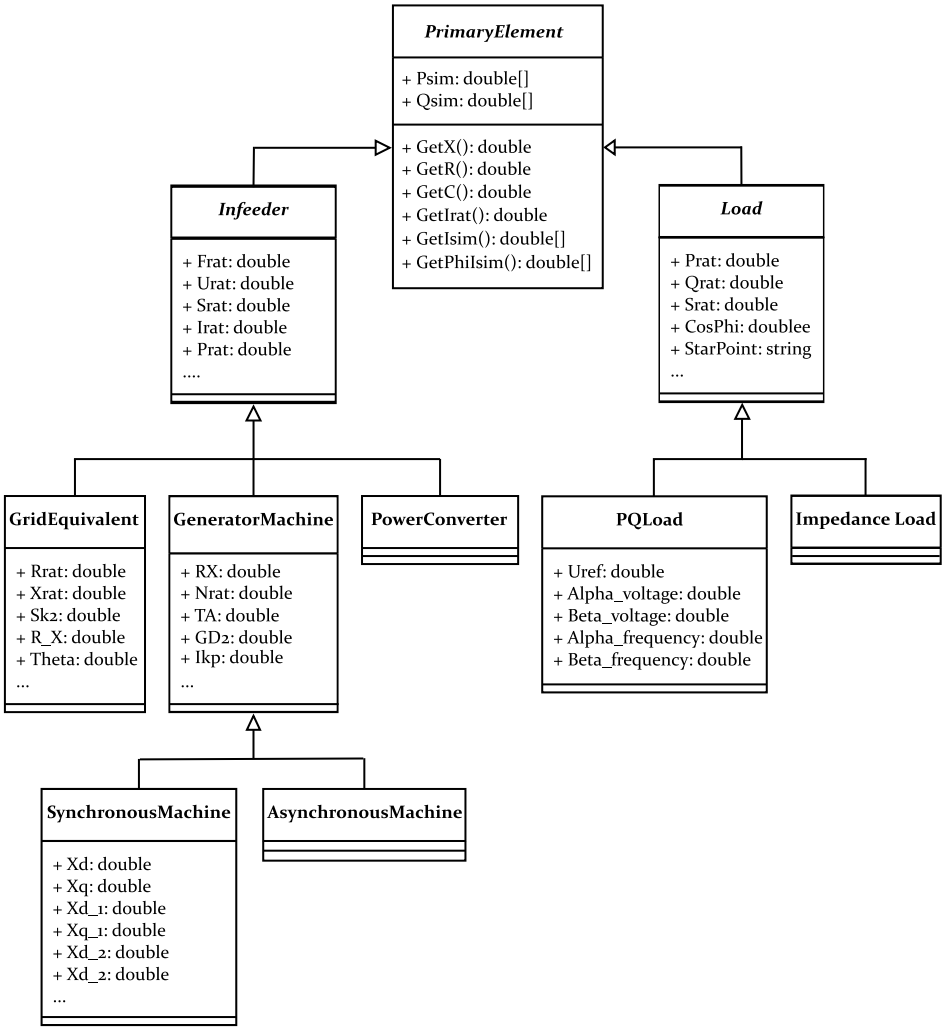

Figure 34: GDM UML class diagram of primary elements supplying and consuming electrical energy.

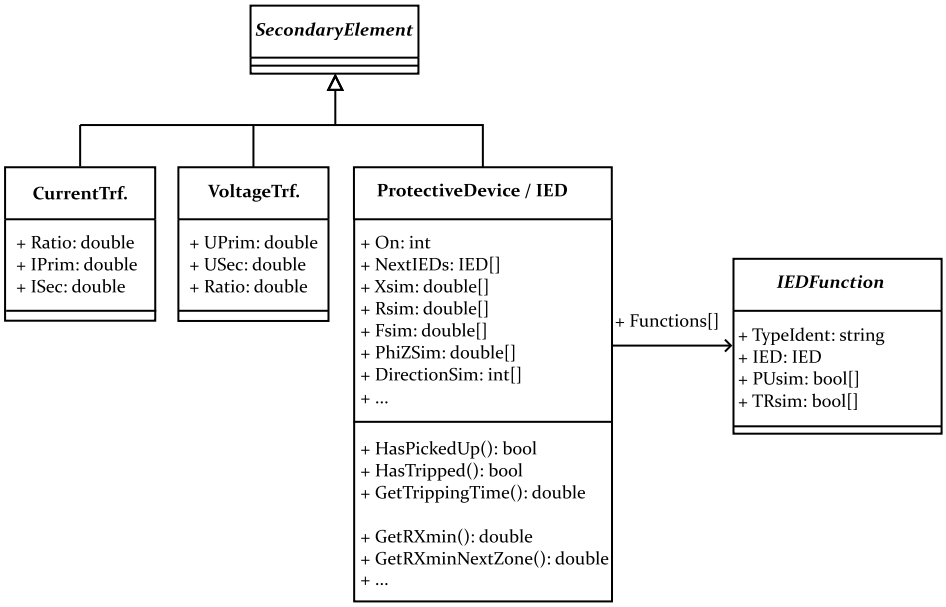

Figure 35: GDM UML class diagram of secondary elements and protective devices / IEDs.

tive devices, protection functions and setting values. For instance, individual minimum and maximum values can be defined for each value, which will still be of importance in chapter 11 when using an optimization algorithm. In perspective, this principle could also be applied in the CIM.

Electrical nodes are instantiated via the *Node* class. Thus, joints, busbars, substations, net stations or cable distribution cabinets are all objects of the *Node* class. Within the node class these can then be specified via attributes proximity. Should an investigation make it necessary to increase the resolution, this is also possible in the GDM as in the CIM by instantiating the appropriate objects. In general, however, the focus of the GDM is on the overall system and the protection system assessment as well as a high compatibility with simulation applications and less on the detailed description of configurations.

In addition to nodes, primary and secondary elements, protection zones or just zones, can be defined using their own objects of the class *Zone*. Zones include a certain amount of primary elements and nodes.

All connections in the GDM are described using objects of the *terminal* class. Terminals, with respect to a graph, represent the edges of the model, while nodes, primary elements, secondary elements and zones are vertices of the graph. Here, a terminal represents an electrical, logical, communicative, or

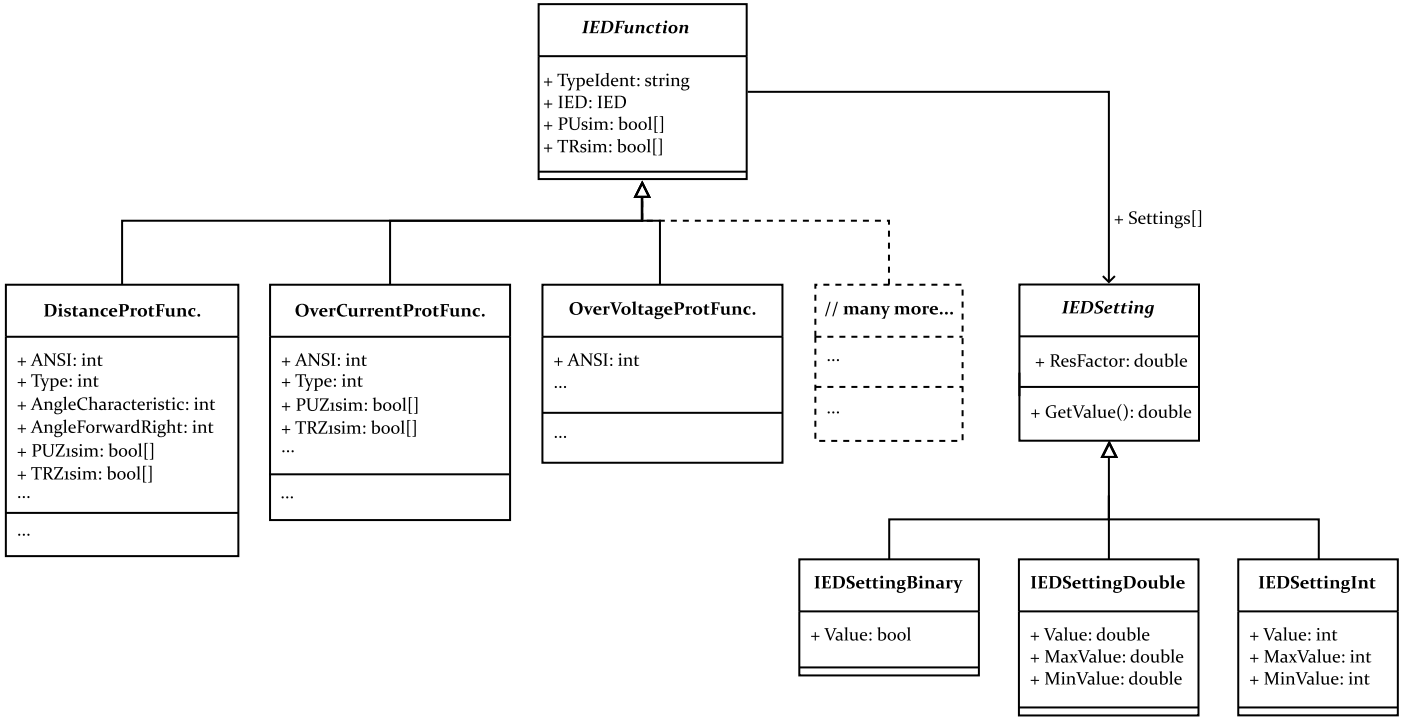

Figure 36: GDM UML class diagram of IED protection functions and IED settings.

more generally an abstract connection between exactly two resources. The semantics is the same for all types of relationships. Only the type of terminal finally decides the type of connection and therefore the type of relationship. Thus, following the model of the CIM, all primary elements are connected via terminals to nodes for building the power system. However, an important difference is that the nodes correspond to electrical nodes and not imaginary points. Therefore, a node always has at least two or more electrical connections to primary elements. Primary elements such as synchronous machines or loads have only one electrical connection to a node. Lines, cables or transformers represent connecting elements and therefore have electrical connections to two nodes. Primary elements also exist with the three-winding transformer, which can even be electrically connected to three nodes.

Secondary elements can be connected to nodes as well as to primary elements and other secondary elements. For example, a protective device is logically connected via a terminal each to a primary element and a node, representing the installation location of the non-defined circuit breaker. A VT is electrically connected to a node via a terminal. A CT is installed between an electrical node and a primary element to measure the flowing current. This is therefore connected to both resources by a terminal. A protective device receives measured values from the CT and CT and is therefore electrically or communicatively connected to both of them. Since not every simulation program provides for and requires the definition of measuring transformers, the GDM does not rely on a separate definition. For all these different multirelational connections, different terminal objects are provided to describe the type of connection in the GDM. Figure 37 shows the corresponding UML class diagram. The status of a connection as well as the status of a switch position is defined by setting a boolean attribute in the terminal object itself. In this way, all connections can be easily opened/activated and closed/deactivated and different system topologies and switch positions can be transferred to the GDM.

Zones are also connected to each other via nodes. This creates a new, higher level of abstraction in which the entire system consists only of zones and nodes.

In summary, the GDM connectivity model provides a generic, flexible, and at the same time comprehensive way to represent multi-relational connections. Figure 38 concludes by comparing a simple grid section in its real physical representation in the form of a single-line diagram with a bus-branch model, the CIM and thus a node-breaker model, and the representation in the GDM.

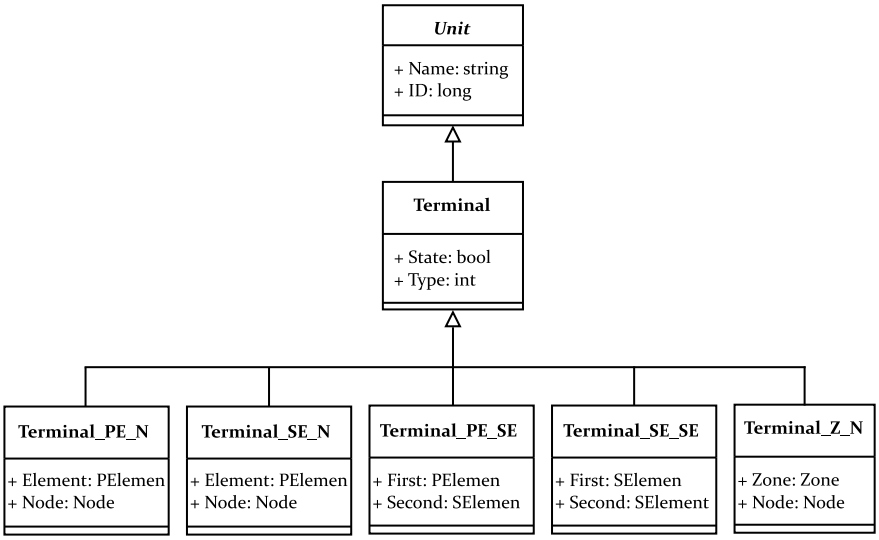

Figure 37: GDM UML class diagram of terminals describing multirelational connections.

(a) Physical model

(b) Simple Bus-branch-model

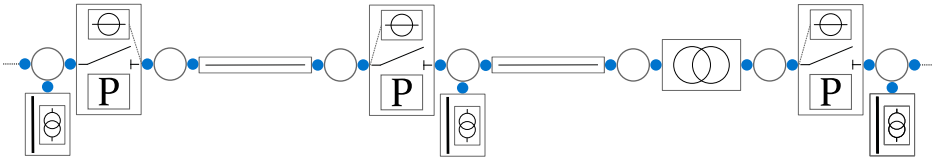

(c) CIM (node-breaker-model)

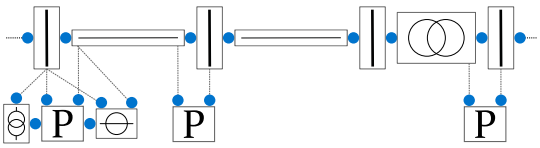

(d) GDM with optional CT and VT definition

Figure 38: Description of a simple grid structure in four different models.

Another important resource in the GDM is the definition of contingencies as objects. A *Contingency* describes a specific event such as the location, type and duration of a short circuit or the failure of a certain resource. In addition, there are further classes that serve as an interface to various simulation programs as well as the execution of simulations and the reading of simulation results. The classes *Simulation*, *SimulationProject* and *SimulationSettings* are intended for this. However, these shall not be discussed in more detail in the following. What is important, however, is the way simulation results are included and processed in the GDM. Measurement and simulation data are stored directly in the individual classes of primary elements, secondary elements and nodes. For example, the measured voltage at a node can be queried directly via the respective node after the simulation of a contingency. The same applies to measured currents, frequencies, impedances and generated pickup and trip signals of the various elements.

A final important feature of the GDM is that the entire power system itself is instantiated as an object via its own *PowerSystem* class. Figure 39 shows the matching UML diagram. In the *PowerSystem* class, all existing primary elements, secondary elements, nodes, zones and terminals are stored in lists and are thus available for analysis and evaluation purposes. In addition, each *PowerSystem* object has exactly one *Contingency* object associated with it. This means that a *PowerSystem* represents exactly one specific incident, one fault or, more generally, one event. Via the stored simulation data in the individual classes, the state of the overall system for this event can ultimately be retrieved via the *PowerSystem* object. This includes all connections, load flows, short circuit currents and reactions of the secondary system. For evaluation and analysis of another event and thus state, the *PowerSystem* is copied via a *DeepCopy* function. This copies the power system including all associated objects. The contingency can then be redefined, the simulation executed and the result data read in. Finally the total system state of a further event is available in a second *PowerSystem* object. About this procedure a simple handling and execution of most diverse contingencies results, which can be analyzed and evaluated all over the same methods. In addition, the data can be exchanged well with other tools and programs.

Conclusion The GDM is a fusion of different data management concepts, whereby particular emphasis was placed on a generic and flexible structure as well as the inclusion of protection data. The required abstraction level can be individually adapted to the task at hand.

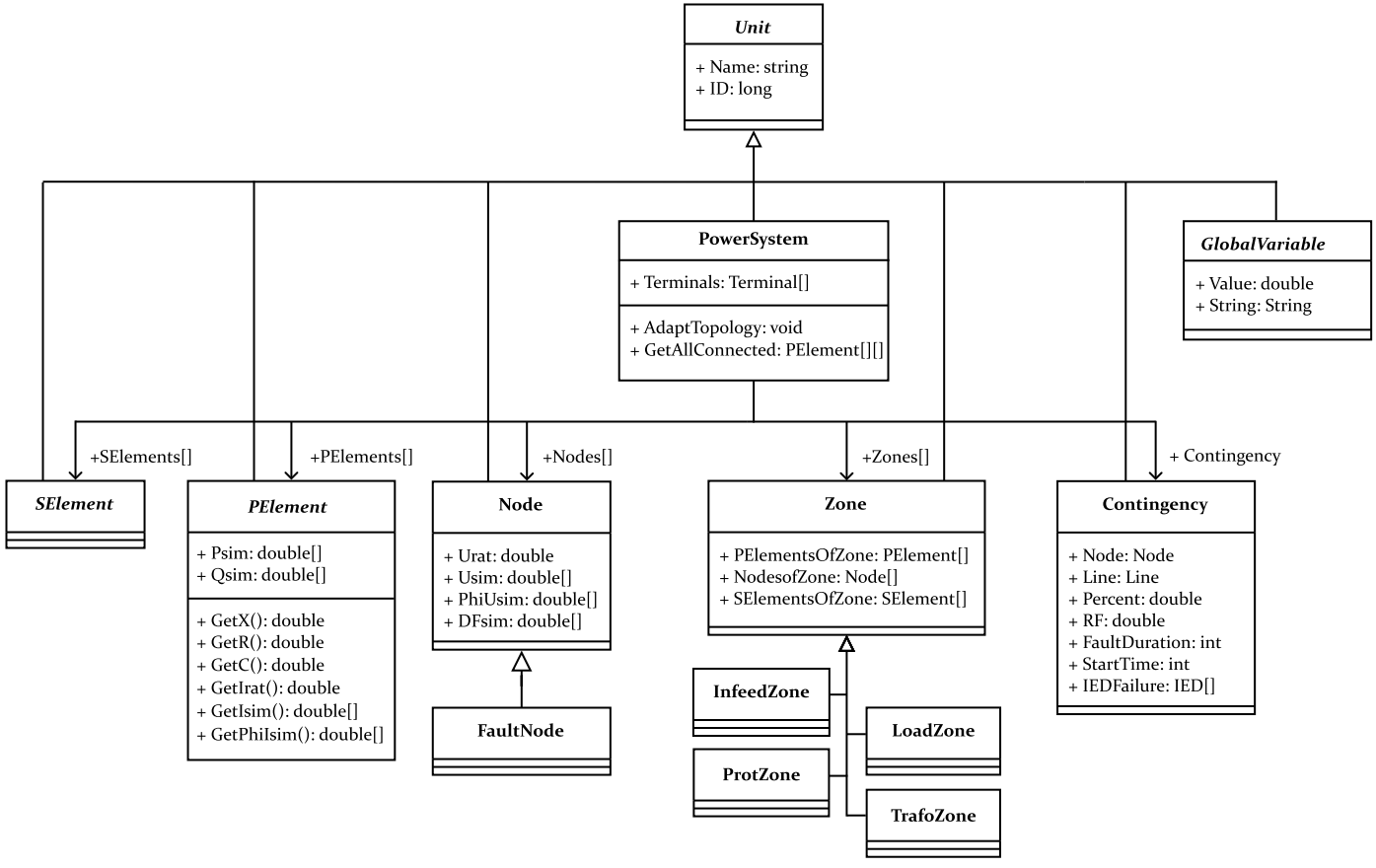

Figure 39: GDM UML class diagram of the PowerSystem class and the associations to the resources.

10.2 Protection Concept Generation

The first application area of the ProToc is automated new planning of protection concepts. The workflow is shown in Figure 40. The various process steps Typical Matching, Pre-Calculation, Algorithm Selection and Setting Calculation are run through one after another.

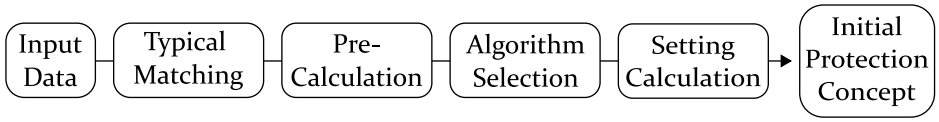

Figure 40: Worflow of the ProToc to generate an initial, first protection concept.

10.2.1 Typical Matching

In a very first step, the Typical Matching Tool loads the necessary input data. This includes the type of power system, existing primary, node and terminal data including voltage levels, as well as any circuit breakers, current and voltage transformers already installed. In the future, soft information such as special customer requirements or the available budget will be added. Subsequently, the loaded structure is analyzed via graph-theoretic approaches and suitable, prefabricated protection typicals, as known from section 9.4, are mapped onto the structure and assigned. Typicals are not necessarily limited to just one resource. They can also cover smaller grid sections in their entirety. The allocation takes place automatically after a hierarchical principle under consideration of the system type. The assigned typicals supplement the loaded input data with the type and installation location of additionally required CTs and VTs as well as circuit breakers, protective devices, protection function and a predefined protection algorithm. The data is then passed on to the next tool.

10.2.2 Pre-Calculation

The Pre-Calculations tool has the task of performing various preliminary calculations for the subsequent tools and providing the results accordingly. One of the most important tasks is to define protection zones. For this task, the GDM is used in combination with a special algorithm. Due to its graph-theoretic structure, the GDM allows to perform a recursive depth-first search through the system starting from the protective devices and thus to establish the individual protection zones. The depth-first search is a search algorithm specially designed for graph or grid structures. A protection zone describes

a contiguous area of equipments which, in the event of a fault, must be jointly isolated from the rest of the system to achieve selective fault clearing. The range of a zone is therefore defined by the installation locations of the protective devices and thus of the breakers. Figure 41 shows an example of the definition of different protection zones on a simple grid section. All primary elements and nodes located within a zone are assigned to the zones respectively.

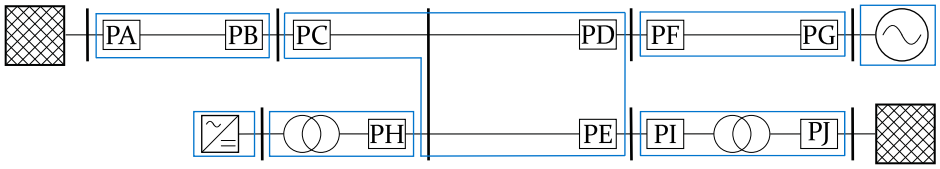

Figure 41: Construction of different zones on a simple grid section based on the topology.

In a next step, from the point of view of each protective device, the minimum and maximum path through its own zone to the end of the zone is calculated and from this the minimum and maximum resistance and reactance values R_{min}, X_{min}, R_{max} and X_{max} are determined. These are based on the resource data of the primary elements. Depending on the settings, parallel paths and transformers can be taken into account in each case. Subsequently, the values $R_{\text{next,min}}$, $X_{\text{next,min}}$, $R_{\text{next,max}}$ and $X_{\text{next,max}}$ are calculated, which are also used in the already presented setting rules (72), (73) and (74). For this purpose, from the point of view of each protection device, the resulting minimum and maximum path through its own and the next adjacent zone is calculated. The determined zones as well as resistance and reactance data are added to the JSON file.

10.2.3 Algorithm Selection

The Algorithm Selection tool has the task of selecting a suitable protection algorithm for each protective device. For this purpose, it uses an expert system to evaluate all available information and, based on this, to select the respective algorithm from an library. Information on the system type, grid topology, primary and secondary elements, zones, existing communication, the selected protection function and, in perspective, customer requirements as well as results of the PSA tool are included. In addition to standard algorithms, for example, the reactance method can be selected for distance protection in the case of longer lines and larger transmission angles, protection algorithms specifically for ring closures [89] or adaptive protection concepts in the case

of high backfeed of RES from the lower-level to the higher-level system [P123]. Adaptation of the filtering algorithm or Automatic Reclosing (AR) time are also possible options. Adaptive algorithm selection may play a more prominent role in the future.

10.2.4 Setting Calculation

After selecting the protection function and algorithm, all protective devices must be initially parameterized. For this purpose, an expert system based on many years of experience and expertise translated into setting rules is used. The system uses the input data system type, typical type, topology, primary and secondary data, protection function and protection algorithm, zone structure as well as additionally calculated parameters from the pre-calculation tool and further soft data such as the applicable grid code. More than 200 different constellations, each representing a so-called *setting unit*, are distinguished and taken into account. Each setting unit has a unique identifier. This identifier can be used to automatically select a suitable setting rule for each setting unit in order to calculate the settings of all protective devices of each typical. The setting instructions also take into account operating conditions and design limits of the equipment. After all settings have been calculated, they are added to the JSON file, which completes the initial protection concept. This is followed by the assessment and possible optimization of the entire protection setup.

10.3 Protection Concept Assessment & Optimization

The second area of application, which follows on seamlessly from the first, is the automated assessment and optimization of protection concepts. This can involve protection concepts initially generated by the ProToc as well as existing ones. The workflow is shown in Figure 42. The GDM is used in both tools as a data management and exchange platform.

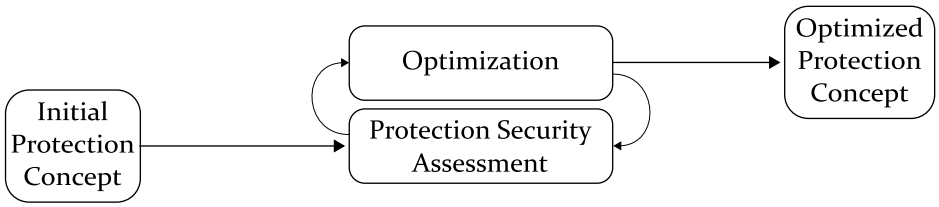

Figure 42: Worflow of ProToc for the assessment and optimization of existing protection concepts.

10.3.1 Protection Security Assessment

The PSA tool has the task of holistically analyzing the overall system consisting of the power and protection system and evaluating the underlying protection concept. It aims to determine whether the protection concepts initially developed by the ProToc or already existing in the field sufficiently meet the requirements for security and dependability, as well as leave the power system as a whole in a state as good and stable as possible after a fault has been cleared. The approach is based on an integrated, dynamic system modeling of the power and protection system behavior as well as a sequential simulation and subsequent evaluation of multivariate contingencies. The reactions and mutual interactions as well as effects of all connected equipment as well as protective devices including various protection functions are dynamically investigated. The evaluation criteria used must be implicit and comprehensible, as well as allow conclusions to be drawn about improvements, which is why the assessment system *Guiding Protection Security Assessment for Optimization* presented in chapter 8 is used. The presented indices allow to make a qualitative statement about the power system and protection system behavior as well as the subsequent use of an optimization method. The assessment tool thus serves as a basis for validating the protection concept, coordination as well as all settings and as a fitness function for the following optimization tool.

Required input data are the existing power system topology consisting of primary elements, nodes and terminals as well as protective devices, transducers, protection functions, the algorithms used and setting values. The installation locations of the protective devices and thus circuit breakers, as well as the defined protection zones, controller and load flow data are also required. In the future, soft data such as the prioritization of equipment, the probability of individual contingencies and customer requirements will be added. In order for the ProToc to be used as an online tool for protection assessment, it must always be supplied with the latest measurement, status and forecast data.

10.3.1.1 Modeling of the Power and Protection System

By using the GDM as well as a separately implemented assessment system, it is possible to perform the execution of simulation as well as subsequent analysis and assessment of the results separately from each other. The approach therefore allows the use of different simulation programs depending on the requirements. In the context of this work, the dynamics engine PSS©NETOMAC (Network Torsion Machine Control) of the power system simulation program PSS©SINCAL of Siemens AG is used. This offers the possibility to perform

transient and dynamic calculations in the time domain and to simulate the behavior of power system elements, electrical machines, converters and controllers.
For transient calculations the momentary value part, also called EMT part, is available. With this, any electromagnetic as well as electromechanical, symmetrical as well as asymmetrical processes can be completely calculated. For this, Netomac solves the state differential equations of the power system according to the differential conductance method. The integration in turn takes place according to the trapezoidal rule, which is also used, among other things, for the calculation of individual evaluation indices.
The stability part, also called RMS part, is available for the calculation of dynamic processes. Here, the power system is assumed to be symmetrical and is described in a single-pole form via complex impedances instead of differential equations. Electrical machines are modeled with reduced order of the differential equations, which means that the flux variation in the d- and q-axes is not considered. This has the consequence that, for example, DC compensation currents do not occur when simulating a short circuit. The stability part allows an effective calculation of the transient stability processes in a multi-machine model reduced to the fundamental frequency model. Thus, only the respective fundamental phasors are calculated. Unbalanced faults can be solved by using symmetrical components, however, the corresponding system data must be specified.

Within the framework of the PSA tool, the consideration of power system and protection behavior in the stability part is sufficient for the assessment of the protection coordination as well as the tripping and pickup behavior of all protective devices in the short-circuit case and during transient stability. [124] In addition, the lower level of detail required for the power and protection system in the stability part reduces the computational effort required, which is especially necessary for subsequent coupling with an optimization method. Cascading protection trips, which lead to partial power system failures, load failures and islanding are taken into account. All protective devices and functions are simulated in the form of simple, phasor-based models with mathematical equations and characteristic curves. These are implemented in the form of controller definitions in Netomac Fortran macro files, which allow logical separation and individual programming of all functionalities. The first generic protection models of this kind were developed in the diploma thesis [125] at the EES of FAU and are described there in detail. In [52] these were further developed and used to build the DPSA system already presented in chapter 7.3. There, their functionality was also validated using Petri nets,

among others. In the context of this work, the following generic protection functions implemented in Netomac macros are available to the PSA tool:

Distance Protection Function

- Characteristics: Quadrilaterals or MHO circles.
- Number of zones: 3
- Direction: Forward, backward or undirected.
- Pickup: Impedance.
- Trip delay: Common timer or zone depending timer.
- PSB: Trajectory movement detection according to [126] or dual-quadrilateral blinder.

Overcurrent Protection Function

- Characteristics: IOC and DTOC.
- Number stages: 2
- Direction: Forward, backward or undirected.
- Pickup: Overcurrent.
- Trip delay: Common timer.

Generator Protection Functions according to [52], [127]

- Over/undervoltage protection with two stages.
- Over/underfrequency protection with two stages.
- Over/underexcitation protection with two stages.
- Out-of-step protection (78) with quadrilateral blinder.

All protective devices and protective functions have:

- Hysteresis functions for the fallback.
- Adjustable circuit breaker opening time.
- Individual timer for all pickup stages.
- Possibility of activation/deactivation.

10.3.1.2 Simulation Process and Result Data

Like the GDM, all controlling, analyzing and evaluating applications of the PSA tool are implemented in the object-oriented and type checking programming language C# from Microsoft.

Parsing Input Data In a first step all necessary input data are parsed and translated into the GDM. Here a check of the data for correctness and completeness takes place. At the end of the process, the object *PowerSystem* is created, through which all information can be accessed.

Definition of all Contingencies Subsequently, all contingencies to be simulated are automatically created in the form of objects depending on settings made. The principle is based on the approach of a running fault already presented in chapter 7.1. Fault duration, fault resistances, failure of protective devices and the rastering of the short-circuit location can be specified individually. However, in order to be able to reduce the computational effort while maintaining the same level of information, short-circuits are not simply simulated all X% on each line but on automatically determined paths. A path describes a continuous section of lines within a zone, which extends from protective device to protective device, from protective device to a junction or from a junction to the end of a zone. Paths thus divide a zone into different, interconnected segments and, from the perspective of each protective device, result in a kind of individual tree structure. The advantage of this is that if the lines simply follow one another, the number of short circuits to be simulated can be reduced. At the same time, the resolution of the rastering at the critical points in the power system remains high. For each contingency created, the *PowerSystem* object is copied and the corresponding association is made. In the end, there is a whole list of *PowerSystem* objects that are passed for simulation.

Simulation Execution In order to make the simulation process as computationally efficient as possible, it is parallelized. The degree of parallelization depends on the available hardware and thus on the number of available processors. A number of parallel simulations of about 1.5 times the available number of virtual cores has proven to be effective.

At the beginning of the simulation process, Netomac projects are created in separate folders according to the defined number of parallel simulations. The individual simulations then take place within these Netomac projects and project folders. The execution of all functions necessary for this as well as

the actual simulation are organized over the class *System.Threading.Tasks* provided by Microsoft. This is available for the *.NET Framework* software platform as well as for the *.NET* platform. Each simulation to be performed is first created as a *Task* object representing an asynchronous task, and thus added to the thread pool. The execution of all simulations and thus the processing of all *Task* objects is then done in parallel, leaving the order to the Windows operating system.

Each task process writes all necessary data into the corresponding Netomac project before starting the actual simulation. Thus, the contingency data to be simulated, the setting values and functions of all protective devices to be used as well as the result data required for the subsequent assessment are first defined and written to the Netomac files required for this purpose. Subsequently, the actual simulation call takes place. For this purpose, the Component Object Model (COM) interfaces provided by Netomac are used, via which various Netomac functions can be accessed [128]. COM is a programming language independent technique created by Microsoft, which allows components to make their functionalities available to other components and applications. After the simulation is finished, all result data is imported into the GDM, assigned to the respective objects and then deleted in the Netomac project itself. The Netomac project is then available again for the next task. Results are stored securely in a respective *PowerSystem* object.

Contingency Evaluation After all simulations are completed, the simulation results are evaluated in parallel. In a first step, the responsibility of each protective device for the existing contingency is determined. This is followed by the calculation of the fault clearing time and fault tripping time. This is followed by the evaluation and thus calculation of the individual indices from chapter 8. In addition, the following indices are determined so that the sequence of events can be traced in detail by a protection engineer.

- Determination of all protective devices that have been picked up as well as the protective functions responsible for it.
- Determination of all correctly as well as unnecessarily tripped protective devices, time of tripping as well as the protection functions that led to tripping.
- Identification of all tripped protective devices as well as the responsible functions that were allowed to trip but were not required to trip.
- Determination of all protective devices that did not trip but should have tripped and basically had the necessary conditions to do so.

- Determination of all protective devices that did not trip, but should have, but could not due to a defined failure.

In the end, the corresponding result value EV_i is obtained for each contingency according to (70).

Total Assessment Finally, the GPI and the final PSA fitness value $PSA(\vec{x})$ are calculated according to (70). The evaluation results of all fault cases are output in the form of a colored matrix, as exemplified in Figure 25. Additionally, all further result data and determined information are stored in a text file.

10.3.2 Optimization

The task of the optimization tool is to improve the existing protection concept. In chapter 7, various methods such as the use of rule-based methods, expert systems, fuzzy sets or deterministic techniques were presented and discussed for this purpose. However, all of them do not sufficiently fulfill the requirements of an automated, efficient and protection function spanning system. Therefore, a metaheuristic optimization method is used in this work, which is able to simultaneously and jointly optimize the setting values of all distance protection and overcurrent protection functions of all protective devices in the system. In combination with a suitable fitness function, different protection systems can be parameterized in the same way, coordinated together and adapted to existing conditions. The determined setting values must meet the requirements of reliability, applicability and comprehensibility. As a result, the generation of a protection concept should be simple, complete, automated and without the need for expert knowledge, and should offer significant added value compared to simple setting rules. In addition, unconventional and thus novel solutions are to be expected with the corresponding freedom granted for the optimization procedure. All PSO optimization methods from chapter 3, which are implemented in the programming language C#, are available in the optimization tool. The PSA tool serves as a fitness function. In order to minimize this like the test functions from chapter 5.2, the function $1 - PSA(\vec{x})$ is used.

10.3.2.1 Selection of the Decision Variables

Which protection setting values of which protective functions of which protective devices are to be optimized can be set individually. Single functions but also all functions and devices in the system can be optimized. For the distance protection function, only the quadrilateral tripping characteristic with three

zones is considered in the following, with which the protection setting values according to Table 15 are available. For the overcurrent protection function, the DTOC characteristic with two zones is used and thus the setting values according to Table 16 are available for selection.

Table 15: Optimizable protection settings, decision variable names, value ranges and resolution factors of a distance protection function.

Setting	Decision variable x_i	Value range $[x_{\min}, x_{\max}]$	Resolution factor rf
Reactance in Ω	X_1, X_2, X_3	Automatic determination	Adjustable default: 0.01
Delay time in s	T_1, T_2, T_3	User definition	Adjustable default: 0.05
Direction	Dir_1, Dir_2, Dir_3	1: Forward 2: Reverse 0: Non-directional	1.0
PSB function	PSB	1: On 0: Off	1.0
OOS function	OOS	1: On 0: Off	1.0

An optimization of the resistance values R_1, R_2, R_3 of the tripping zones of the distance protection functions is not performed within the scope of this work. They are directly coupled to the corresponding reactance values via (84). A limitation takes place via the maximum allowed R-range according to (86). The angle α describes the angle of inclination of the quadrilateral tripping characteristic of the distance protection function, which is often oriented to the angle of the line characteristic in the high and extra-high voltage system. The minimum load impedance $Z_{\text{Load-max}}$ is calculated from the maximum load current $I_{\text{Load-max}}$ and a freely selectable security factor SF according to (85). [93] On the one hand, this approach simplifies the optimization process and, on the other hand, it prevents coordination based on the resistance rather than reactance values.

$$R_i = \begin{cases} 4X_i & X_i < 6.25\,\Omega \\ 25\,\Omega & 6.25\,\Omega \leq X_i \leq 62.5\,\Omega \\ 0.4X_i & X_i > 62.5\,\Omega \end{cases} \tag{84}$$

Table 16: Optimizable protection settings, decision variable names, value ranges and resolution factors of an overcurrent protection function.

Setting	Decision variable x_i	Value range $[x_{\min}, x_{\max}]$	Resolution factor rf
Current in kA	$I_{>>}$ and $I_{>}$	Automatic determination	Adjustable default: 0.1
Delay time in s	$T_{>>}$ and $T_{>}$	User definition	Adjustable default: 0.05
Direction	Dir_1 and Dir_2	1: Forward 2: Reverse 0: Non-directional	1.0

$$Z_{\text{Load-max}} = SF \cdot \frac{U_{\text{r}}}{\sqrt{3} \cdot I_{\text{Load-max}}} \tag{85}$$

$$R_{\text{Quad-max}} = Z_{\text{Load-max}} \cdot \left(\cos(\varphi_{\text{Load-max}}) - \frac{\sin(\varphi_{\text{Load-max}})}{\tan(\alpha)} \right) \tag{86}$$

10.3.2.2 Determination of the Value Ranges

The value ranges of the protection settings to be complied with have a decisive influence on the runtime of the optimization process as well as on the result. These should be as small as possible so that the optimization method can find a solution quickly. At the same time, however, they should also be large enough so that the best coordination solution can be found. For the test functions from chapter 5, the respective value ranges were predefined and the same for all decision variables. However, since different protection setting values and thus different decision variables are now used to optimize the protection coordination, it is necessary to use individual and adapted value ranges. In this case, the range of values to be assumed is clearly defined for some protection setting values. For example, additional functions can only be switched on or off and for the direction view to be defined there are exactly three possibilities with the options forward, backward or undirected. For the delay times of the individual tripping zones, the permissible times can be defined individually for each zone. In this way, the free space available to

the optimization method can be defined and, at the same time, applicable specifications and guidelines for delay times to be met can be realized. However, the value ranges and thus the minimum and maximum reactance and current values to be assumed for the distance and the overcurrent protection function of the individual tripping zones represent a particular challenge. The value range of the individual setting values must be large enough for an optimization method to determine the best solutions. At the same time, the optimization method should be goal-oriented and efficient, providing logical and practical results. Traditional approaches such as the (72), (73), and (74) equations rely solely on equipment data. However, as shown in section 9.3, numerous effects influence the measurement result of protective devices, so this approach is not accurate enough.

To be able to define the value ranges more specifically, a PSA pre-analysis is performed to determine the value ranges of the reactance and current values simulatively. This was first published in [P71]. As with the PSA procedure, a running fault is simulated in the power system. Here, for each individual fault simulation, all measured fault impedances and all fault currents of all protective devices are individually recorded and stored. Thus, what each protective device measures in response to a fault is recorded. Each individual measured value of each protective device is then assigned to a specific protection zone (*ProtZone1*, *ProtZone2* or *ProtZone3*) of the protective device. For this purpose, similar to selectivity evaluation, the responsibility of a protective device is determined for each fault. Thus, a protective device may be primarily, secondarily, or tertiary responsible for fault clearing. Depending on the result, the measured values are then assigned to the corresponding protection zones. Figure 43 illustrates the assignment process based on a fault in the already known example system from section 10.2.2.

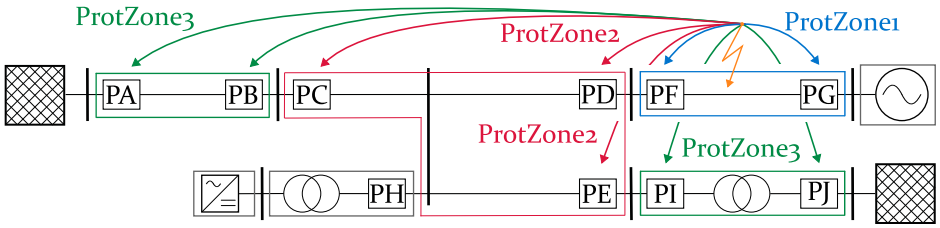

Figure 43: Assignment of the individual measuring values of each protective device depending on the responsibility for the present fault to the respective protection zone ProtZone1, ProtZone2 or ProtZone3.

The fault is located between the protective devices PF and PG. These are therefore primarily responsible for the fault and assign their measured values

to the protection zone *ProtZone1*. PC, PD and PE represent the first backup protection and are therefore secondarily responsible for the fault. They assign their measured values to *ProtZone2*. Accordingly, PA, PI and PJ are tertiary responsible and assign their measured values to *ProtZone3*. This process is repeated for all the topologies and states of the power system to be investigated simultaneously. Thus, all contingencies and measurement effects are considered and the respective measured values are stored.

Finally, the formation of value ranges of the reactance and current setting values of all tripping zones takes place. Depending on the topology, the minimum $x_{\min}$ and maximum $x_{\max}$ setting value to be taken is determined based on the minimum and maximum measured values. Since the smallest measured reactance value of the protection zone *ProtZone1* is always close to 0 Ω, the minimum reactance value $X_{\min}$ of the own zone is used by the Pre-Calculation Tool instead. For the determination of the smallest current value to be assumed, the maximum load current is taken additionally. The value ranges formed in this way serve only as a framework for the subsequent optimization process. They neither have the task nor should they meet selectivity requirements. This task falls to the fitness function, where the tripping behavior is also evaluated with respect to selectivity. After setting up all value ranges, the GDM automatically calculates the still missing bit lengths n_b according to (25) depending on the defined resolution factor rf. Finally, the data is passed to the optimization tool.

Two things are necessary to our work: Tireless perseverance and the willingness to throw away something in which you have put a lot of time and effort.

Albert Einstein
German theoretical physicist
* 1879, + 1955

11 Applications of the Protection Toolchain

In this chapter, the ProToc is brought to bear and different scenarios are tested, evaluated and optimized. In a first step, different protection concepts for a real existing 20 kV distribution system are investigated and compared. Subsequently, analyses are carried out to show which setting values the use of the ProToc leads to and which strengths and weaknesses a fully automatic concept generation has. In a second step, the ProToc is used to evaluate and improve protection concepts on the well-known Nordic Test System (NTS). This is an ultra-high-voltage and high-voltage transmission system that is particularly suitable for investigating dynamic phenomena and their effects on stability.

The entire ProToc including all parallel dynamic short-circuit simulations of the PSA system is run on a ProLiant DL380 Gen10 server from Hewlett Packard Enterprise. The server has two Intel© Xeon© Gold processors 6136, each of which has 12 physical cores and thus 24 virtual cores. The base clock frequency of the processors is 3 GHz. The installed RAM is 192 GB and the operating system used is Microsoft Windows Server 2019 Standard.

11.1 Protection Concepts for a Distribution System

11.1.1 Power System Model & Protection Data

The 20 kV, 50 Hz city grid used in the following is a modified version of a real existing grid section in Germany. It was extended by various fictitious

Distributed Energy Resource (DER) in [129] and subsequently used for investigations of protection systems and protection concepts. The system is a ring grid with open disconnectors. The grid topology and the installation location of all installed lines, generators, transformers and protective devices are shown in Figure 44. The corresponding equipment data can be found in the Appendix C, thus enabling the reconstruction of the power system model and the plausibility check of the protection settings given below.

Compared to [129], the installation location of the DER G1 has been changed and the outputs of all units have been reduced to make the model more realistic. The DERs G1 to G5 are biogas, combined heat and power, hydroelectric or small thermal power plants, all of which have a synchronous generator. The corresponding plant data can be found in Table 24 and the data of the associated transformers T1 to T5 in Table 25 in the Appendix. The PSS©E standard controllers *TGOV1* and *HYGOV* are used as rotational speed controllers depending on the particular machine. The *SEXS* model for excitation systems is used as voltage regulator. The IEEE and PSS©E standard *PSS2A* model is used as grid stabilizer. For all controllers default values are used. The main infeed is from the 110 kV level above with a short-circuit power of 4.7 GVA and a R/X ratio of 0.1.

The main busbars Bus1 and Bus2 are located in the center of the system. From them depart 14 line feeders A to N, each feeder being protected by a protective device PA to PN with distance protection function. Each of them has a quadrilateral tripping characteristic with two or three forward zones. The PA, PB and PI protective devices are followed in the respective feeders by PA2, PB2 and PB3 and PI2 with overcurrent protection function. Connected line outlets to the DERs are protected by the protective devices PG1E to PG5E with overcurrent function. They all have DTOC characteristics with one or two direction-independent zones each. Every DER also has its own overfrequency and underfrequency protection as generator protection. The setting values from PG1E to PG5E as well as the generator protection settings are given in the Appendix C in the Tables 28 and 29 and remain the same for all subsequent studies. The breaker delay time of all devices is assumed to be 0.1 s, which is a conservative value and an on-the-safe-side estimate. All protective devices always calculate with directly measured voltages.

11.1.2 General Framework Conditions

For the performance of all tests, the following general conditions apply when calculating or optimizing the protection setting values.

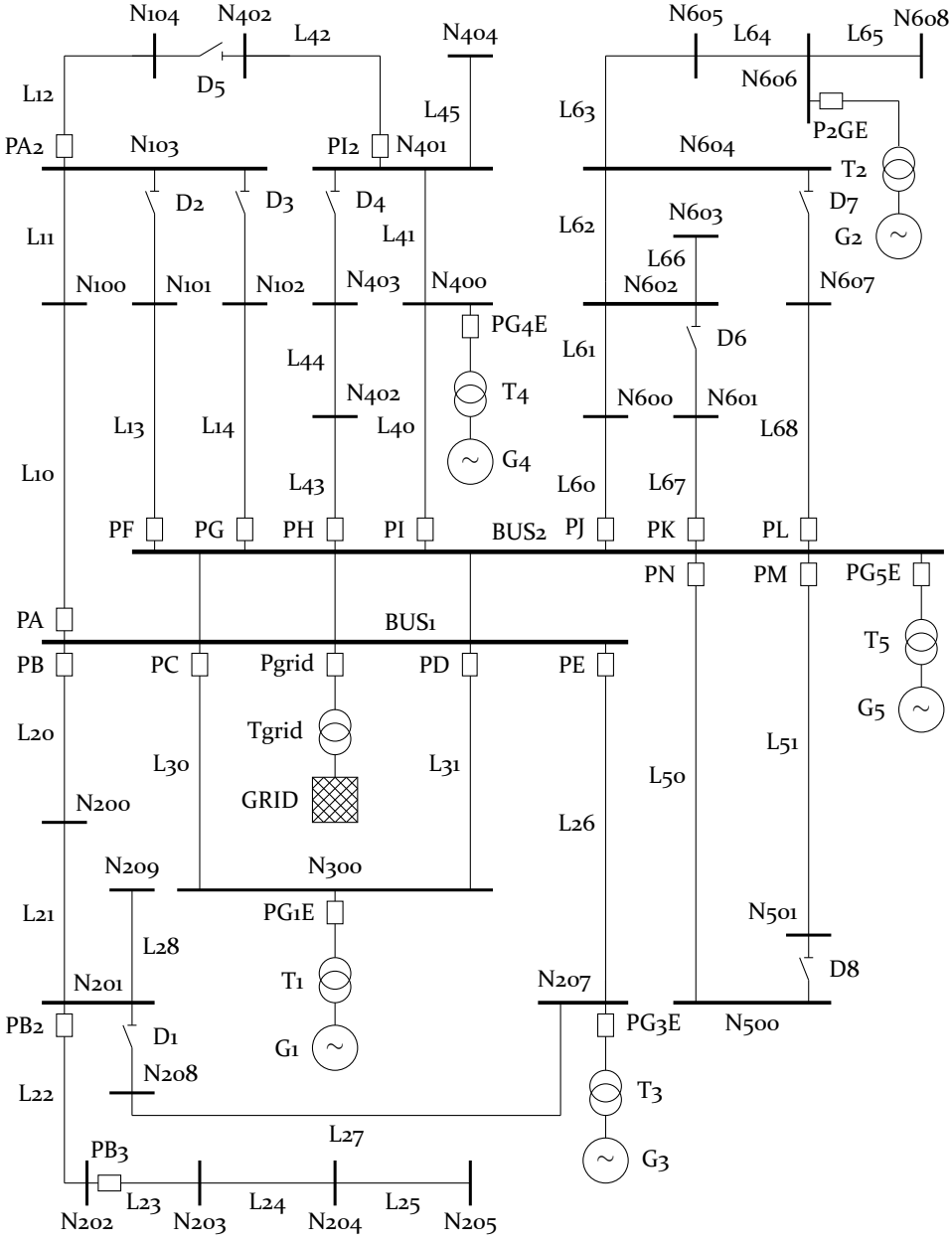

Figure 44: Single line diagram of the 20 kV medium voltage grid.

- The first two zones of all distance protection functions are always enabled. A third zone is used by the ProToc only if the respective protective device has a subsequent zone or there is an intermediate infeed to its own zone. When calculating or optimizing all setting values, outgoing feeder stations in the line sections are not taken into account and are therefore overstaggered accordingly. This is acceptable as far as the reactances of local distribution transformers can be assumed to be sufficiently large so that the zones of the distance protection do not extend unselectively into the underlying low-voltage systems. Should faults occur directly at the beginning of the local distribution transformers, unselective fault clearing would be accepted.
- For all overcurrent protection functions to be set, only one zone is initially activated. For PA2 and PI2, this is set to $I_{>>} = 2I_N$ with $t_{>>} = 0.1\,s$. PB3 as upstream device to PB2 is parameterized to $I_{>>} = 1.1I_N$ with $t_{>>} = 0\,s$ and PB2 correspondingly to the same threshold $I_{>} = 1.1I_N$ with a higher delay time of $t_{>} = 0.3\,s$.
- Only 3ph and thus symmetrical short circuits without fault resistance are simulated.
- The raster of the fault location is set to 1 %, 10 %, 30 %,... 90 %, 99 % for the optimization process. The failure of protective devices is also taken into account. For this purpose, in the case of a zone with two protective devices, first one, then the other, and finally both devices are blocked and the corresponding failure on the paths is regenerated. In case of failure of one of the distance protective devices, a directional overcurrent protective device is available as backup protection, which trips 0.6 s after fault detection.
- As simulation time 3 s and as time step 5 ms are used. For transient stability studies with electrical machines, even time steps of 10 ms to 20 ms are basically sufficient [52], [130]. Modern, digital protective devices have an internal sampling frequency of 16 kHz and more. However, for a wide variety of measurement and protection applications, only 20 samples per cycle are used, resulting in exactly one sample per 1 ms at a system frequency of 50 Hz. Digital Finite Impulse Response (FIR) filters and adaptive algorithms are used for filtering. If there are abrupt changes in the measurement inputs, the filtering data window is reduced to 5 ms and then filled for increased accuracy. The first measured value of the fault impedance is therefore available after 5 ms at the earliest. [93], [99], [131]

- The number of maximum FES is set to 5000 as a good tradeoff of computation time and accuracy. As optimization method $BPSO_{DE}$-4 is used, which has shown the best performance in chapter 5.
- The fitness function used is FV $= 1 - PSA(\vec{x})$ to (70) with a weighting factor of $w = 0.5$. Thus, the selectivity evaluation expressed by PSI is incorporated into FV as much as the dynamic stability evaluation by DSI and the security of supply by SRI.

The following modified conditions apply in the final assessment of the protection concepts.

- The rasterization of the fault location is increased to 1 %, 10 %, 20 %,... 90 %, 99 %.
- The simulation time is increased to 5 s.
- The overall result is FV $= PSA(\vec{x})$, which means that larger values represent better results and are therefore more convenient to compare.

11.1.3 Operated as a Radial System

If all disconnectors of the system are open, the present ring grid results in the form of a radial system. For this condition, the protective devices PA to PN with distance protection function and PA2, PB2, PB3 and PI2 with overcurrent protection function are to be set in the following. During the optimization process, the topology leads to 378 dynamic short-circuit simulations per PSA run. This results in a total of 1.89 million dynamic short-circuit simulations during an optimization run, so the process takes approx. 44 h. For the final assessment of the protection concept with finer rasterization of the fault location and extended simulation duration, this results in 594 dynamic short-circuit simulations per PSA-run. One run thereby takes approx. 4 min.

11.1.3.1 Use of Standard Setting Rules for Distance & Overcurrent Protection

Procedure With the use of the ProToc, in a first step all distance protection functions are parameterized according to (72) and all overcurrent functions according to (75). The individual values $X_{\mathrm{AB,min}}$, $X_{\mathrm{AB,max}}$ and $X_{\mathrm{next,max}}$ from the protective device perspective are automatically calculated based on the line data, topology and zone structure. If there is no subsequent zone, then X_3 is set to $2X_{\mathrm{AB,max}}$. All calculated values, as well as all future optimized values, are clearly listed in Table 30 in the Appendix D, summarized for easy comparison.

Results The result matrix of the PSI is shown in Figure 45 and gives a result value of 0.989. The joint result of of the DSI and the SRI is shown in Figure 46 and gives a result of 0.894. The overall assessment result is 0.942. It can be seen that most of the faults are selectively cleared. However, especially in the range of 1 % and 10 % faults with simultaneous protective device failure and thus delayed fault clearing, unselective behavior of the protection system occurs. Table 17 lists the corresponding unselective tripping devices in relation to the simulated fault. It is noticeable that especially the protective devices PE, PI and PJ tend to overfunction. Figures 47, 48 and 49 show the R-X impedance diagrams of the respective three protective devices during a fault on 1 % of path L10-L11 when PA fails. It can be clearly seen that the measured impedance trajectories of all three devices move along elliptical paths during the fault. In doing so, they penetrate backwards into Zone1 of the tripping characteristics of the distance protection functions, causing the generation of instantaneous trip signals and unselective tripping.

Table 17: Marking of the unselectively tripped protective devices by fault location. All disconnectors are open and calculated setting values are used.

Fault on path	PE	PI	PJ	PB
Fault on L10-L11-1 % (PA)	x	x	x	
Fault on L13-1 % (PF)		x	x	
Fault on L14-1 % (PG)		x	x	
Fault on L20-L21-1 % (PB)	x		x	
Fault on L22-1 %-10 %				x
Fault on L26-1 % (PE)		x	x	
Fault on L30-1 % (PC)	x		x	
Fault on L30-1 % (PC PD)	x		x	
Fault on L31-1 % (PD)	x		x	
Fault on L31-1 % (PC PD)	x		x	
Fault on L40-1 %-10 % (PI)			x	
Fault on L43-L44-1 % (PH)		x	x	
Fault on L50-1 %-10 % (PN)		x	x	
Fault on L51-1 %-10 % (PM)		x	x	
Fault on L60-L61-1 % (PJ)		x		
Fault on L67-1 % (PK)		x	x	
Fault on L68-1 % (PL)		x	x	

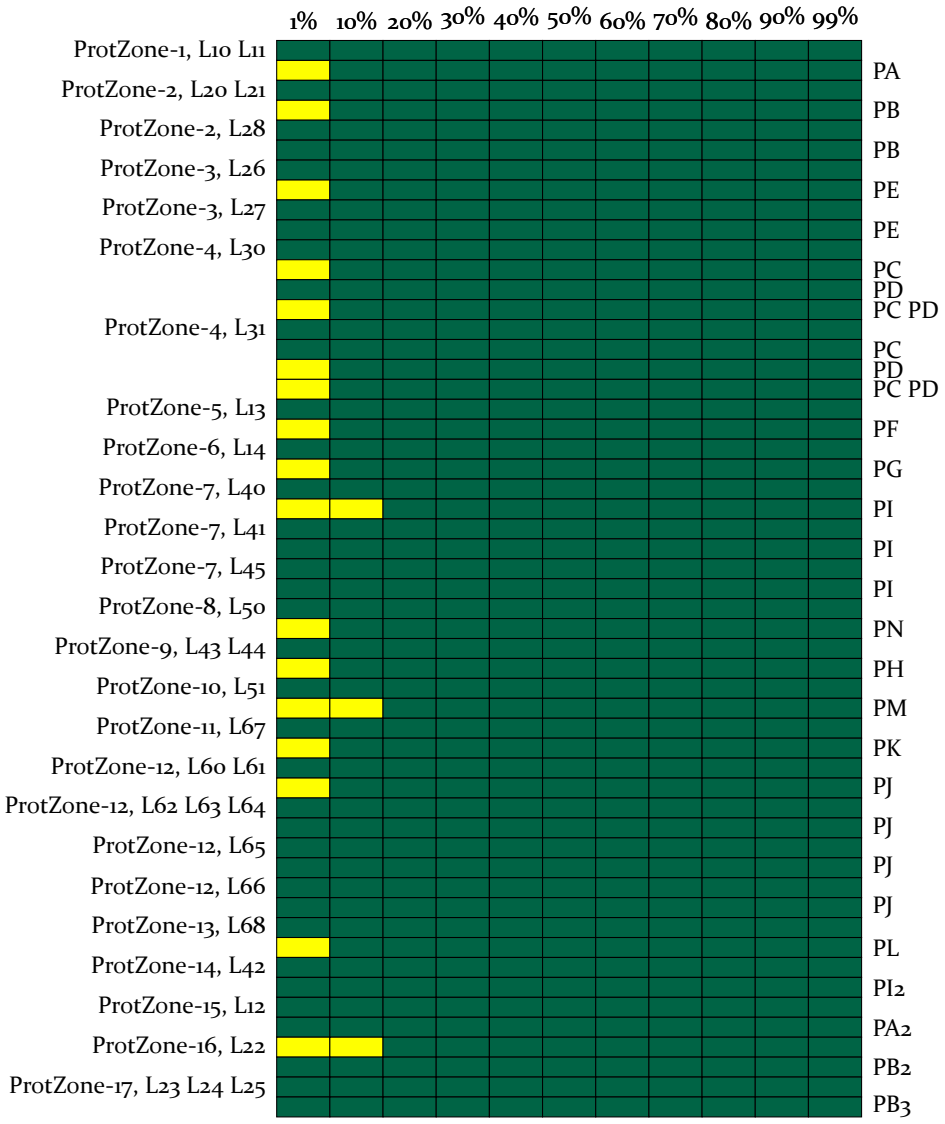

Figure 45: PSI result matrix with open disconnectors and calculated protection setting values.

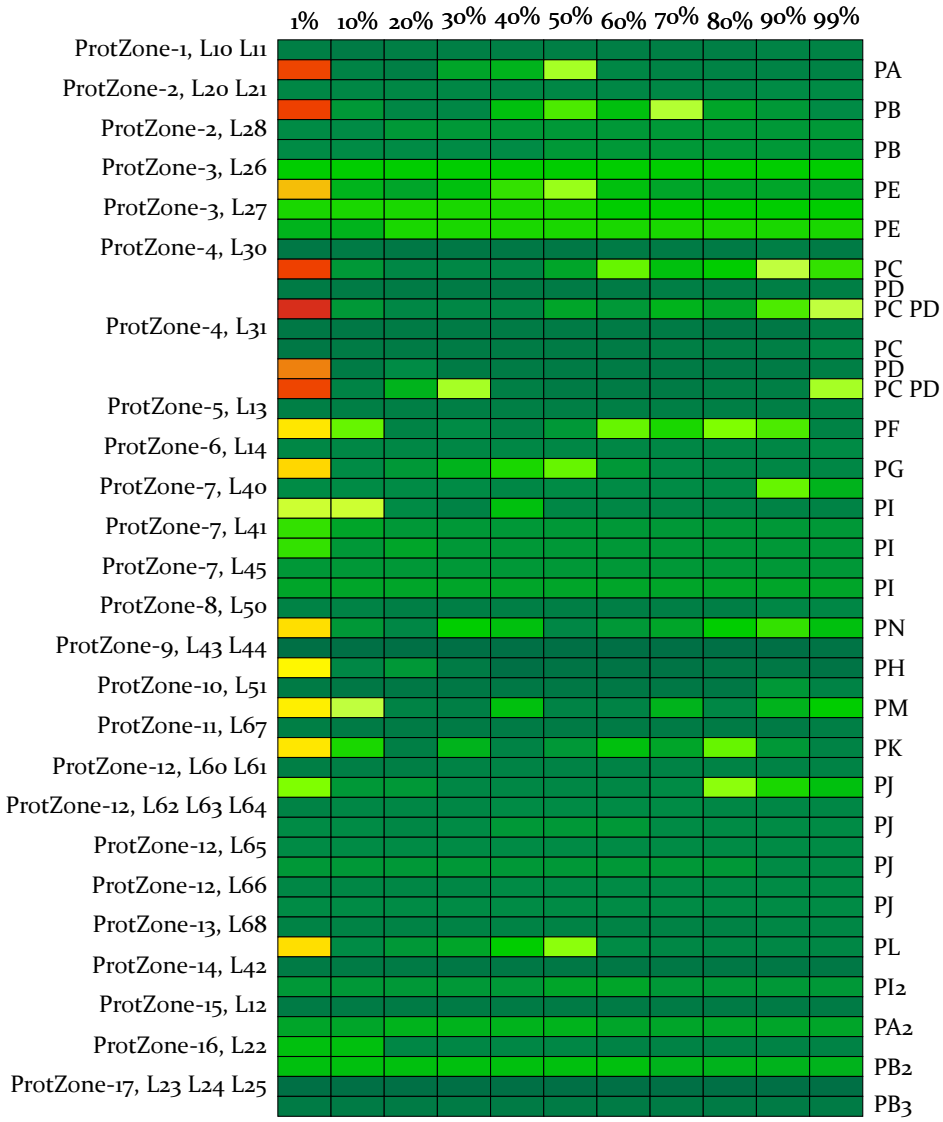

Figure 46: DSI and SRI result matrix with open disconnectors and calculated protection setting values.

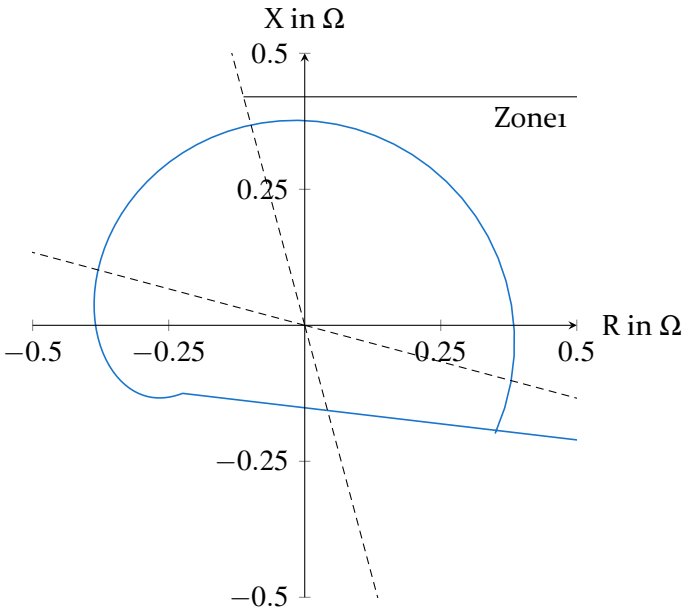

Figure 47: R-X diagram of protective device PE for a fault at 1 % on L10 for failure of protective device PA.

This phenomenon is caused by the DERs G2, G3 and G4 connected to the feeders E, I and J and has already been analytically studied in the work [129]. When a fault occurs, there is an abrupt change in the internal impedance of the power system, which is mainly composed of the parallel connection of the impedances of all feeders and the series-connected line and transformer impedances. Depending on the level of internal impedance, the change results in correspondingly high short-circuit currents and small voltages in the system. [51] This also affects the respective connection nodes and thus the DERs stator voltages. As a result, there is a reduction in the dissipated active electric power P_{el} of the DERs according to (83). The input drive power P_T can in turn be assumed to be constant to a first approximation. Thus, as P_{el} is less than P_T, the rotors of the synchronous machines accelerate as the excess input energy is converted into kinetic energy. This process is enhanced by the low inertia of the connected DERs, which is reflected, among other things, in their start-up time constants TA of only 3 s or 4 s, respectively. Smaller machines thus have a larger angular acceleration than machines with a large inertia or than the connected ideal voltage source, which is enormously strong relative to the DERs and has an infinitely large inertia.

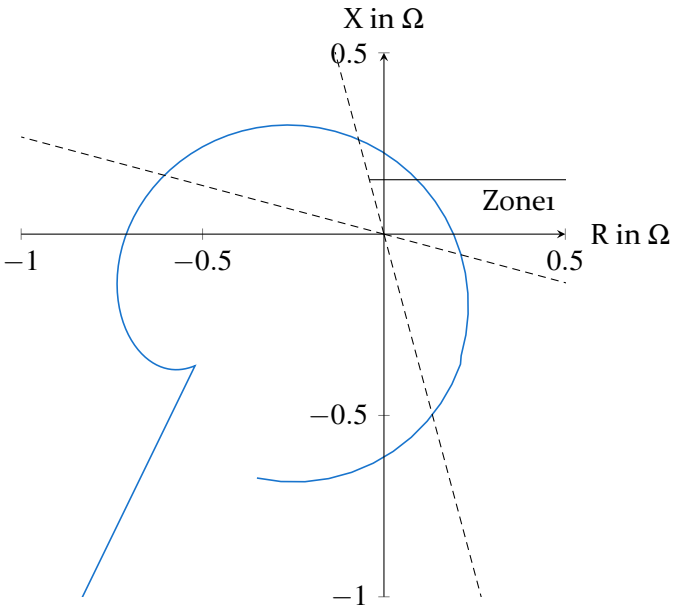

Figure 48: R-X diagram of protective device PI for a fault at 1 % on L10 for failure of protective device PA.

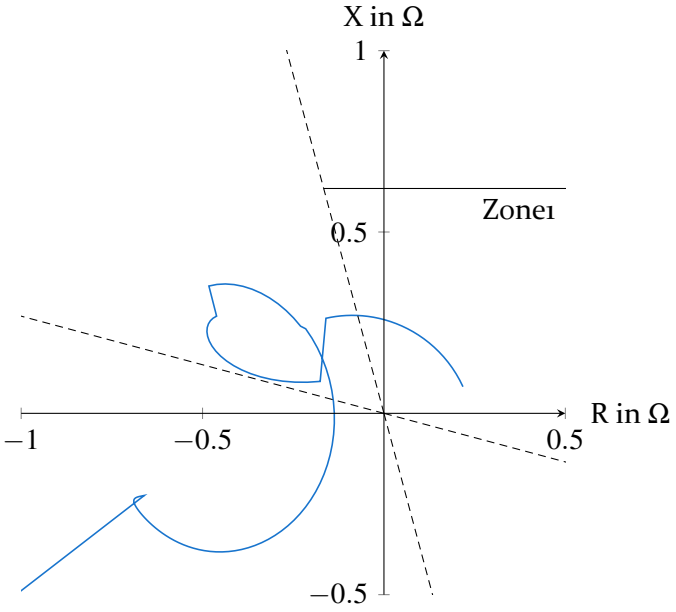

Figure 49: R-X diagram of protective device PJ for a fault at 1 % on L10 for failure of protective device PA.

After the onset of the fault, all connected DERs in the system accelerate, inducing a rotating transient voltage and current in their stator. The DERs G3, G4 and G5 thereby accelerate more strongly than the DERs G1 and G2 due to their installation location and their preload. The voltages at the main busbars Bus1 and Bus2 are mainly determined by the ideal voltage source and the DER G5. During the fault, there is an increasing power angle ϑ between the main busbars Bus1 and Bus2, respectively, and the stator voltages of DERs G3, G4 and G5. This results in a clockwise rotating measured impedance in the R-X diagram of PE and PI, as seen in Figure 47 and 48. This causes the moving impedance trajectory to enter Zone1 of PE at $t = 230$ ms after fault occurrence. The generated trip signal leads 100 ms later to the complete opening of the circuit breaker. In the case of PI, the impedance trajectory enters Zone1 after $t = 290$ ms after fault occurrence.

Figure 49 shows the R-X diagram of the protective device PJ. The impedance trajectory shown here initially turns to the left and not to the right. This is due to the fact that the power angle between the main busbar Bus2 and the stator voltage of G2 initially decreases during the fault. This is partly because the rotor of G2 accelerates less rapidly, and partly because the voltage phasor of Bus2 is affected by the strongly accelerating DER G5. At $t = 330$ ms after fault occurrence, the circuit breaker of PE opens, resulting in the first jump in the measured impedance trajectory of PJ. At $t = 390$ ms the circuit breaker of PI opens, causing the second jump in the measured impedance trajectory. The third jump occurs at $t = 490$ ms after the fault, where the frequency protection of G5 disconnects the machine from the rest of the system. From this point on, the power angle between Bus2 and G2 increases, which means that the impedance trajectory now follows a right-hand curve. At $t = 530$ ms, the measured impedance enters Zone1, causing the circuit breaker to open at $t = 630$ ms, stopping the measurement.
If PJ were to use buffered voltages in the event of a fault, then the last measured voltage angles of the fault-free state would be used. This would then also lead to exclusively right-handed impedance trajectories.

Another unselectivity that stands out when looking at the PSI according to Figure 45 and Table 17 are the faults on line L22 at 1 % and 10 % of the line length. In this case, there is an overfunction of PB, which reaches too far with its second zone and therefore trips faults simultaneously with PB2. The overcurrent protection functions of PB2 and PB3 have been set to be time selective with respect to each other, so PB2 only trips with $t_> = 300$ ms time delay. Traditional setting rules are usually not able to coordinate different protection functions and handle special situations.

The result matrix of the DSI and SRI confirms the selectivity evaluation and provides some additional information about the state of the system after fault clearing. It can be seen that the DSI and SRI also take worse values for faults where there is unselective fault clearing or failure of devices.
For example, in the case of the already discussed fault on 1 % of path L10-L11 with simultaneous failure of PA, major load disconnections occur in the system. Following the unselective trips of PE, PI, and PJ, the DERs G2, G3, and G4 are unable to transition to safe islanding operation and are disconnected from their generator protection. The LLI, which evaluates the additional and thus avoidable load disconnections, therefore assumes a value of 0.68. The FCI, which evaluates the amount and duration of short-circuit current that occurs, does not fall below 0.95 for any of the simulated faults, so all faults are disconnected in a reasonable time for the system. The GLI, which evaluates the utilization of the system after fault clearing, is also in an optimal range for all simulated faults and therefore always takes a value of 1.0. Thus, the value of the SRI is largely determined by the LLI.

The DSI evaluates the dynamic stability of the entire system after fault clearing based on the voltages, frequencies, and angles that occur. In the case of the fault L10-L11-1 % (PA), significant degradation occurs. As the unselective protective devices trip and disconnect DERs sequentially, numerous nodes become de-energized. In addition, some nodes still experience excessive voltages after fault clearing, which is caused by the control of G2. This does not switch off until $t = 1060\,\mathrm{ms}$ after fault occurrence and thus 400 ms after actual fault clearing. The VFI and the VQI evaluate the resulting node voltages in the system with 0.54 and 0.51, respectively. The quality of the system frequency evaluated by the FQI is very good at 0.93. This is mainly due to the strong ideal voltage source. The FDI, in turn, takes a value of 0.66, which is due to the slightly accelerating DER G1 and the strongly accelerating DER G2. The angular stability is very good despite and because of the many tripping DERs. Thus, AQI and AFI both take a value of 1.0. This is because the individual machines disconnected from the system are not included in the evaluation and G1, which remains connected to the system, always has a rotor angle smaller than 60° with respect to δ_{COI}. In addition, its inertia and hence its influence is small compared to the ideal voltage source.
Finally, the overall result for this fault is a value of 0.61. This is composed of 50 % from the value of PSI with 0.7 and 50 % from the multiplication of DSI with 0.77 and SRI with 0.67.

Conclusion The radial system topology is easy to handle. Most faults are selectively cleared when traditional setting rules are applied. However,

these are not able to establish a directly usable coordination with downstream devices with overcurrent protection function. Therefore, overlapping occurs at two fault locations, resulting in unselective protection behavior. If protective devices fail, high fault clearing times occur, leading to transient effects and thus to numerous unselective trips.

11.1.3.2 Optimization of X of the Distance Protection

Procedure In the following, the reactance setting values X_1, X_2 and X_3 of all distance protection functions are optimized by the ProToc. All other setting values of all protection functions and devices remain constant. Thus, the extent to which the ProToc is able to simultaneously set and match the different zone ranges of many protection functions is investigated, and whether it provides reasonable and applicable results. The resulting values, as well as the calculated ones, are listed in the Table 30 in the Appendix D.

Results The result matrix of the PSI is shown in Figure 50 and gives a result value of 0.991. The joint result of the DSI and SRI is shown in Figure 51 and gives a result of 0.895. The overall result of the assessment is 0.944, which is higher than the result obtained by the calculated values. The assessment shows that only 17 of the previous 20 unselectivities are still present. Thus, the fault L60-L61-1 % (PJ) and the faults on L22 at 1 % and 10 % are now selectively tripped.

The reason for this is that the measured impedance trajectory of the protective device PI at fault L60-L61-1 % (PJ) no longer penetrates backwards into Zone1 during the fault. It does penetrate into Zone2 and Zone3, but only for a maximum of 10 ms, so that no tripping occurs. To achieve this, the ProToc reduced the X_1 value of PI to 0.9 Ω, covering only 9.4 % of its own zone. In turn, the value of X_2 was increased to 1.7 Ω, covering the entire branch to the end of line L42. Thus, in the event of a failure of PI2, PI takes over in the second zone. A third zone is therefore no longer needed under the current conditions and faults. The ProToc set the X_3 value to 2.55 Ω, which was the maximum value allowed. Since a wide-ranging Zone3 does not cause any disadvantages in the assessment, this is considered acceptable.

In the event of faults at the beginning of L22, protective device PB now no longer overlaps PB2. Since all delay times of all protective devices were fixed and PB2 was time-selectively set with $t_> = 0.3$ s, the ProToc set the X_1 and X_2 value of PB to 0.35 Ω, which exactly corresponds to $X_{\mathrm{AB,min}}$ of the zone as seen by PB. The third zone was set to 2.29 Ω, which fully covers even the most distant fault at 99 % on line L25 with a fault impedance of 2.2 Ω. This solution

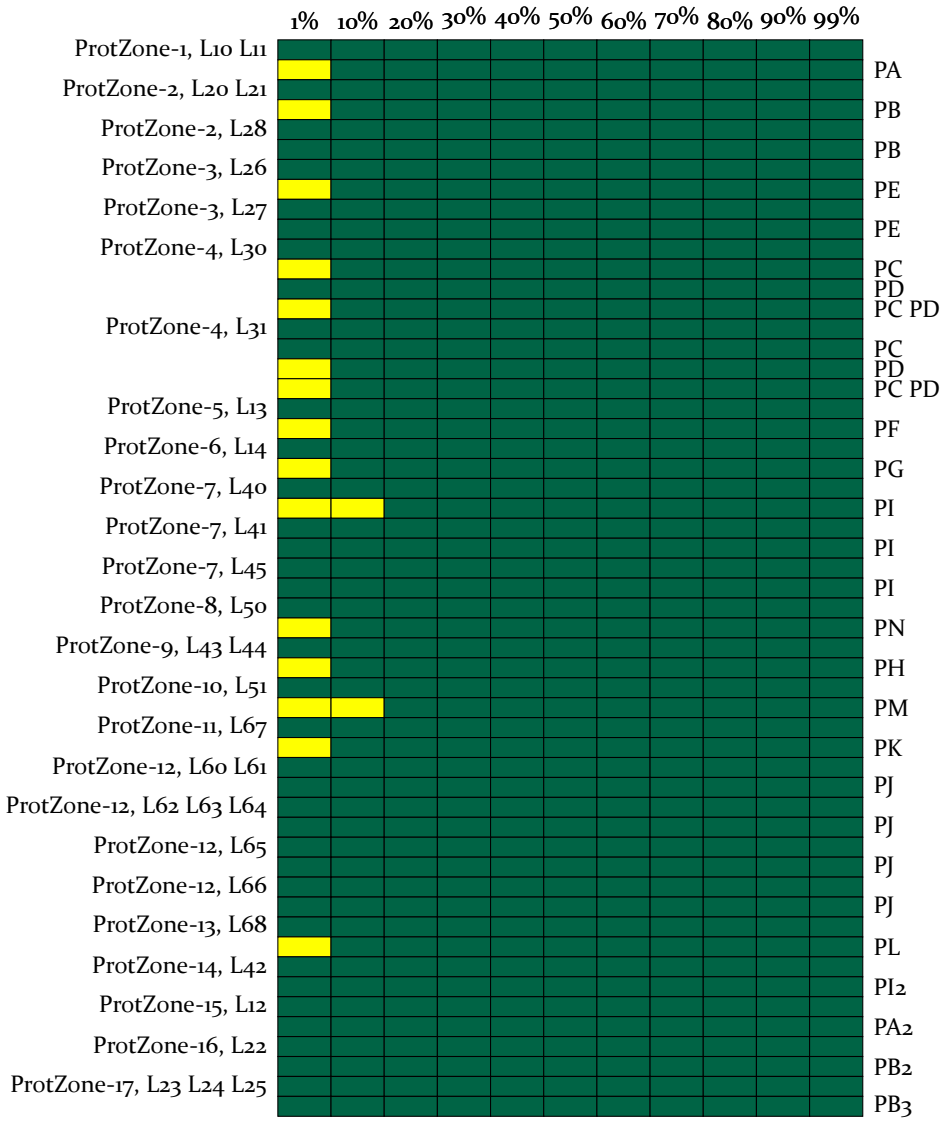

Figure 50: PSI result matrix with open disconnectors and optimized X values of the distance protection.

Figure 51: DSI and SRI result matrix with open disconnectors and optimized X values of the disance protection.

proves the capability of the system to handle even difficult situations with accuracy.

For the protective devices PH, PK, PM and PN, the first zone X_1 was set exactly to $X_{\mathrm{AB,min}} = X_{\mathrm{AB,max}}$ of the respective zone. All faults within the own zone are thus disconnected directly in Zone1 and thus in fast time. Zone2 is not used for all devices. Therefore, the ProToc could not determine optimal values for the respective zones, because the settings did not lead to any change in the assessment. However, this problem could be solved by an addition to the fitness function or detailed specifications of the limit values for zones without subsequent zones.

The first zone of PL was set to 0.43 Ω and the second zone to 0.44 Ω. The minimum and maximum zone values $X_{\mathrm{AB,min}} = X_{\mathrm{AB,max}}$ are also at 0.44 Ω. This disconnects all faults on line L68 in Zone1 and only the fault at 99 % on L68 in Zone2. The reason for this rather unusual parameterization is that the maximum allowed value for Zone1 during optimization was only 0.43 Ω. This circumstance came about because the measured value of fault impedance for a fault at 99 % of L68 is at a value of 0.431 Ω and according to the settings of Table 15 was rounded down to 0.43 Ω accordingly. Finally, the X_2 value covers the last fault at the end of L68.

The first zone of PJ was set to $X_1 = 0.66\,\Omega$ only slightly larger compared to the calculated value of 0.62 Ω, with the maximum fault impedance for a fault on line L65 at 99 % at 1.31 Ω. The reason for this is that above a setting value of 0.8 Ω, there is unselective tripping of PJ for the fault L50-10 % (PN). Thus, the X_1 value could have been slightly larger, but as it is, it already provides good selectivity behavior. The unselective tripping at fault L50-1 % (PN) could not be prevented by the ProToc. This would have required a X_1 value of just 0.035 Ω, which would have been outside the allowed limits. Zone2 of PJ was set to 2.0 Ω, which fully protects the feeder. Zone3 is not used and was set to the allowed maximum value of 3.93 Ω.

The first zone of protective device PA was set to $X_1 = 0.48\,\Omega$. Thus, the first zone is slightly shorter than the minimum and maximum zone values $X_{\mathrm{AB,min}} = X_{\mathrm{AB,max}} = 0.5\,\Omega$ and the fault L12-99 % (PA2) is cleared only in Zone2 of PA. A slightly larger Zone1 with 0.5 Ω would have led to a better overall result. The circumstance can be explained by the fact that the optimization of the ProToc is still an iterative search process that is terminated after 5000 FES. The probability is high that the optimization method would have continued to approach 0.5 Ω as it progressed. Overall, however, Zone1 was selectively

adjusted to the subsequent device PA2. The second zone of PA assumes a value of 1.07 Ω, covering all faults up to the end of line L12.

The protective devices PC and PD are located at the beginning and end of a ring line consisting of the lines L30 and L31. The DER G1 is connected to this ring and represents an intermediate infeed for both devices in the event of a fault. The setting values of PC are therefore with $X_1 = X_2 = 3.98\,\Omega$ also well above $X_{\mathrm{AB,max}}$ with 1.5 Ω. X_3 of PC was set to the maximum allowed value of 12.0 Ω, with Zone3 never used. When a fault occurs on 1 % of line L31, PC initially sees the fault due to the transient current from G1 in the reverse direction. Only when PD trips, the fault impedance jumps into Zone1 with a value of 1.49 Ω. With a fault on 10 % of line L31, the fault impedance is directly in the forward direction with 2.1 Ω and thus within Zone1. The setting values are therefore well chosen to clear faults as quickly as possible. However, they are also significantly larger than they need to be. Since this is not considered further in the assessment, however, the optimization process has worked satisfactorily.
PD initially sees the fault at 1 % of line L30 also in reverse direction. The fault impedance here jumps to 1.51 Ω after the trip of PC and is thus into Zone1 with $X_1 = 2.07\,\Omega$. A fault on 10 % of line L30 results in a fault impedance of 2.24 Ω, placing it initially into Zone2 with $X_2 = 5.81\,\Omega$. However, due to the transient current injected by G3, the fault impedance moves into Zone1 of PD on an eleptic trajectory within 40 ms after fault occurrence, ensuring fast tripping. Overall, it still would have been better, if the ProToc had further increased the X_1 value so that faults at the beginning of line L30 were cleared even faster. Possibly this would have happened had the process not terminated after a maximum number of 5000 FES. As with the PC, the X_3 value of PD is not used.

Conclusion The optimization process resulted in plausible and applicable reactance values. The selectivity of the protection system was improved overall. Coordination with subsequent overcurrent functions was successfully performed so that unselective tripping no longer occurs. For certain distance protection functions, the first zone was shortened so that transient effects no longer lead to unselective tripping. This is a simple and at the same time effective solution to the problem. In some places, however, the ProToc could have determined slightly more accurate results. This can be attributed to the maximum number of 5000 FES during the optimization process. The high coverage of some zones results from the fact that this was not considered disadvantageous within the assessment system. This could be easily solved by appropriate extensions in the future.

11.1.3.3 Optimization of X & T of the Distance Protection

Procedure The reactance setting values X_1, X_2 and X_3 as well as the corresponding delay times T_1, T_2 and T_3 of all distance protection functions are now optimized by the ProToc. All other setting values of all protection functions and devices remain unchanged. Thus, it is investigated whether the system is also capable of optimizing different types of setting values simultaneously, matching them to each other and generating added value by exploiting the higher freedom. Furthermore, it is tested whether the ProToc is able to generate a suitable time grading in addition to a pure grading via reactances. The resulting values, like the calculated values, are listed in Table 30 in the Appendix D.

Results The result matrix of the PSI is shown in Figure 52 and gives a result value of 0.9909. The joint result of the DSI and SRI is shown in Figure 53 and gives a result of 0.8989. The overall assessment result is 0.945, which is higher than the result obtained by optimizing only the reactance settings. The evaluation result of the PSI shows that, compared to the calculated values, there are two less unselectivities but one more unselectivity than with the purely optimized reactance values. Table 18 lists accordingly all unselective tripping protective devices in relation to the fault.

In contrast to the use of the purely optimized reactance values for the fault L13-10 % (PF), PI now trips unselectively 440 ms after fault occurrence. The reason for this is an impedance trajectory penetrating backwards into Zone1. This is because PI's Zone1 is now set much larger than the previous 0.09 Ω with $X_1 = 0.61\,\Omega$. As a result, Zone1 now fully covers line L40 and 75 % covers line L41, which means that faults in this section are disconnected much faster. At the same time, the ProToc has also increased the delay time to $T_1 = 100$ ms. This has the great advantage that for the faults L10-1 % (PA), L20-1 % (PB), L30-1 % (PC), L30-1 % (PC PD), L31-1 % (PD), and L31-1 % (PC PD) PI no longer trips unselectively, which significantly improves the DSI and SRI results. Thus, in favor of better dynamic behavior and five fewer unselective trips, the ProToc was able to set the delay time upward.
The same applies to the delay time $X_1 = 100$ ms of PE. Also here, with the faults L30-1 % (PC PD), L31-1 % (PD) and L31-1 % (PC PD), there is now no more unselective tripping of PE.

For PA, X_1 was now set exactly to $X_{\mathrm{AB,min}} = X_{\mathrm{AB,max}}$ and a delay time of $T_1 = 0$ ms was selected. Zone2 fully secures the following zone with 1.5 Ω. At first glance, the delay time of $T_2 = 350$ ms could have been lower with 250 ms. Indeed, the delay time of the fast stage of PA2 was fixed at 100 ms. To this must

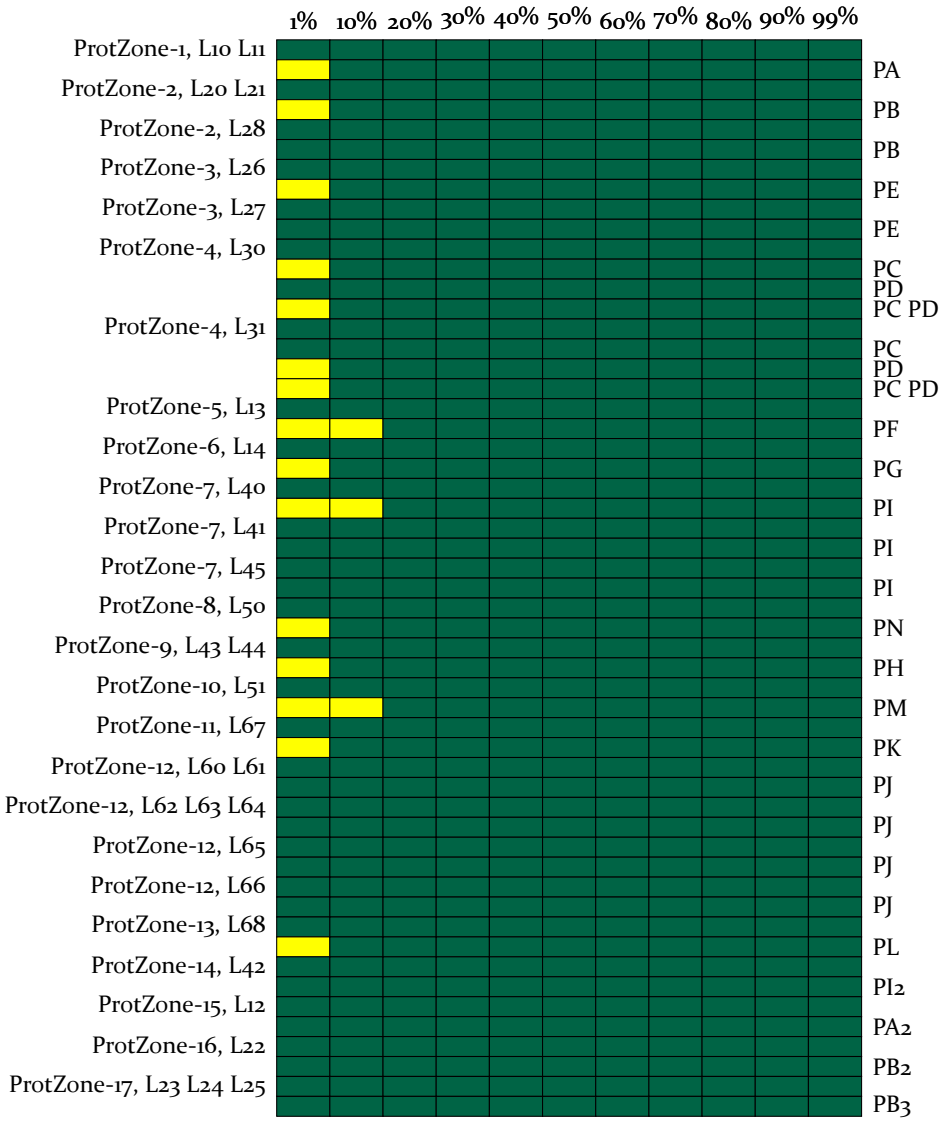

Figure 52: PSI result matrix with open disconnectors and optimized X and T values of the distance protection.

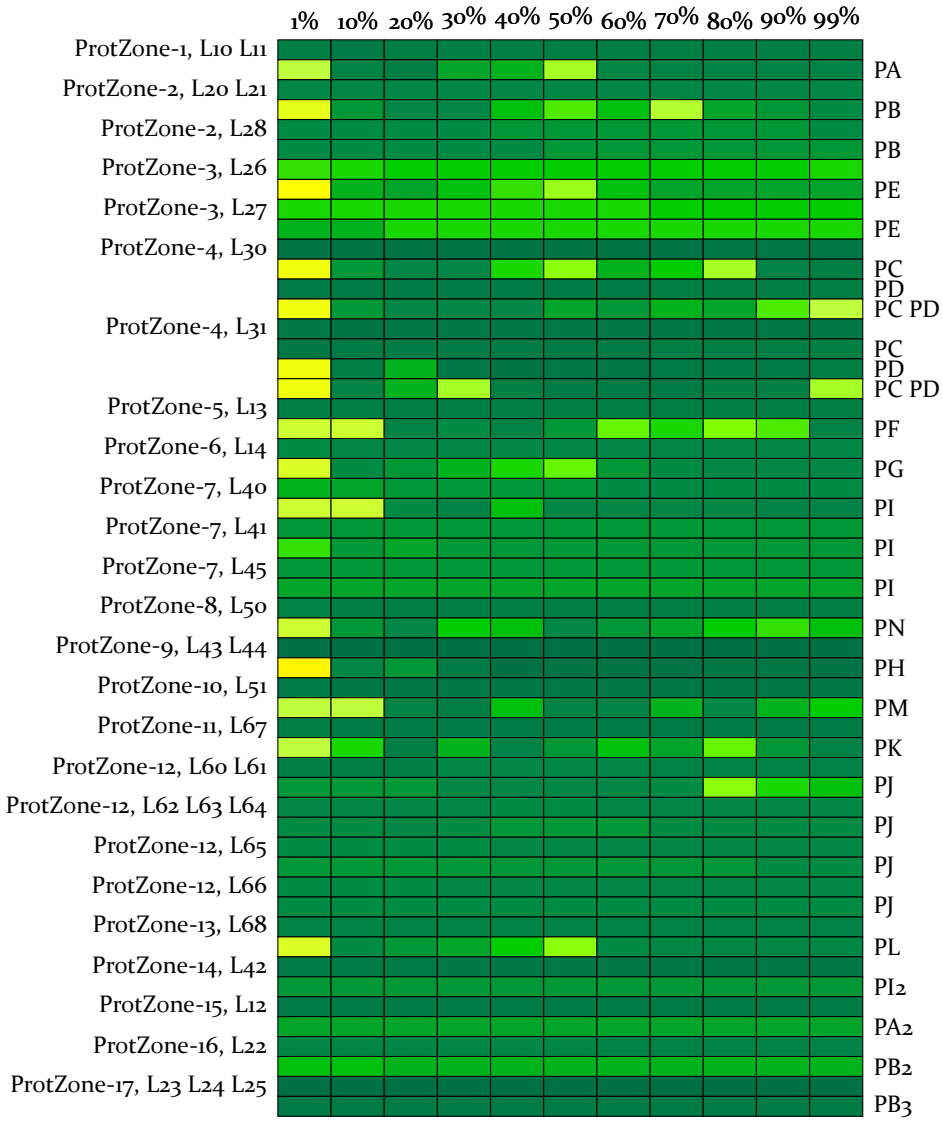

Figure 53: DSI and SRI result matrix with open disconnectors and optimized X and T values of the distance protection.

Table 18: Marking of the unselectively tripped protective devices by fault location. All disconnectors are open and X & T optmized setting values are used.

Fault on path	PE	PI	PJ	PB
Fault on L10-L11-1 % (PA)			x	
Fault on L13-1 % (PF)			x	
Fault on L13-10 % (PF)		x		
Fault on L14-1 % (PG)			x	
Fault on L20-L21-1 % (PB)			x	
Fault on L26-1 % (PE)			x	
Fault on L30-1 % (PC)			x	
Fault on L30-1 % (PC PD)			x	
Fault on L31-1 % (PD)			x	
Fault on L31-1 % (PC PD)			x	
Fault on L40-1 %-10 % (PI)			x	
Fault on L43-L44-1 % (PH)		x	x	
Fault on L50-1 % (PN)			x	
Fault on L51-1 %-10 % (PM)			x	
Fault on L67-1 % (PK)			x	
Fault on L68-1 % (PL)			x	

be added 100 ms circuit breaker opening time and 50 ms self-defined step size to trip selectively to PA2 in Zone2. However, the frequency response of G2 and G5 to faults on line L12 with simultaneous failure of PA2 is better, if the faults are tripped 100 ms later. Overshoots and undershoots turn out slightly better in this case. The DSI therefore assumes an overall better assessment value with a higher delay time.

For PB, X_1 was increased by 0.01 Ω to 0.36 Ω, which means that the value is now greater than $X_{\text{AB,min}}$. However, the circumstance does not lead to unselective tripping, since the measured fault impedance for the fault at 1 % of line L22 is still larger. However, for faults with a distance of 0.1 % and less on L22, the measured fault impedance is now within Zone1 of PA and would thus cause unselective tripping. This shows that in perspective it would be even better to include node faults or line faults with a smaller distance to the node. The protective devices PF, PH, PK, PN, PM, were set according to the expectations. The range of the first zone X_1 was set exactly to $X_{\text{AB,min}} = X_{\text{AB,max}}$ with a delay time of $T_1 = 0$ millis in each case.

However, the situation is different for PG and PL. For these, the X_1 value was set slightly smaller than $X_{\text{AB,min}} = X_{\text{AB,max}}$ and the delay time T_1 was set to 50 mills. Here the ProToc could have achieved an even better FV.
The delay times of Zone1 of PC and PD were each optimally set with $T_1 = 0$ ms. Both first zones also reach far enough to disconnect all faults on the ring L30-L31 in Zone1.

Conclusion The results show that the ProToc was able to parameterize reactance and time values together and in a coordinated manner. Compared to the use of setting rules, two less unselectivities occur. The overall stability of the system has been noticeably improved. Many delay times were set to a minimum, resulting in fast fault clearing. However, for some distance protection functions, the ProToc has increased the times to prevent unselective tripping due to transient effects. Also, some delay times were increased when this resulted in an better dynamic assessment. All this proves how powerful and precise the ProToc can generate protection settings and determine the best compromise of different criteria.

11.1.3.4 Optimization of X, T & PSB of the Distance Protection

Procedure The reactance setting values X_1, X_2 and X_3, the associated delay times T_1, T_2 and T_3 as well as the use of PSB functions are optimized simultaneously by all distance protection functions of all protective devices in the system in a next step. All other setting values of all functions and devices remain

unchanged. It is thus investigated whether the ProToc is able to activate the PSB function selectively at protective devices and to use this further degree of freedom effectively. The resulting values are listed like the calculated values in Table 30 in the Appendix D.

Results The result matrix of the PSI is shown in Figure 54 and gives a result value of 1.0. The joint result of the DSI and SRI is shown in Figure 55 and gives a result of 0.905. The overall result of the evaluation is thus 0.9525 and is the best value achieved so far. The PSB has been activated for the protective devices PD, PE, PI, PJ and PL. The protection system no longer behaves unselectively in the event of a fault.

For PE, the ProToc was able to reduce the delay time of the first zone due to the activated PSB from 100 ms to 0 ms. However, at the same time, the X_1 value was also reduced from 0.47 Ω to the minimum allowable value of 0.23 Ω, clearing faults only up to and including 40 % on line L26 in Zone1. Zone2 with 1.67 Ω is subsequently large enough to clear all further faults on the branch with a delay time of $T_2 = 400$ ms. Two reasons can be given for reducing the size of Zone1. On the one hand, a higher fault clearing time now does not lead to an unselective tripping of other protective devices, since moving impedance trajectories are detected accordingly and a tripping is blocked. On the other hand, this leads to a slightly improved FV, since the negative effects and reactions of G3 are no longer included in the assessment result. Due to its closeness to the fault, G3 quickly loses its synchronism and is disconnected from the system by the overfrequency protection in time and before fault clearing. Thus, the negative impacts of G3 drop out of the assessment. This is at the expense of the VFI, but both the VQI and the FDI show improvement. To achieve this, the delay time of Zone2 had to be increased accordingly to 400 mseconds. This method represents an unconventional and less practical solution, but still corresponds to an improvement of the assessment under the given conditions. The prerequisite of this solution approach is, of course, that a powerful voltage source that ensures grid stability.

Also for PI, the range of the first zone was lowered and the delay time has been reduced. The same effect as with PE occurs here as well, so that the negative effects of G4, which also loses its synchronism, are less influential. The overall coverage of Zone2 could have been slightly larger to ensure that all faults on L42 are cleared within Zone2. However, the FV would have been only marginally better under these circumstances. Thus, although generally higher fault clearing times lead to poorer dynamic results, with sufficient distance to the main busbars onto which the ideal voltage source feeds, this has only

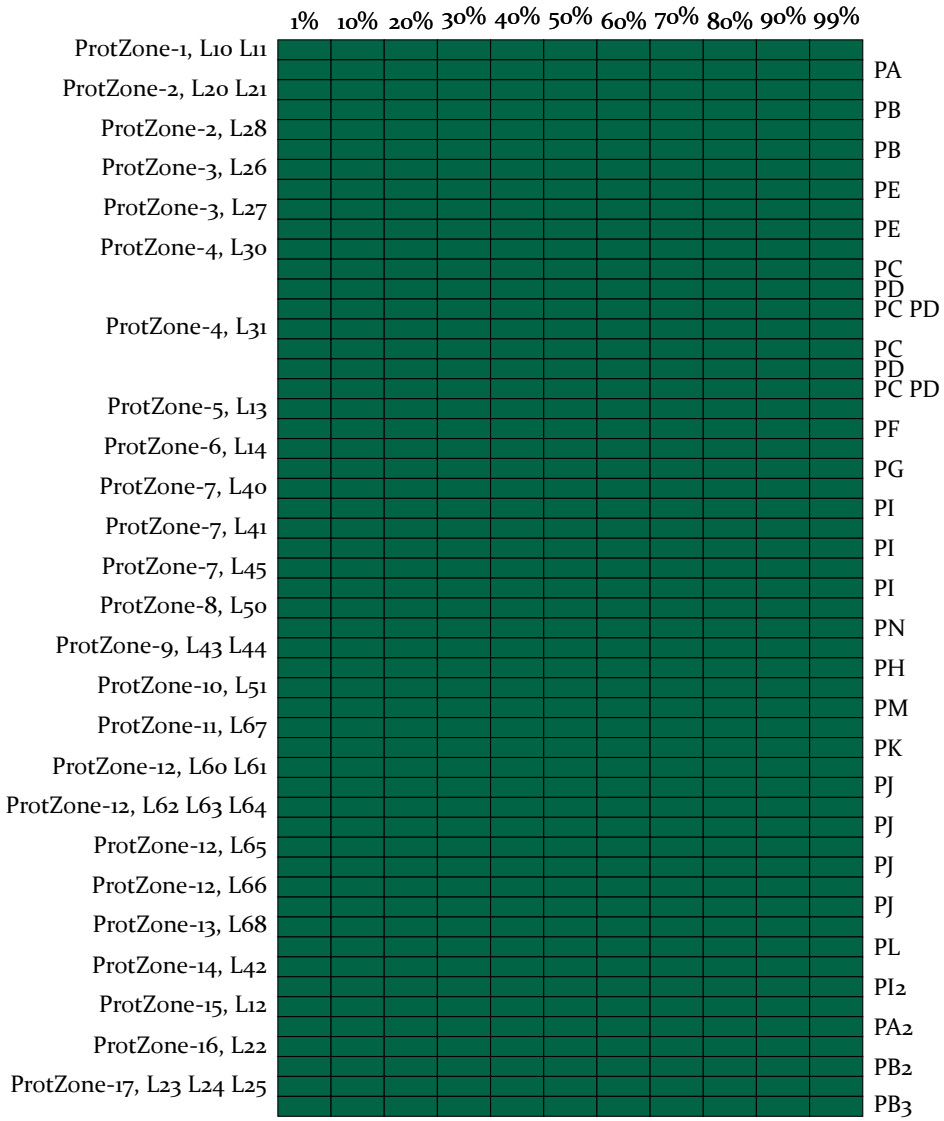

Figure 54: PSI result matrix with open disconnectors and optimized X, T and PSB values of the distance protection.

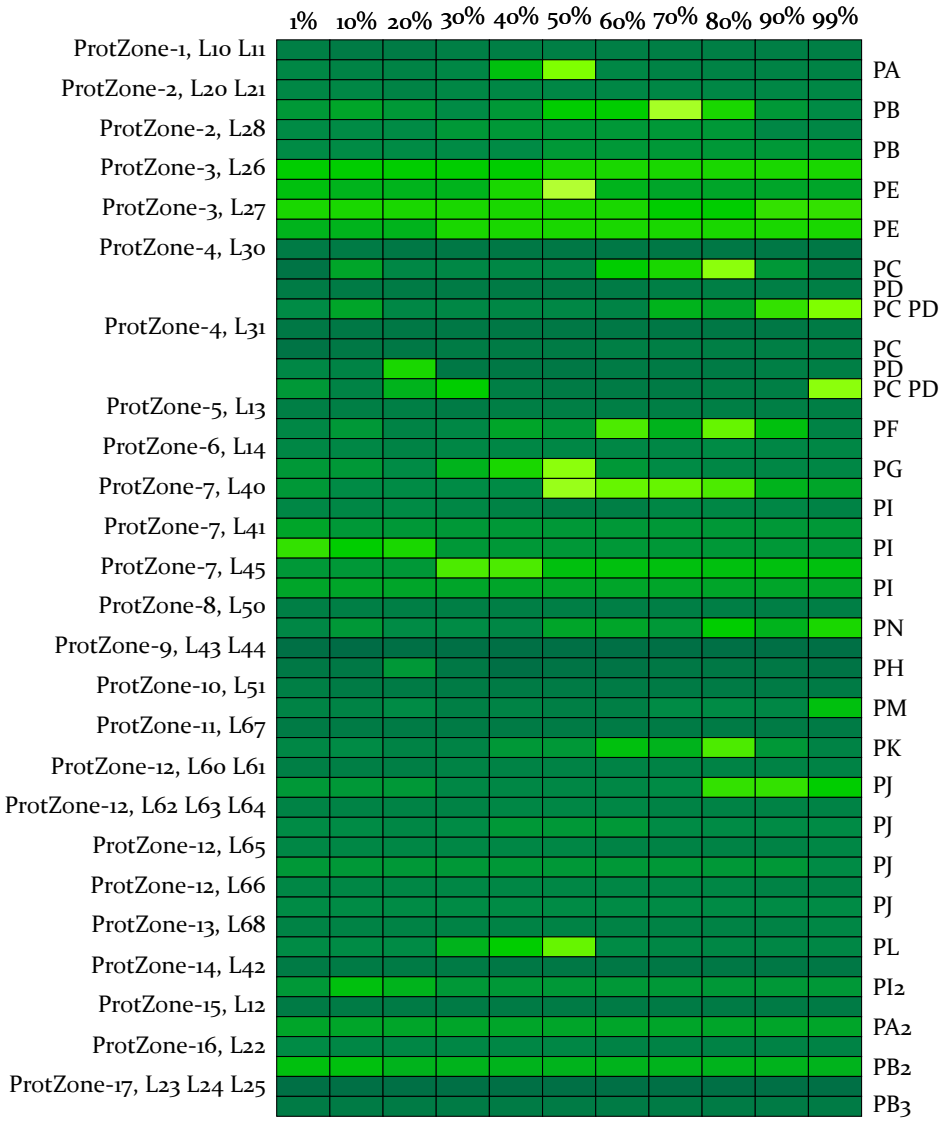

Figure 55: DSI and SRI result matrix with open disconnectors and optimized X, T and PSB values of the distance protection.

a minor effect. The lack of fine-tuning can be explained by the fact that the total number of FES has been kept constant, but the number of variables to be optimized has increased. In principle, the runtime of the optimization process should be increased together with the complexity in order to achieve consistently optimal results.

For PJ, due to the active PSB, the X_1 value could be raised from 0.36 Ω to 1.31 Ω, thus disconnecting almost all faults of the branch in Zone1. Only the fault L65-99 % is cleared in Zone2.

The activation of the PSB for PD and PL is surprising.
In case of PL, the activation has no effect at all, since it is not used in any fault. The FV would therefore have been slightly better if the ProToc had not activated it for PL.
This is in contrast to the activation of the PSB function for PD. Here, the activation actually leads to a better overall result, but at the same time represents an unusual approach and solution. For example, the measured fault impedance of PD at fault L30-1 % (PC) is initially in the reverse direction due to the transient current of G1. The onset of impedance trajectory movement is detected by PD and the PSB function is activated accordingly. After PC is tripped, the measured fault impedance of PD jumps into Zone1 in forward direction and would lead to immediate tripping, if the PSB function was not activated. However, tripping is thus initially prevented. Due to the trip of PC, however, an impedance jump measured by PD occurs, which 600 ms later leads to deactivation of tripping block. In the meantime, PG1E disconnects G1 from the system, thus excluding it from the subsequent DSI evaluation. The bottom line is that this again leads to a better dynamic assessment, which is why the ProToc provides for an activated PSB in the case of PD. However, this approach represents an increased risk should the dynamic behavior in reality deviate from that in the simulation. At the same time, the ProToc thus proves to formulate completely new solution approaches.

Conclusion The best outcome so far has been achieved by simultaneously optimizing reactance, time values and PSB functions. As a result, there is no longer any unselective behavior of the protection system. Tripping times could be reduced again by activating the PSB function, since moving impedance trajectories are detected and unselective trips are blocked. The ProToc has once again proven that it is capable of configuring and matching different setting values.
Although some delay times have been increased, so that individual faults are cleared later, ultimately this leads to a better result in the dynamic assessment.

The basic prerequisite for this is of course that the rest of the system is still very stable despite longer fault clearing times. Nevertheless, the fact shows that the ProToc can identify unconventional and optimal solutions within the framework of the assessment system used and find a balance of different criteria.

11.1.3.5 Optimization of X, T, PSB of the Distance Protection & I, T of the Overcurrent Protection

Procedure The reactance setting values X_1, X_2 and X_3, the associated delay times T_1, T_2 and T_3 as well as the use of PSB functions are optimized by all distance protection functions in the system. At the same time, the current levels $I_{>>}$ and/or $I_{>}$ of the overcurrent protection functions of PA2, PB2, PB3 and PI2 as well as the associated delay times $T_{>>}$ and $T_{>}$ are also optimized. All other setting values of all functions and devices remain unchanged. The ProToc must therefore parameterize setting values of different protection functions and coordinate them within a common protection coordination. The resulting values are listed like the calculated values in Table 30 in Appendix D.

Results The result matrix of the PSI is shown in Figure 56 and also gives a result value of 1.0. The joint result of the DSI and SRI is shown in Figure 57 and gives a result of 0.9061. The overall assessment result is 0.953, which is slightly higher than the result obtained by optimizing the distance protection functions only.

The ProToc parameterized the overcurrent protection function of PA2 with $I_{>>} = 3.6\,\text{kA}$ and $T_{>>} = 0\,\text{ms}$. The smallest measured short-circuit current at fault L12-99 % is 4 kA, allowing PA2 to clear all faults at L12 in the shortest possible time.

For PI2, $I_{>>}$ was set to 2.3 kA with $T_{>>} = 0\,\text{ms}$. The minimum short-circuit current is reached for the fault L42-99 % with 2.5 kA. Thus, PI2 also clears all faults in fast time.
Reducing the delay time $T_{>>}$, also allowed the delay time of Zone2 T_2 from the upstream device PI to be set to the minimum allowable value of 200 ms. Overall, faults on lines L40, L41 and L42 are thus cleared more quickly and yet selectively.

Protective device PB3, located downstream of PB2, was set to $I_{>>} = 1.8\,\text{kA}$ with $T_{>>} = 0\,\text{ms}$. Fault L25-99 % results in a minimum short circuit current

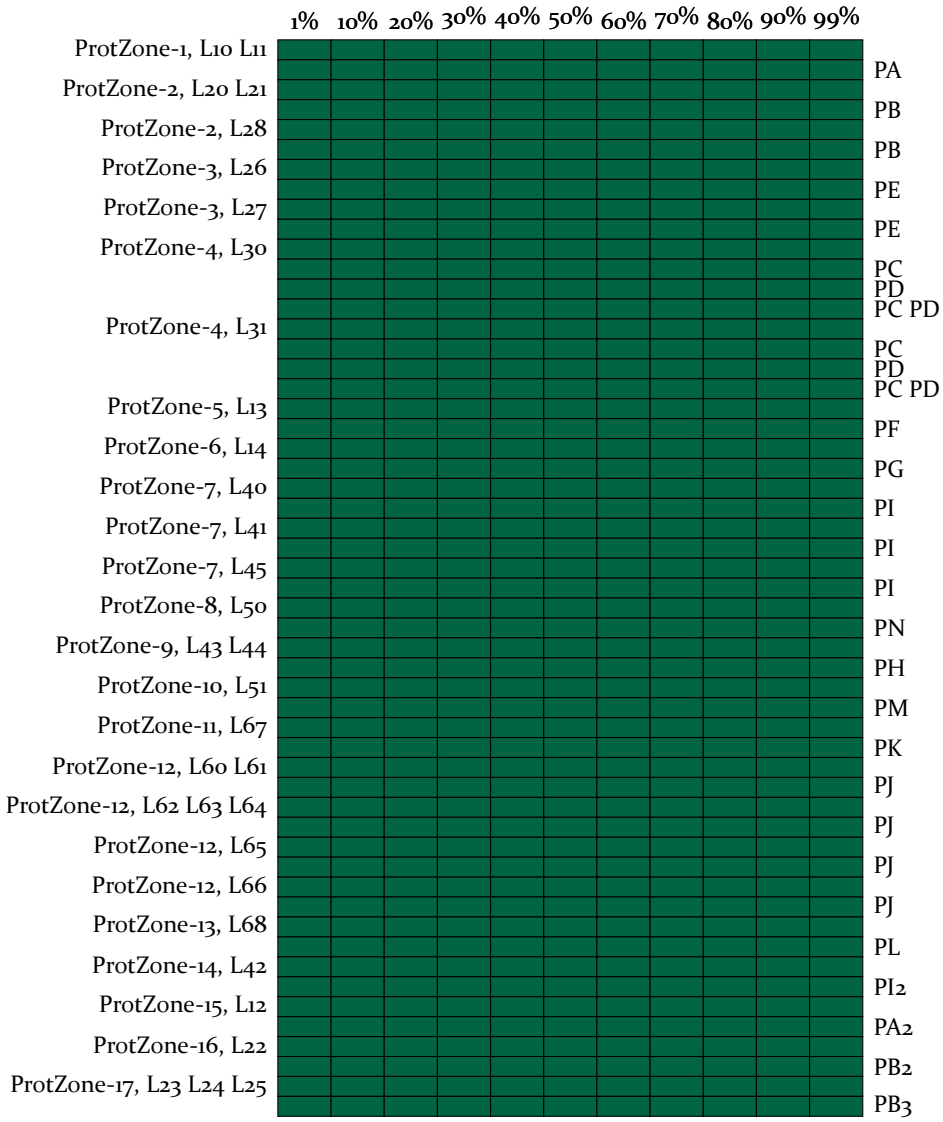

Figure 56: PSI result matrix with open disconnectors and optimized X, T, PSB values of the distance protection and I, T values of the overcurrent protection.

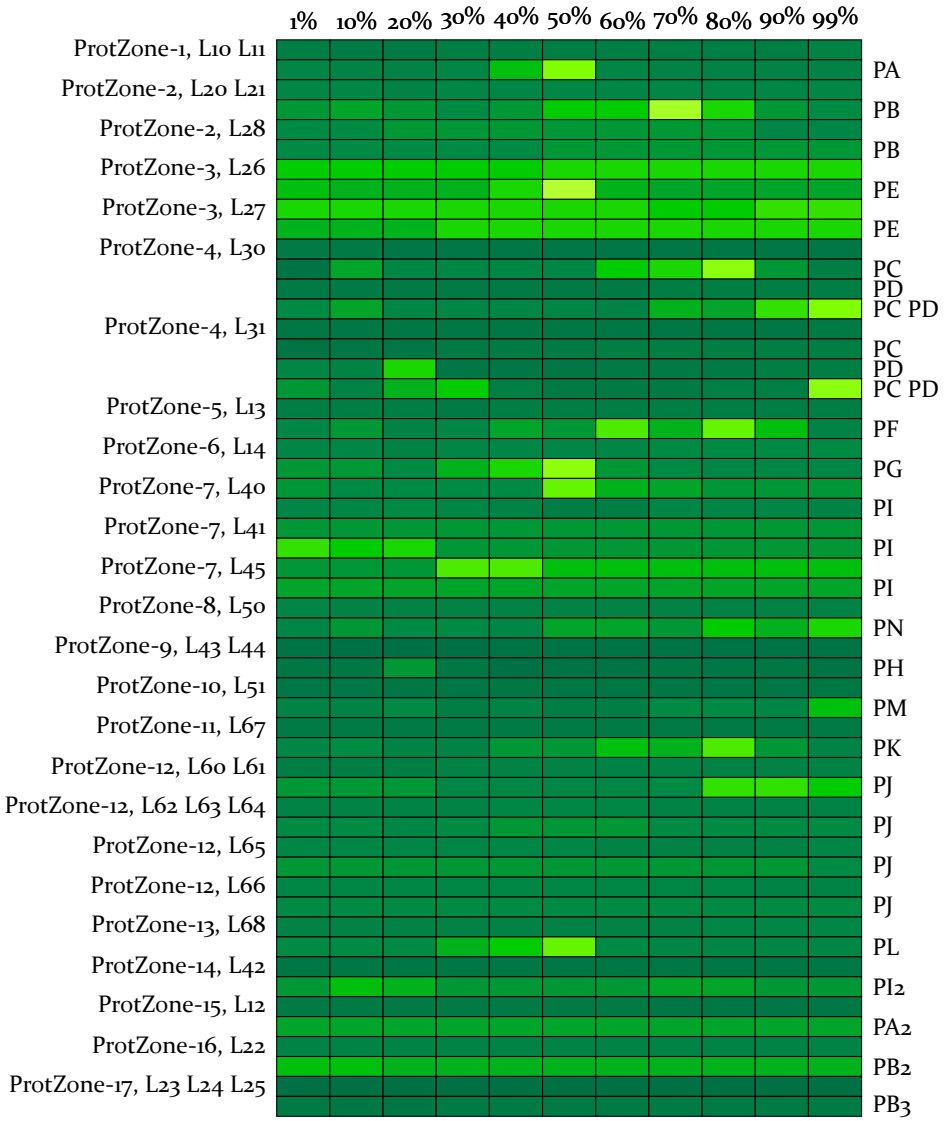

Figure 57: DSI and SRI result matrix with open disconnectors and optimized X, T, PSB values of the distance protection and I, T values of the overcurrent protection.

of 2.4 kA. All faults on lines L23, L24 and L25 are therefore disconnected by PB3 in optimal time.

The parameterization of PB2 was the most challenging part of the optimization process. The fast stage $I_>$ was set to 3.7 kA with $T_{>>} = 0$ ms and the delayed stage $I_>$ to 0.6 kA with $T_> = 200$ ms. This clears faults up to and including 60 % on line L22 from PB2 in fast time. After that, the delayed stage comes into effect, which is set for PB3 with 200 ms optimal time selectivity. The delay time of Zone2 from the upstream device PB was set to 350 ms, which is an optimal value. Thus, unselective tripping does not occur even in case of faults at the end of line L22. Zone2 of PB becomes active and clears faults only in the case of a failure of PB2.

Conclusion Plausible and applicable values for the overcurrent functions were determined. The result obtained represents the best protection coordination achieved so far. The ProToc proves that it is able to set distance and overcurrent protection functions including setting values together and in coordination with each other.

11.1.4 Closing a Ring Inside the System

The extension and connection of DERs can lead to impermissible voltages, especially in low and medium voltage systems, and thus to a violation of the permissible voltage band. For instance, the active power injection of a DER leads to an increase in the voltage at the grid connection node depending on the impedance between the connection node and the system. A simple and quickly implemented measure to counteract this problem is to close open disconnection points and thus form a ring. This reduces the connection impedance, which reduces losses and counteracts voltage peaks. However, from a protection point of view, this approach has a number of disadvantages. In the event of a fault, the entire ring must be disconnected, not just the faulty branch. Because of the lower impedance, the short-circuit current increases over the entire ring. However, in the case of faults that are particularly close to the common busbar, the problem arises that the fault current is distributed very differently between the two half-rings. The protective device located on the fault-free half-ring and thus remote from the fault initially measures a much lower current in the event of a fault. In the case of overcurrent protection functions, this may be lower than the actual tripping value. The distance protection function, in turn, initially calculates a fault impedance that is too high, so that the fault appears to be further away. This effect is enhanced by the intermediate infeed of the DER. The result is often a delayed

tripping of the remote device, which accordingly trips only after the other one near the fault. [55], [88], [89]

The effects of such a ring closure on the protection security of the present test system are investigated in the following. For this purpose, the disconnector D1 is closed, creating a ring between PB and PE. G3 feeds onto this ring in form of an intermediate infeed. First, the protection behavior is analyzed while maintaining the last optimized protection setting values.

11.1.4.1 Keeping Optimized Settings for Open Ring

Procedure The exact settings determined from section 11.1.3.5 are used for all protective devices in the system. These have been optimized for a topology with open disconnector D1 and are now being investigated in terms of their suitability for the closed ring. This situation would occur if protection settings are not adjusted after power system changes. For reasons of clarity, only the closed ring between PB and PE and the connected branch of PB2 and PB3 will be considered subsequently.

Results The result matrix of the PSI is shown in Figure 58 and gives a result value of 1.0. The joint result of the DSI and SRI is shown in Figure 59 and gives a result of 0.8555. The overall assessment result is 0.928. All faults are cleared selectively. However, the evaluation of the DSI and SRI shows that many faults are tripped late and the ring closure therefore leads to a degradation of stability and load losses. Although PB trips faults on line L20 and at the beginning of L21 in Zone1, PE measures and clears these faults only in Zone3 and only after PB has tripped before. Faults on L26 are disconnected by PE in Zone1 and by PB only in Zone2. The negative evaluation in the case of faults on line L22 with simultaneous failure of PB2 is notable. In this case PB sees the faults only in Zone2 and PE even only in Zone3. Due to the late fault clearing, the VQI and VFI evaluate the voltage stability worse and the LLI evaluates the additional load loss negatively. The latter occurs due to the now closed ring and cannot be prevented.

Conclusion Many faults are disconnected late, resulting in stability degradation and load losses. Protection settings should also be adjusted accordingly after changes in the power system to maintain power system and protection security.

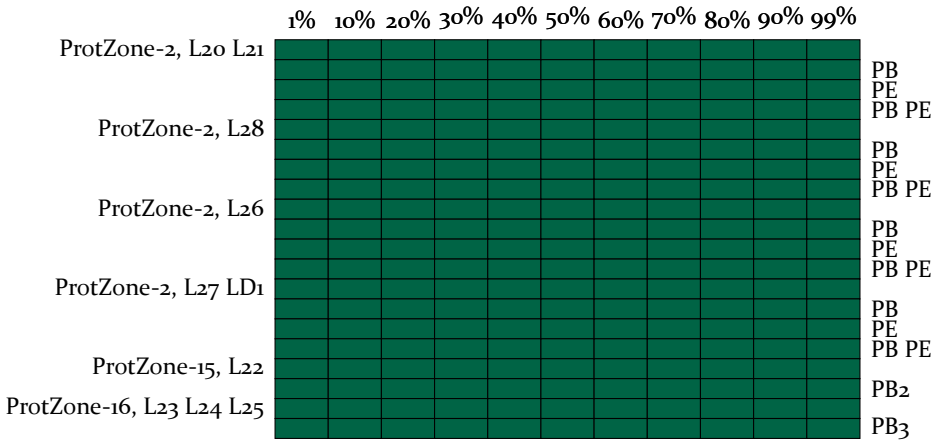

Figure 58: PSI result matrix for the state that the disconnector D1 is closed, but optimized values for the open state are used.

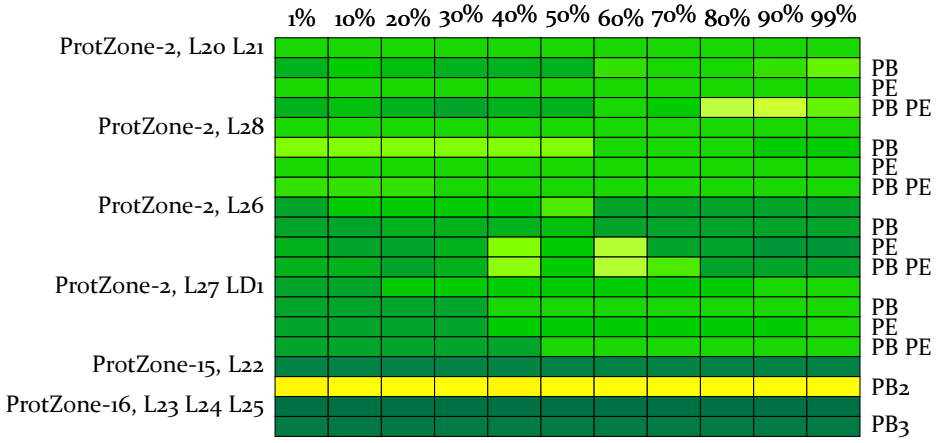

Figure 59: DSI and SRI result matrix for the state that the disconnector D1 is closed, but optimized values for the open state are used.

11.1.4.2 Use of Standard Setting Rules for Distance & Overcurrent Protection

To increase the stability of the system, the setting values of the protection shall be adjusted. For this purpose, default setting rules are used first.

Procedure Using (72) the distance protection functions of PB and PE are readjusted to the present ring topology. The basic procedure for calculating $X_{\mathrm{AB,min}}$, $X_{\mathrm{AB,max}}$, etc. from section 11.1.3.1 remains unchanged. All other setting values also remain the same. The calculated values are listed in Table 31 in the Appendix D.

Results The result matrix of the PSI is shown in Figure 60 and gives a result value of 0.988. The joint result of the DSI and SRI is shown in Figure 61 and gives a result of 0.856. The overall assessment result is 0.922, worsening compared to keeping the optimized setting values from section 11.1.3.5. The joint value of DSI and SRI has improved slightly.

Conclusion Conventional setting rules fail at this point. They are not well suited for coordinating the protection system in closed ring topologies with intermediate infeed and lead to increased unselectivities. Adaptation of protection settings to new conditions requires the use of suitable tools.

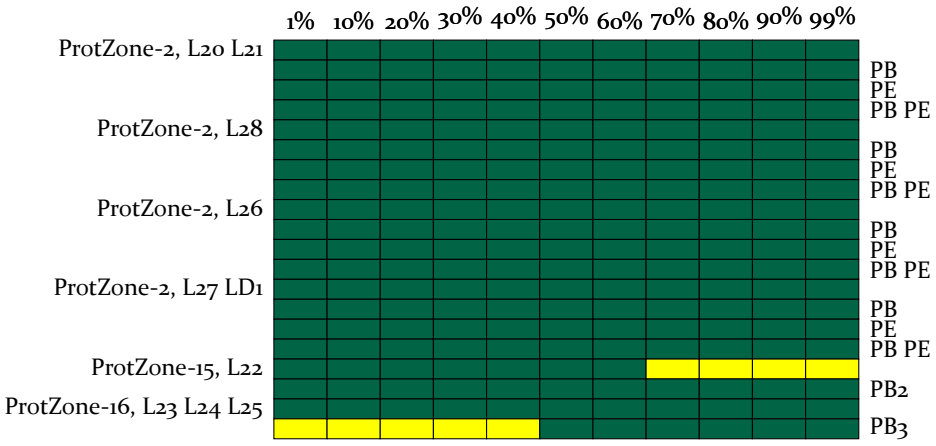

Figure 60: PSI result matrix for the state that the disconnector D1 is closed and values calculated for it are used.

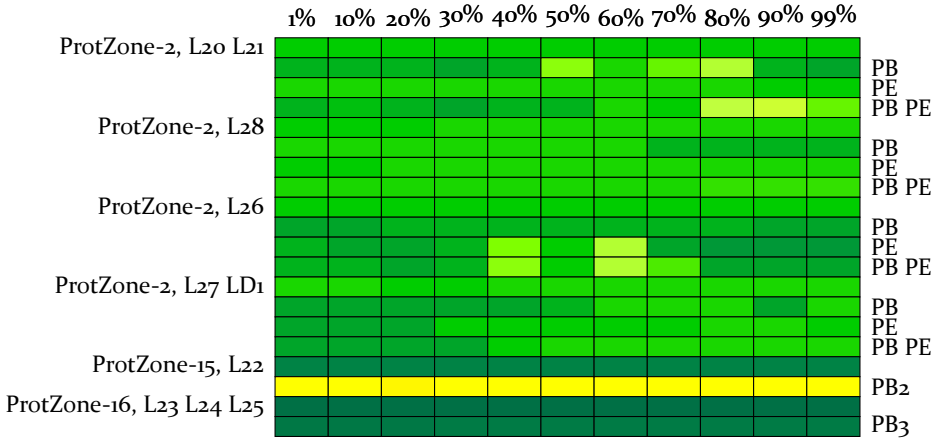

Figure 61: DSI result matrix for the state that the disconnector D1 is closed and values calculated for it are used.

11.1.4.3 Optimization of X, T, PSB of the Distance Protection & I , T of the Overcurrent Protection

In the following, the ProToc is used to optimize new setting values for the closed-loop state.

Procedure The reactance setting values X_1, X_2 and X_3, the associated delay times T_1, T_2 and T_3 as well as the use of PSB functions are optimized by the protective devices PB and PE. At the same time, the current values $I_{>>}$ of the overcurrent functions of PB2 and PB3 and $I_{>}$ of PB2 and the associated delay times $T_{>>}$ and $T_{>}$ are also optimized. All other setting values of all protection functions and devices are otherwise the same as in section 11.1.3.5. This is used to examine how well the system performs when only parts of the system are optimized and adjusted to changing conditions. The resulting values, like the calculated ones, are listed in the Table 31 in the Appendix D.

Results The result matrix of the PSI is shown in Figure 62 and gives a result value of 0.999. The joint result of the DSI and SRI is shown in Figure 63 and gives a result of 0.863. The overall assessment result is 0.931, which is the best result for the closed-ring case. Except for the fault at 1 % on line L22, all faults are selectively cleared. The ProToc accepts this in favor of a significantly better stability assessment. Thus, Zone1 and Zone2 of PE have been significantly increased and the associated delay times reduced to a minimum of 0 ms and 250 ms. The setting values are chosen so that, from the PE's point of view, all faults on the ring up to and including line L21 are measured directly in

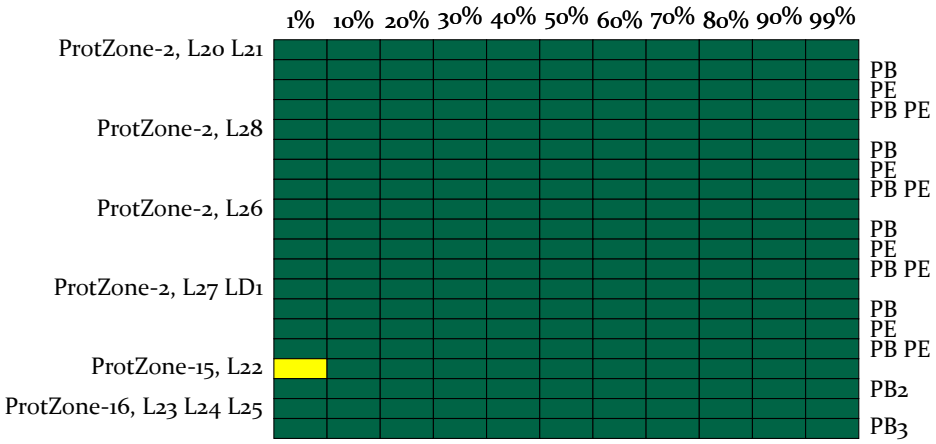

Figure 62: PSI result matrix for the state that the disconnector D1 is closed and optimized values are used for this.

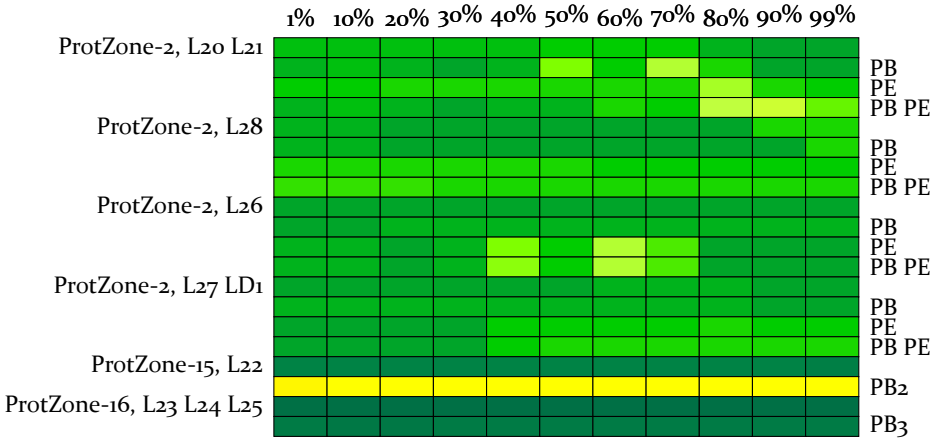

Figure 63: DSI and SRI matrix for the state that the disconnector D1 is closed and optimized values are used for this.

Zone1. For faults on line L20, the fault impedance jumps to Zone1 after PB has previously tripped the fault in Zone1. PB disconnects faults up to and including 50 % on line L21 in Zone1. This is done with a delay time of 50 ms. Thus, all faults on the ring between PB and PE are cleared in two stages with a small time delay.
The fault L22-1 % is located at the beginning of the branch of PB2 and PB3 and thus in the downstream zone from the point of view of PE. The fault impedance measured by PE is 1.81 Ω, which is within Zone1 and results in unselective tripping. For the subsequent faults on the feeder, the measured fault impedances are much larger due to the strong intermediate infeed. Thus, the fault impedance for L22-10 % is already 2.7 Ω and thus in Zone2. The ProToc therefore accepts unselective fault clearing right at the beginning of L22 in order to be able to look much further into the ring.
The PSB function is not needed for PB or PE and was therefore deactivated for both.

Conclusion The ProToc has reacted flexibly to the new ring topology and optimized new setting values. In favor of better dynamic stability, it accepted the unselective clearing of one fault. Otherwise, it has optimally adapted the setting values to the existing conditions and achieved an excellent compromise between selectivity and dependability.

11.1.5 Forming a Highly Meshed System

In chapter 9 numerous changes and challenges of power systems were mentioned, which are present or upcoming to achieve the global climate goals. These include the rapid expansion of RES and increasing electrification. The increasing energy exchange via distribution systems requires a corresponding grid expansion and/or the application of unconventional solutions. One of these solutions could be to operate distribution grids temporarily or even permanently meshed to better handle feed-in fluctuations and load peaks [132], [133]. To investigate the protection security and applicability of the ProToc, disconnectors D2, D3, D4 and D5 are now closed, resulting in a highly meshed grid section in the northwest of the test system.

11.1.5.1 Use of Standard Setting Rules for Distance & Overcurrent Protection

Procedure The distance protection functions of the protective devices PA, PF, PG, PI and PH are re-parameterized according to (72) and the overcurrent functions of PA2 and PI2 are re-parameterized according to (75). All other

setting values of all protection functions and devices are otherwise the same as those from section 11.1.3.5. This is used to investigate how well traditional setting rules are suited for unconventional topologies. All calculated values, as well as all future optimized values, are summarized in Table 32 in the Appendix D.

Results The result matrix of the PSI is shown in Figure 64 and gives a result value of 0.708. The joint result of the DSI and SRI is shown in Figure 65 and gives a result of 0.786. The overall result of the assessment is 0.755. The PSI matrix clearly shows that the protection system does not have good selective behavior. Since the overcurrent protective devices PA2 and PI2 often trip simultaneously, many faults are tripped with overfunction. This is due to the direction setting, which is still set to undirectional with $DIR_1 = 2$.

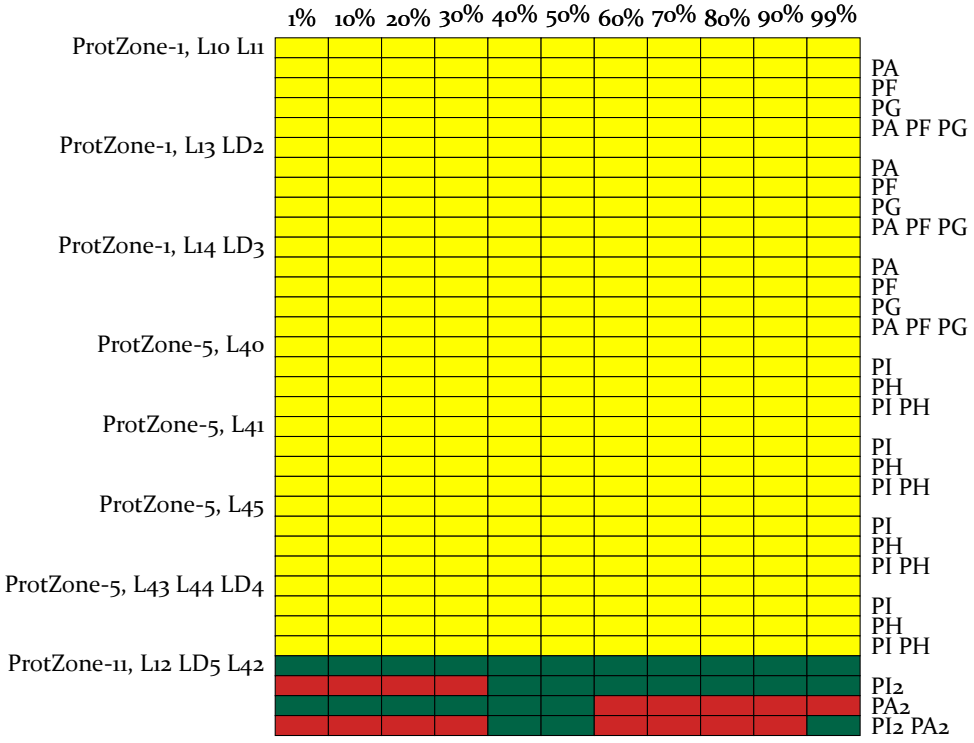

Figure 64: PSI result matrix with closed disconnector D2, D3, D4 and D5 as well as calculated values for PA, PF, PG, PI, PH, PA2 and PI2.

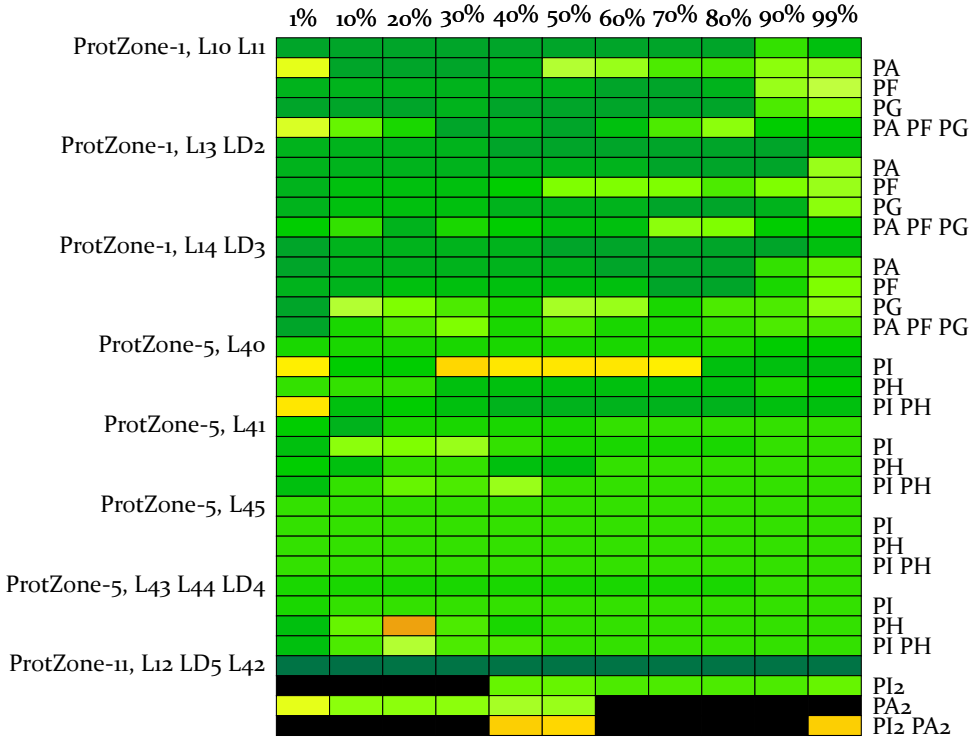

Figure 65: DSI and SRI result matrix with closed disconnector D2, D3, D4 and D5 as well as calculated values for PA, PF, PG, PI, PH, PA2 and PI2.

Fault clearing with under function occurs for faults at the beginning of path L12-D5-L42 where PI2 fails. The distance protective devices PI and PH both fail to trip, with the result that 4 s after the fault occurrence, PgridE trips. Subsequently, the ideal voltage source is disconnected from the system, causing all DERs still connected up to this point to trip as well. Eventually, no load in the system is supplied anymore.
The same applies to faults at the end of the path L12-D5-L42, when PA2 fails. In this case, PA, PF and PG do not trip, so the PgridE finally disconnects the fault and the system is no longer supplied. An exception to this is fault L12-D5-L42-99 % (PI2 PA2), where protective device PA detects and trips the fault in Zone3. This is followed by subsequent tripping of PF and finally PG, which disconnects the fault 1.6 s after its occurrence.

Conclusion The use of traditional setting rules fails with such unconventional topology. The high degree of meshing cannot be accounted for, so there

is no protection or power system security. This also shows how important it is to seriously review protection system security after power system changes.

11.1.5.2 Optimization of X, T, PSB of the Distance Protection and I, T, DIR of the Overcurrent Protection

Procedure From the protective devices PA, PF, PG, PI and PH the setting values X_1, X_2 and X_3, the associated delay times T_1, T_2 and T_3 as well as the use of PSB functions are optimized. For PA2 and PI2, the current stages $I_{>>}$ and $I_{>}$, the associated delay times $T_{>>}$ and $T_{>}$, and the direction settings DIR_1 and DIR_2 of the overcurrent protection functions are optimized in parallel. All other setting values of all functions and devices are otherwise the same as those in section 11.1.3.5. This is used to investigate how well the ProToc handles such unconventional situations and whether it is also able to select the direction setting appropriately well for overcurrent functions. The resulting values, like the calculated values, are listed in Table 32 in the Appendix D.

Results The result matrix of the PSI is shown in Figure 66 and gives a result value of 0.989. The joint result of the DSI and SRI is shown in Figure 67 and gives a result of 0.879. The overall result of the assessment is 0.934. The ProToc set both stages of the overcurrent function of PA2 to forward and of PI2 to non-directional. This corresponds to the best possible solution, since a mixture of forward and reverse stages was not possible due to the small difference in short-circuit current for faults upstream and downstream of PA2 and PI2, respectively. The tripping threshold of the fast stage of PA2 takes $I_{>>} = 2.2$ kA, which is more than three times the value of the fast stage of PI2 with 0.7 kA. At the delayed stage, the value of PA2 with 1.3 kA is also significantly larger than PI2 with 0.5 kA, which corresponds to the minimum allowed value. Both fast stages were set to the minimum possible delay time of 0 ms. The delayed stage of PA2 trips slightly later with 250 ms than the delayed stage of PI2 with 200 ms. The protective device PI2 with short delay times, low tripping thresholds, and non-directional current stages thus acts as a fast system separator, disconnecting the three left parallel feeders A, F, G from the two right feeders I and H in the event of a fault. This reduces the complexity of the system and the negative influence of the measuring accuracy on the distance protection functions. After tripping, corresponding short-circuit currents then flow only in the paths of the system half affected by the fault, making it easier for the protective devices to detect and disconnect it.

However, the PSI matrix shows an unselective behavior of the protection system in the event of some faults. For faults at 1 % on line L13 or L14 with simultaneous failure of PF or PG, unselective tripping of PI occurs due to transient effects. An activation of the PSB function could have prevented the unselective behavior, but would lead to negative consequences in case of other faults. For example, in the case of faults at the beginning of path L43-L44-D4, PI would then not trip due to blocking, so that the PgridE would have to disconnect the entire subsystem at the end. Therefore, during optimization, the PSB was explicitly not enabled for PI.
In the event of a fault at 1 % on line L40 and a failure of PI, PJ trips unselectively due to transients and a failure of the activated PSB. PA trips unselectively in Zone2 because the flowing short-circuit current is too low for the overcurrent protection functions of PA2 and PI2 to adequately respond and trip beforehand.

The situation is similar for faults at the beginning of L43 and a failure of PH. Due to an impedance trajectory that enters backwards into the tripping characteristic, PI trips about 270 ms after the occurrence of the fault. Then PA trips in Zone2, followed by PG in Zone2. After the backup protection of PH finally trips, PI2 and also PG follow, the latter tripping unselectively. PA2 falls back without tripping.
Particularly noticeable are the unselective fault clearings up to and including 30 % of the path L12-D5-L42. Here, overfunctions of PA, PF, and PG occur. This has been set by the ProToc in favor of much better dynamic behavior. Thus, faults along paths L10-L11, L13-D2, L14-D3 and on L12-D5-L42 (PI2) are cleared much faster and thus dynamically more secure for the system.

Conclusion It becomes clear that such unconventional and highly meshed structures are more difficult to protect and higher tripping times as well as unselectivities cannot be prevented. At the same time, unlike traditional approaches, the ProToc was able to provide a reasonable, usable and satisfactory result and identify suitable protection settings. In the course of dynamic meshing approaches and more variable and flexible grid structures in general, a regular assessment and appropriate adaptation of all protection setting values to newly emerging conditions is necessary. The ProToc has proven its potential, flexibility and variability in this respect.

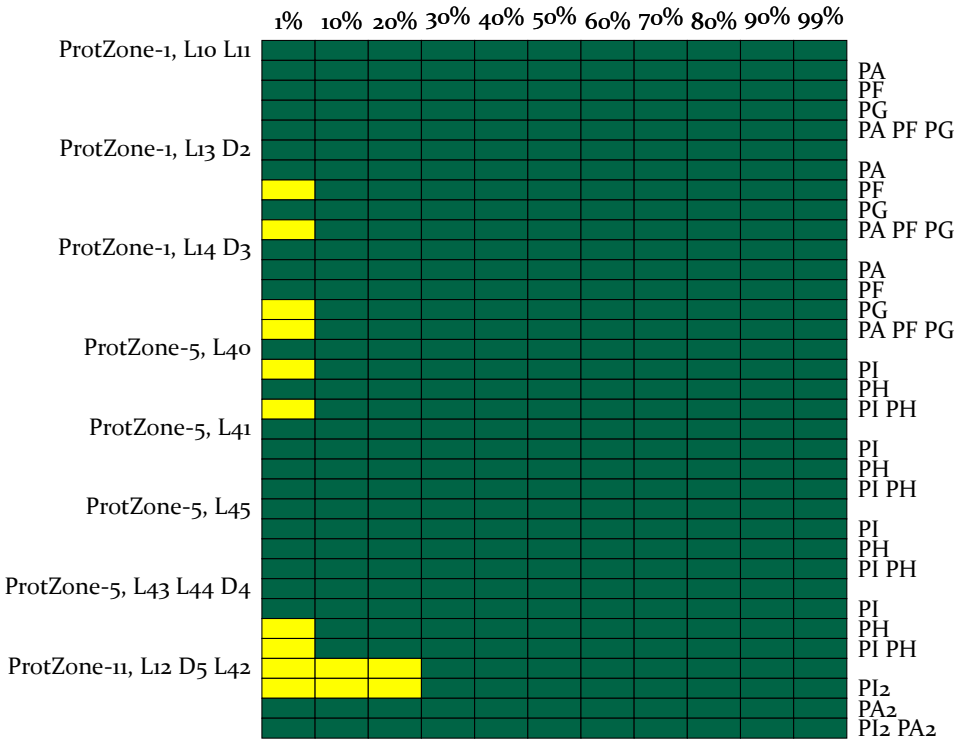

Figure 66: PSI result matrix with closed disconnector D2, D3, D4 and D5 as well as optimized values for PA, PF, PG, PI, PH, PA2 and PI2.

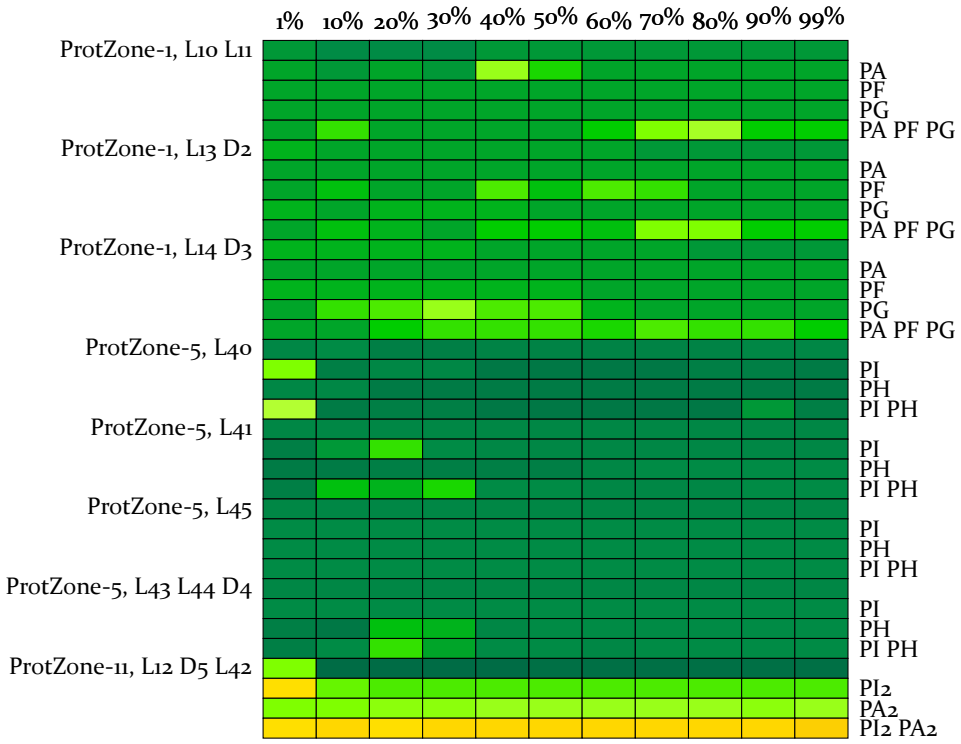

Figure 67: DSI and SRI result matrix with closed disconnector D2, D3, D4 and D5 as well as optimized values for PA, PF, PG, PI, PH, PA2 and PI2.

11.2 Protection Concepts for a Transmission System

11.2.1 Power System Model & Protection Data

The transmission system used in the following is the widely known NTS. This is a fictitious 50 Hz, extra-high voltage transmission system based on the 1983 Swedish transmission system, which experienced a voltage collapse. The system is a modified version of the Nordic32 system and has the three voltage levels 400 kV, 220 kV, and 130 kV. The NTS standard model now available in PSS©Netomac is used. In this, 19 generators, 1 synchronous capacitor, 22 loads, and 11 shunts are interconnected via 76 nodes, 50 lines, and 50 transformers. The total generation is 11.5 GW and the total consumption 11 GW. The grid topology and installation location of all resources are shown in Figure 68. Resource data, input as well as output power and used controllers can be taken from the following sources. These also form the basis for the standard model in Netomac. [134], [135]

The NTS is suitable to consider both long-term and short-term transient disturbances. It has therefore also been proposed by the IEEE PES Task Force on *Test Systems for Voltage Stability Analysis and Security Assessment* as a test system for voltage stability studies. The system can also be used to study small-signal stability and power restoration phenomena, and is now being used for protection studies as part of this work. [135] Characteristically, it is divided into the four sections *North*, *Central*, *South* and *Equiv.*. The latter represents a simply constructed section in which the largest generators are connected and which can therefore be used as a reference system. In the *North* there is a high amount of generation at low load. The opposite is true for the *Central* area, resulting in a high load flow from *North* to *Central*. In total, more than 3.2 GW flow over the five interconnected transmission lines, resulting in between 42 % and 51 % utilization of the lines. The *South* covers only a small area and is connected to the *Central* via two 400 kV lines. [134], [136]

The standard NTS model used is not initially equipped with a protection system, so it is automatically added via the ProToc. Thus, a protective device with current and voltage transformers is installed at each line start and end. An emulated line current differential protection is used as primary protection and a distance protection is used as backup protection. Current differential protection systems are more expensive because of the communication technology required, but they are the state of the art in transmission systems. They have the advantage of being inherently selective, quickly disconnecting faults within the area to be protected. This minimizes the impact of faults on the rest

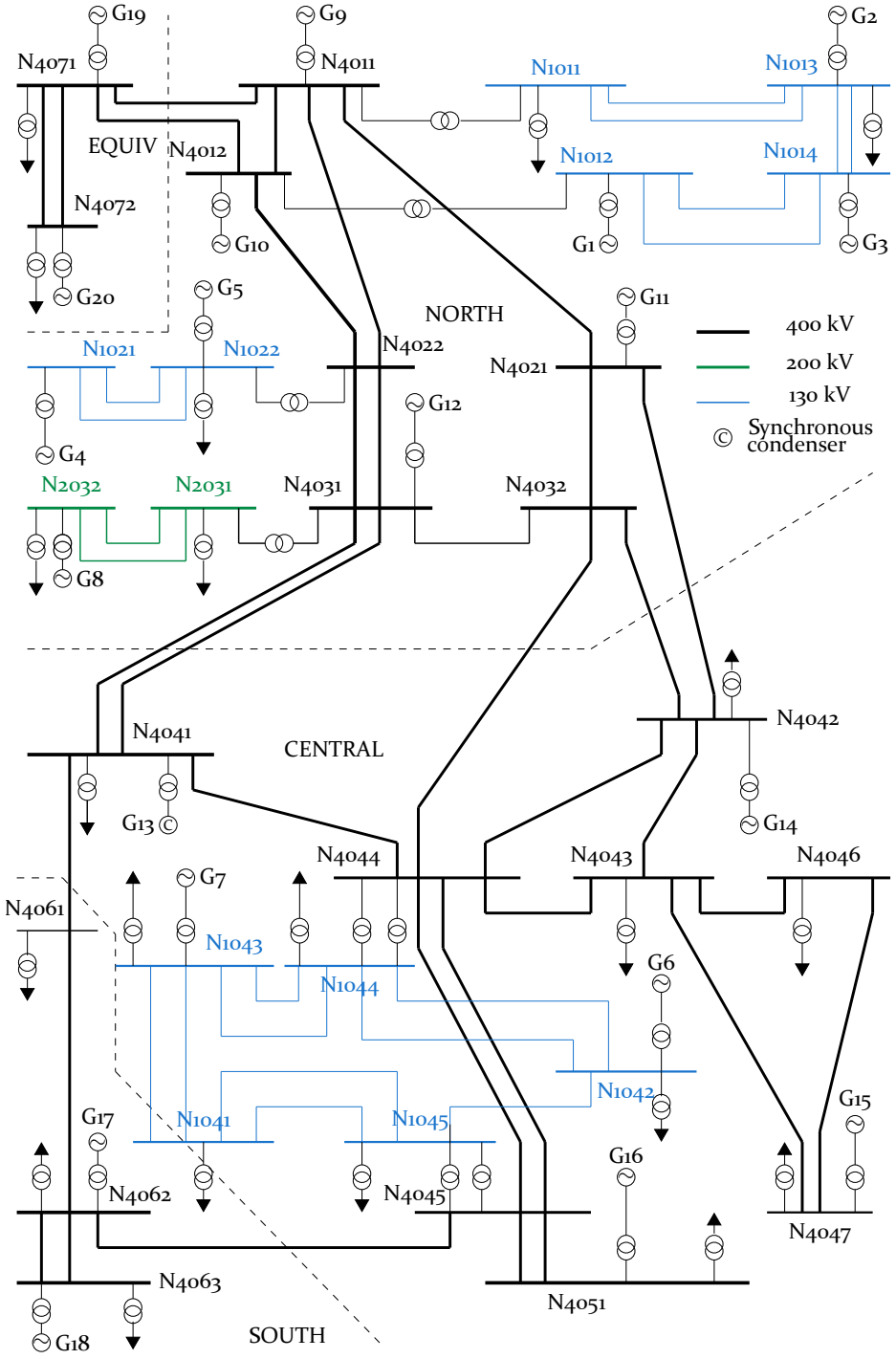

Figure 68: Single-line diagram of the Nordic Test System.

of the system. Backup protection becomes active if the primary protection fails or malfunctions due to disturbed communication. The functions are designed to be equivalent but to trip with different delay times. The line current differential protection is set to a delay time of 0 ms. The distance protection is parameterized according to formula (72) and the delay times are set to $T_1 = 40$ ms, $T_2 = 200$ ms and $T_3 = 400$ ms. Therefore, only the current differential protection is initially used to clear a fault. Zone3 of the distance protection is used as breaker failure protection and the breaker delay time remains at 100 ms.
All synchronous generators are protected by additional generator protection functions. This is neglected in many studies, although it has a major impact on the results. Generator protection includes under/overvoltage protection, under/overfrequency protection, under/overexcitation protection, and out-of-step protection. The latter trips when the specified characteristic is crossed once. All other setting values are listed in the Appendix E in the Tables 33, 34 and 35.

11.2.2 General Framework Conditions

For the performance of the tests, the following conditions apply:

- Only 3ph and thus symmetrical short circuits without fault resistance are simulated.
- The grid of the fault location is set to 1 %, 50 % and 99 % for the optimization process.
- The simulation time used is 20 s and the time step is 5 ms.
- The number of maximum FES is 5000. As optimization method BPSO_{DE}-4 is used.
- The fitness function used is $\text{FV} = 1 - PSA(\vec{x})$ according to (70) with a weighting factor of $w = 0.5$.

For the sole assessment of protection concepts, the grid of the fault location is set to 1 %, 10 %, 20 %,... 90 %, 99 %.

11.2.3 Use of Differential Protection as Main and Distance Protection as Backup Protection

Procedure The power and protection system is first examined as described above. The differential protection works properly, the distance protection runs along as backup protection.

Results The selectivity result matrix based on the PSI is shown in Figure 69 and the joint result matrix of the DSI and SRI is shown in Figure 70. An overall very selective behavior of the protection system can be seen. However, two points are noticeable.

On the one hand, unselective tripping occurs in the event of faults at the beginning and end of the parallel line between nodes N1021 and N1022. In this case, the protective device of the fault-free line located at node N1021 always trips after the actual disconnection of the fault. The reason for this is the transient current supplied by generator G4. With fault occurrence, G4 starts to accelerate strongly and lose synchronism with the rest of the system. After fault clearing by the differential protection and thus disconnection of one of the parallel lines, all the current injected by G4 flows through the remaining line. The impedance measured by the protective device is already in Zone3 at that point. It subsequently moves through Zone2 into Zone1 and, after fault clearing, causes the backup protection to trip unselectively. However, the dynamic stability assessment makes it clear that this does not endanger the rest of the system and that the loss of generation power can be compensated. Figure 71 proves this with the voltage curves of the 400 kV main nodes for the fault L-N1021-N1022-20 %. The voltage assessment gives a value of 0.87 for the VQI and the VFI is at 0.88.

On the other hand, all faults on the line between N4011 and N4021 result in unselective tripping. This line is a 400 kV transmission line in the northern area of the system. There is one transmission line from node N4021 and two transmission lines from the following node N4032 to the *Central* area. The failure of the line L-N4011-N4021 causes cascading protection trips that result in almost complete failure of the entire system. Only the generators G6 as well as G19 and G20 remain connected to the system and form two separate islanding grids. After disconnection of the faults by the differential protection, the first two unselective trips occur about 1.4 s later due to power swings. 1 s after that, the next three and about 400 ms after that, the next four protective devices trip. The generators G1, G2, G3 and G4 are tripped approx. 4 s after fault clearing by the overvoltage protection. This is followed by the generators G5, G7, G8, G9, G10, G15 and G18 due to undervoltage and overvoltage. The cascade continues accordingly. Figure 72 illustrates the situation with the corresponding voltage curves for the fault L-N4011-N4021-20 %. The voltage assessment results in 0.21 for the VQI and 0.32 for the VFI.

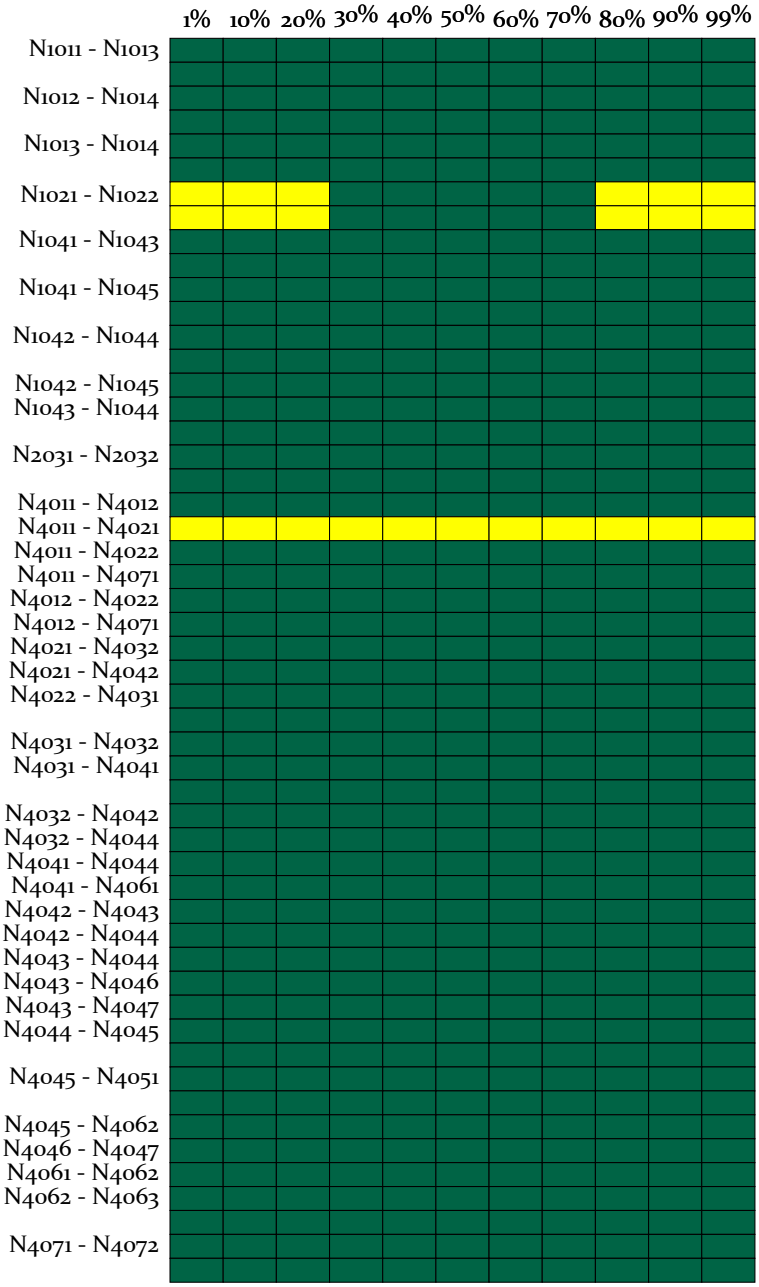

Figure 69: PSI result matrix using line current differential protection as main und distance protection as backup protection.

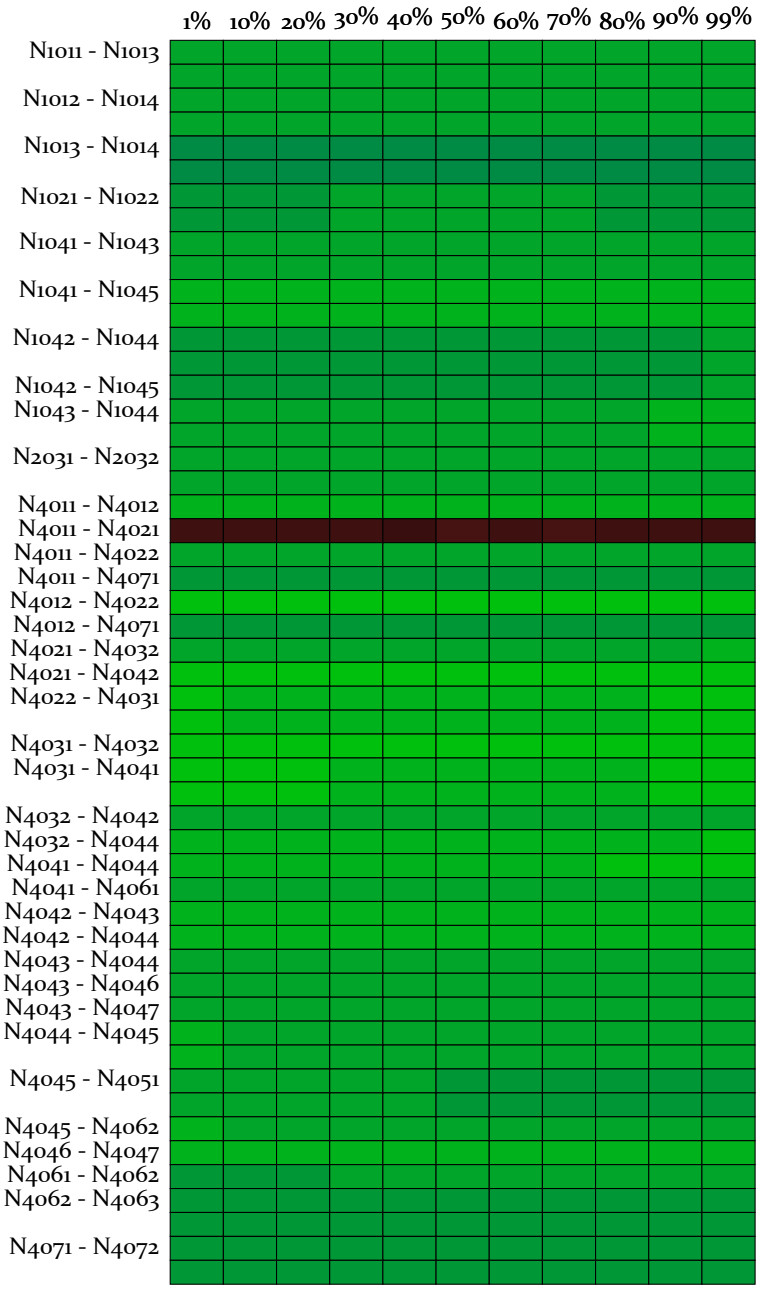

Figure 70: DSI and SRI result matrix using line current differential protection as main und distance protection as backup protection.

Conclusion Even when differential protection systems are used, faults can lead to consequential reactions that endanger system stability and supply security. Distance protection in particular is at risk to trip unselectively in case of transient events such as power swings. This has already been demonstrated by numerous analyses of power outages and system splits [72], [74]. A regular review of primary and backup protection is therefore necessary.

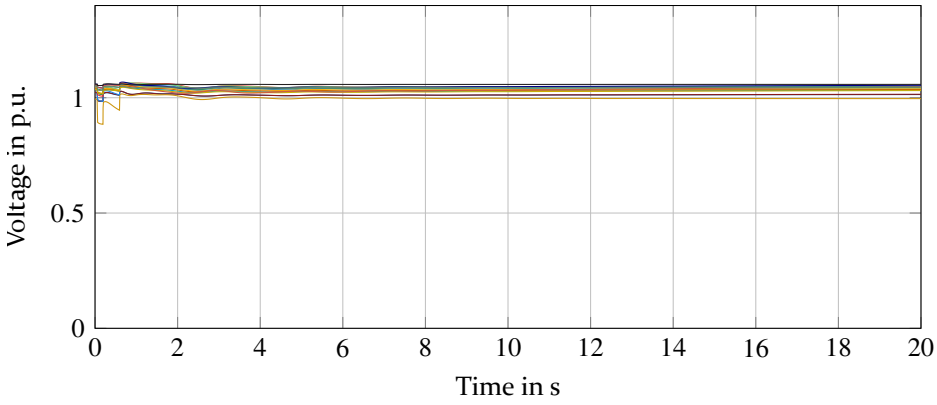

Figure 71: Voltage curves of the main 400 kV nodes for the fault L-N1021-N1022-20 %.

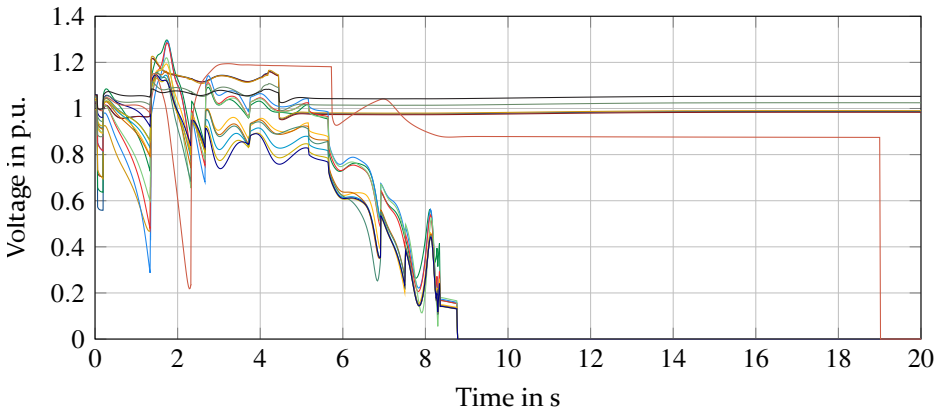

Figure 72: Voltage curves of the main 400 kV nodes for the fault L-N4011-N4021-20 %.

11.2.4 Use of the Distance Protection as Main and Backup Protection

11.2.4.1 Using Calculated Values

Procedure In the following, a communication failure and thus a failure of the differential protection is assumed. The distance protection therefore now functions as primary and backup protection. The setting values of the distance protection remain unchanged.

Results The selectivity result matrix based on the PSI is shown in Figure 73 and the joint result of the DSI and SRI is shown in Figure 74. For clarity, only the faults and lines where selectivity or stability problems occur are shown in the following. Overall, both criteria have deteriorated compared to the use of differential protection. On the one hand, this is due to the fact that now all faults are cleared with at least an additional time delay of 40 ms. On the

Figure 73: PSI result matrix using distance protection as main and backup protection.

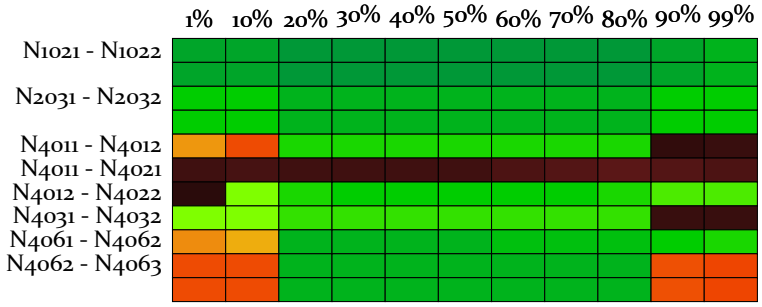

Figure 74: DSI and SRI result matrix using distance protection as main and backup protection.

other hand, the faults in the range 0 % to 20 % from the beginning of the line and 80 % to 100 % from the end of the line are now disconnected in two stages, with the more distant protective device tripping only in Zone2 and thus with a delay time of 200 ms.

The unselective behavior of section 11.2.3 is still present and now also affects all faults on the parallel line between N1021 and N1022. In addition, there are other faults that have little to no effect on and jeopardize system stability. For faults on the parallel line between the nodes N2021 and N2023, the same phenomenon occurs as for N1021 and N1022. Here, however, it is generator G8 that loses synchronism. But this also has little effect on the rest of the system. The situation is different for the faults at the beginning and end of the lines between the nodes N4061 and N4062 as well as N4062 and N4063. Here, due to transients, there is unselective tripping of some protective devices and disconnection of the generators G17 and G18 in the southern part of the system. In particular, angular stability is at risk. However, the voltage and frequency stability remains reasonably stable and there are no widespread consequential reactions.

The situation is different for individual faults at the end and beginning on the lines between the nodes N4011 and N4012, N4012 and N4022, and N4031 and N4032, all of which are in the *North* area. For these, there are massive consequential and unselective protection trips due to the fault and numerous generator failures. The voltage stability assessment indices VQI and VFI drop to as low as 0.15 for these faults and all generators in the system except G6, G19 and G20 are disconnected from the system.

Conclusion The backup protection has the task of taking over in the event of a failure of the primary protection and reliably disconnecting faults. However, it must be reviewed whether the backup protection fulfills this task sufficiently and whether the minimum fault clearing time is respected.

11.2.4.2 Optimization of PSB and OOS of the Distance Protection

Procedure The ProToc is to optimize the activation/deactivation of all PSB and OOS functions of all distance protection functions in the following. The reactance setting values and delay times remain unchanged. The intent is to determine if power system protection and security can be improved by blocking trips at certain locations and allowing trips at other locations when instability is detected. While blocking a trip may have a positive effect on some faults, an early separation of the system may be better for other faults.

Results The selectivity result matrix using the PSI is shown in Figure 75 and the joint result of the DSI and SRI is shown in Figure 76. Overall, the selectivity behavior of the protection system and the stability behavior of the power systems have been significantly improved. However, there are still some fault situations where stability is still severely impaired. The PSB function was activated in half and the OOS function in a quarter of all protective devices.

Faults at the beginning of the line between the nodes N4011 and N4012 as well as the parallel line between the nodes N4062 and N4063 still lead to unselective tripping, but there are significantly fewer to no generator outages anymore. This has a positive effect on system stability. Most noticeable is the good result for the fault at 1% on the line L-N4012-N4022. There are now no more unselective protection trips and consequently no cascading disconnections of generators.

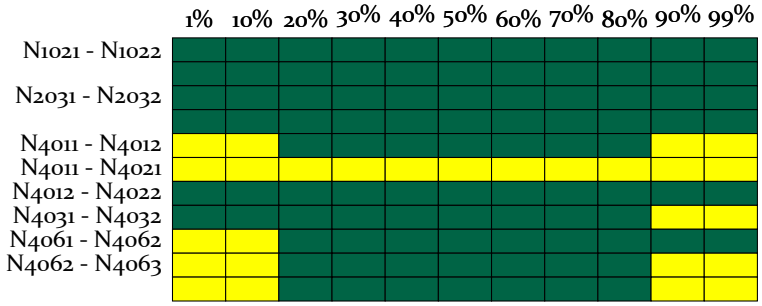

Figure 75: PSI result matrix using distance protection as main and backup protection with optimized protection functions.

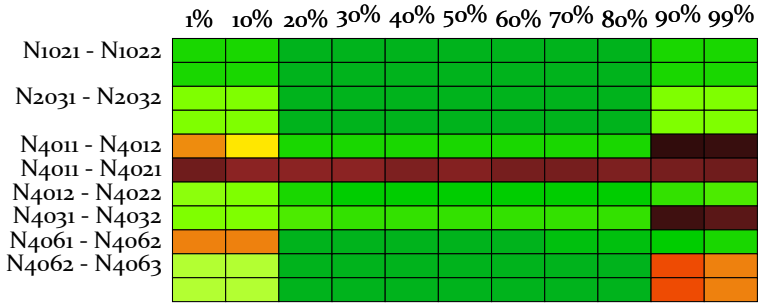

Figure 76: DSI and SRI result matrix using distance protection as main and backup protection with optimized protection functions.

The stability behavior for all faults on the line L-N4011-N4021 has also been greatly improved. For these, only a maximum of 11 generators and once 13 generators are disconnected instead of 16 generators as before. Here, generators G17 and G18 in the *South* area and generator G6 each form an island grid. In addition, the generators G4, G5, G9, G10 from the *North* area and G19 and G20 from the *EQUIV* area are still interconnected and in operation. Figure 77 shows the resulting voltage curves as before for the fault L-N4011-N4021-20 %. In this case, the voltage assessment yields 0.24 for the VQI and 0.25 for the VFI.

The only thing that has deteriorated is the stability assessment for faults at the beginning and end of the line L-N2031-N2032. Although there are no more unselective trips, this has a slightly worsening effect on all three stability criteria.

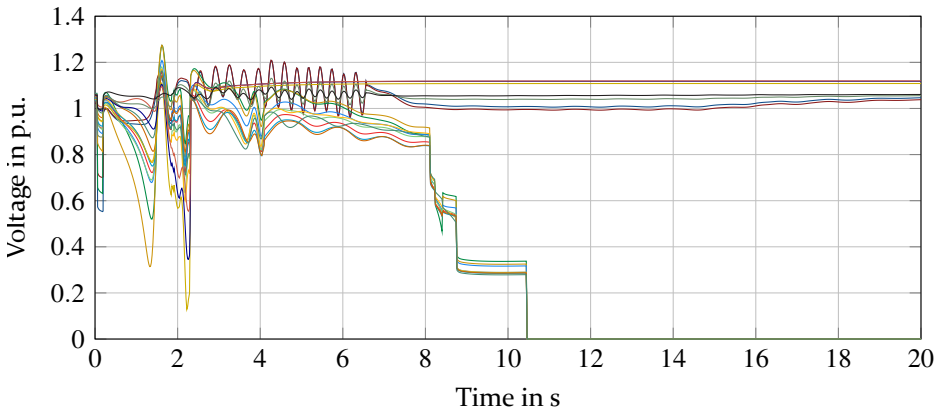

Figure 77: Voltage curves of the main 400 kV nodes for the fault L-N4011-N4021-20 % using optimized protection functions.

Conclusion The ProToc was able to optimize the protection and security of the power system in the best possible way under the given conditions and requirements. The PSB and OOS functions were turned on or off individually for each protective device, weighing selectivity and stability criteria. This proves that ProToc can also generate significant added value for transmission systems. It is also suitable for primary and backup protection.

The greatest enemy of knowledge is not ignorance, it is the illusion of knowledge.

Stephen Hawking
English theoretical physicist
* 1942 + 2018

12 Laboratory Tests for Verification

In order to validate the results of the ProToc, which are based on generic protection functions and dynamic simulations, some of the optimized setting values and effects will be verified using real protection devices and a real-time simulation system. The simulation grid used is the 20 kV distribution system from section 11.1.1.

12.1 Setup

The laboratory setup is shown pictorially and schematically in Figure 78. It consists of a Real Time Digital Simulator (RTDS) NovaCor™ system from RTDS Technologies Inc, four CMS 365 current and voltage amplifiers from OMICRON electronics GmbH, and four SIPROTEC 5 7SX85 universal protection devices from Siemens AG. The laboratory is located on the premises of EES in Nuremberg. As part of the Kopernikus ENSURE project [114], the power system model from section 11.1.1, Figure 44, was converted to RSCAD. For this purpose, the existing Root Mean Square (RMS) model from PSS©Netomac was first converted to an Electromagnetic Transients (EMT) model using PSS©E software and then imported into RSCAD©. Equipment, topology, and all DERs are replicated according to the original model. However, for the voltage regulator of the DERs, the *IEEE Type 1* standard model is used instead of the *SEXS* model since the latter was not available. Default parameters are used for all controllers. All loads are grounded, CTs, VTs and breakers are modeled. The fault implementation in RSCAD uses a fault transfer resistor of 0.01 Ω and

(a) Real setup consisting of an RTDS system (left) and protective devices as well as voltage and current amplifiers (right).

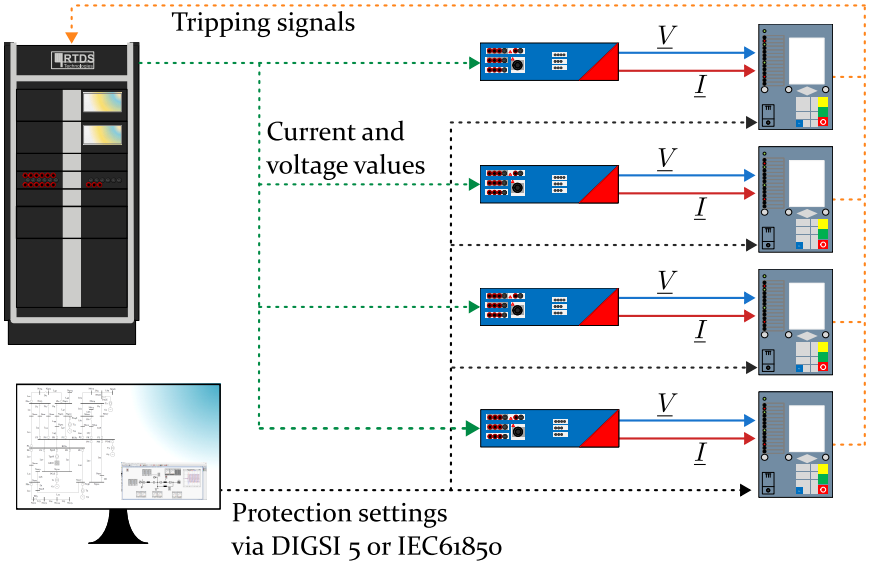

(b) Schematic representation of the setup including signal and data transmission.

Figure 78: Real-time laboratory setup.

connects all phases of the system to ground simultaneously through three switches. The dynamic behavior of the system is therefore different in some respects from the original model in PSS©Netomac, which is not a problem for the upcoming studies, but must be taken into account. Via the CMS 365, the analog, low-level current and voltage signals from the RTDS are amplified according to the measurement circuits of the 7SX85 universal protection devices used. Instrument transformers are considered within the power system model. The four available real protection devices represent the protective devices PB, PE, PJ and PgridE. Distance protection and overcurrent protection are accordingly used as protection functions. The DIGSI 5 software or a client communicating via IEC 61850 as in [P137] is used for parameterization. When one of the real protection devices trips, the binary trip signal is fed back to the RTDS via a hardware connection, ensuring that the circuit breaker is opened within the simulation according to the implemented opening logic.

In the following, various tests are performed with the disconnector D1 open and closed.

12.2 Accuracy & Comparability Analysis

Procedure All disconnectors are initially open. For this condition, the ProToc has often determined a setting value for the protective device PB for the first zone of $X_1 = 0.36\,\Omega$, which is thus higher by 0.01 Ω than the corresponding minimum and maximum zone value $X_{\mathrm{AB,min}} = X_{\mathrm{AB,max}}$ of 0.35 Ω of path L10-L11. Nevertheless, the assessment does not show an unselective behavior of PB for faults in the downstream zone on line L22. The reason is that the PSA tool simulates all faults exclusively in the range of 1 % to 99 % on the corresponding paths. For the fault L22-1 % the measured fault impedance is 0.3625 Ω and thus outside Zone1 of PB. To check and compare this fact and at the same time the accuracy of the measured values and the resulting optimization results, the following two faults in the RTDS are investigated:

1. 3phE fault at 1 % on line L22.
2. 3phE fault directly after the CT, which is like a fault at 0 % on line L22.

Result Figure 79 shows the real measurement result of the phase-phase impedances of a 7SX85 at the installation location of PB for the first case and Figure 80 for the second case. It is good to see that the measured impedance are just outside Zone1 of the 7SX85 in the first case and just inside Zone1 in the second case.

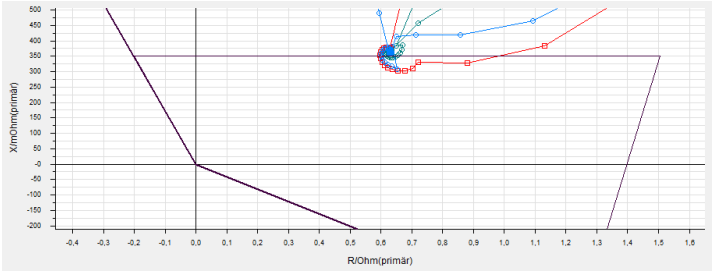

(a) Fault impedance and tripping characteristic of Zone1.

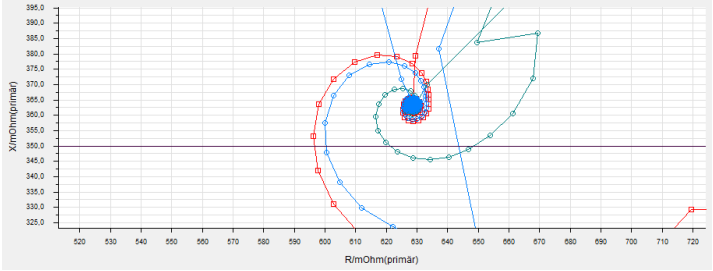

(b) Zoomed in view.

Figure 79: Measured impedances $\underline{Z}_{12}$ (blue), $\underline{Z}_{23}$ (green) and $\underline{Z}_{31}$ (red) of the 7SX85 at the installation location of PB for a fault at 1 % on line L22.

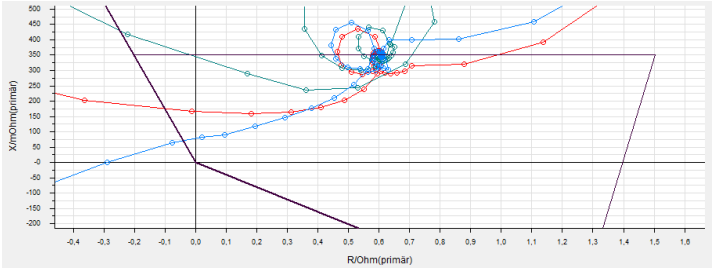

(a) Fault impedance and tripping characteristic of Zone1.

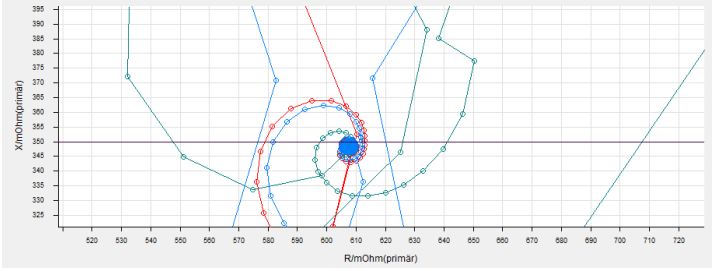

(b) Zoomed in view.

Figure 80: Measured impedances $\underline{Z}_{12}$ (blue), $\underline{Z}_{23}$ (green) and $\underline{Z}_{31}$ (red) ofthe 7SX85 at the PB installation location for a fault directly behind the current transformer.

Therefore, the 7SX85 does not trip in the first case and the following protective device PB2 clears the fault in fast time. In the second case, there is an unselective fault clearing of PB.

Conclusion The laboratory test confirms assumptions and statements made. The accuracy and thus the applicability of fault simulations with generic protection functions is hence able to generate realistic and applicable protection settings through optimization. The measured fault impedances of the generic protection functions within the Netomac simulation agree well with those of the real 7SX85 protection devices in combination with an RTDS simulation. However, the rasterization of the fault location has a decisive influence on the assessment, optimization and thus the determined setting values and should, in perspective, be done with a smaller distance to the node or even include node faults.

12.3 Advantages of Topology-dependent Adaptation

Procedure When the disconnector D1 is closed, a ring is formed between PB and PE. For this topology, the ProToc has determined adapted protection setting values. For analysis, the following two faults are considered at 20 % on line L21 for the closed ring:

1. Using the optimized setting values for the open ring from section 11.1.3.5.
2. Using the optimized closed-ring setting values from section 11.1.4.3.

Result Figure 81 shows the real measurement results of the phase-phase impedances of the 7SX85 at the installation location of PE for the first case and Figure 82 for the second case. Using the optimized open-ring setting values, the measured fault impedances $\underline{Z}_{12}$, $\underline{Z}_{23}$, and $\underline{Z}_{31}$ are in Zone3, so the trip signal is not output until 600 ms after the fault occurs and the fault is then sequentially disconnected. The measured fault impedances at the time before and after the tripping of the opposite device PB, which clears the fault in its Zone1, can be clearly seen in the RX diagram.
The situation is different when using the optimized values for the closed ring. Here, the real 7SX85 sees the fault directly in Zone1 and issues a trip signal immediately after fault occurrence.
Figure 83 shows the respective timing trip signals of the two 7SX85 protection devices at the installation locations of PB and PE as they arrive in the RTDS for both cases and lead to the corresponding circuit breaker openings.

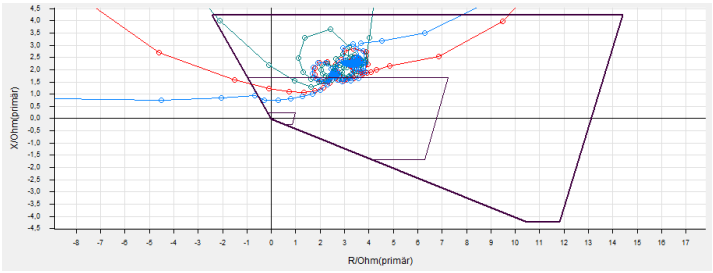

(a) Fault impedance and tripping characteristic of Zone1, Zone2 and Zone3.

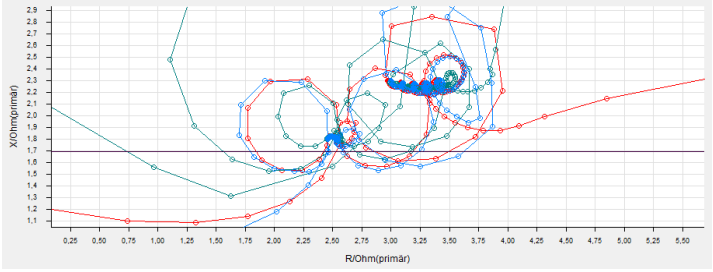

(b) Zoomed in view.

Figure 81: Measured impedances $\underline{Z}_{12}$ (blue), $\underline{Z}_{23}$ (green) and $\underline{Z}_{31}$ (red) of the 7SX85 at the PE installation location for a fault at 20 % on line L21 using optimized settings for the open ring.

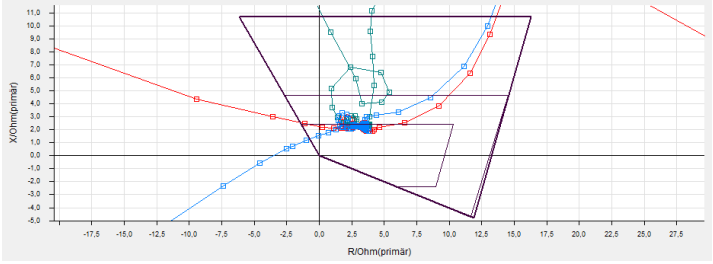

(a) Fault impedance and tripping characteristic of Zone1, Zone2 and Zone3.

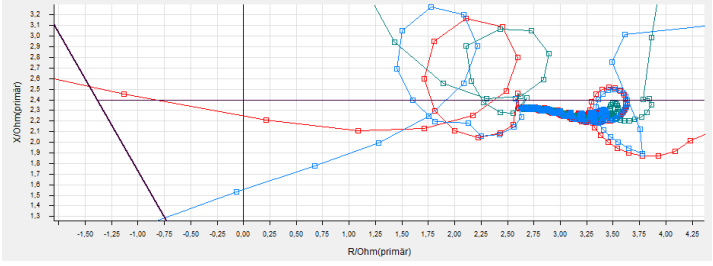

(b) Zoomed in view.

Figure 82: Measured impedances $\underline{Z}_{12}$ (blue), $\underline{Z}_{23}$ (green) and $\underline{Z}_{31}$ (red) of the 7SX85 at PE for a fault at 20 % on line L21 using optimized settings for the closed ring.

The earlier disconnection also has a corresponding positive effect on the stability and the DERs located in the system. Figure 84 shows the injected active and reactive powers of all DERs from both cases investigated. It can be seen that in the upper case (a), with later fault clearing, the responses are stronger and last longer. The situation is different for an early fault clearing (b). Here, a reduced transient and thus more stable behavior of the individual DERs results.

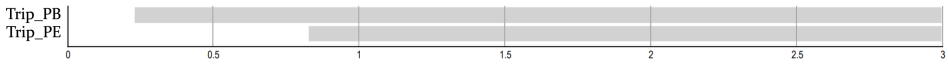

(a) Using optimized settings for the open ring.

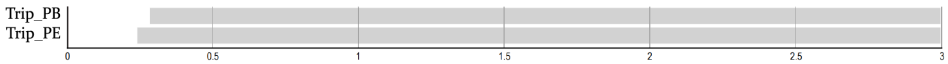

(b) Using optimized settings for the closed ring.

Figure 83: Time sequence of the trip signals of PB and PE measured inside the RTDS.

Conclusion The laboratory test confirms the analysis and assessment of the PSA tool with regard to the transient system behavior for different protection settings. The new closed-loop setting values optimized by the ProToc also lead to significantly improved performance of the protection system under real laboratory conditions.

12.4 Comparison of the Impact of Transient Events

PSB Function Disabled

Procedure Finally, the transient behavior of the power systems and the associated effects on real protection devices are to be tested. For this purpose, the calculated setting values from section 11.1.3.1 are used and a fault at 1 % of line L10 with simultaneous failure of protective device PA and open disconnector D1 in the RTDS is simulated. This fault had caused unselective tripping of PE in the Netomac simulation during the fault due to an elliptically moving impedance trajectory.

Result Figure 85 shows the corresponding measurement result of the phase-phase impedances of the real 7SX85 protection device at the installation location of PE. The result and the curve of the impedance trajectory is very similar to the one from the previously performed Netomac simulation, which is shown in Figure 47 at the beginning of this chapter. Also in this case, the measured fault impedance is initially in the reverse direction and then

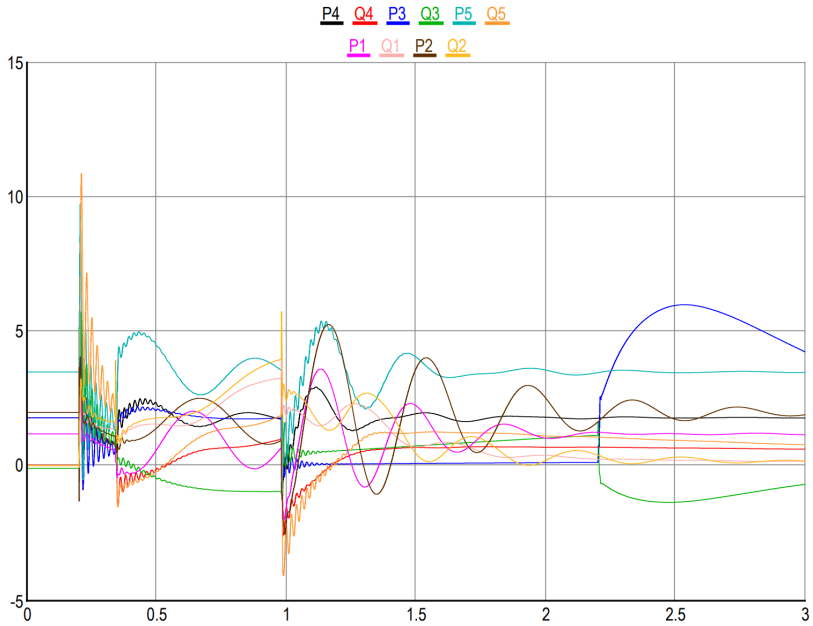

(a) Late fault clearing in Zone3 by protection device PE.

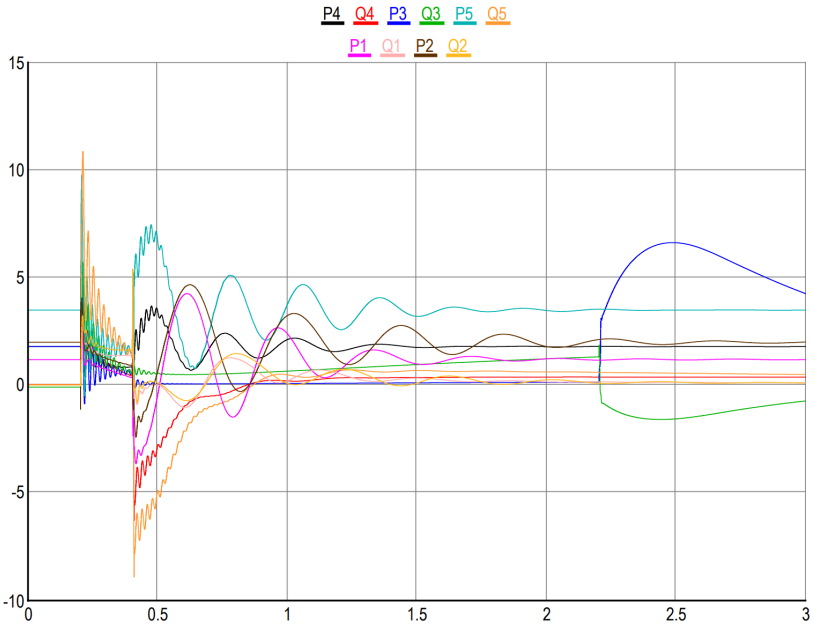

(b) Early fault clearing in Zone3 by protection device PE.

Figure 84: Active (P) and reactive (Q) power output of all DERs in MW as reaction for a fault at 20 % on line L21.

moves in a clockwise elliptical trajectory into Zone1 of the 7sX85, providing unselective tripping. The measured impedance values of the 7SX85 show a slight deviation from those of the generic protective devices, which can be explained by the different model designs and simulation modes used by Netomac and RSCAD.

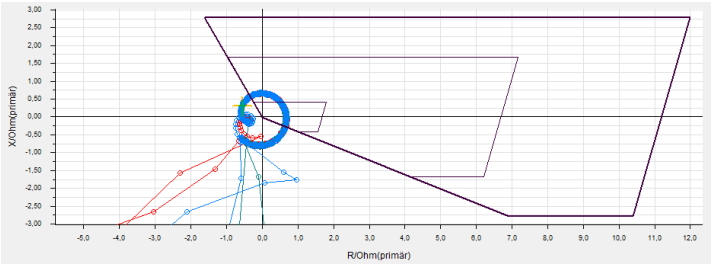

(a) Impedance trajectory and tripping characteristic of Zone1, Zone2 and Zone3.

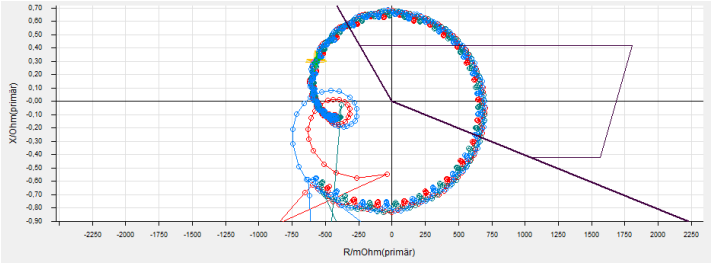

(b) Zoomed in view.

Figure 85: Measured impedances $\underline{Z}_{12}$ (blue), $\underline{Z}_{23}$ (green) and $\underline{Z}_{31}$ (red) of the 7SX85 at the installation location of PE for a fault at 1 % on line L10 when PA fails and the calculated open-ring settings are used.

Conclusion Overall, the laboratory test confirms the problem of possible false tripping due to transient effects during the fault in distribution systems. This is caused by too high fault clearing times and the resulting acceleration of rotating machines with low inertia. In addition, the larger R/X ratio in distribution compared to transmission systems already leads to an initial fault impedance which is closer to the direction lines and thus the zone boundaries of protective devices.

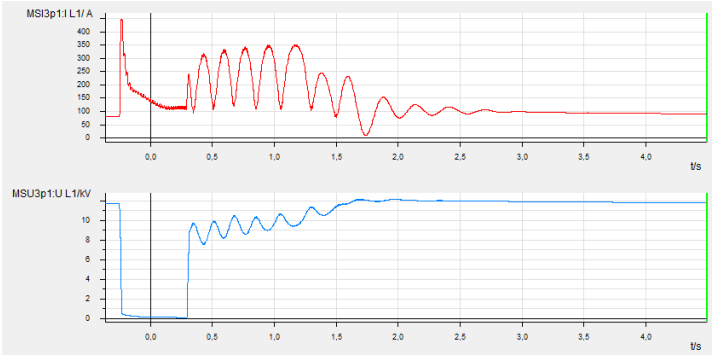

Figure 86: Measured RMS voltage and current of phase 1 of the 7SX85 at the installation location of PE for a fault at 1 % on line L10, when PA fails, the calculated open-ring settings are used and the PSB function is activated.

PSB Function Enabled

Procedure For a final test, the implemented PSB function is enabled on the real 7SX85 protection device. This tests whether transient movements are successfully detected and whether the function should not also be used in distribution systems in the future.

Result The currents and voltages measured by the 7SX85 device for the same simulated fault at 1 % of line L10 with simultaneous failure of protective device PA and open disconnector D1 are shown in Figure 86. Figure 87 shows the corresponding impedance trajectory in the RX diagram. It can be seen that the 7SX85 was able to successfully detect the elliptical movement of the impedance trajectory and prevent a false trip. The trajectory passes through Zone1 and jumps well outside the tripping characteristics of the protection device after successful fault clearing. In the comprehensive overall view of Figure 87 (a), the final transients of the DER G3 can be seen in the impedance plane of the 7SX85.

Conclusion The laboratory test again confirms a good match of Netomac simulations with generic protection functions and the RTDS along with real protection devices. The proof is thus provided that fully automatically generated and optimized protection concepts as well as setting values meet requirements for accuracy, plausibility and applicability.

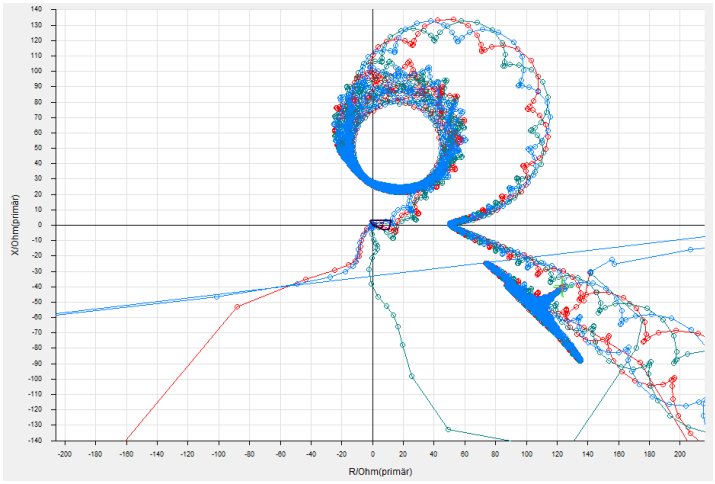

(a) Overall view of the impedance trajectory.

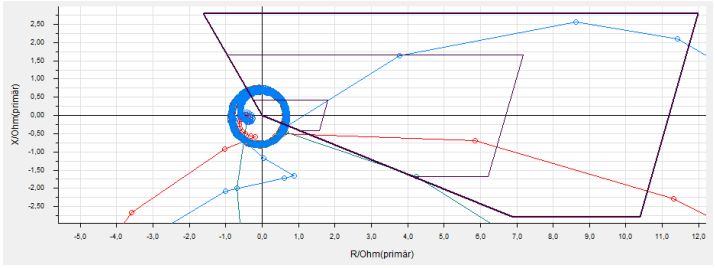

(b) Impedance trajectory and tripping characteristic of Zone1, Zone2 and Zone3.

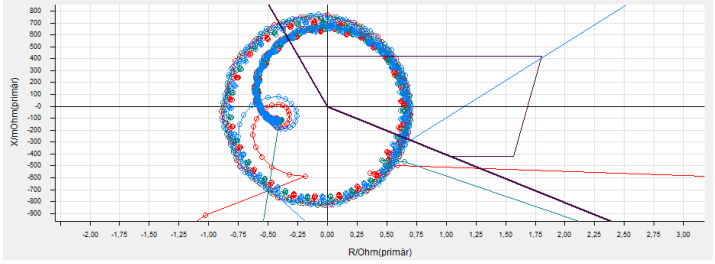

(c) Zoomed in view.

Figure 87: Measured impedances $\underline{Z}_{12}$ (blue), $\underline{Z}_{23}$ (green) and $\underline{Z}_{31}$ (red) of the 7SX85 at the PE installation location for a fault at 1 % on line L10, when PA fails, the calculated open-ring settings are used and the PSB function is activated.

The world as we have created it is a process of our thinking. It cannot be changed without changing our thinking.

Albert Einstein
German physicist
* 1879, + 1955

13 Conclusion & Outlook

Power systems worldwide are facing the major challenge of advancing the expansion and integration of RES. In the future, green electricity is expected to supply the energy, transport, heating and industrial sectors in an efficient, secure and climate-neutral manner. This has far-reaching implications for transmission and distribution systems.
Consequently, more prosumers will have to be connected, more storage integrated, and more RES connected. The total energy exchange via the power grid will increase. In the process, the infeed and load behavior will become significantly more variable, depending on the yields from wind and sun as well as the respective time of year and day. Grid planning, system management and protection concepts will therefore be confronted with a variety of new grid operating and fault conditions as well as bidirectional and volatile load flows, all of which must be managed securely.

It is common practice to rely on proven and typical protection schemes and traditional setting standards that focus primarily on selectivity when creating protection concepts. Protection experts with many years of experience usually develop them using only table lists and short-circuit simulation programs in close coordination with the existing grid structure. The workflow is rarely automated and therefore labor-intensive, time-consuming and requires a high level of technical expertise. Regular review of system-wide protection after changes often does not take place, or only inadequately, for reasons of time, staff, and costs.

Therefore, the ProToc consisting of six different and interlinked tools is presented, which enables protection concepts and the corresponding setting values to be automatically generated, dynamically evaluated and holistically optimized. The entire approach is digitized and flexibly designed to best handle and protect future multivariable grid structures and fault situations. All tools are executed sequentially, resulting in a continuous workflow.
Connecting element is the object-oriented, generic data model GDM, which was developed especially for the processing of primary and secondary power grid and simulation data. It is a CIM-based data management system, independent of proprietary programs, which combines data from different sources, validates them and makes them available for further processing. The GDM enables automated data exchange within the ProToc and the execution of various analysis, evaluation and protection calculation functions. The main focus is on a high compatibility with simulation programs in order to be able to execute numerous fault simulations in parallel, to read in result data and to evaluate them afterwards. Due to the structural separation and detailed description of the protective device, protection function and protection setting objects, it forms the basis for the optimization.

More advanced, adapted and hybrid PSO methods are proposed as optimization techniques. PSO is a population based metaheuristic, which belongs to the fields of SI and EC. The hybrid versions additionally add elements from the fields of EA and DE to improve the search behavior and thus achieve faster and more accurate results. By using these methods, it is possible to handle diverse, variable and highly complex problems without having to adapt the optimization algorithm in detail, anew and specifically each time. Therefore, protection coordination can be optimized regardless of the power system state, topology, and protection system design. This also means that distance and overcurrent protection functions can be coordinated together, detached from traditional setting rules. Individual activation or deactivation of protection functions for individual or all protective devices is also made possible by the use of the newly introduced binary PSO variants. To compare all optimization methods described and to review their suitability, a benchmark test was performed with various test functions proposed. In the process, the maximum available number of FES was varied. The test showed that with a maximum number of 3E3 FES, the $EPSO_{DE}$2-4 method yields the best results on average. However, when optimizing the pure binary OneMax test function, the $BPSO_{DE}$-4 method proved to be better. At a maximum specification of 3E4 FES, $BPSO_{DE}$-4 unerringly delivered the best results. For 3E5 FES, the $BPSO_{DE}$2-1 method performed best. Finally, the $BPSO_{DE}$-4 method emerges as the overall winner, which performed best on average across all test functions

and available FES. However, not only the optimization but also the evaluation method used has a significant impact on the feasibility and efficiency of the ProToc.

In recent years, DSA has made a name for itself in the field of evaluating the dynamic stability of power systems, and PSA has become well-known in the field of evaluating protection security based on selectivity. However, both methods have deficiencies in considering and evaluating protection responses and the resulting impact on power systems.
Therefore, a modified PSA system was developed to generate a coherent overall assessment value and adequately guide an optimization method, leading to improved and correct protection settings. The approach envisages that the performance of a protection system is no longer determined solely by selectivity behavior. Instead, a whole-system perspective is taken, and the behavior of the protection system is evaluated according to how well it contributes to securing and maintaining the overall system stability and the reliability of supply. This is based on dynamic RMS simulations in which time-delayed, unselective and cascading protection system behavior is reflected quantitatively and qualitatively accordingly. Thus, the gap between protection analyses and dynamic stability considerations is bridged. The new stability indices evaluate the course of voltages, frequencies and angles with the simple but consistent and coherent WE evaluation method. This uses different rectangular time windows to extract specific features from a signal under analysis and is thus similar in its approach to the wavelet transform and the short-time Fourier transform. The WE allows the evaluation of all primary and secondary system responses to a fault and the resulting impact on stability. In addition, the reliability of the supply is determined based on the criteria load loss, grid loading and fault current. Finally, the new indices, together with the evaluation of the selectivity behavior, form the FV and allow an optimization method to efficiently advance, make tradeoffs, and identify unconventional solutions.

The performance as well as advantages and disadvantages of an automatically generated protection coordination are demonstrated by numerous investigations on a distribution and transmission system. Various topological states ranging from simple stubs and rings to a highly meshed structures are investigated. The results obtained are analyzed and compared in accordance with the conditions and specifications present in each case. They prove that a system consisting of a suitable assessment methodology and optimization methods is capable of parameterizing distance and overcurrent protection functions jointly and in a coordinated manner.
The advantages are that the system can be used regardless of the grid type

and topology. Individual or even all protective devices, protective functions or setting values can be coordinated flexibly at the same time, and the best compromise is determined automatically. Even when coordinating unconventional structures, where the application of traditional setting rules fails, the system is able to achieve a usable result and generate applicable protection settings. It can therefore be seen as a pioneer of the widely discussed dynamic meshing approaches to protect multivariable grid structures in the future. The disadvantage are that the optimized result is strongly tailored to the underlying structure and load flow situation. In addition, a dynamic power system model is required, which should be as detailed as possible and correspond to real conditions. Furthermore, an optimization run involves a large number of simulations, so appropriate computing power is required. Since it is not known in advance what the best possible result will be, a maximum number of FES must be defined in advance. If this number is too low, the optimization process may not complete sufficiently well in the end. If the chosen number is too high, the computational effort will increase unnecessarily. As with all metaheuristics, there is the disadvantage that each optimization run leads to new, changed values due to the stochastic elements used. The results may have the same quality and lead to the same protection security, but the setting values may differ. This can be limited by defining appropriately tighter limits for each setting value in the search process. The narrower the limits, the simpler the optimization process and the more similar the results. Larger search spaces, in contrast, give the optimization method more freedom to identify unconventional solutions. This can lead to new possibilities and efficient strategies. However, less feasible solutions are also possible. Therefore, a precise control of the optimization process is always necessary. In perspective, further evaluation and penalty functions can be added. A final manual review of the setting values for plausibility and applicability is still necessary with the state of the system described in this work.

Finally, to demonstrate the realistic applicability of the ProToc, protection tests were performed with 7SX85 universal protection devices in a real-time laboratory. The optimized protection settings proved to meet the requirements for accuracy, applicability and plausibility. The results validate the assumptions and statements on the usability of automatically generated protection concepts. Even transient effects such as impedance trajectories that already move in elliptical paths during a fault, which can lead to unselective tripping, are confirmed.

Unquestionably, the ProToc as well as the fully automated generation and optimization of protection concepts and setting values is still in its early stages and

part of current research. In perspective, however, the system offers numerous possibilities and advantages to meet upcoming challenges.
For example, further development of the system in terms of parameterization for detection and disconnection of additional fault types such as single-phase and two-phase faults with and without ground contact, double faults, etc. is advisable. Also an extension for parameterization of the R-range of the distance protection function including earth faults would be useful. Moreover, other protection functions could be added and optimized in the same way. An essential addition would be the simultaneous consideration of different states of the power systems. In this way, optimized setting values could be used equally for all states. However, this would require that all states are simulated and assessed one after the other during the optimization process and combined into a common return value. In this sense, it would be necessary to investigate how many and which system states should be covered simultaneously by a single protection coordination and how they should be weighted among each other. The optimization would then be able to determine the best compromise for all system states.
Further validation and fine-tuning based on intensive testing with other power system models, including boundary conditions, special features and individual challenges is desired. This would also be a basic prerequisite for the ProToc to be able and gain the necessary confidence in the future to determine protection setting values that can be applied directly to devices in the field without further testing. As soon as this technical level is reached, an online variant would also be conceivable that permanently and routinely reviews the protection system and optimally adapts it to newly occurring conditions as required.
Beyond that, it is possible to use the setup of the ProToc for training machine learning algorithms. Already in [P138] and [P139] this was done to generate training data for an Artificial Neural Network. Its task was to determine the exact location of a fault using measurement data from distributed measurement stations in the power system. This could be a solution, especially in view of the advancing cabling and the negative influence on measurement accuracy of the distance protection function. In general, the approach could be extended to a variety of use cases, as long as they can be simulated.

Appendix

A Result Graphs and Data of the Optimization of the Test Functions

A.1 Shifted Sphere's Function

The following are the optimization results of all PSO variants for the shifted Sphere's function.

Table 19: Average FV at 25 runs after 3E3, 3E4 and 3E5 FES at shifted Sphere's function.

3E3 FES		3E4 FES		3E5 FES	
Method	FV	Method	FV	Method	FV
$EPSO_{DE}2$-4	3,998	EPSO-4	1.004	$EBPSO_{DE}$-1	1
$EPSO_{DE}2$-3	4,806	EPSO-3	1.005	$EBPSO_{DE}$-2	1
$EPSO_{DE}2$-2	4,858	EPSO-2	1.02	$EBPSO_{DE}$-3	1
$EPSO_{DE}2$-1	5,408	$BPSO_{DE}$-4	1.69	$EBPSO_{DE}$-4	1
$EPSO_{DE}$-4	5,694	$BPSO_{DE}2$-4	2.27	$EBPSO_{DE}2$-1	1
$EPSO_{DE}$-3	6,104	$BPSO_{DE}$-3	2.64	$EBPSO_{DE}2$-2	1
$EPSO_{DE}$-2	7,355	$BPSO_{DE}2$-3	4.11	$EBPSO_{DE}2$-3	1
EPSO-4	8,562	$BPSO_{DE}$-2	4.22	$EBPSO_{DE}2$-4	1
EPSO-3	8,723	EPSO-1	9.79	$BPSO_{DE}$-1	1
EPSO-2	12,057	$EPSO_{DE}2$-2	11.78	$BPSO_{DE}$-2	1
$BPSO_{DE}$-4	14,378	$EBPSO_{DE}$-4	18.61	$BPSO_{DE}$-3	1
DEEPSO-1	15,266	$EPSO_{DE}2$-3	21.30	$BPSO_{DE}$-4	1
$BPSO_{DE}2$-4	15,950	$BPSO_{DE}2$-2	21.71	$BPSO_{DE}2$-1	1
DEEPSO-4	16,1301	$BPSO_{DE}$-1	21.94	$BPSO_{DE}2$-2	1
$EPSO_{DE}$-1	16,259	$EBPSO_{DE}2$-4	27.34	$BPSO_{DE}2$-3	1
DEEPSO-3	16,539	$EBPSO_{DE}$-3	34.62	$BPSO_{DE}2$-4	1
$BPSO_{DE}$-3	16,843	$EPSO_{DE}2$-4	39.69	$EPSO_{DE}2$-1	1.0004
PSO-2	17,056	$EPSO_{DE}2$-1	47.87	EPSO-1	1.00044
BPSO-2	17,600	DEEPSO-4	49.06	EPSO-2	1.00084
DEEPSO-2	17,692	$EBPSO_{DE}2$-3	49.60	EPSO-3	1.00011
EPSO-1	18,912	DEEPSO-3	49.63	EPSO-4	1.0012
$BPSO_{DE}2$-3	24,758	$EBPSO_{DE}$-2	49.97	$EPSO_{DE}2$-2	1.01
$BPSO_{DE}$-2	25,580	$EPSO_{DE}$-1	51.63	$EPSO_{DE}$-1	1.17
$EBPSO_{DE}$-4	28,333	DEEPSO-2	81.32	$EPSO_{DE}2$-3	1.25
$EBPSO_{DE}2$-4	32,262	$EPSO_{DE}$-2	105.47	DEEPSO-3	2.70
$EBPSO_{DE}$-3	32,665	$EPSO_{DE}$-4	114.53	$EPSO_{DE}$-2	3.93
$EBPSO_{DE}$-2	39,915	$BPSO_{DE}2$-1	116.72	$EPSO_{DE}2$-4	3.95
$EBPSO_{DE}2$-3	42,275	DEEPSO-1	118.4	DEEPSO-4	5.99
PSO-1	47,119	$EPSO_{DE}$-3	130.1	DEEPSO-2	7.49
$BPSO_{DE}2$-2	48,904	$EBPSO_{DE}$-1	264.5	$EPSO_{DE}$-3	7.53
$BPSO_{DE}$-1	49,923	$EBPSO_{DE}2$-2	266.5	DEEPSO-1	13.83
$EBPSO_{DE}$-1	64,094	BPSO-2	694.6	BPSO-2	15.40
$EBPSO_{DE}2$-2	67,434	$EBPSO_{DE}2$-1	877.7	$EPSO_{DE}$-4	16.88
$BPSO_{DE}2$-1	67,493	PSO-2	10,762	PSO-2	6,015
$EBPSO_{DE}2$-1	81,034	PSO-1	12,045	PSO-1	17,243
BPSO-1	1.23E5	BPSO-1	91,713	BPSO-1	61,210

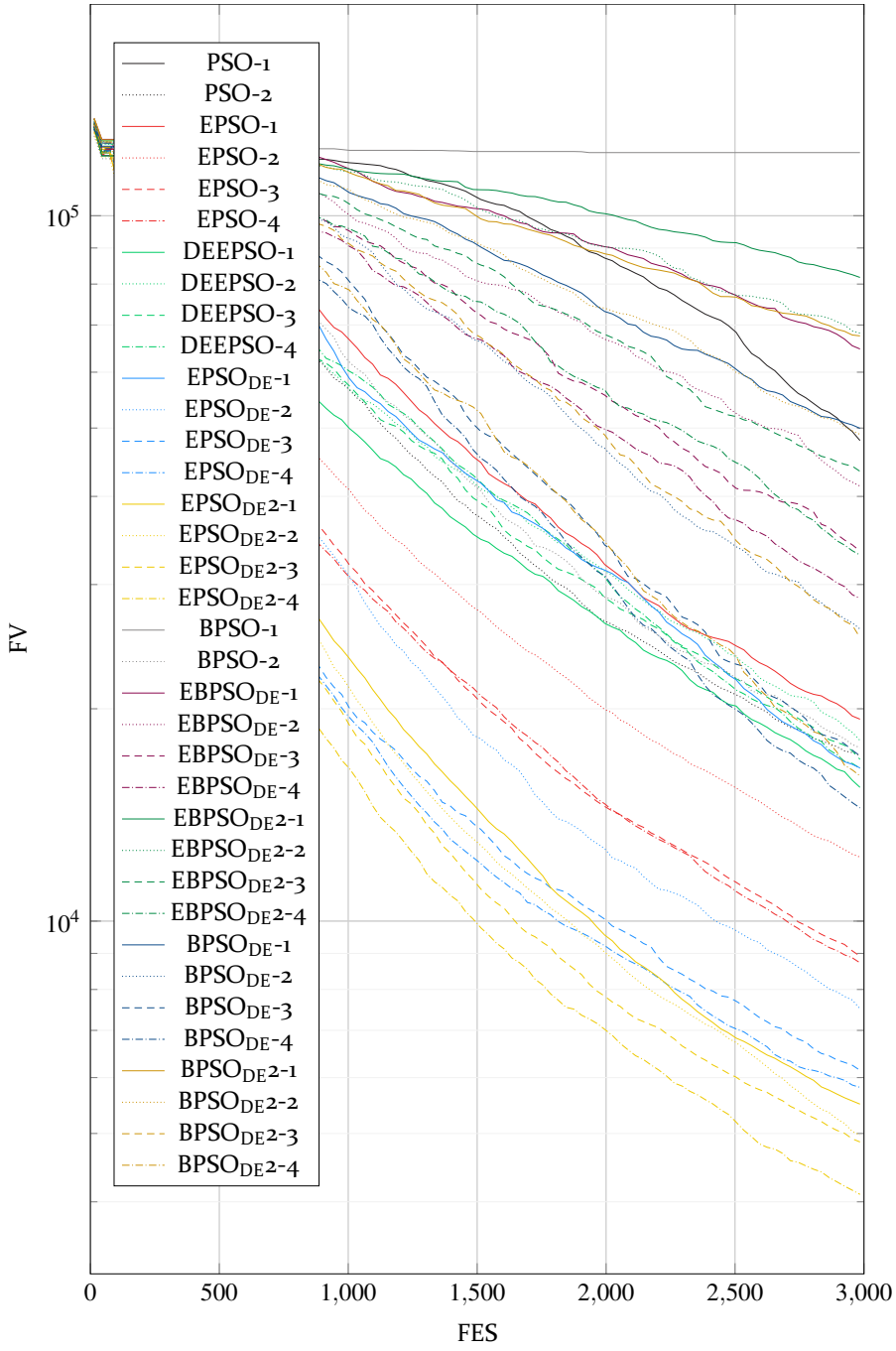

Figure 88: Result graph of the optimization of the shifted Sphere's function with a maximum number of 3E3 FES.

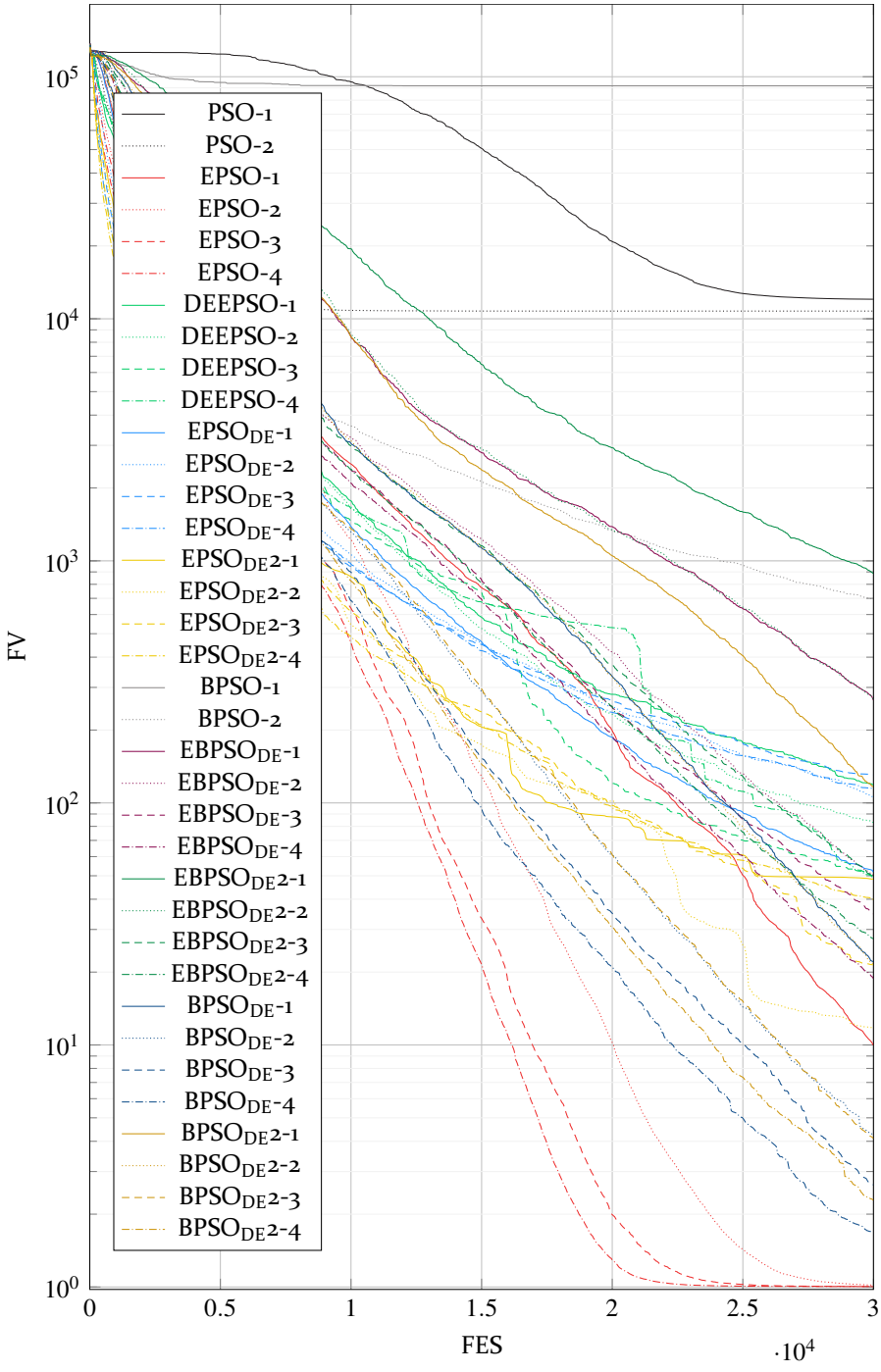

Figure 89: Result graph of the optimization of the shifted Sphere's function with a maximum number of 3E4 FES.

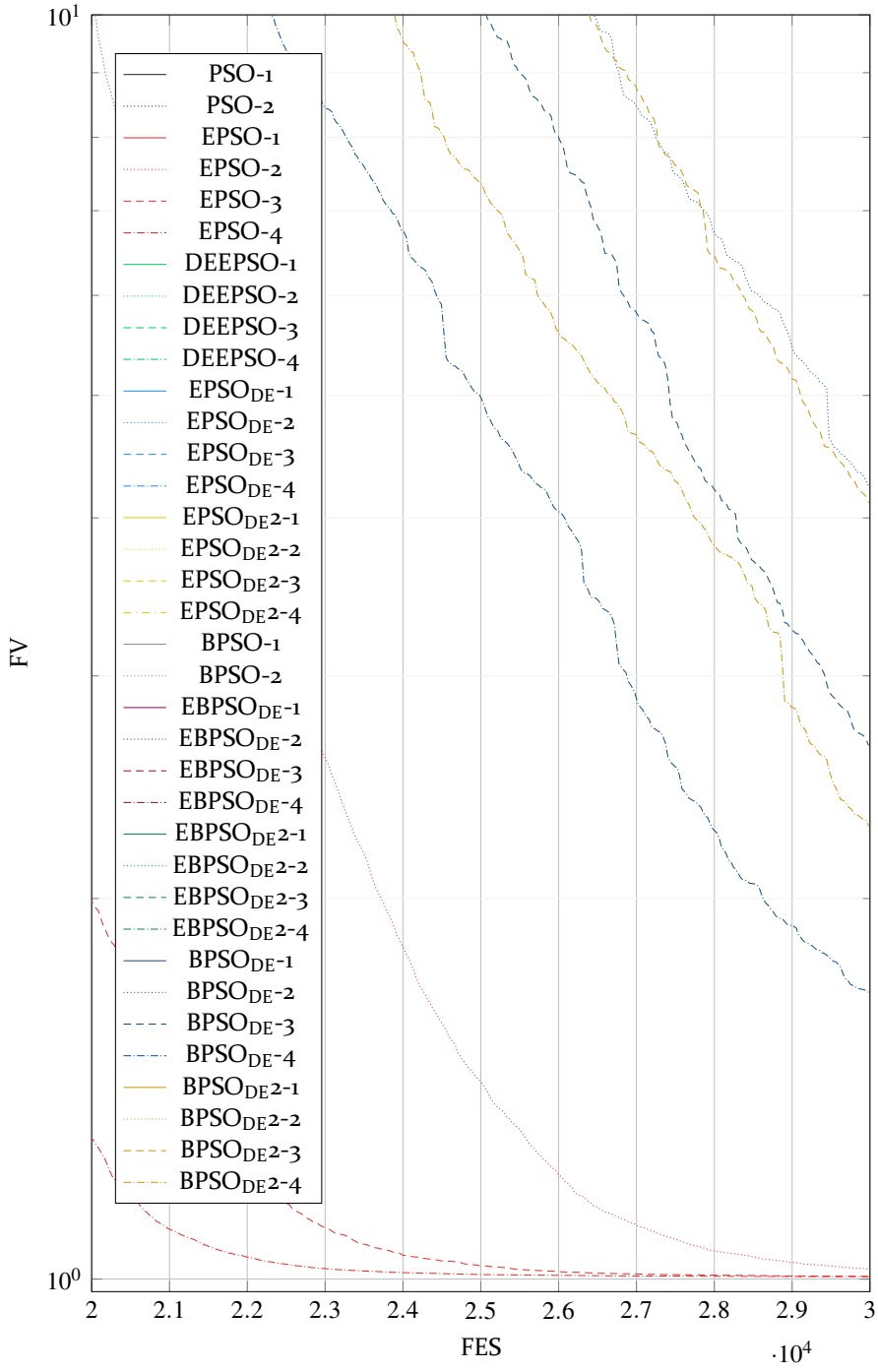

Figure 90: Zoomed partial section of the result graph of the optimization of the shifted Sphere's function with a maximum number of 3E4 FES.

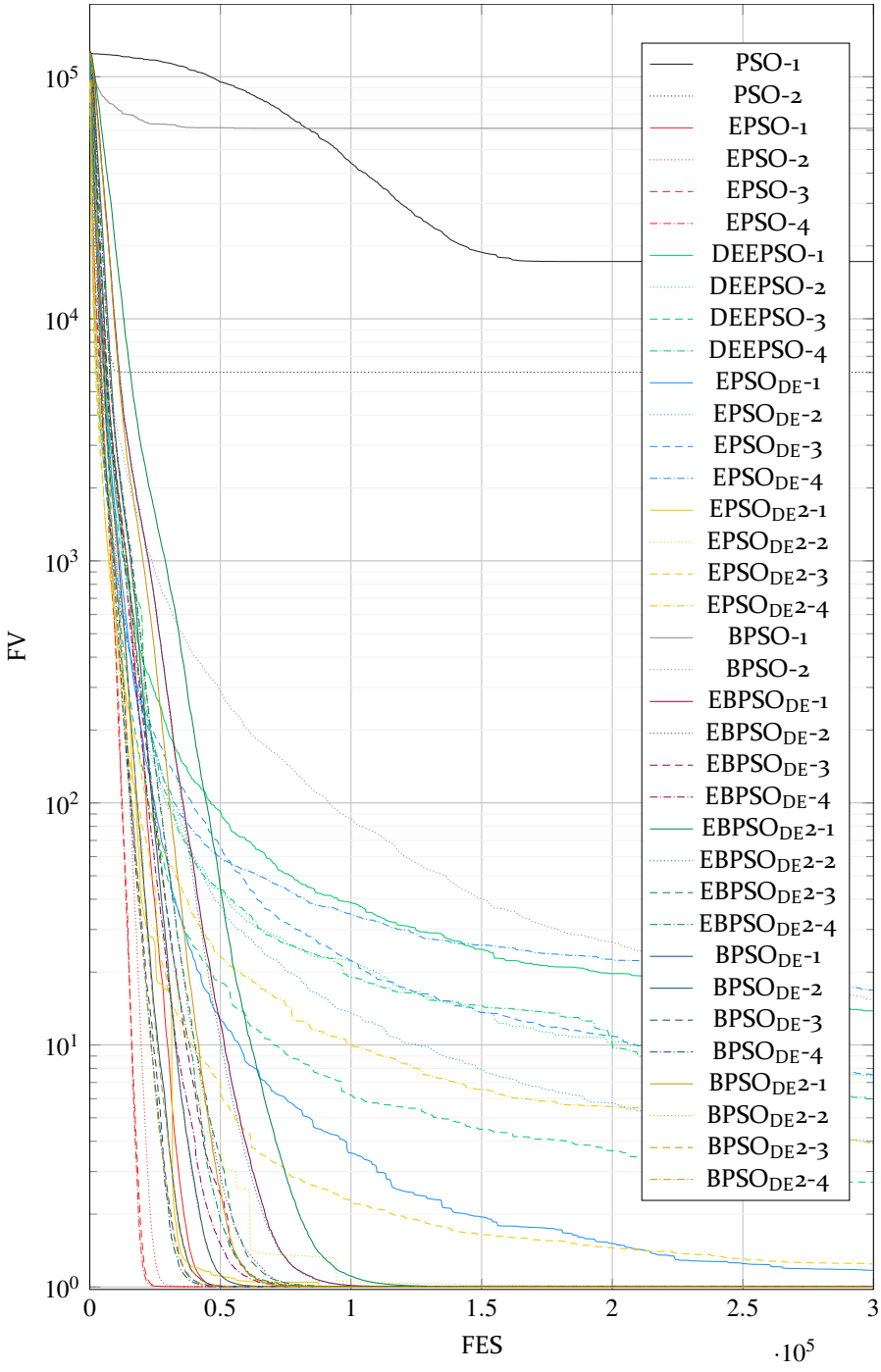

Figure 91: Result graph of the optimization of the shifted Sphere's function with a maximum number of 3E5 FES.

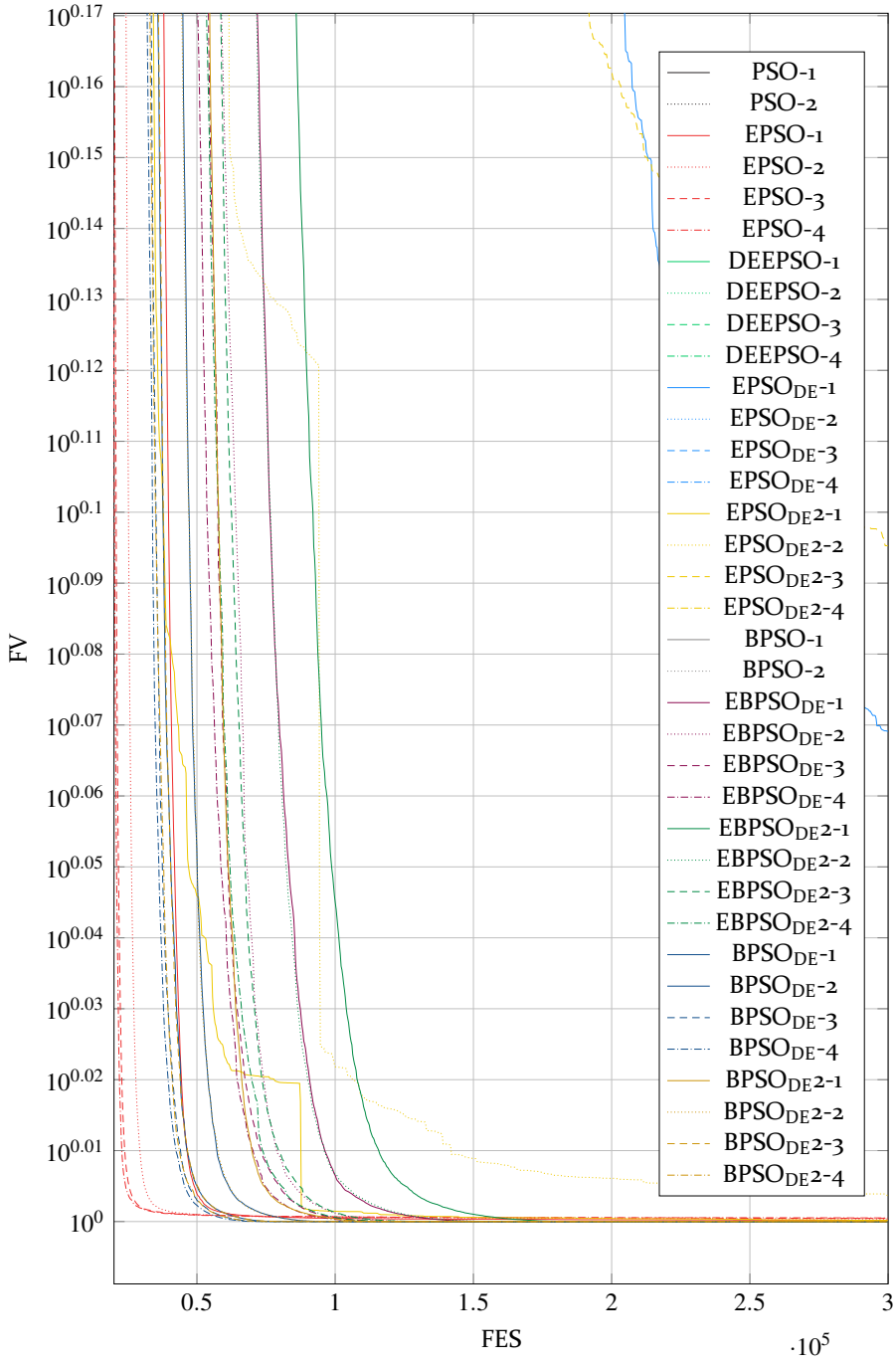

Figure 92: Zoomed partial section of the result graph of the optimization of the shifted Sphere's function with a maximum number of 3E5 FES.

A.2 Shifted Rosenbrock's Function

The following are the optimization results of all PSO variants for the shifted Rosenbrock's function.

Table 20: Average FV at 25 runs after 3E3, 3E4 and 3E5 FES at shifted Rosenbrock's function.

3E3 FES		3E4 FES		3E5 FES	
Method	FV	Method	FV	Method	FV
$EPSO_{DE}$2-2	2.32E6	EPSO-3	147.6	$BPSO_{DE}$2-1	28.3
$EPSO_{DE}$2-1	3.30E6	$EPSO_{DE}$2-1	177.2	$EBPSO_{DE}$2-1	58.8
EPSO-4	5.66E6	EPSO-4	209.5	EPSO-1	87.1
$EPSO_{DE}$2-3	5.75E6	EPSO-2	223.5	EPSO-4	89.8
$EPSO_{DE}$2-4	7.78E6	$EPSO_{DE}$2-2	356.4	$BPSO_{DE}$-1	94.4
EPSO-3	1.61E7	EPSO-1	467.2	$BPSO_{DE}$2-2	95.7
PSO-2	1.89E7	$EPSO_{DE}$2-3	1,123	DEEPSO-1	107.5
$EPSO_{DE}$-4	2.74E7	$BPSO_{DE}$-1	1,583	$EPSO_{DE}$2-2	114.8
$EPSO_{DE}$-3	3.32E7	$BPSO_{DE}$-2	1,743	EPSO-2	116.6
EPSO-2	3.50E7	$BPSO_{DE}$2-2	1,750	$EPSO_{DE}$-1	117.4
DEEPSO-4	4.47E7	$BPSO_{DE}$2-3	1,757	DEEPSO-4	122.2
$EPSO_{DE}$-2	5.10E7	$EPSO_{DE}$-1	1,861	EPSO-3	131.6
DEEPSO-3	7.10E7	$EPSO_{DE}$2-4	2,068	DEEPSO-3	132.0
DEEPSO-2	1.18E8	$BPSO_{DE}$-4	2,278	DEEPSO-2	139.2
DEEPSO-1	1.94E8	$BPSO_{DE}$2-4	2,480	$EPSO_{DE}$2-3	159.0
EPSO-1	3.26E8	$EBPSO_{DE}$-4	3,118	$EPSO_{DE}$2-4	161.4
BPSO-2	3.33E8	$EBPSO_{DE}$-3	3,766	$EPSO_{DE}$-2	164.9
$EPSO_{DE}$-1	3.57E8	$BPSO_{DE}$-3	3,799	$EPSO_{DE}$2-1	206.4
$BPSO_{DE}$-4	5.14E8	DEEPSO-4	4,013	$EPSO_{DE}$-3	207.0
$BPSO_{DE}$-3	6.41E8	$EPSO_{DE}$-3	4,641	$EPSO_{DE}$-4	383.8
$BPSO_{DE}$2-4	7.24E8	$EBPSO_{DE}$2-4	4,876	$EBPSO_{DE}$2-2	394.8
$BPSO_{DE}$-2	1.22E9	$EPSO_{DE}$-2	5,039	$BPSO_{DE}$-4	488.7
$BPSO_{DE}$2-3	1.33E9	$EBPSO_{DE}$2-3	5,503	$BPSO_{DE}$-3	554.0
PSO-1	1.36E9	DEEPSO-3	5,766	$BPSO_{DE}$-2	599.8
$EBPSO_{DE}$2-4	2.15E9	$EPSO_{DE}$-4	6,432	$EBPSO_{DE}$-1	788.1
$EBPSO_{DE}$-4	2.20E9	$EBPSO_{DE}$-2	8,082	$EBPSO_{DE}$2-3	841.0
$EBPSO_{DE}$-3	2.41E9	BPSO-2	10,295	$BPSO_{DE}$2-4	865.7
$EBPSO_{DE}$-2	3.41E9	$BPSO_{DE}$2-1	12,114	$EBPSO_{DE}$-4	981.1
$BPSO_{DE}$2-2	3.42E9	DEEPSO-2	16,090	$BPSO_{DE}$2-3	1,060
$EBPSO_{DE}$2-3	3.47E9	DEEPSO-1	37,368	$EBPSO_{DE}$-2	1,130
$BPSO_{DE}$-1	4.00E9	$EBPSO_{DE}$-1	69,272	$EBPSO_{DE}$-3	1,205
$BPSO_{DE}$2-1	5.83E9	$EBPSO_{DE}$2-2	79,167	BPSO-2	1,221
$EBPSO_{DE}$-1	6.50E9	PSO-2	2.46E5	$EBPSO_{DE}$2-4	1,314
$EBPSO_{DE}$2-2	7.46E9	$EBPSO_{DE}$2-1	7.41E5	PSO-2	2.46E5
$EBPSO_{DE}$2-1	1.16E10	PSO-1	7.41E9	PSO-1	3.69E5
BPSO-1	2.57E10	BPSO-1	1.20E10	BPSO-1	2.32E9

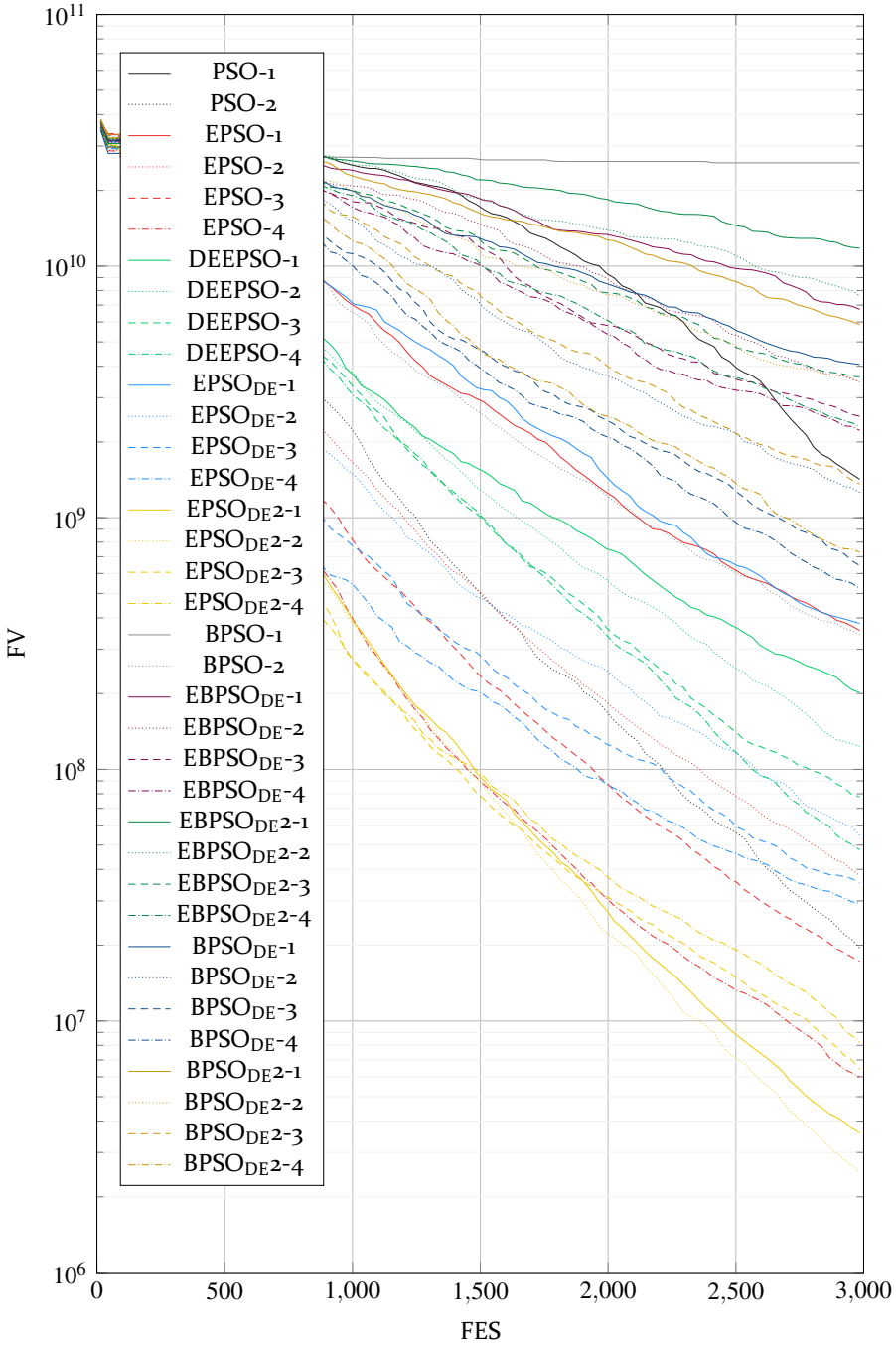

Figure 93: Result graph of the optimization of the shifted Rosenbrock's function with a maximum number of 3E3 FES.

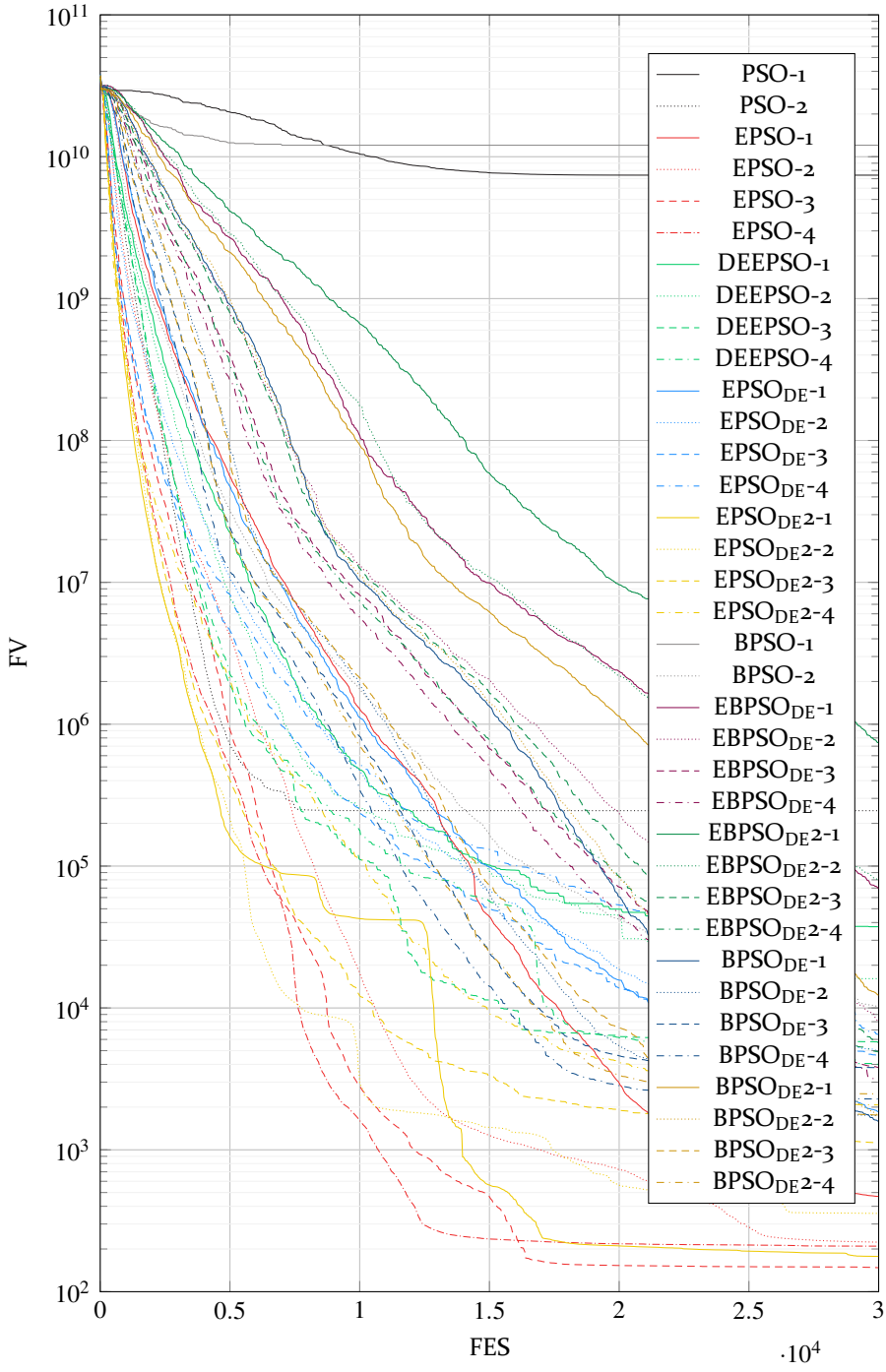

Figure 94: Result graph of the optimization of the shifted Rosenbrock's function with a maximum number of 3E4 FES.

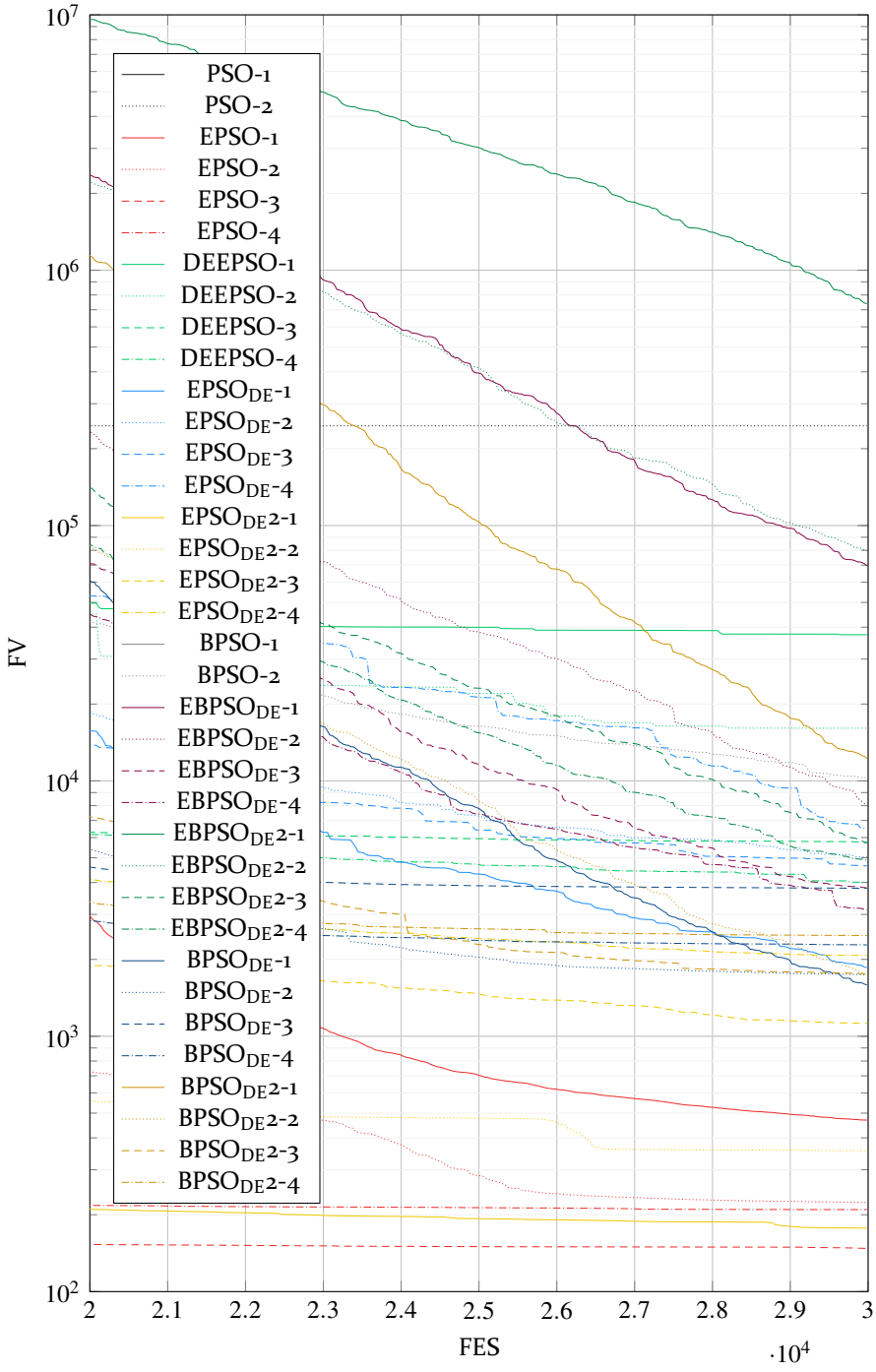

Figure 95: Zoomed partial section of the result graph of the optimization of the shifted Rosenbrock's function with a maximum number of 3E4 FES.

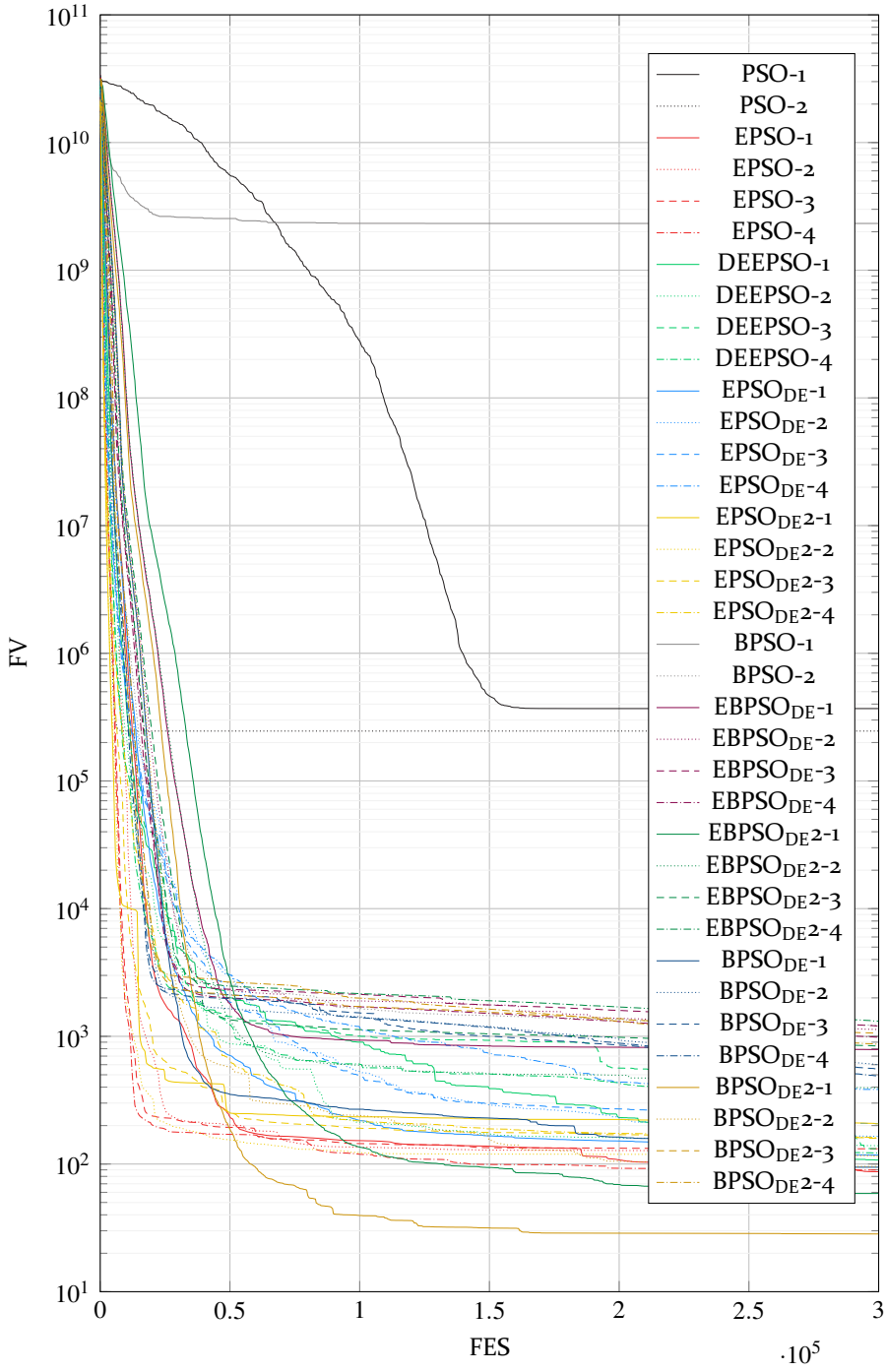

Figure 96: Result graph of the optimization of the shifted Rosenbrock's function with a maximum number of 3E5 FES.

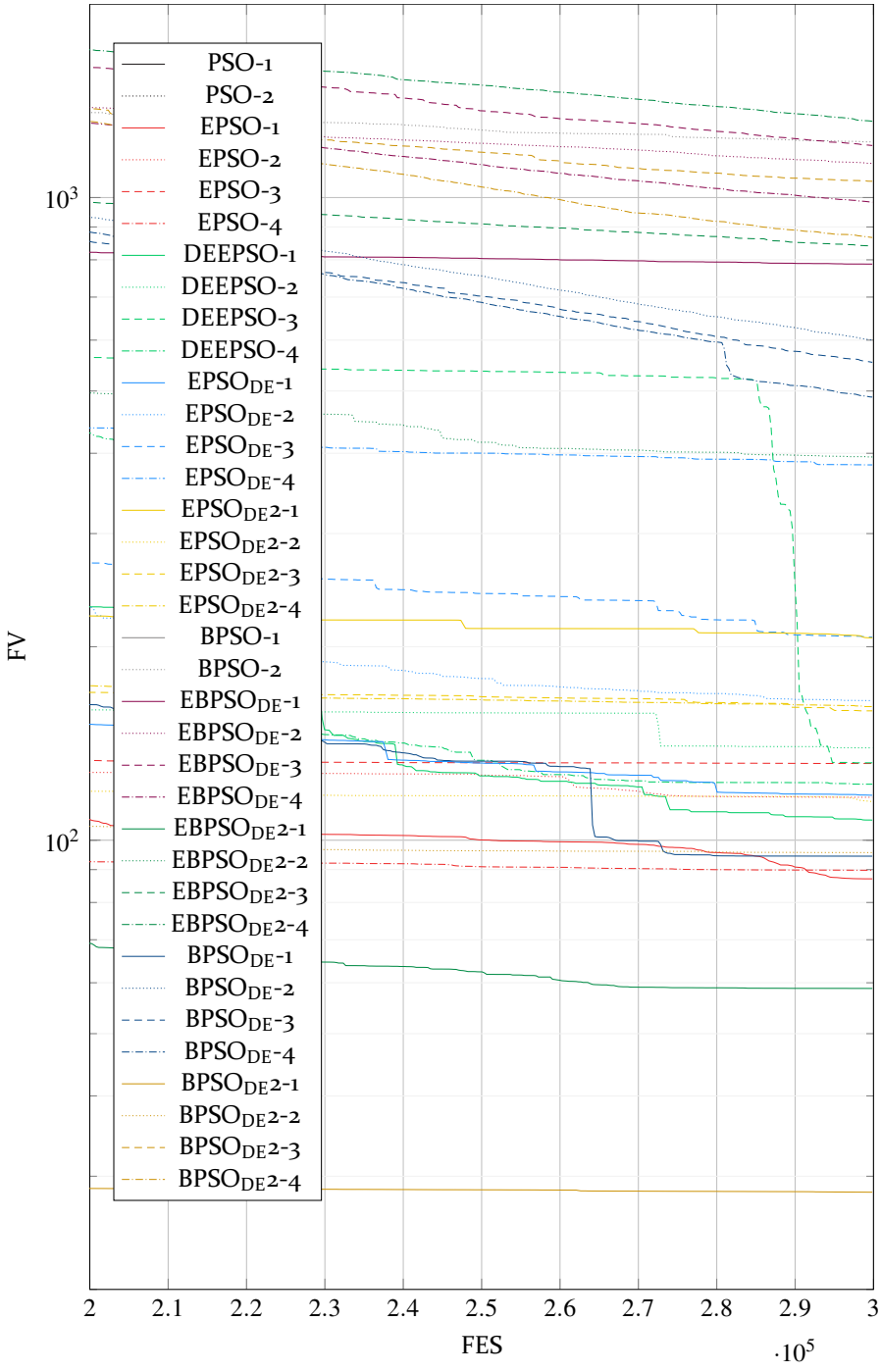

Figure 97: Zoomed partial section of the result graph of the optimization of the shifted Rosenbrock's function with a maximum number of 3E5 FES.

A.3 Shifted Griewank's Function

The following are the optimization results of all PSO variants for the shifted Griewank's function.

Table 21: Average FV at 25 runs after 3E3, 3E4 and 3E5 FES at shifted Griewank's function.

3E3 FES		3E4 FES		3E5 FES	
Method	FV	Method	FV	Method	FV
$EPSO_{DE}2$-4	4.65	$BPSO_{DE}$-3	1.021	$EBPSO_{DE}2$-1	1
$EPSO_{DE}2$-3	4.78	$BPSO_{DE}$-4	1.023	$BPSO_{DE}$-1	1
$EPSO_{DE}$-4	8.45	EPSO-4	1.023	$BPSO_{DE}2$-1	1
BPSO-2	8.87	$BPSO_{DE}2$-4	1.024	$BPSO_{DE}2$-2	1
DEEPSO-1	9.04	EPSO-3	1.024	$EBPSO_{DE}2$-2	1.0005
DEEPSO-2	9.44	EPSO-1	1.031	$EBPSO_{DE}$-1	1.0013
$BPSO_{DE}$-4	9.48	EPSO-2	1.034	$EPSO_{DE}$-1	1.0018
DEEPSO-3	9.67	$BPSO_{DE}2$-3	1.057	$BPSO_{DE}2$-4	1.0039
$BPSO_{DE}$-3	10.05	$BPSO_{DE}$-2	1.057	$BPSO_{DE}$-2	1.0046
$BPSO_{DE}2$-4	10.34	DEEPSO-2	1.075	$EBPSO_{DE}$-3	1.0049
$EPSO_{DE}$-3	10.38	DEEPSO-4	1.122	$EBPSO_{DE}$-2	1.0051
EPSO-3	11.53	DEEPSO-3	1.144	$BPSO_{DE}$-4	1.0067
EPSO-2	11.68	$EBPSO_{DE}$-4	1.164	$BPSO_{DE}2$-3	1.0073
$BPSO_{DE}$-2	12.12	$BPSO_{DE}$-1	1.179	$EBPSO_{DE}2$-4	1.0096
$EPSO_{DE}2$-2	12.22	$EPSO_{DE}2$-4	1.186	$BPSO_{DE}$-3	1.0104
$BPSO_{DE}2$-3	12.34	$BPSO_{DE}2$-2	1.188	$EBPSO_{DE}2$-3	1.0108
DEEPSO-4	13.28	$EPSO_{DE}2$-3	1.192	DEEPSO-4	1.0145
EPSO-4	13.52	$EBPSO_{DE}2$-4	1.207	DEEPSO-1	1.0165
$EPSO_{DE}2$-1	14.00	$EBPSO_{DE}$-3	1.217	EPSO-4	1.0179
$EPSO_{DE}$-2	15.27	$EPSO_{DE}$-1	1.262	EPSO-3	1.0185
$EBPSO_{DE}$-4	15.71	DEEPSO-1	1.270	DEEPSO-2	1.0187
$EBPSO_{DE}$-3	16.57	$EPSO_{DE}$-3	1.385	$EBPSO_{DE}$-4	1.0194
$EBPSO_{DE}2$-4	17.48	$EBPSO_{DE}$-2	1.401	$EPSO_{DE}$-2	1.0200
EPSO-1	17.89	$EPSO_{DE}$-2	1.420	EPSO-1	1.0202
$EBPSO_{DE}$-2	24.13	$EPSO_{DE}$-4	1.427	$EPSO_{DE}2$-4	1.0229
$EBPSO_{DE}2$-3	25.10	$EBPSO_{DE}2$-3	1.432	EPSO-2	1.0243
$BPSO_{DE}$-1	27.72	$BPSO_{DE}2$-1	1.555	DEEPSO-3	1.0252
$BPSO_{DE}2$-2	27.97	BPSO-2	1.857	BPSO-2	1.0274
$EPSO_{DE}$-1	40.41	$EBPSO_{DE}2$-2	1.900	$EPSO_{DE}$-3	1.0366
$BPSO_{DE}2$-1	55.83	$EBPSO_{DE}$-1	1.927	$EPSO_{DE}2$-2	1.0377
PSO-2	59.20	$EBPSO_{DE}2$-1	2.093	$EPSO_{DE}$-4	1.0380
PSO-1	60.30	$EPSO_{DE}2$-2	3.679	$EPSO_{DE}2$-3	1.0568
$EBPSO_{DE}2$-2	68.84	$EPSO_{DE}2$-1	4.962	$EPSO_{DE}2$-1	1.0628
$EBPSO_{DE}$-1	68.93	BPSO-1	58.74	BPSO-1	17.62
$EBPSO_{DE}2$-1	101.6	PSO-2	68.20	PSO-2	59.30
BPSO-1	162.9	PSO-1	73.60	PSO-1	61.90

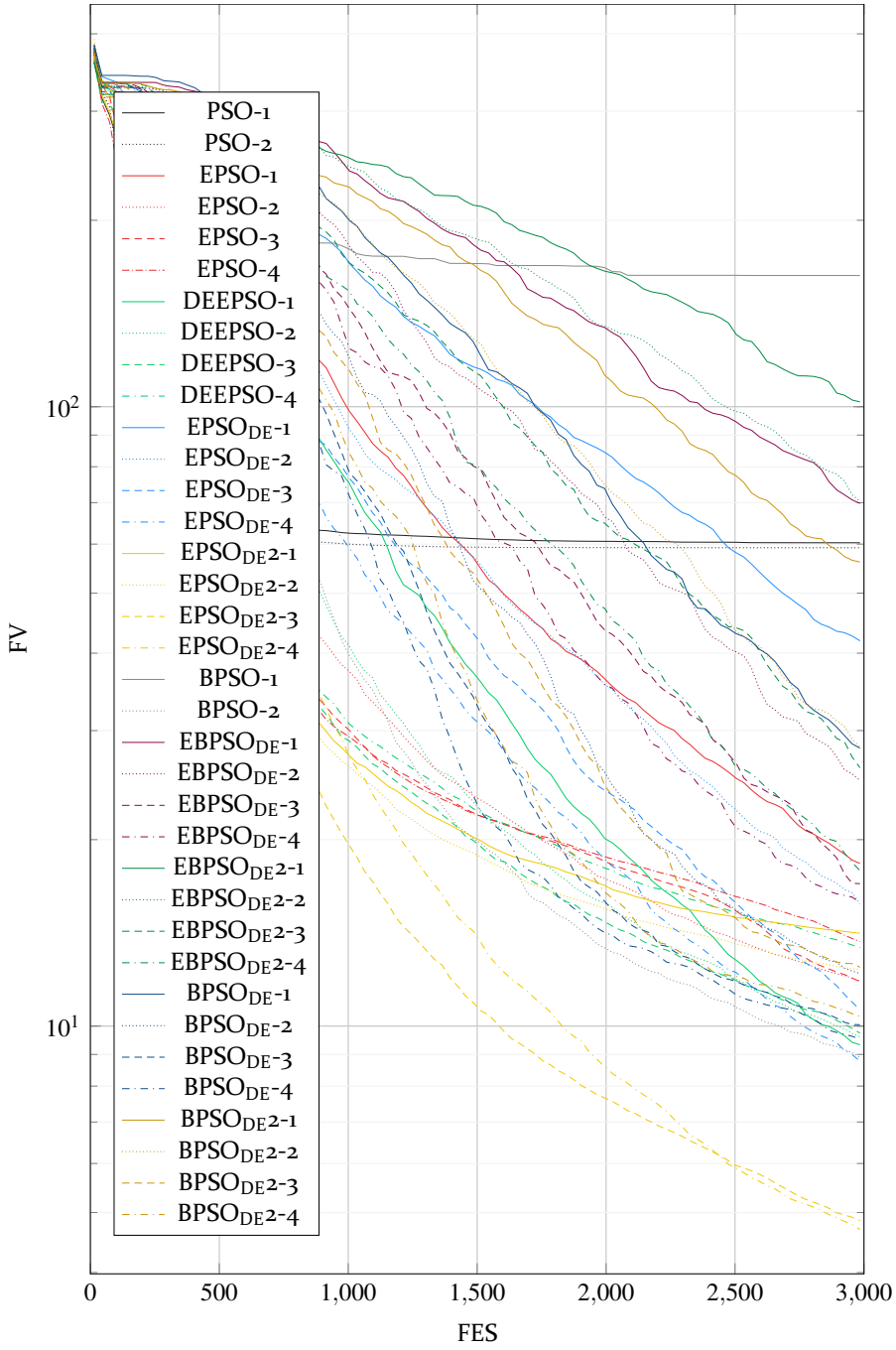

Figure 98: Result graph of the optimization of the shifted Griewank's function with a maximum number of 3E3 FES.

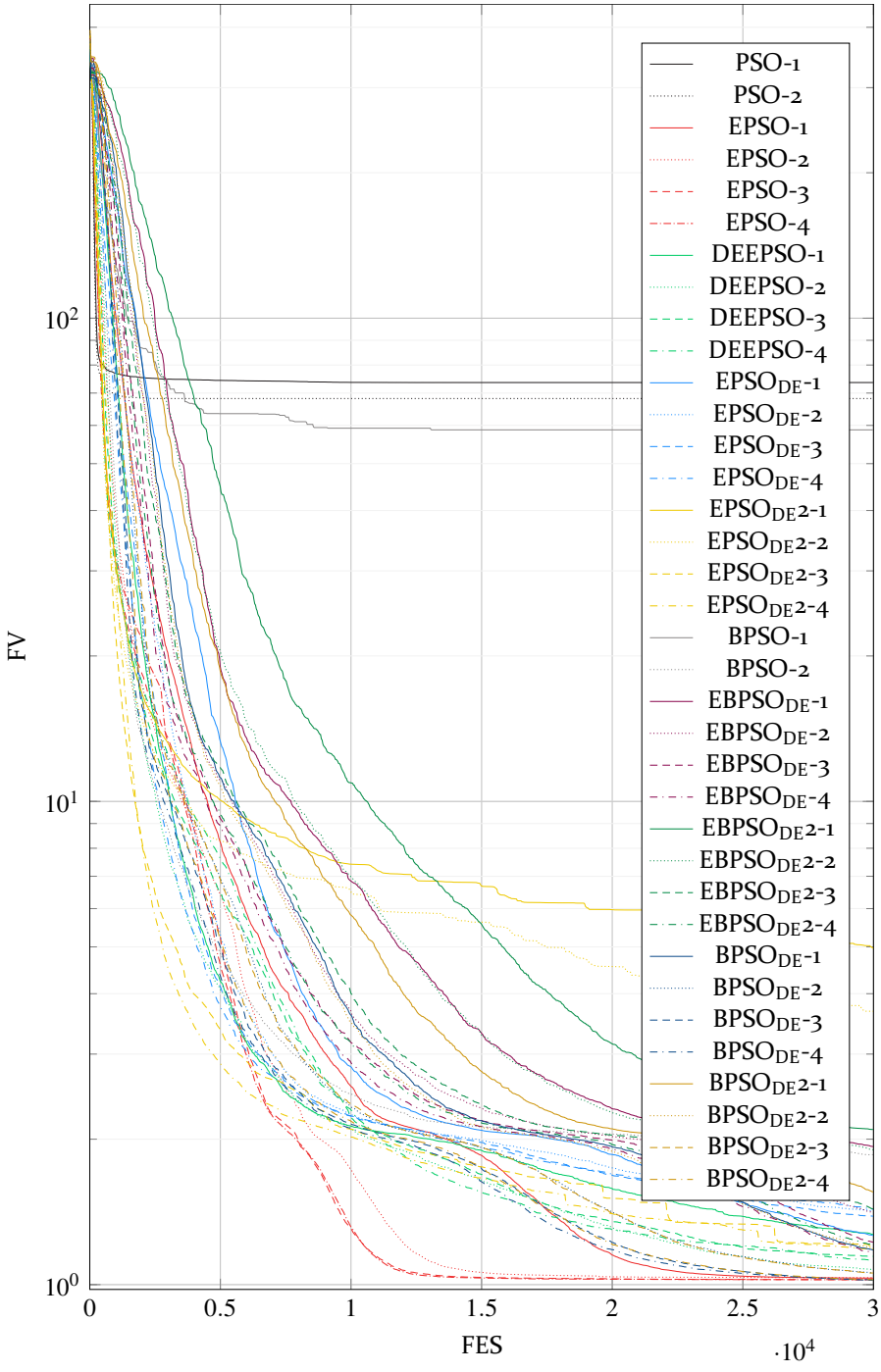

Figure 99: Result graph of the optimization of the shifted Griewank's function with a maximum number of 3E4 FES.

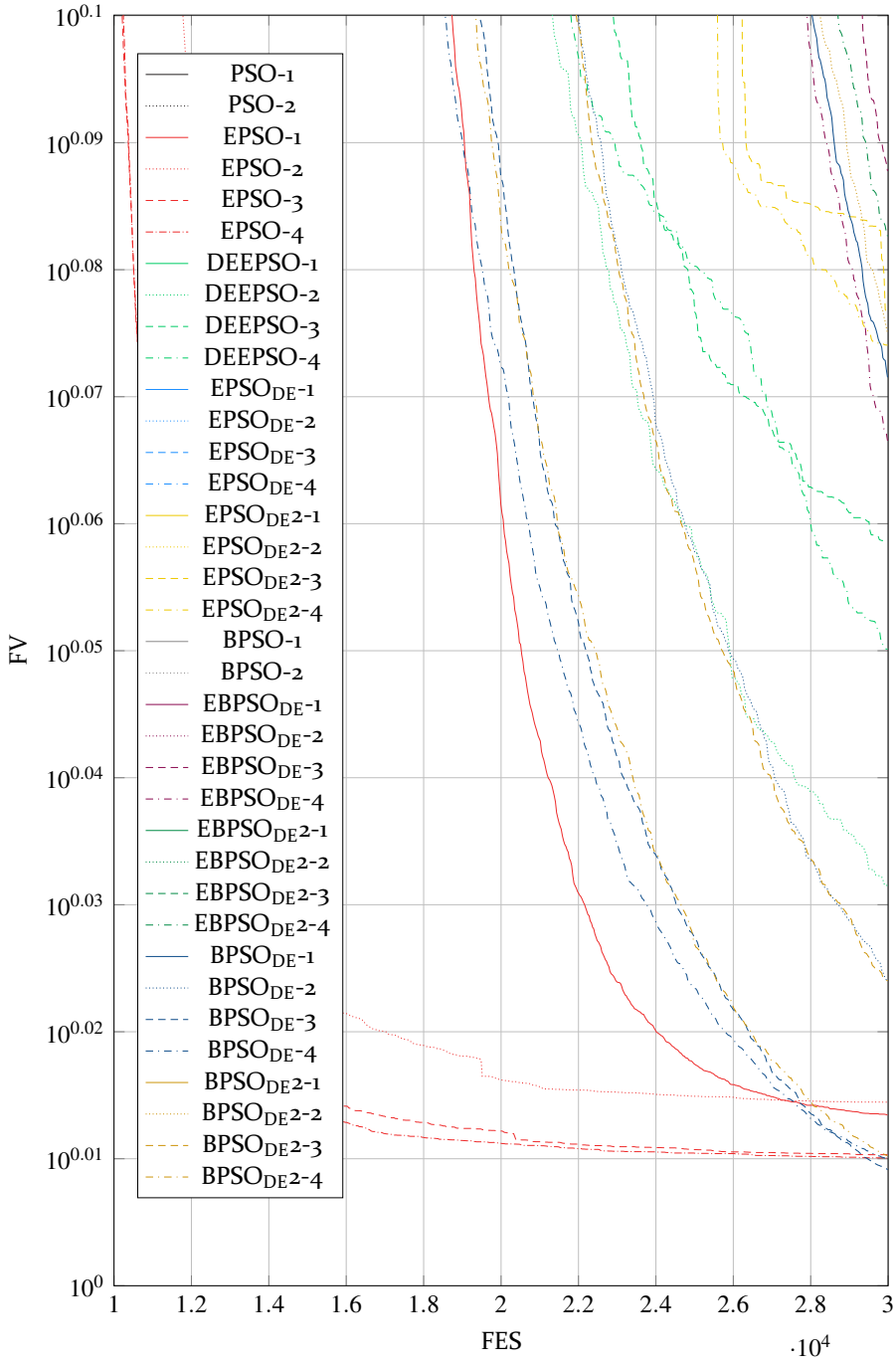

Figure 100: Zoomed partial section of the result graph of the optimization of the shifted Griewank's function with a maximum number of 3E4 FES.

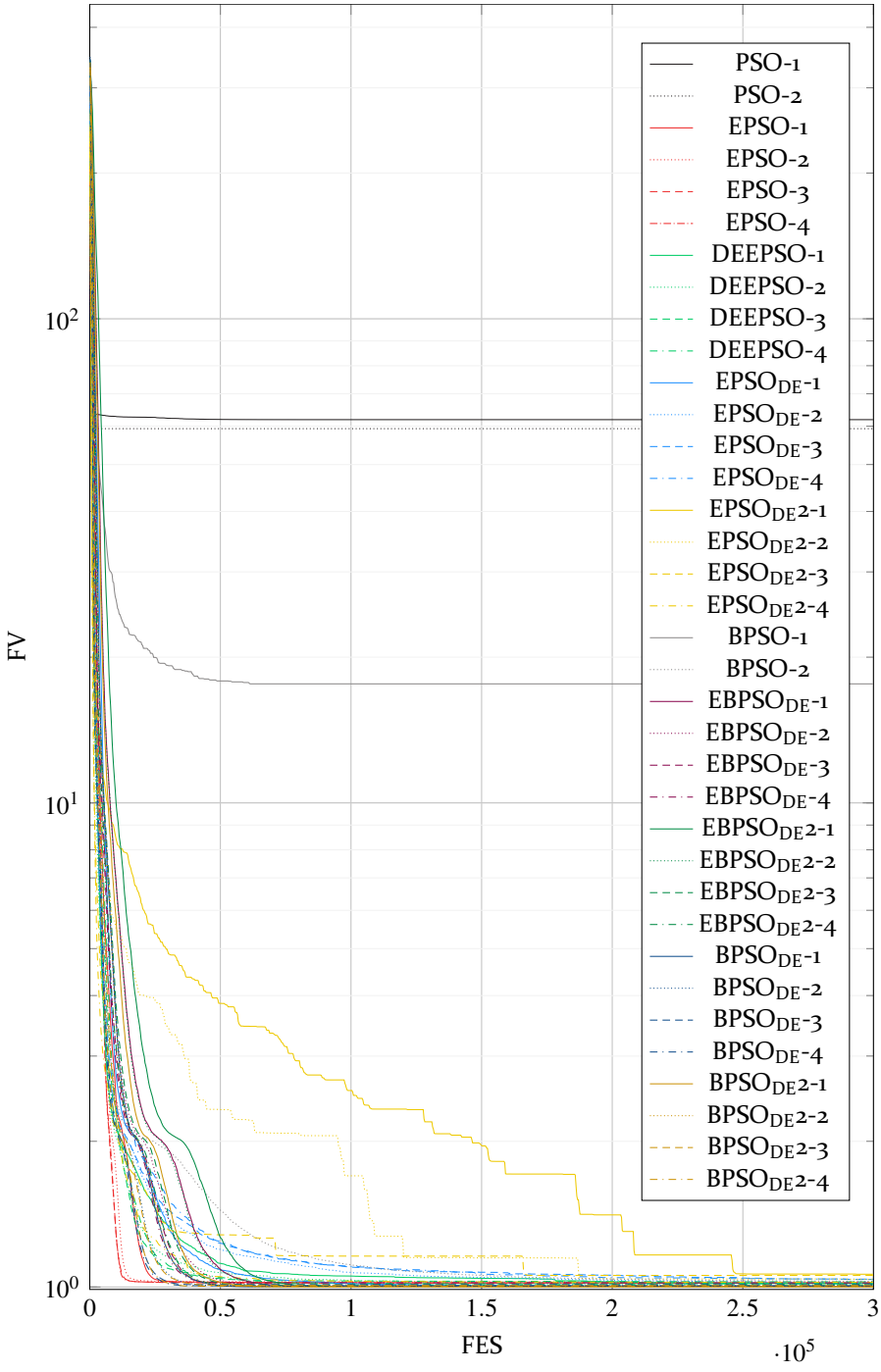

Figure 101: Result graph of the optimization of the shifted Griewank's function with a maximum number of 3E5 FES.

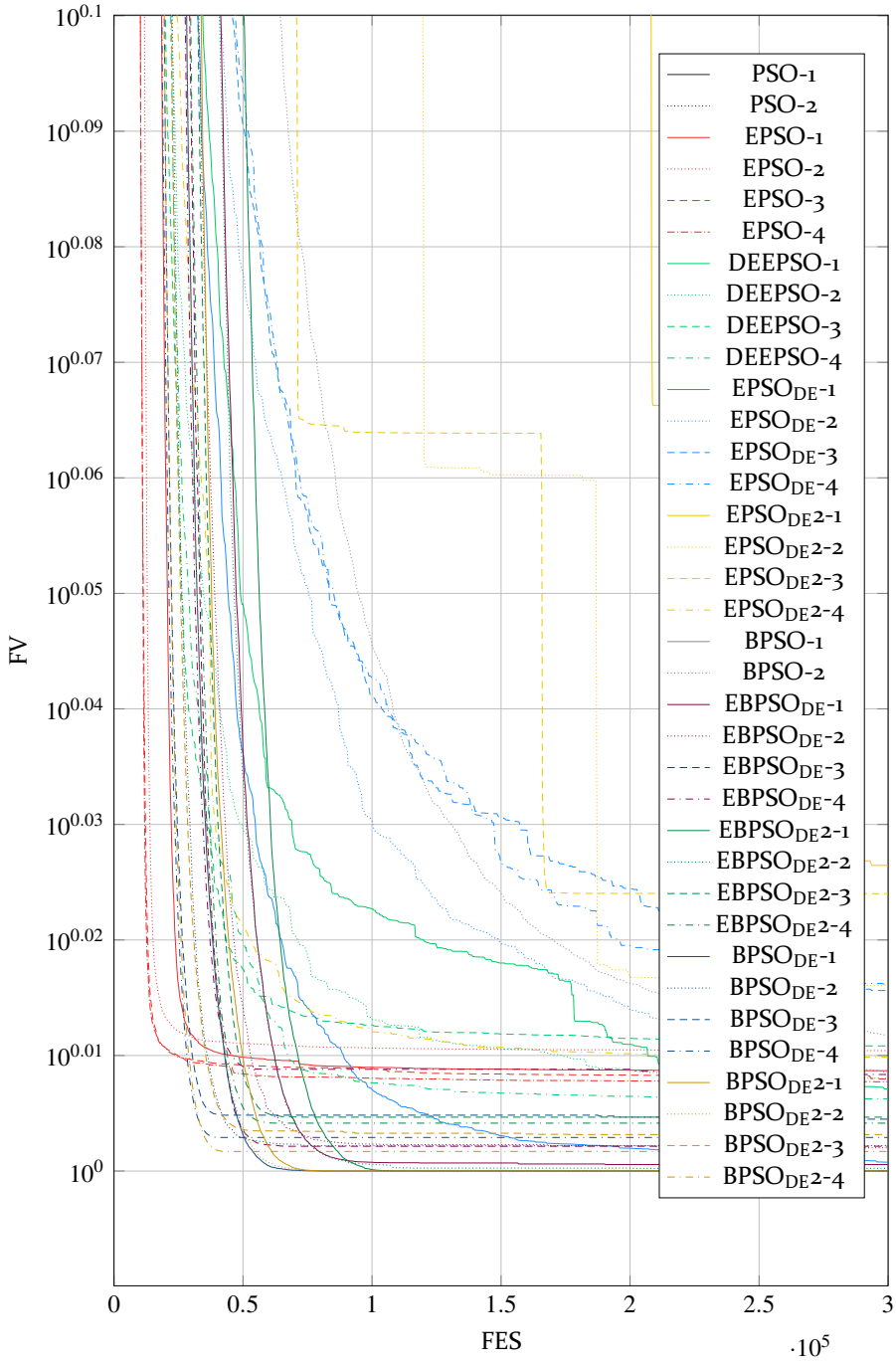

Figure 102: Zoomed partial section of the result graph of the optimization of the shifted Griewank's function with a maximum number of 3E5 FES.

A.4 Shifted Rastrigin's Function

The following are the optimization results of all PSO variants for the shifted Rastrigin's function.

Table 22: Average FV at 25 runs after 3E3, 3E4 and 3E5 FES at shifted Rastrigin's function.

3E3 FES		3E4 FES		3E5 FES	
Method	FV	Method	FV	Method	FV
$EPSO_{DE}2$-1	129.8	$BPSO_{DE}2$-4	10.29	$EBPSO_{DE}2$-1	1
EPSO-3	139.7	$BPSO_{DE}$-4	11.00	$BPSO_{DE}2$-1	1
BPSO-2	145.5	$BPSO_{DE}$-3	11.10	$EBPSO_{DE}$-1	1.080
$EPSO_{DE}2$-2	149.6	$BPSO_{DE}$-2	13.28	$BPSO_{DE}2$-2	1.119
EPSO-4	159.4	$BPSO_{DE}2$-3	16.22	$BPSO_{DE}$-1	1.159
EPSO-2	164.6	$EBPSO_{DE}2$-4	21.21	EPSO-1	2.275
$BPSO_{DE}$-4	187.5	$EBPSO_{DE}$-3	25.01	$BPSO_{DE}$-2	2.970
$BPSO_{DE}$-3	192.6	$BPSO_{DE}2$-2	25.47	EPSO-2	3.031
$BPSO_{DE}2$-4	204.6	$BPSO_{DE}$-1	26.18	$BPSO_{DE}2$-3	3.218
$EPSO_{DE}2$-3	206.9	BPSO-2	26.97	$EBPSO_{DE}2$-3	3.437
$EPSO_{DE}2$-4	213.1	$BPSO_{DE}2$-1	27.31	$EBPSO_{DE}$-2	3.783
DEEPSO-4	221.2	$EBPSO_{DE}2$-3	31.31	BPSO-2	3.835
$EPSO_{DE}$-4	221.5	DEEPSO-1	32.86	$BPSO_{DE}2$-4	3.941
PSO-2	223.2	$EBPSO_{DE}$-2	33.14	EPSO-3	4.268
EPSO-1	223.5	$EBPSO_{DE}2$-2	40.78	$BPSO_{DE}$-3	4.472
DEEPSO-1	226.1	EPSO-1	41.10	$BPSO_{DE}$-4	4.801
DEEPSO-3	226.5	$EBPSO_{DE}$-1	41.41	EPSO-4	5.222
$BPSO_{DE}$-2	229.0	DEEPSO-2	44.49	$EBPSO_{DE}$-3	6.066
$BPSO_{DE}2$-3	229.1	$EBPSO_{DE}2$-1	45.21	$EBPSO_{DE}$-4	6.140
$EPSO_{DE}$-3	229.6	$EPSO_{DE}2$-3	51.91	$EBPSO_{DE}2$-4	6.190
DEEPSO-2	232.3	DEEPSO-3	53.94	DEEPSO-4	7.956
$EPSO_{DE}$-2	237.3	EPSO-2	55.09	DEEPSO-3	10.36
$EBPSO_{DE}$-4	242.6	$EPSO_{DE}2$-2	57.27	DEEPSO-1	11.88
$EBPSO_{DE}$-3	253.2	DEEPSO-4	60.60	DEEPSO-2	11.95
$EBPSO_{DE}2$-4	255.2	EPSO-3	61.32	$EPSO_{DE}2$-1	15.01
$BPSO_{DE}$-1	260.4	EPSO-4	65.05	$EPSO_{DE}2$-2	23.06
$EPSO_{DE}$-1	262.9	$EPSO_{DE}2$-1	65.58	$EPSO_{DE}2$-3	24.15
$BPSO_{DE}2$-2	263.0	NBPSO-1	127.2	$EPSO_{DE}2$-4	45.32
$EBPSO_{DE}2$-3	270.9	$EPSO_{DE}2$-4	134.8	NBPSO-2	78.87
$EBPSO_{DE}$-2	271.5	$EPSO_{DE}$-1	149.6	$EPSO_{DE}$-1	79.2
$BPSO_{DE}2$-1	273.4	PSO-2	153.6	$EPSO_{DE}$-3	109.1
$EBPSO_{DE}$-1	292.8	NBPSO-2	159.4	$EPSO_{DE}$-4	111.2
$EBPSO_{DE}2$-2	296.1	$EPSO_{DE}$-3	166.7	NBPSO-1	130.5
PSO-1	302.7	$EPSO_{DE}$-4	168.1	PSO-2	157.8
$EBPSO_{DE}2$-1	308.8	PSO-1	219.8	PSO-1	207.3
BPSO-1	346.7	BPSO-1	295.5	BPSO-1	252.0

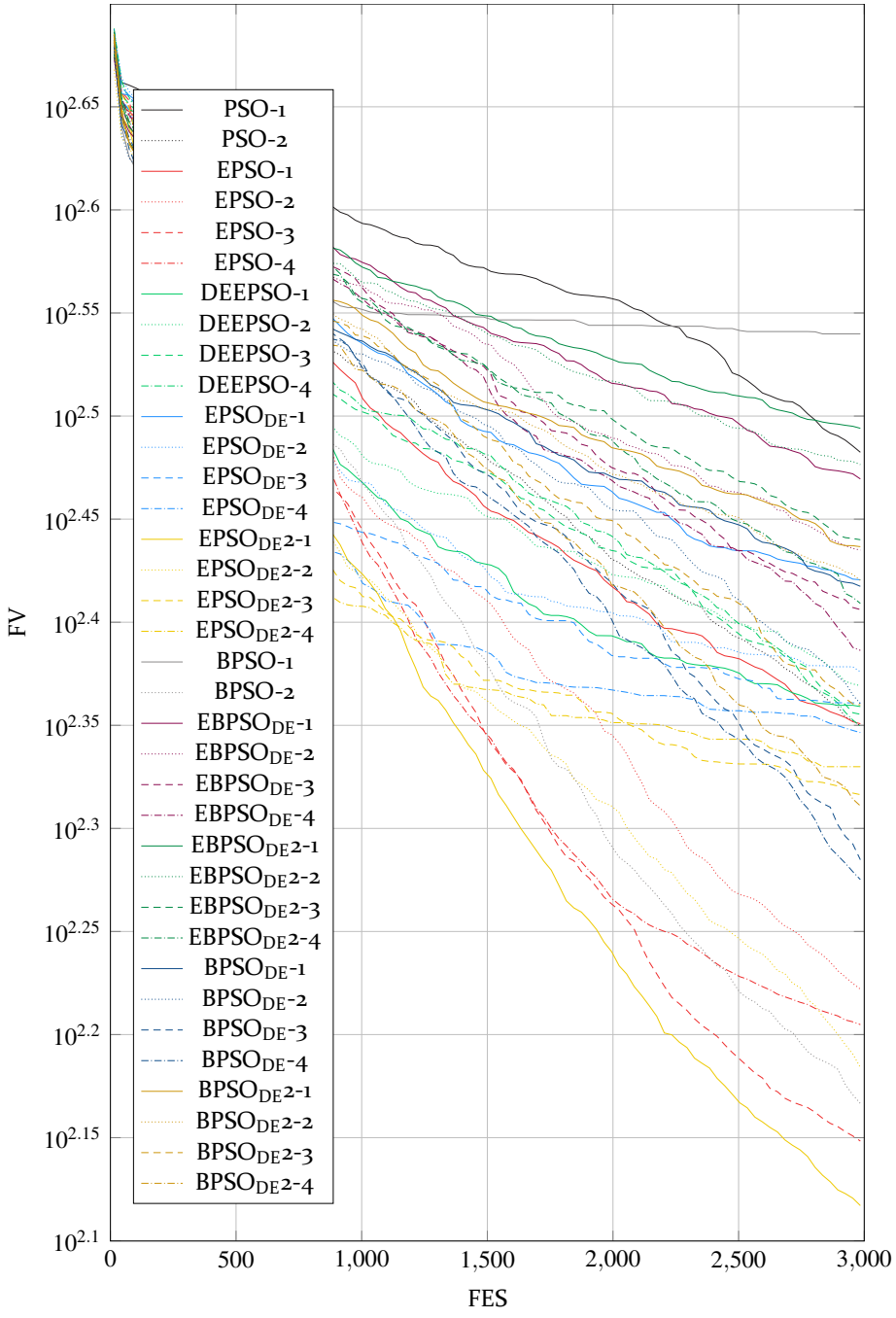

Figure 103: Result graph of the optimization of the shifted Rastrigin's function with a maximum number of 3E3 FES.

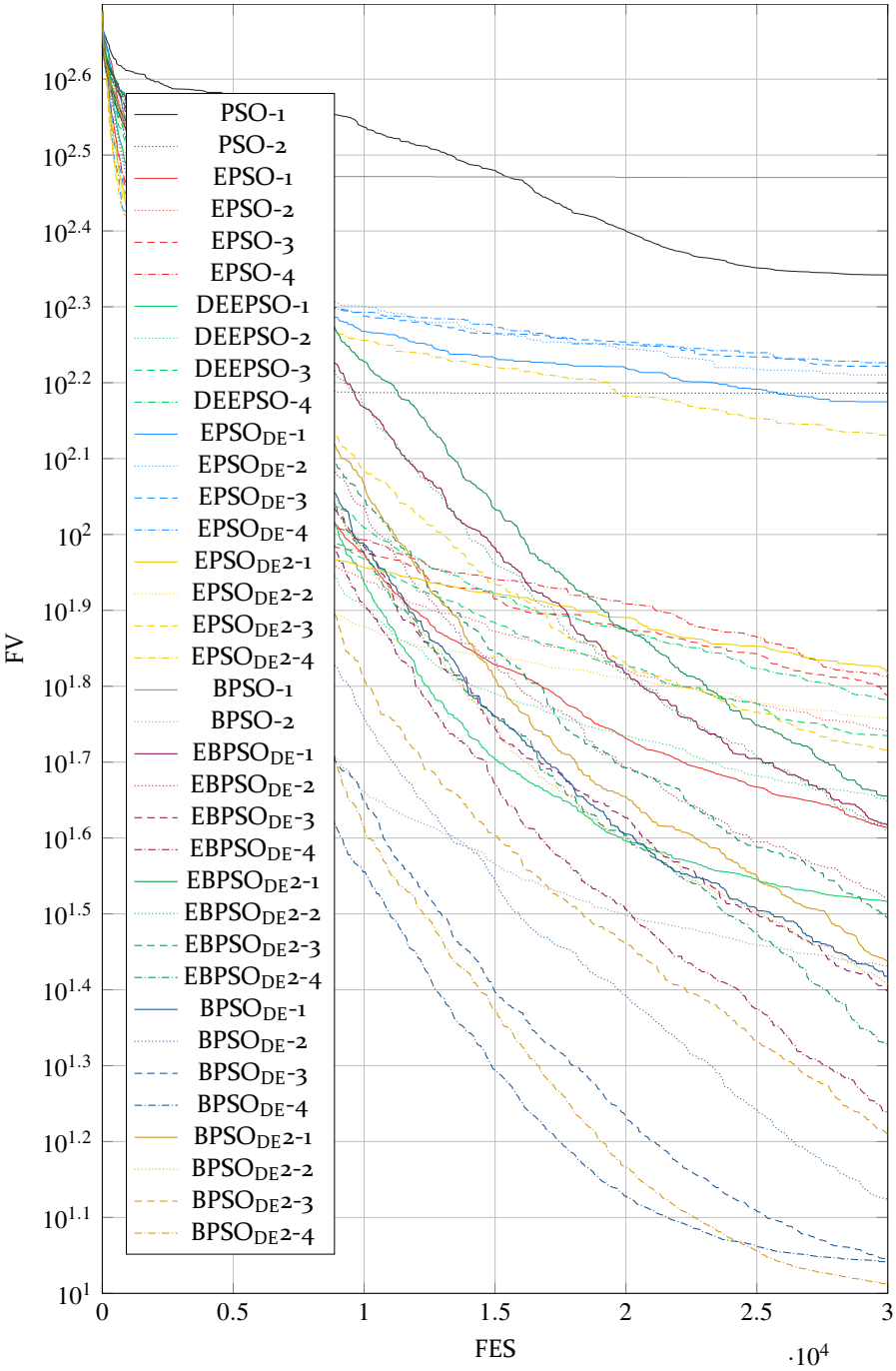

Figure 104: Result graph of the optimization of the shifted Rastrigin's function with a maximum number of 3E4 FES.

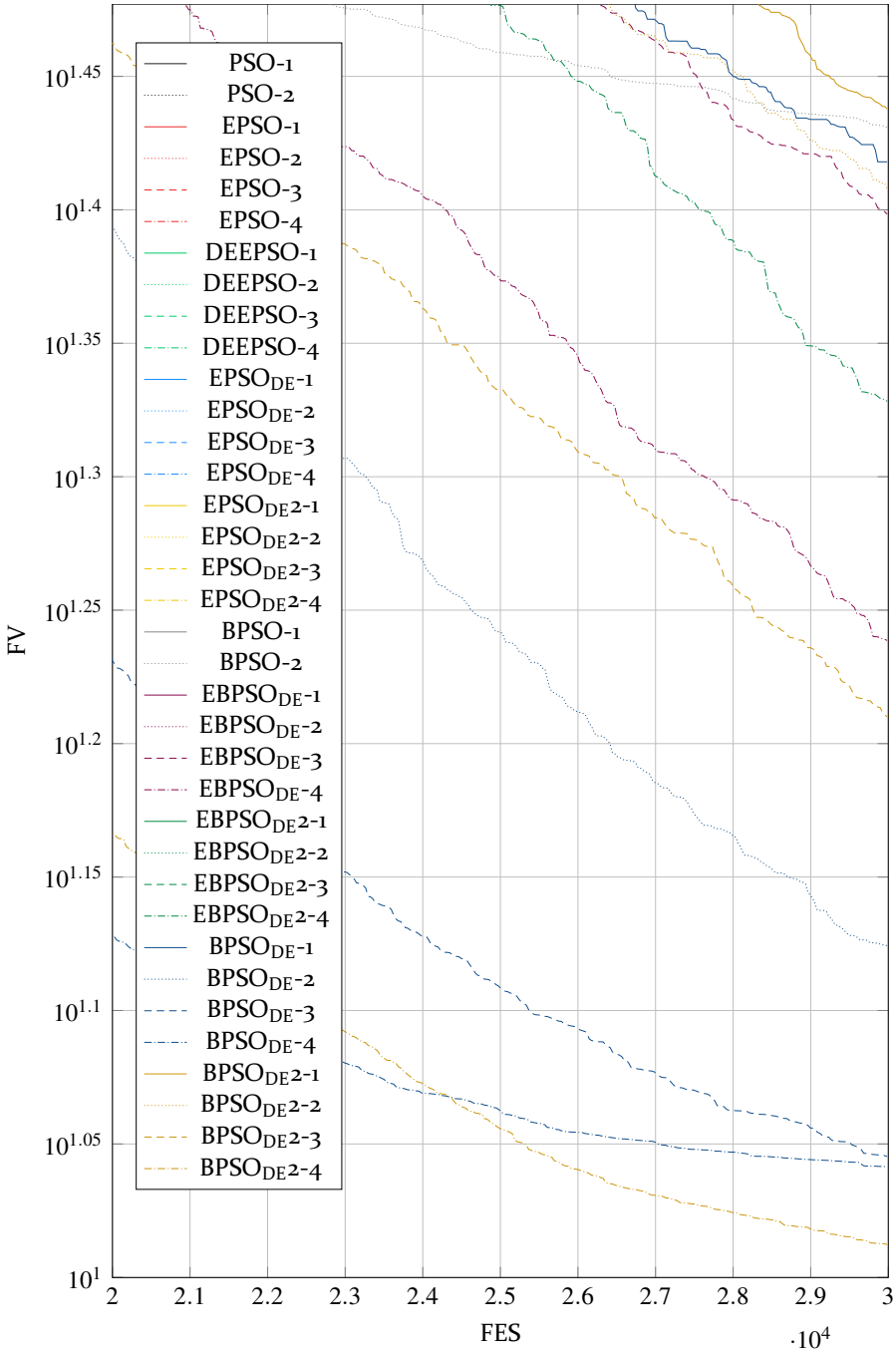

Figure 105: Zoomed partial section of the result graph of the optimization of the shifted Rastrigin's function with a maximum number of 3E4 FES.

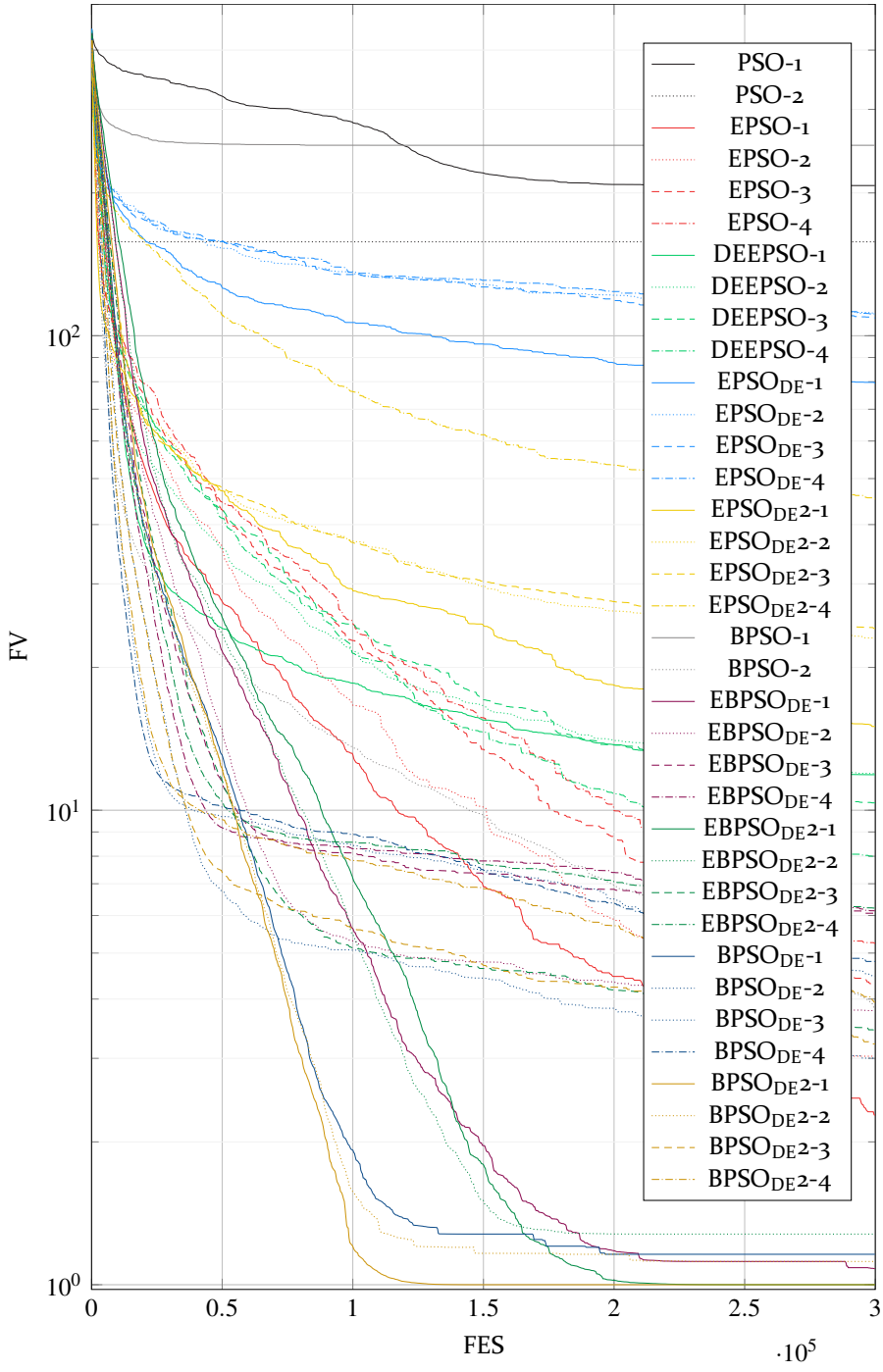

Figure 106: Result graph of the optimization of the shifted Rastrigin's function with a maximum number of 3E5 FES.

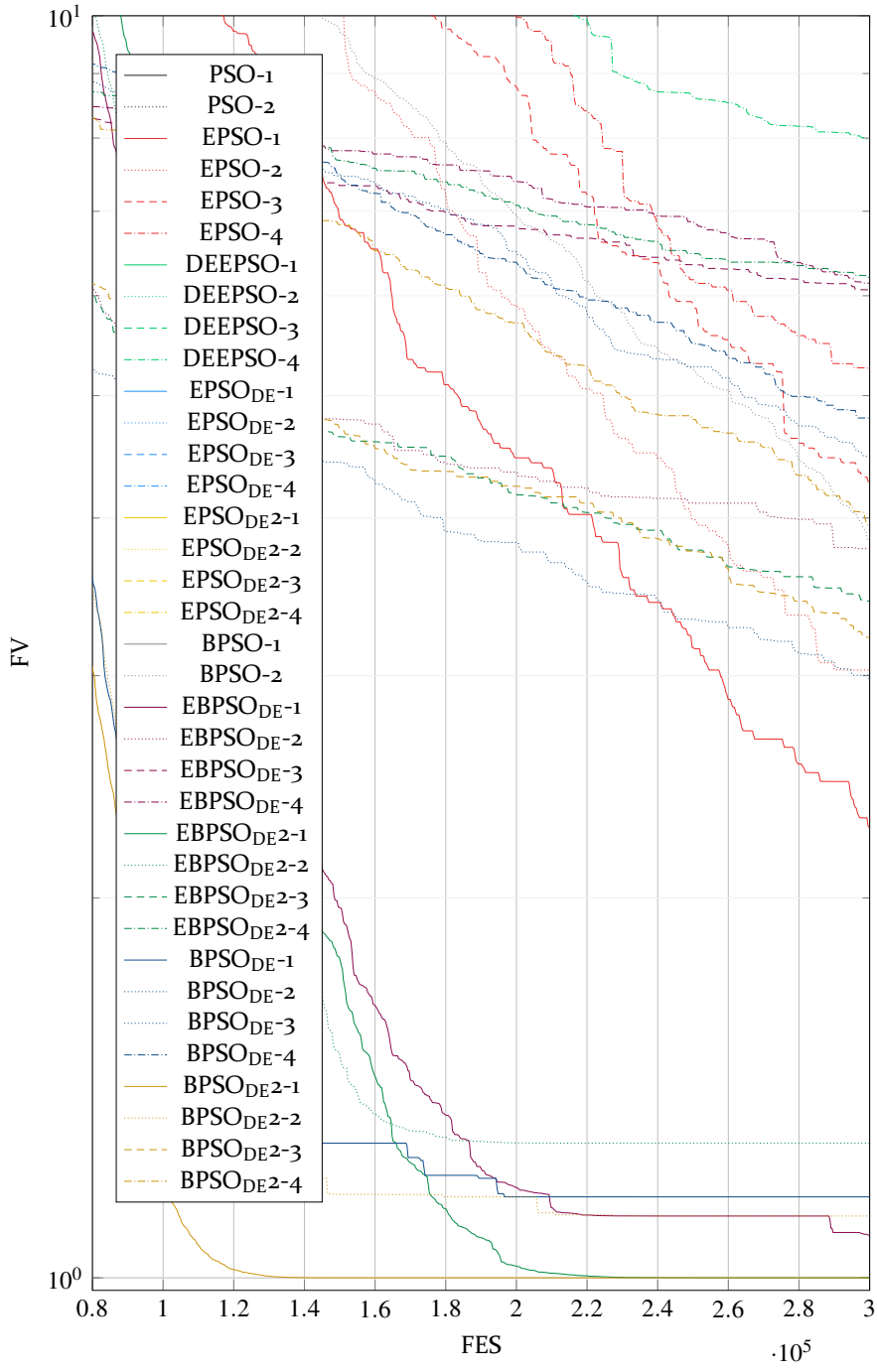

Figure 107: Result graph of the optimization of the shifted Rastrigin's function with a maximum number of 3E5 FES.

A.5 OneMax Function

The following are the optimization results of all PSO variants for the OneMax function.

Table 23: Average FV at 25 runs after 3E3, 3E4 and 3E5 FES at OneMax function.

3E3 FES		3E4 FES		3E5 FES	
Method	FV	Method	FV	Method	FV
$BPSO_{DE}$-4	217.8	$BPSO_{DE}$-2	1	$EBPSO_{DE}$-1	1
$BPSO_{DE}$-3	235.2	$BPSO_{DE}$-3	1	$EBPSO_{DE}$-2	1
$BPSO_{DE}$2-4	235.4	$BPSO_{DE}$-4	1	$EBPSO_{DE}$-3	1
BPSO-2	246.8	$BPSO_{DE}$2-3	1	$EBPSO_{DE}$2-1	1
$BPSO_{DE}$-2	267.7	$BPSO_{DE}$2-4	1	$EBPSO_{DE}$2-2	1
$BPSO_{DE}$2-3	269.7	$BPSO_{DE}$2-2	1.16	$EBPSO_{DE}$2-3	1
$EBPSO_{DE}$-4	286.1	$BPSO_{DE}$-1	1.20	$BPSO_{DE}$-1	1
$EBPSO_{DE}$-3	294.6	$EBPSO_{DE}$-4	2.48	$BPSO_{DE}$-2	1
$EBPSO_{DE}$2-4	295.5	$EBPSO_{DE}$-3	2.56	$BPSO_{DE}$-3	1
$EPSO_{DE}$2-4	313.3	$EBPSO_{DE}$2-4	2.84	$BPSO_{DE}$-4	1
$EPSO_{DE}$-4	317.1	$EBPSO_{DE}$2-3	3.36	$BPSO_{DE}$2-1	1
$EBPSO_{DE}$2-3	320.0	$EBPSO_{DE}$-2	3.68	$BPSO_{DE}$2-2	1
$EBPSO_{DE}$-2	321.1	$BPSO_{DE}$2-1	10.84	$BPSO_{DE}$2-3	1
$EPSO_{DE}$2-3	327.8	$EBPSO_{DE}$-1	15.32	$BPSO_{DE}$2-4	1
$BPSO_{DE}$-1	331.0	$EBPSO_{DE}$2-2	15.88	$EBPSO_{DE}$-4	1.040
$BPSO_{DE}$2-2	331.8	$EBPSO_{DE}$2-1	52.40	$EBPSO_{DE}$2-4	1.040
$EPSO_{DE}$-3	332.5	BPSO-2	98.84	EPSO-1	19.20
DEEPSO-2	333.1	$EPSO_{DE}$-1	130.0	DEEPSO-1	26.76
DEEPSO-3	334.3	DEEPSO-1	130.7	EPSO-2	27.00
DEEPSO-1	334.6	$EPSO_{DE}$-2	146.9	$EPSO_{DE}$-1	34.24
DEEPSO-4	339.4	DEEPSO-2	155.3	$EPSO_{DE}$2-3	35.60
$EPSO_{DE}$-2	339.7	$EPSO_{DE}$2-4	155.9	EPSO-3	37.00
$EPSO_{DE}$2-2	347.5	$EPSO_{DE}$-3	157.4	DEEPSO-2	38.80
EPSO-2	350.4	$EPSO_{DE}$2-3	161.6	DEEPSO-3	42.72
EPSO-3	354.0	$EPSO_{DE}$-4	162.6	EPSO-4	42.80
EPSO-1	355.0	DEEPSO-3	167.1	DEEPSO-4	46.72
$EPSO_{DE}$2-1	356.7	EPSO-4	168.1	$EPSO_{DE}$2-4	49.76
$EBPSO_{DE}$-1	361.6	$EPSO_{DE}$2-2	192.1	$EPSO_{DE}$2-2	50.72
EPSO-4	361.9	EPSO-3	170.0	BPSO-2	56.88
$BPSO_{DE}$2-1	364.9	DEEPSO-4	173.8	$EPSO_{DE}$-2	58.00
$EBPSO_{DE}$2-2	365.0	EPSO-2	177.0	$EPSO_{DE}$-3	68.60
PSO-2	379.6	EPSO-1	183.2	$EPSO_{DE}$-4	71.56
$EPSO_{DE}$-1	381.4	$EPSO_{DE}$2-1	215.6	$EPSO_{DE}$2-1	93.48
PSO-1	387.8	PSO-2	374.9	BPSO-1	347.8
$EBPSO_{DE}$2-1	390.2	BPSO-1	377.1	PSO-2	377.4
BPSO-1	408.3	PSO-1	391.9	PSO-1	394.7

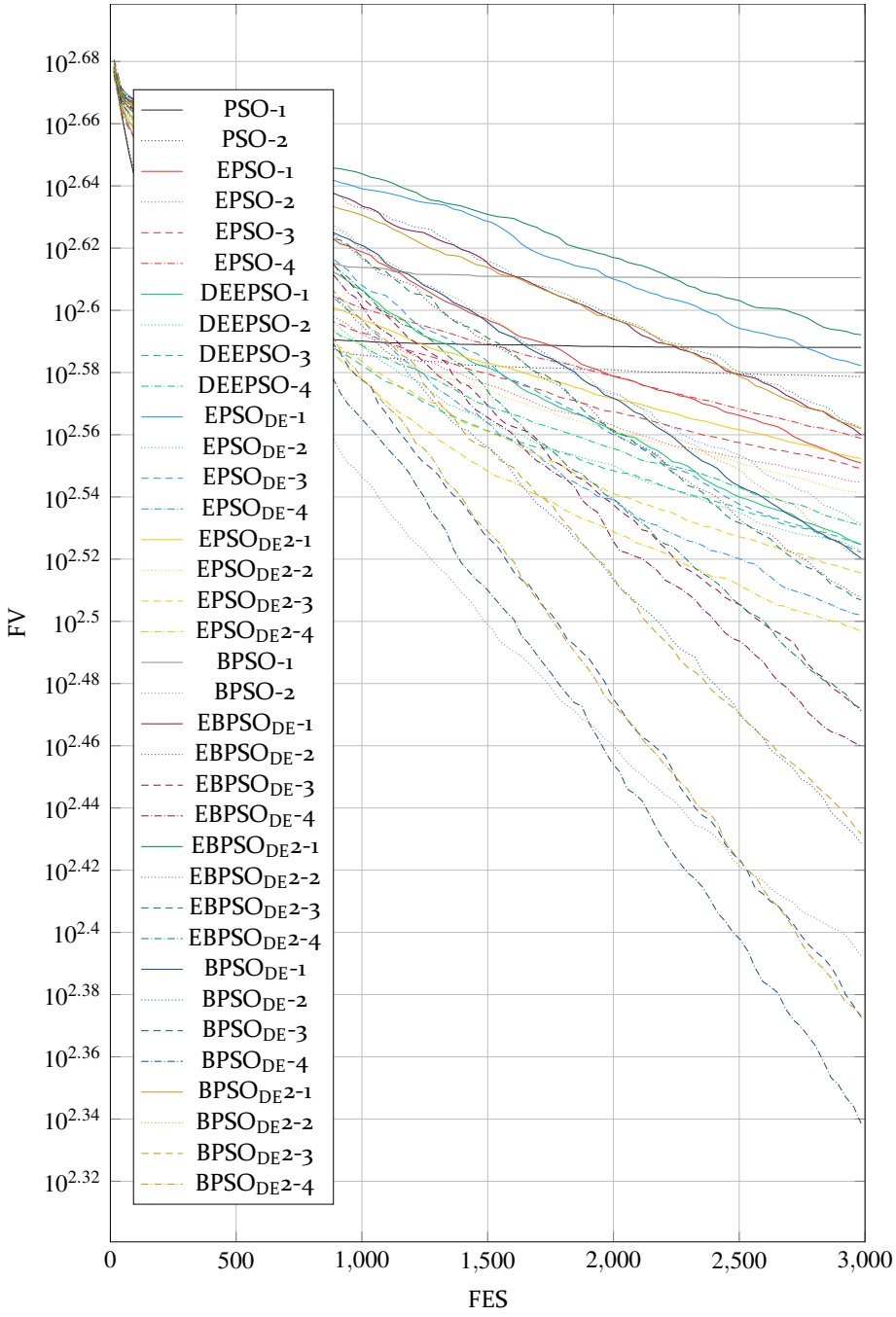

Figure 108: Result graph of the optimization of the OneMax function with a maximum number of 3E3 FES.

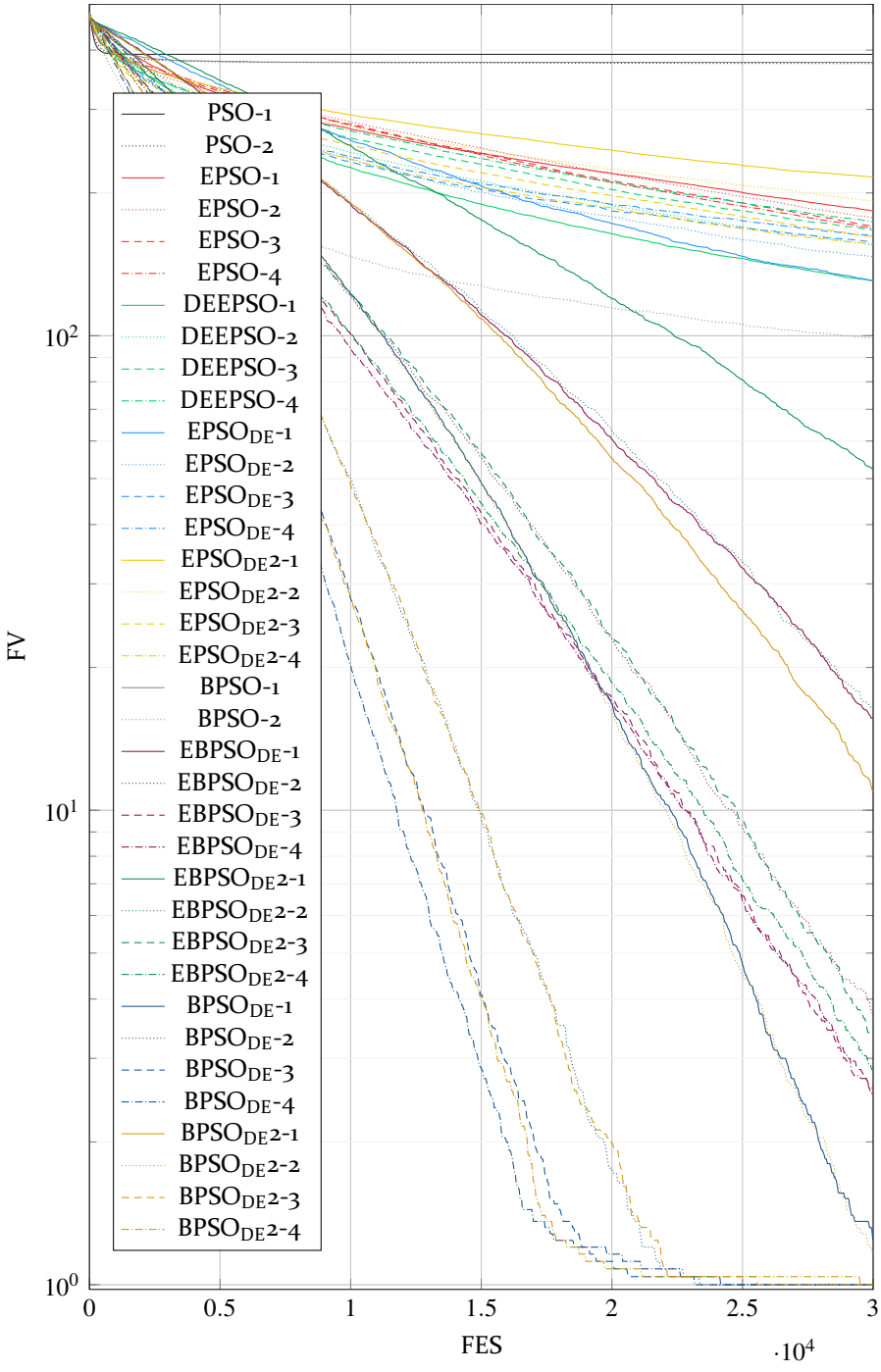

Figure 109: Result graph of the optimization of the OneMax function with a maximum number of 3E4 FES.

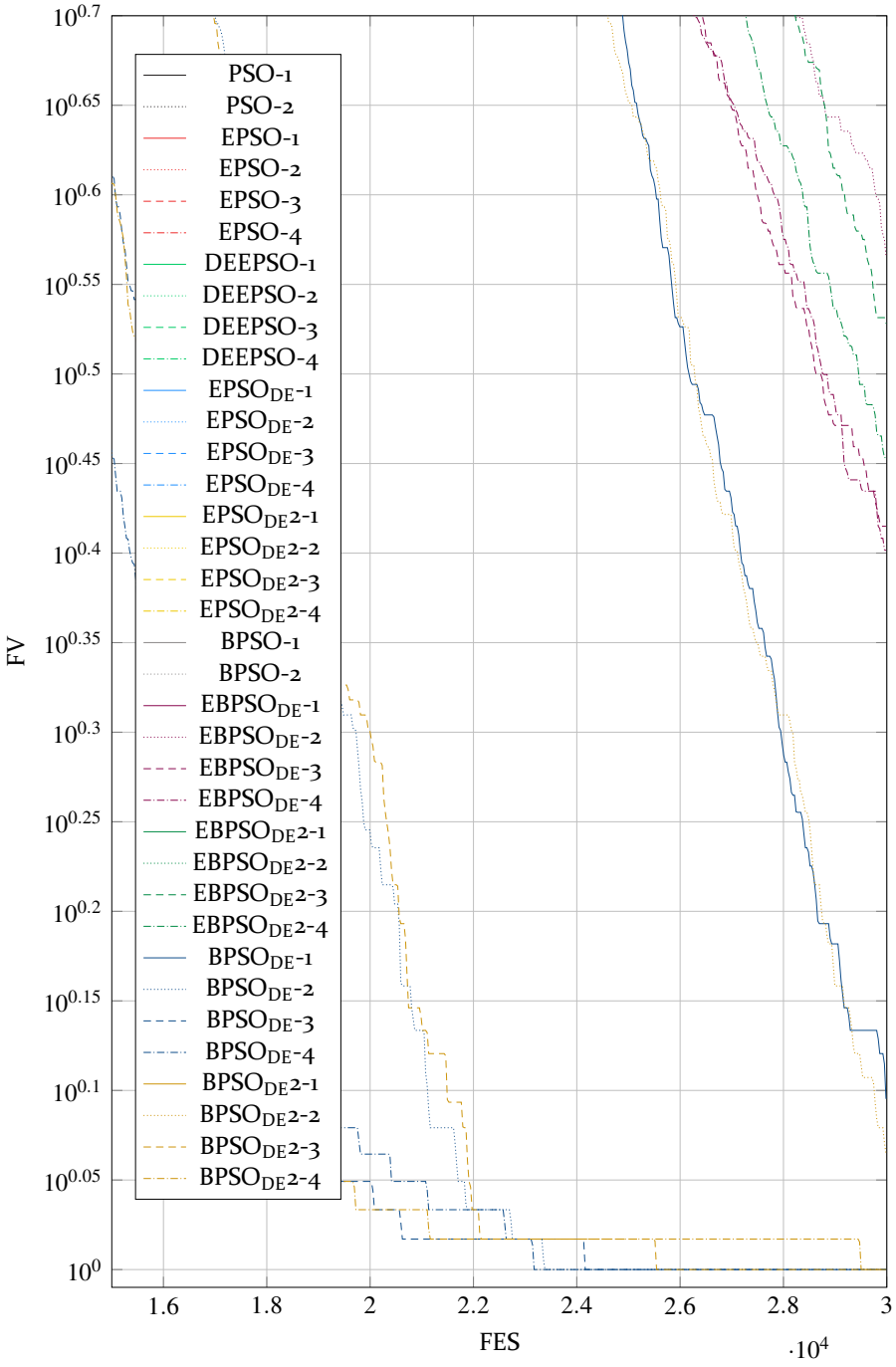

Figure 110: Zoomed partial section of the result graph of the optimization of the OneMax function with a maximum number of 3E4 FES.

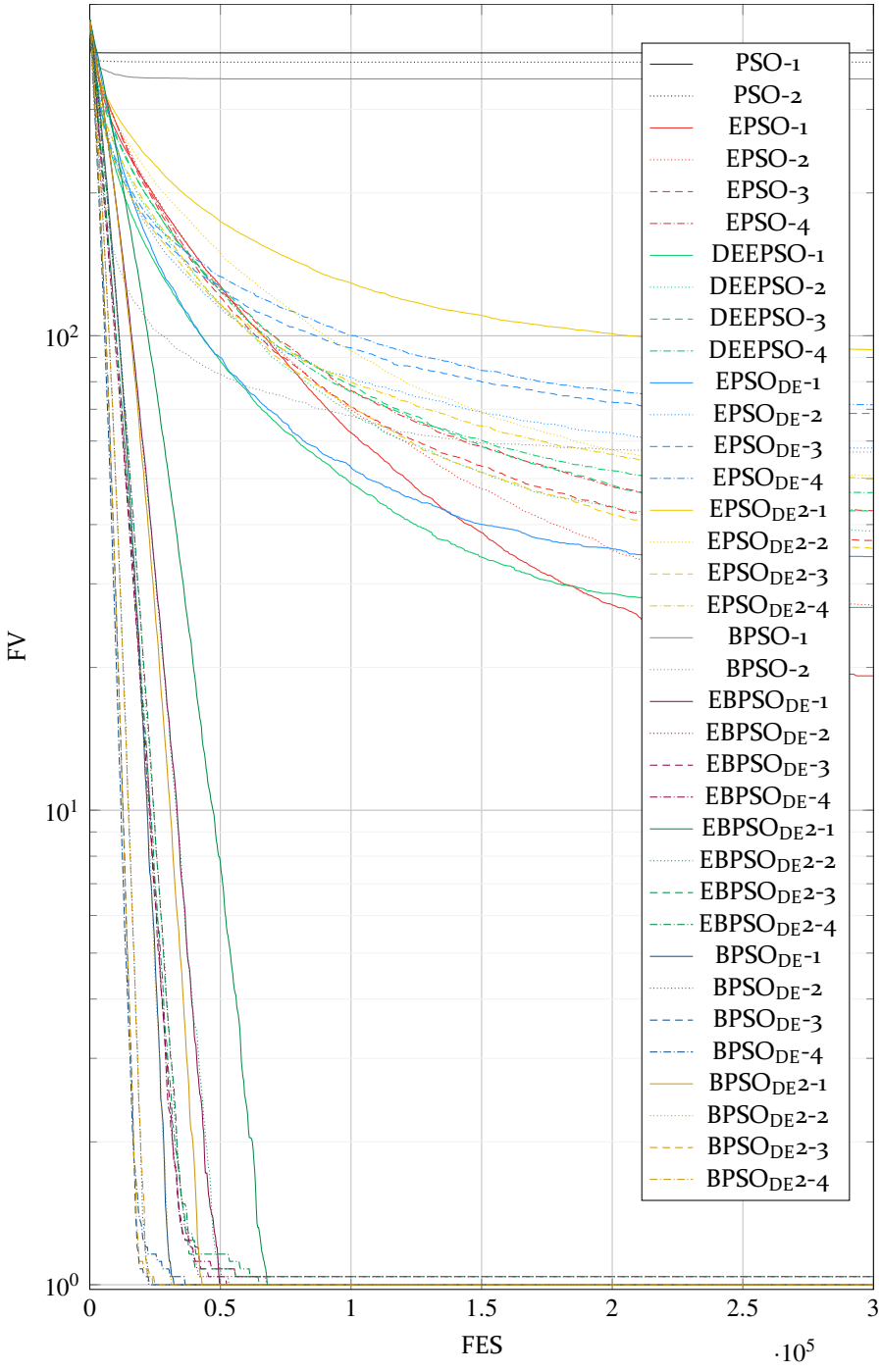

Figure 111: Result graph of the optimization of the OneMax function with a maximum number of 3E5 FES.

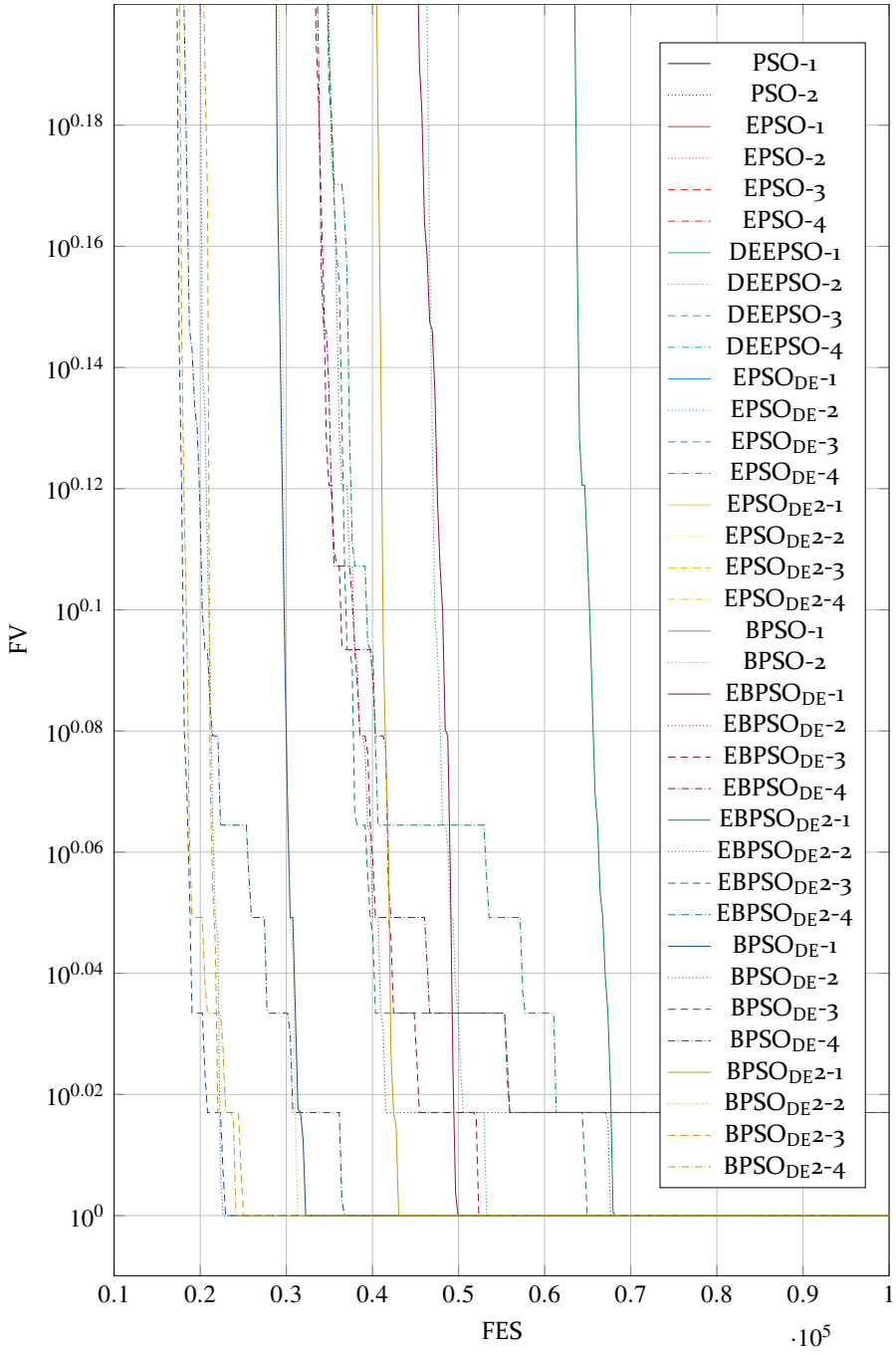

Figure 112: Result graph of the optimization of the OneMax function with a maximum number of 3E5 FES.

B Voltage and Reactance Calculations

In the following, the different voltage as well as reactance calculations including conversion steps of the chapter 9.3 related to Figure 29 and 30 are listed.

1) S1, S2, S3 open

$$U_{\mathrm{A}} = \begin{cases} I_{\mathrm{A}} \cdot x \cdot X'_{\mathrm{AB}} & \text{fault on section AB} \\ I_{\mathrm{A}} \cdot (X_{\mathrm{AB}} + y \cdot X'_{\mathrm{BC}}) & \text{fault on section BC} \end{cases} \tag{87}$$

$$X_{\mathrm{PA,meas.}} = \begin{cases} x \cdot X'_{\mathrm{AB}} & \text{fault on section AB} \\ X_{\mathrm{AB}} + y \cdot X'_{\mathrm{BC}} & \text{fault on section BC} \end{cases} \tag{88}$$

2) S1 open, S2 closed, S3 open

$$\begin{aligned} U_{\mathrm{A}} &= I_{\mathrm{A}} \cdot X_{\mathrm{AB}} + I_{\mathrm{A}} \cdot (yX_{\mathrm{BC}} || ((2-y)X_{\mathrm{BC}})) \\ &= I_{\mathrm{A}} \cdot X_{\mathrm{AB}} + I_{\mathrm{A}} \cdot X_{\mathrm{BC}}(y - 0.5y^2) \\ &= I_{\mathrm{A}} \cdot \left(X_{\mathrm{AB}} + X_{\mathrm{BC}}(y - 0.5y^2)\right) \end{aligned} \tag{89}$$

$$X_{\mathrm{PA,meas.}} = \frac{U_{\mathrm{A}}}{I_{\mathrm{A}}} = X_{\mathrm{AB}} + X_{\mathrm{BC}}(y - 0.5y^2) \tag{90}$$

3) S1 closed, S2 open, S3 open

$$U_{\mathrm{A}} = I_{\mathrm{A}} \cdot 0.5X_{\mathrm{AB}} + I_{\mathrm{A}} \cdot yX_{\mathrm{BC}} = I_{\mathrm{A}} \cdot (0.5X_{\mathrm{AB}} + yX_{\mathrm{BC}}) \tag{91}$$

$$\begin{aligned} X_{\mathrm{PA,meas.}} &= \frac{U_{\mathrm{A}}}{I_{\mathrm{A1}}} = \frac{I_{\mathrm{A}}}{I_{\mathrm{A1}}} \cdot (0.5X_{\mathrm{AB}} + yX_{\mathrm{BC}}) \\ &= 2 \cdot (0.5X_{\mathrm{AB}} + yX_{\mathrm{BC}}) = X_{\mathrm{AB}} + 2yX_{\mathrm{BC}} \end{aligned} \tag{92}$$

4) S1 closed, S2 closed, S3 open

$$\begin{aligned} U_{\mathrm{A}} &= I_{\mathrm{A}} \cdot 0.5X_{\mathrm{AB}} + I_{\mathrm{A}} \cdot (yX_{\mathrm{BC}} || ((2-y)X_{\mathrm{BC}})) \\ &= I_{\mathrm{A}} \cdot 0.5X_{\mathrm{AB}} + I_{\mathrm{A}} \cdot 0.5X_{\mathrm{BC}}(2y - y^2) \\ &= I_{\mathrm{A}} \cdot \left(0.5X_{\mathrm{AB}} + 0.5X_{\mathrm{BC}}(2y - y^2)\right) \end{aligned} \tag{93}$$

$$\begin{aligned} X_{\text{PA,meas.}} &= \frac{U_\text{A}}{I_{\text{A}1}} = \frac{I_\text{A}}{I_{\text{A}1}} \cdot \left(0.5X_\text{AB} + 0.5X_\text{BC}(2y - y^2)\right) \\ &= 2\left(0.5X_\text{AB} + 0.5X_\text{BC}(2y - y^2)\right) = X_\text{AB} + X_\text{BC}(2y - y^2) \end{aligned} \tag{94}$$

5) S1 closed, S2 closed, S3 closed To calculate the voltage drop through $I_{\text{C}1}$, the current divider rule is suitable.

$$\begin{aligned} U_\text{A} &= I_\text{A} \cdot \left(0.5X_\text{AB} + 0.5X_\text{BC}(2y - y^2)\right) + I_{\text{C}1} \cdot yX_\text{BC} \\ &= I_\text{A} \cdot \left(0.5X_\text{AB} + 0.5X_\text{BC}(2y - y^2)\right) + I_\text{C} \cdot \frac{1-y}{(1+y)+(1-y)} yX_\text{BC} \\ &= I_\text{A} \cdot \left(0.5X_\text{AB} + 0.5X_\text{BC}(2y - y^2)\right) + I_\text{C} \cdot 0.5X_\text{BC}(y - y^2) \\ &= I_\text{A} \cdot \left(0.5X_\text{AB} + 0.5X_\text{BC}\left((2y - y^2) + \frac{I_\text{C}}{I_\text{A}} \cdot (y - y^2)\right)\right) \end{aligned} \tag{95}$$

$$\begin{aligned} X_{\text{PA,meas.}} &= \frac{U_\text{A}}{I_{\text{A}1}} = \frac{I_\text{A}}{I_{\text{A}1}} \cdot \left(0.5X_\text{AB} + 0.5X_\text{BC}\left((2y - y^2) + \frac{I_\text{C}}{I_\text{A}} \cdot (y - y^2)\right)\right) \\ &= X_\text{AB} + X_\text{BC}\left((2y - y^2) + \frac{I_\text{C}}{I_\text{A}} \cdot (y - y^2)\right) \\ &= X_\text{AB} + X_\text{BC}\left((2y - y^2) + (2y - 2y^2)\right) \\ &= X_\text{AB} + X_\text{BC}(4y - 3y^2) \end{aligned} \tag{96}$$

Source Currents in Phase

$$\begin{aligned} \underline{U}_\text{A} &= \underline{I}_\text{A} \cdot yX_\text{AC} + (\underline{I}_\text{A} + \underline{I}_\text{C})R_\text{F} \\ &= \underline{I}_\text{A} \cdot (yX_\text{AC} + R_\text{F}) + \underline{I}_\text{C} \cdot R_\text{F} \end{aligned} \tag{97}$$

$$\underline{Z}_{\text{PA,meas.}} = \frac{\underline{U}_\text{A}}{\underline{I}_\text{A}} = yX_\text{AC} + R_\text{F} + \frac{\underline{I}_\text{C}}{\underline{I}_\text{A}} \cdot R_\text{F} \tag{98}$$

C Equipment and Protection Data of the Distribution System

C.1 Equipment Data

C.1.1 Machine Data

Table 24: Machine data with rated apparent power S_r, sub-transient reactance X'', transient reactance X', synchronous reactance X, armature resistance ra and starting time TA.

DER	G1	G2	G3	G4	G5
S_r in MV A	2	2.4	2	2	4
X'' in p.u.	0.168	0.168	0.128	0.128	0.128
X' in p.u.	0.256	0.256	0.3	0.3	0.3
X in p.u.	1.5	1.5	2.0	2.0	2.0
T'' in s	0.03	0.03	0.05	0.05	0.05
T' in s	0.53	0.53	1.0	1.0	1.0
TA in s	4	4	3	3	3
ra in p.u.	0.05	0.05	0.0036	0.0036	0.0036

C.1.2 Transformer Data

Table 25: Transfomrer data with rated apparent power S_r, impedance voltage u_k, high voltage level V_{HV} and low voltage level V_{LV}.

Transformer	T1	T2	T3	T4	T5	TGrid
S_r in MV A	3	3.5	3	3	5	31.5
u_k in %	6	7	6	6	7	11.5
V_{HV} in kV	20	20	20	20	20	110
V_{LV} in kV	0.69	10	0.69	13.8	10	20

C.1.3 Line Data

Table 26: Line data with length l, reactance X', resistance R' and capacitance C'.

Line	l in km	X' in Ω/km	R' in Ω/km	C' in nF/km
L10	1.61			
L11	2.65			
L12	4.87			
L13	2.71			
L20	1.30			
L21	1.65			
L22	12.52			
L23	0.71			
L24	1.41			
L25	0.86			
L26	3.98			
L27	7.82			
L30	2.76	0.118	0.169	273
L31	9.99			
L40	1.45			
L41	5.49			
L44	2.06			
L45	1.21			
L50	2.1			
L51	1.61			
L60	1.29			
L62	1.28			
L63	0.81			
L66	0.88			
L67	2.79			
L14	3.51			
L61	3.57	0.12	0.21	367
L64	3.2			
L68	3.63			
L28	0.98	0.122	0.105	245
L42	6.43	0.128	0.323	310
L43	2.49			
L65	0.83	0.149	0.868	222

C.1.4 Disconnector Data

Table 27: Disconnector data with length l, reactance X', resistance R' and capacitance C'.

Disconnector	l in km	X' in Ω/km	R' in Ω/km	C' in nF/km
D1	1.25			
D2	1.3			
D3	2.4			
D4	0.5	0.188	0.169	273
D5	1.8			
D6	1.8			
D7	2.6			
D8	0.76			

Thermal limit current of lines and disconnectors $I_{\text{th}} = 361\,\text{A}$.

C.2 Protection Data

C.2.1 Overcurrent Protection Settings for P1GE to P5GE

Table 28: Overcurrent protection settings for P1GE to P5GE with high current stage $I_{>>}$, low current stage $I_{>}$, delay times $t_{>>}$, $t_{>}$ and nominal current I_{N}.

Setting	Value
$I_{>>}$	$5.0 I_{\text{N}}$
$t_{>>}$	0.05 s
$I_{>}$	$1.5 I_{\text{N}}$
$t_{>}$	1.0 s

C.2.2 Generator Over/Underfrequency Protection Settings for G1 to G5

Table 29: Generator over/underfrequency protection settings for G1 to G5 with fast overfrequency stage $f_{>>}$, slow overfrequency stage $f_{>}$, fast underfrequency stage $f_{<<}$, slow underfrequency stage $f_{<}$, delay times $t_{>>}$, $t_{>}$, $t_{<<}$, $t_{<}$ and nominal frequency f_{N}.

Setting	Value
$f_{>>}$	$1.05 f_{\mathrm{N}}$
$t_{>>}$	0.15 s
$f_{>}$	$1.03 f_{\mathrm{N}}$
$t_{>}$	3.0 s
$f_{<<}$	$0.95 f_{\mathrm{N}}$
$t_{<<}$	0.15 s
$f_{<}$	$0.97 f_{\mathrm{N}}$
$t_{<}$	3.0 s

D Optimization Results of the Distribution System

X in Ω, T in s and I in kA.
$PSB = 1$ means enabled and $PSB = 0$ means disabled.
Numbers in gray color were fixed regardless of the calculation or optimization method.

D.1 Operated as a Radial System

Calculated and optimized setting values for the condition that all disconnectors of the system are open.
All overcurrent protection functions are designed as undirectional functions.

Prot. Dev.	Setting	Calc.	X	X, T	X, T PSB	X, T PSB, I
PA	X1	0.45	0.48	0.50	0.50	0.47
	T1	0.00	0.00	0.00	0.00	0.00
	X2	0.60	1.07	1.50	1.36	1.45
	T2	0.30	0.30	0.35	0.30	0.25
	X3	1.08	1.61	1.61	1.61	1.61
	T3	0.60	0.60	0.60	0.60	0.60
	PSB	0	0	0	0	0
PB	X1	0.31	0.35	0.36	0.36	0.36
	T1	0.00	0.00	0.00	0.00	0.00
	X2	0.56	0.35	2.3	2.1	1.95
	T2	0.30	0.30	0.45	0.45	0.35
	X3	1.83	2.29	2.7	2.7	2.7
	T3	0.60	0.60	0.75	0.65	0.60
	PSB	0	0	0	0	0

Continued on next page

Prot. Dev.	Setting	Calc.	X	X, T	X, T PSB	X, T PSB, I
PC	X1	0.29	3.98	3.6	2.88	3.50
	T1	0.00	0.00	0.00	0.05	0.05
	X2	1.81	3.98	5.18	7.45	4.90
	T2	0.30	0.30	0.25	0.35	0.35
	X3	3.01	12,00	11.79	11.78	10.42
	T3	0.60	0.60	0.75	0.65	0.70
	PSB	0	0	0	0	0
PD	X1	1.06	2.07	2.39	2.2	3.81
	T1	0.00	0.00	0.00	0.05	0.05
	X2	1.81	5.81	5.34	2.45	8.42
	T2	0.30	0.30	0.50	0.50	0.50
	X3	3.01	11.17	9.55	8.3	12.00
	T3	0.60	0.60	0.65	0.75	0.65
	PSB	0	0	0	1	1
PE	X1	0.42	0.50	0.47	0.23	0.23
	T1	0.00	0.00	0.10	0.00	0.00
	X2	1.67	1.97	2.3	1.67	1.69
	T2	0.30	0.30	0.25	0.40	0.40
	X3	2.79	4.23	4.23	3.47	4.23
	T3	0.60	0.60	0.60	0.75	0.60
	PSB	0	0	0	1	1
PF	X1	0.29	0.32	0.32	0.32	0.32
	T1	0.00	0.00	0.00	0.00	0.00
	X2	0.38	0.64	0.32	0.36	0.64
	T2	0.30	0.30	0.20	0.25	0.35
	PSB	0	0	0	0	0

Continued on next page

Prot. Dev.	Setting	Calc.	X	X, T	X, T PSB	X, T PSB, I
PG	X1	0.38	0.42	0.39	0.33	0.29
	T1	0,00	0,00	0.05	0.00	0.00
	X2	0.51	0.64	0.84	0.57	0.58
	T2	0.30	0.30	0.50	0.40	0.20
	PSB	0	0	0	0	0
PH	X1	0.51	0.56	0.56	0.56	0.56
	T1	0.00	0.00	0.00	0.00	0.05
	X2	0.67	1.13	1.12	1.13	0.96
	T2	0.30	0.30	0.50	0.30	0.25
	PSB	0	0	0	0	0
PI	X1	0.15	0.09	0	0.08	0.08
	T1	0.00	0.00	0.10	0.05	0.00
	X2	1.15	1.7	1.76	1.56	1.29
	T2	0.30	0.30	0.25	0.25	0.20
	X3	1.64	2.55	2.55	2.25	2.55
	T3	0.60	0.60	0.70	0.70	0.75
	PSB	0	0	0	1	1
PJ	X1	0.62	0.66	0.36	1.31	1.31
	T1	0.00	0.00	0.00	0.00	0.00
	X2	1.6	2,00	2.19	2.7	3.69
	T2	0.30	0.30	0.20	0.20	0.50
	X3	2.67	3.93	3.93	3.93	3.93
	T3	0.60	0.60	0.75	0.70	0.75
	PSB	0	0	0	1	1

Continued on next page

Prot. Dev.	Setting	Calc.	X	X, T	X, T PSB	X, T PSB, I
PK	X1	0.30	0.33	0.33	0.33	0.33
	T1	0.00	0.00	0.00	0.00	0.00
	X2	0.39	0.60	0.66	0.66	0.64
	T2	0.30	0.30	0.20	0.45	0.50
	PSB	0	0	0	0	0
PL	X1	0.39	0.43	0.37	0.42	0.34
	T1	0.00	0.00	0.05	0.00	0.00
	X2	0.52	0.44	0.54	0.71	0.67
	T2	0.30	0.30	0.20	0.35	0.35
	PSB	0	0	0	1	0
PM	X1	0.17	0.19	0.19	0.19	0.19
	T1	0.00	0.00	0,00	0.05	0.00
	X2	0.23	0.33	0.33	0.38	0.36
	T2	0.30	0.30	0.20	0.25	0.20
	PSB	0	0	0	0	1
PN	X1	0.22	0.25	0.25	0.25	0.25
	T1	0.00	0.00	0.00	0.00	0.05
	X2	0.30	0.30	0.28	0.38	0.28
	T2	0.30	0.30	0.25	0.40	0.30
	PSB	0	0	0	0	0

Continued on next page

Prot. Dev.	Setting	Calc.	X	X, T	X, T PSB	X, T PSB, I
PA2	**I1**	0.6	0.6	0.6	0.6	3.6
	T1	0.10	0.10	0.10	0.10	0.00
PB2	**I1**	/	/	/	/	3.7
	T1	/	/	/	/	0.00
	I2	0.6	0.6	0.6	0.6	0.6
	T2	0.30	0.30	0.30	0.30	0.20
PB3	**I1**	0.6	0.6	0.6	0.6	1.8
	T1	0,00	0.00	0.00	0.00	0.00

D.2 Closing a Ring Inside the System

Calculated and optimized setting values for the condition that disconnector D1 is closed.
All overcurrent protection functions are designed as undirectional functions.

Prot. Device	Setting	Optimised for D1 open	Calculated for D1 closed	Optimized for D1 closed
PB	X1	0.36	0.31	0.25
	T1	0.00	0.00	0.00
	X2	1.95	2.27	2.38
	T2	0.35	0.30	0.60
	X3	2.70	3.78	3.55
	T3	0.60	0.60	0.60
	PSB	0	0	0
PE	X1	0.23	0.42	2.4
	T1	0.00	0.00	0.00
	X2	1.69	2.27	4.65
	T2	0.4	0.3	0.25
	X3	4.23	3.02	10.67
	T3	0.60	0.60	0.60
	PSB	1	0	0
PB2	I1	3.7	/	2.9
	T1	0.00	/	0.00
	I2	0.6	0.6	1.3
	T2	0.20	0.30	0.20
PB3	I1	1.8	0.6	1.8
	T1	0.00	0.00	0.00

D.3 Highly Meshed System

Calculated and optimized setting values for the condition that disconnectors D2, D3, D4 and D5 are closed.
Dir = 1 means vorward, = 0 means backward and = 2 means undirected.

Prot. Device	Setting	Calculated	Optimized
PA	X1	0.45	0.72
	T1	0.00	0.00
	X2	0.94	0.93
	T2	0.30	0.40
	X3	2.23	4.14
	T3	0.60	0.8
	PSB	0	1
PF	X1	0.43	1.53
	T1	0.00	0.00
	X2	1.41	4.24
	T2	0.30	0.40
	X3	2.48	7.76
	T3	0.60	0.60
	PSB	0	0
PG	X1	0.63	2.18
	T1	0.00	0.00
	X2	1.45	6.51
	T2	0.30	0.20
	X3	2.71	10.84
	T3	0.60	0.80
	PSB	0	0

Continued on next page

Prot. Device	Setting	Calculated	Optimized
PH	X1	0.56	0.63
	T1	0.00	0.00
	X2	1.73	7.21
	T2	0.30	0.20
	X3	2.23	8.92
	T3	0.60	0.60
	PSB	0	1
PI	X1	0.15	0.52
	T1	0.00	0.05
	X2	1.73	3.30
	T2	0.30	0.40
	X3	2.43	9.55
	T3	0.60	0.60
	PSB	0	0
PA2	I1	0.6	0.7
	T1	0.10	0.00
	Dir1	1	2
	I2	/	0.5
	T2	/	0.25
	Dir2	/	2
PI2	I1	0.6	2.2
	T1	0.10	0.00
	Dir1	1	2
	I2	/	1.3
	T2	/	0.20
	Dir2	/	2

E Generator Protection Data of the Transmission System

Table 33: Generator over/underfrequency protection settings for all generator with fast overfrequency stage $f_{>>}$, slow overfrequency stage $f_{>}$, underfrequency stage $f_{<}$, delay times $t_{>>}$, $t_{>}$, $t_{<}$ and nominal frequency f_{N}.

Setting	Value
$f_{>>}$	$1.05 f_{\mathrm{N}}$
$t_{>>}$	5 s
$f_{>}$	$1.03 f_{\mathrm{N}}$
$t_{>}$	10 s
$f_{<}$	$0.95 f_{\mathrm{N}}$
$t_{<}$	10 s

Table 34: Generator over/undervoltage protection settings for all generator with overvoltage stage $V_{>}$, undervoltage stage $V_{<}$, delay times $t_{>}$, $t_{<}$ and nominal voltage V_{N}.

Setting	Value
$V_{>}$	$1.1 V_{\mathrm{N}}$
$t_{>}$	3 s
$V_{<}$	$0.9 V_{\mathrm{N}}$
$t_{<}$	3 s

Table 35: Generator over/underexcitation protection settings for all generator with overexcitation OE, underexcitation UE and delay times t_{OE}, t_{UE}.

Setting	Value
t_{OE}	1.0 s
t_{UE}	1.5 s

Bibliography

[1] Mattheij, R. M. M.; Rienstra, S. W.; Boonkkamp, J. H. M. t. T., *Partial Differential Equations, Modeling, Analysis, Computation*. Philadelphia, Pennsylvania, USA: Society for Industrial and Applied Mathematics (SIAM Press), 2005, ISBN: 978-0-89871-827-0. DOI: 10.1137/1.9780898718270.

[2] Ortlieb, C. P., Dresky, C. von, Gasser, I., Günzel, S., Eds.: *Mathematische Modellierung, Eine Einführung in zwölf Fallstudien*, 2., aktualisierte Aufl., Wiesbaden: Springer Spektrum, 2013, ISBN: 3658005343. DOI: 10.1007/978-3-662-54335-1.

[3] Burkard, R. E.; Zimmermann, U. T., *Einführung in die Mathematische Optimierung*. Berlin, Heidelberg: Springer Berlin Heidelberg, 2012, vol. 5045, 313 pp., ISBN: 978-3-642-28672-8. DOI: 10.1007/978-3-642-28673-5.

[4] Suhl, L.; Mellouli, T., *Optimierungssysteme, Modelle, Verfahren, Software, Anwendungen*, 3. korrigierte und aktualisierte Aufl. Berlin, Heidelberg: Springer Gabler, 2013, ISBN: 978-3-642-38937-5. DOI: 10.1007/978-3-642-38937-5.

[5] Lee, K. Y., El-Sharkawi, M. A., Eds.: *Modern heuristic optimization techniques, Theory and applications to power systems*, IEEE Press series on power engineering, Hoboken, NJ: Wiley-Interscience, 2008, ISBN: 9780471457114. DOI: 10.1002/9780470225868.

[6] Soliman, S. A.-H.; Mantawy, A.-A. H., *Modern Optimization Techniques with Applications in Electric Power Systems*. New York, NY: Springer New York, 2012, 430 pp., ISBN: 978-1-4614-1751-4. DOI: 10.1007/978-1-4614-1752-1.

[7] Scholz, D., *Optimierung interaktiv*. Berlin, Heidelberg: Springer Berlin Heidelberg, 2018, 245 pp., ISBN: 978-3-662-57952-7. DOI: 10.1007/978-3-662-57953-4.

[8] Korte, B.; Vygen, J., *Kombinatorische Optimierung*. Berlin, Heidelberg: Springer Berlin Heidelberg, 2012, 707 pp., ISBN: 978-3-642-25400-0. DOI: 10.1007/978-3-642-25401-7.

[9] Papageorgiou, M.; Leibold, M.; Buss, M., *Optimierung*. Berlin, Heidelberg: Springer Berlin Heidelberg, 2015, 543 pp., ISBN: 978-3-662-46935-4. DOI: 10.1007/978-3-662-46936-1.

[10] Thomas Weise, *Optimization Algorithms*. Hefei, Anhui, China: Institute of Applied Optimization, School of Artificial Intelligence and Big Data, 2023. [Online]. Available: http://thomasweise.github.io/oa/ (visited on 05/25/2023).

[11] Stork, J.; Eiben, A. E.; Bartz-Beielstein, T., A new taxonomy of global optimization algorithms, *Natural Computing*, 2020, ISSN: 1567-7818. DOI: 10.1007/s11047-020-09820-4.

[12] Stein, O., *Grundzüge der Globalen Optimierung*. Berlin, Heidelberg: Springer Berlin Heidelberg, 2018. DOI: 10.1007/978-3-662-55360-2.

[13] Wolpert, D. H.; Macready, W. G., No free lunch theorems for optimization, *IEEE Transactions on Evolutionary Computation*, vol. 1, no. 1, 67–82, 1997. DOI: 10.1109/4235.585893.

[14] Yu-Chi Ho; Pepyne, D. L., *Simple explanation of the no free lunch theorem of optimization*, in *Proceedings of the 40th IEEE Conference on Decision and Control*, vol. 5, 2001, 4409–4414 vol.5. DOI: 10.1109/CDC.2001.980896.

[15] McDermott, J., When and Why Metaheuristics Researchers can Ignore "No Free Lunch" Theorems, *SN Computer Science*, vol. 1, no. 1, 60, 2020, ISSN: 2661-8907. DOI: 10.1007/s42979-020-0063-3.

[16] Borenstein, Y., Moraglio, A., Eds.: *Theory and Principled Methods for the Design of Metaheuristics*, Berlin, Heidelberg: Springer Berlin Heidelberg, 2014, ISBN: 978-3-642-33206-7.

[17] Storn, R.; Price, K., Differential Evolution – A Simple and Efficient Heuristic for global Optimization over Continuous Spaces, *Journal of Global Optimization*, vol. 11, no. 4, 341–359, 1997. DOI: 10.1023/A:1008202821328.

[18] Kramer, O., *Computational Intelligence*. Berlin, Heidelberg: Springer Berlin Heidelberg, 2009. DOI: 10.1007/978-3-540-79739-5.

[19] Kennedy, J.; Eberhart, R.; Shi, Y., *Swarm Intelligence*. Morgan Kaufmann Publishers, 2001.

[20] Beni, G.; Wang, J., Swarm Intelligence in Cellular Robotic Systems, in *Proceed. NATO Advanced Workshop on Robots and Biological Systems*, Tuscany, Italy, 1989. DOI: 10.1007/978-3-642-58069-7_38.

[21] Beni, G., *From Swarm Intelligence to Swarm Robotics*, in *Swarm Robotics*, Şahin, E., Spears, W. M., Eds., Berlin, Heidelberg: Springer Berlin Heidelberg, 2005, 1–9, ISBN: 978-3-540-30552-1.

[22] Bonabeau, E.; Dorigo, M.; Theraulaz, G., *Swarm Intelligence: From Natural to Artificial Systems*, eng. New York: Oxford University Press, 1999, 307 pp., ISBN: 9780195131581. DOI: 10.1093/oso/9780195131581.001.0001.

[23] Dorigo, M.; Di Caro, G., *Ant colony optimization: a new meta-heuristic*, in *Proceedings of the 1999 Congress on Evolutionary Computation*, vol. 2, 1999, 1470–1477 Vol. 2. DOI: 10.1109/CEC.1999.782657.

[24] Eberhart, R.; Kennedy, J., *A new optimizer using particle swarm theory*, in *MHS'95. Proceedings of the Sixth International Symposium on Micro Machine and Human Science*, 1995, 39–43. DOI: 10.1109/MHS.1995.494215.

[25] Kennedy, J.; Eberhart, R., *Particle Swarm Optimization*, in *Proceedings of ICNN'95 - International Conference on Neural Networks*, vol. 4, 1995, 1942–1948 vol.4. DOI: 10.1109/ICNN.1995.488968.

[26] Clerc, M.; Kennedy, J., The particle swarm - explosion, stability, and convergence in a multidimensional complex space, *IEEE Transactions on Evolutionary Computation*, vol. 6, no. 1, 58–73, 2002. DOI: 10.1109/4235.985692.

[27] Eberhart, R. C.; Shi, Y., *Tracking and optimizing dynamic systems with particle swarms*, in *Proceedings of the 2001 Congress on Evolutionary Computation*, vol. 1, 2001. DOI: 10.1109/CEC.2001.934376.

[28] Shi, Y.; Eberhart, R., *A modified particle swarm optimizer*, in *1998 IEEE International Conference on Evolutionary Computation Proceedings. IEEE World Congress on Computational Intelligence*, 1998, 69–73. DOI: 10.1109/ICEC.1998.699146.

[29] Miranda, V.; Fonseca, N., *EPSO - best-of-two-worlds meta-heuristic applied to power system problems*, in *2002 Congress on Evolutionary Computation*, vol. 2, 2002, 1080–1085 vol.2. DOI: 10.1109/CEC.2002.1004393.

[30] Miranda, V.; Fonseca, N., *EPSO-evolutionary particle swarm optimization, a new algorithm with applications in power systems*, in *IEEE/PES Transmission and Distribution Conference and Exhibition*, vol. 2, 2002, 745–750 vol.2. DOI: 10.1109/TDC.2002.1177567.

[31] Miranda, V.; Alves, R., *Differential Evolutionary Particle Swarm Optimization (DEEPSO): A Successful Hybrid*, in *2013 BRICS Congress on Computational Intelligence and 11th Brazilian Congress on Computational Intelligence*, 2013, 368–374. DOI: 10.1109/BRICS-CCI-CBIC.2013.68.

[32] Loureiro, F. M. S.: Development and Testing of the Meta-Heuristic Hybrid DEEPSO, Faculty of engineering in electrical and computer engineering, University of porto, Porto, 2014. [Online]. Available: https://repositorio-aberto.up.pt/bitstream/10216/73472/2/31811.pdf (visited on 05/25/2023).

[33] Kennedy, J.; Eberhart, R. C., *A discrete binary version of the particle swarm algorithm*, in *1997 IEEE International Conference on Systems, Man, and Cybernetics. Computational Cybernetics and Simulation*, vol. 5, 1997, 4104–4108 vol.5. DOI: 10.1109/ICSMC.1997.637339.

[34] Nezamabadi-pour, H.; Rostami-Shahrbabaki, M.; Farsangi, M., Binary Particle Swarm Optimization: challenges and New Solutions, *The Journal of Computer Society of Iran (CSI) On Computer Science and Engineering (JCSE)*, vol. 6, 21–32, 2008.

[35] IEEE Standard for Floating-Point Arithmetic, *IEEE Std 754-2019 (Revision of IEEE 754-2008)*, 1–84, 2019. DOI: 10.1109/IEEESTD.2019.8766229.

[36] Martin Gardner, *Knotted Doughnuts and Other Mathematical Entertainments*. New York: W. H. Freeman and Company, 1986, 289 pp., ISBN: 0-7167-1794-8.

[38] Suganthan, P.; Hansen, N.; Liang, J., *et al.*, Problem Definitions and Evaluation Criteria for the CEC 2005 Special Session on Real-Parameter Optimization, *Natural Computing*, vol. 341-357, 2005, ISSN: 1567-7818.

[39] Jamil, M.; Yang, X. S., A Literature Survey of Benchmark Functions for Global Optimisation Problems, *Int. Journal of Mathematical Modelling and Numerical Optimisation (IJMMNO)*, no. 4, 150–194, 2013. DOI: 10.1504/IJMMNO.2013.055204.

[40] Montes de Oca, Marco A.; Stutzle, T.; Birattari, M.; Dorigo, M., Frankenstein's PSO: A Composite Particle Swarm Optimization Algorithm, *IEEE Transactions on Evolutionary Computation*, vol. 13, no. 5, 1120–1132, 2009. DOI: 10.1109/TEVC.2009.2021465.

[41] Bratton, D.; Kennedy, J., *Defining a Standard for Particle Swarm Optimization*, in *2007 IEEE Swarm Intelligence Symposium*, 2007, 120–127. DOI: 10.1109/SIS.2007.368035.

[42] Tang, K.; Li, X.; Suganthan, P.; Yang, Z.; Weise, T.: Benchmark functions for the CEC'2008 special session and competition on large scale global optimization, 12, 2009.

[43] Li, X.; Tang, K.; Omidvar, M. N.; Yang, Z.; Qin, K., Benchmark Functions for the CEC'2013 Special Session and Competition on Large-Scale Global Optimization, 2013.

[44] Liang, J.; Qu, B.; Suganthan, P.: Problem definitions and evaluation criteria for the CEC 2014 special session and competition on single objective real-parameter numerical optimization, 12, 2013.

[45] Bundesministerium für Wirtschaft und Klimaschutz: Definition und Monitoring der Versorgungssicherheit an den europäischen Strommärkten, Projekt Nr. 047/16, ger, 2019. [Online]. Available: https://www.bmwk.de/Redaktion/DE/Publikationen/Studien/definition-und-monitoring-der-versorgungssicherheit-an-den-europaeischen-strommaerkten.html (visited on 05/25/2023).

[46] DIN EN 50160, Voltage characteristics of electricity supplied by public electricity networks; German version. DOI: 10.31030/3187943.

[47] IEEE/CIGRE Joint Task Force on Stability Terms and Definitions: Definition and Classification of Power System Stability, IEEE Transaction on Power Systems, Ed., version VOL. 19, NO. 2, 2004. DOI: 10.1109/TPWRS.2004.825981.

[48] Cigre Working Group C 4.601: Review of On-Line Dynamic Security Assessment Tools and Techniques, Cigre, Ed., 2007.

[49] Hatziargyriou, N.; Milanovic, J.; Rahmann, C., *et al.*, Definition and Classification of Power System Stability – Revisited & Extended, *IEEE Transactions on Power Systems*, vol. 36, no. 4, 3271–3281, 2021, ISSN: 0885-8950. DOI: 10.1109/TPWRS.2020.3041774.

[50] Padiyar; R, K., *Power System Dynamics, Stability and Control*, 2. Hyderabad, India: BS Publications, 2008, 584 pp., ISBN: 81-7800-186-1.

[51] Schwab, A. J., *Elektroenergiesysteme, Erzeugung, Transport, Übertragung und Verteilung elektrischer Energie*, 2., aktualisierte Aufl. Berlin and Heidelberg: Springer, 2009, ISBN: 9783540922261.

[52] Romeis, C.: Dynamische Schutzsicherheit unter Berücksichtigung elektromechanischer Ausgleichsvorgänge in Hochspannungsnetzen, Dissertation, Friedrich-Alexander-Universität Erlangen-Nürnberg, Erlangen, 2017.

[53] Romeis, C.; Jaeger, J., *Dynamic protection security assessment, a technique for blackout prevention*, in *2013 IEEE Grenoble Conference*, 2013, 1–6. DOI: 10.1109/PTC.2013.6652176.

[54] Machowski, J.; Bialek, J. W.; Bumby, J. R., *Power system dynamics, Stability and control*, 2nd edition. Chichester: Wiley, 2012, ISBN: 978-0470725580.

[55] Mahr, F.; Henninger, S.; Biller, M.; Jäger, J., *Elektrische Energiesysteme*. Wiesbaden: Springer Fachmedien Wiesbaden, 2021, 558 pp. DOI: 10.1007/978-3-658-34908-0. (visited on 10/27/2022).

[56] IEEE Guide for Protection System Redundancy for Power System Reliability, *IEEE Std C37.120-2021*, 1–72, 2022. DOI: 10.1109/IEEESTD.2022.9726141.

[57] Cigre working group B 5.47: Network protection performance audits, Cigre, Ed., 2020.

[58] IEEE Guide for Protective Relay Applications to Transmission Lines, *IEEE Std C37.113-2015 (Revision of IEEE Std C37.113-1999)*, 1–141, 2016. DOI: 10.1109/IEEESTD.2016.7502047.

[59] Fouad, A. A.; Aboytes, F.; Carvalho, V. F.; Corey, S. L.; Dhir, K. J.; Vierra, R., Dynamic security assessment practices in North America, *IEEE Transactions on Power Systems*, vol. 3, no. 3, 1310–1321, 1988, Aug, ISSN: 0885-8950. DOI: 10.1109/59.14597.

[60] Morison, K.; Hamadanizadeh, H.; Lei Wang, *Dynamic security assessment tools*, in *1999 IEEE Power Engineering Society Summer Meeting*, 1999, 282–286. DOI: 10.1109/PESS.1999.784360.

[61] Morison, K.; Lei Wang; Kundur, P., Power system security assessment, *IEEE Power and Energy Magazine*, vol. 2, no. 5, 30–39, 2004, ISSN: 1540-7977. DOI: 10.1109/MPAE.2004.1338120.

[62] Chris Oliver Heyde: Dynamic Voltage Security Assessment for On-Line Control Room Application, Fakultät für Elektrotechnik und Informationstechnik, Dissertation, Otto-von-Guericke-Universität Magdeburg, Magdeburg, 2009.

[63] Uros Kerin: Development of tools for dynamic security assessment of electric power systems, Faculty of Electrical Engineering, Dissertation, Univerity of Ljubjana, Ljubjana, 2010, 156 pp.

[64] Kerin, U.; Krebs, R.: PMU and DSA Based Wide Area Control System, Ohrid, Macedonia: IEEE EUROCON 2017 -17th International Conference on Smart Technologies, 2017. DOI: 10.1109/EUROCON.2017.8011220.

[65] Jaeger, J.; Krebs, R., *Automated protection security assessment of today's and future power grids*, in *IEEE PES General Meeting*, 2010, 1–6. DOI: 10.1109/PES.2010.5588076.

[66] Jaeger, J.; Fuchs, J.; Dauer, M.; Bopp, T.; Krebs, R., *Protection security assessment — Innovative strategies and methods for future networks*, in *2012 IEEE Power and Energy Society General Meeting (PESGM)*, 2012, 1–6. DOI: 10.1109/PESGM.2012.6344804.

[67] Dauer, M.; Jaeger, J.; Bopp, T.; Krebs, R., *Protection security assessment - System evaluation based on fuzzification of protection settings*, in *IEEE PES ISGT Europe 2013*, (Copenhagen, Denmark), 2013, 1–4. DOI: 10.1109/ISGTEurope.2013.6695385.

[68] Fuchs, J.: Koordination von Schutzsystemen für multivariate Netzzustände mit Hilfe von mathematischer Optimierung und Bewertung, Institute of Electrical Energy Systems, Dissertation, Friedrich-Alexander-Universität Erlangen-Nürnberg, Erlangen, 2016.

[69] Ganjavi, R.; Mangold, M.; Friedrich, M.; Krebs, R.; Dauer, M.; Worch, M., *Automated Protection Security Assessment of Main and Backup Protection for Distribution Networks*, in *2018 International Conference on Smart Energy Systems and Technologies (SEST)*, 2018, 1–5. DOI: 10.1109/SEST.2018.8495864.

[72] UCTE, Final Report of the Investigation Committee on the 28 September 2003 Blackout Italy, 2004. [Online]. Available: https://eepublicdownloads.entsoe.eu/clean-documents/pre2015/publications/ce/otherreports/20040427%5C_UCTE%5C_IC%5C_Final%5C_report.pdf (visited on 05/25/2023).

[73] Gomes, P.; Aquino, A. F.; Ticom, S. D.; Fernandes, B.; Feltes, J., How Brazil Aims for Gold in Reliability: From Past Blackouts to Preparedness for the 2016 Summer Olympic and Paralympic Games, *IEEE Power and Energy Magazine*, vol. 14, no. 6, 40–51, 2016, ISSN: 1540-7977. DOI: 10.1109/MPE.2016.2593782.

[74] ENTSO-E 2021, Continental Europe Synchronous Area Separation on 08 January 2021, Final Report, [Online]. Available: https://eepublicdownloads.azureedge.net/clean-

documents/SOC%20documents/SOC%20Reports/entso-e_CESysSep_Final_Report_210715.pdf (visited on 05/25/2023).

[75] Raab, A.; Mehlmann, G.; Schindler, J., *et al.*, *Security assessment for higher loaded power system operation to 2030*, in *ETG Congress 2021*, 2021.

[80] Sobajic, D. J.; Pao, Y.-H., Artificial neural-net based dynamic security assessment for electric power systems, *IEEE Transactions on Power Systems*, vol. 4, no. 1, 220–228, 1989, ISSN: 0885-8950. DOI: 10.1109/59.32481.

[81] Hashim, H.; Zulkepali, M. R.; Omar, Y. R.; Ismail, N.; Abidin, I. Z.; Yusof, S., *An analysis of Transient Stability using Center-of-Inertia: Angle and speed*, in *2010 IEEE International Conference on Power and Energy*, 2010, 402–407. DOI: 10.1109/PECON.2010.5697617.

[82] Ting-Jian, L.; Jun-Yong, L.; You-Bo, L.; Jia-Shi, Y.; Ya-Qi, N., *Multi-performance criterion evaluation for severe disturbance screening regarding transient impacts*, in *2014 International Conference on Power System Technology Impacts*, (Chengdu, China), IEEE, 2014, 594–600, ISBN: 978-1-4799-5032-4. DOI: 10.1109/POWERCON.2014.6993779.

[83] Sajadi, A.; Preece, R.; Milanovic, J.: Evaluation of Suitability of Different Transient Stability Indices for Identification of Critical System States, 10th Bulk Power Systems Dynamics and Control Symposium, Ed., 2020. DOI: 10.48550/arXiv.2001.03519.

[84] Soni, B. P.; Saxena, A.; Gupta, V.; Surana, S. L.; Chiodo, E., Assessment of Transient Stability through Coherent Machine Identification by Using Least-Square Support Vector Machine, *Modelling and Simulation in Engineering*, 2018, ISSN: 1687-5591. DOI: 10.1155/2018/5608591.

[85] Guang Li; Rovnyak, S. M., Integral square generator angle index for stability ranking and control, *IEEE Transactions on Power Systems*, vol. 20, no. 2, 926–934, 2005, ISSN: 0885-8950. DOI: 10.1109/TPWRS.2005.846118.

[86] Oeding, D.; Oswald, B. R., *Elektrische Kraftwerke und Netze*, ger, 8. Auflage. Berlin: Springer Vieweg, 2016, 1107 pp., Oeding, Dietrich (VerfasserIn) Oswald, Bernd R. (VerfasserIn), ISBN: 978-3-662-52702-3. DOI: 10.1007/978-3-662-52703-0.

[87] H.-O. Pörtner, D.C. Roberts, M. Tignor, E.S. Poloczanska, K. Mintenbeck, A. Alegría, M. Craig, S. Langsdorf: IPCC, 2022: Climate Change 2022: Impacts, Adaptation and Vulnerability, Working Group II Contribution to the Sixth Assessment Report of the Intergovernmental Panel on Climate Change, Cambridge University Press., Ed., Cambridge, UK and New York, NY, USA: Cambridge University Press., 2022. DOI: 10.1017/9781009325844.

[88] Harnisch, S.; Steffens, P.; Thies, H. H., *et al.*: Planungs- und Betriebsgrundsätze für ländliche Verteilungsnetze, Leitfaden zur Ausrichtung der Netze an ihren zukünftigen Anforderungen, Zdrallek, M., Ed., Wuppertal: Bergische Universität Wuppertal and Siemens AG, 2016.

[89] Biller, M.: Schutzalgorithmen für dynamisch vermaschte Ringnetzstrukturen mit dezentraler Einspeisung, Institute of Electrical Energy Systems, Dissertation, Friedrich-Alexander-Universität Erlangen-Nürnberg, Erlangen, 2021. [Online]. Available: 10.25593/978-3-96147-432-5.

[90] Raab, A.; Mehlmann, G.; Luther, M.; Sennewald, T.; Schlegel, S.; Westermann, D., *Steady-State and Dynamic Security Assessment for System Operation*, in *2021 International Conference on Smart Energy Systems and Technologies (SEST)*, 2021, 1–6. DOI: 10.1109/SEST50973.2021.9543423.

[91] Mario Paolone; Trevor Gaunt; Xavier Guillaud, *et al.*, Fundamentals of power systems modelling in the presence of converter-interfaced generation, *Electric Power Systems Research*, vol. 189, 106811, 2020, ISSN: 0378-7796. DOI: 10.1016/j.epsr.2020.106811.

[92] Verbundpartner: InnoSys 2030 - Innovationen in der Systemführung bis 2030, Abschlussbericht Gesamtverbund, 2022. [Online]. Available: https://www.innosys2030.de/wp-content/uploads/InnoSys2030_Abschlussbericht.pdf (visited on 05/25/2023).

[93] Ziegler, G., *Numerical distance protection, Principles and applications*, 4 vols. Erlangen: Publicis Puplishing, 2011, ISBN: 978-3-89578-381-4.

[94] Blackburn, J. L.; Domin, T. J., *Protective Relaying, Principles and Applications*. Boca Raton, FL, USA: CRC Press, 2007, vol. thrid edition, ISBN: 1-57444-716-5.

[95] Anderson, P. M.; Henville, C.; Rifaat, R.; Johnson, B.; Meliopoulos, S., *Power System Protection* (IEEE Press Series on Power and Energy Systems Ser), 2nd ed. Hoboken, New Jersey: John Wiley & Sons, Inc, 2022, ISBN: 1-119-51311-1.

[96] Horowitz, S. H.; Phadke, A. G.; Henville, C. F., *Power system relaying*, Fifth edition. Hoboken, NJ: Wiley, 2023, 498 pp., ISBN: 9781119838432.

[97] G. Hosemann, W. B., *Grundlagen der elektrischen Energietechnik, Versorgung, Betrisbsmittel, Netzbetrieb, Überspannungen und Isolation, Sicherheit*, 2. Berlin, Heidelberg, New York: Springer, 1983.

[98] Valentin Crastan, *Elektrische Energieversrogung 1, Netzelemente, Modellierung, stationäres Verhalten, Bemessung, Schalt- und Schutztechnik*, 4. Auflage vols. Berlin, Heidelberg: Springer Vieweg, 2015, ISBN: 978-3-662-45984-3. DOI: 10.1007/978-3-662-45985-0.

[99] Siemens: SIPROTEC 5, Distance Protection, Line Differential Protection, and Breaker Management for 1-Pole and 3-Pole Tripping, 7SA87, 7SD87, 7SL87, 7VK87 Manual, 2022.

[100] Siemens AG, Power Engineering Guide, Transmission and Distribution, no. 4th Edition, 2014.

[101] Siemens AG, Power Engineering Guide, no. 8th Edition, 2017.

[102] Walter Schossig, Netzschutz - Das Magazin für Schutztechnik, Reichweiten und Staffelzeiten Grundsätze, no. 02, 2017.

[103] Forum Netztechnik/Netzbetrieb im VDE: Leitfaden zum Einsatz von Schutzsystemen in elektrischen Netzen, 2009.

[104] Sidhu, T. S.; Baltazar, D. S.; Palomino, R. M.; Sachdev, M. S., A new approach for calculating zone-2 setting of distance relays and its use in an adaptive protection system, *Power Delivery, IEEE Transactions on*, vol. 19, no. 1, 70–77, 2004.

[105] Keil, T.; Jager, J., Advanced Coordination Method for Overcurrent Protection Relays Using Nonstandard Tripping Characteristics, *IEEE Transactions on Power Delivery*, vol. 23, no. 1, 52–57, 2008. DOI: 10.1109/TPWRD.2007.905337.

[106] Sadeh, J.; Amintojjar, V.; Bashir, M., *Coordination of overcurrent and distance relays using hybrid Particle Swarm Optimization*, in *2011 International Conference on Advanced Power System Automation and Protection*, vol. 2, 2011, 1130–1134. DOI: 10.1109/APAP.2011.6180975.

[107] Damchi, Y.; Sadeh, J.; Mashhadi, H. R., Optimal coordination of distance and overcurrent relays considering a non-standard tripping characteristic for distance relays, *IET Generation, Transmission & Distribution*, 1448–1457, 2016. DOI: 10.1049/iet-gtd.2015.1087.

[108] Saleh, K. A.; Mehrizi-Sani, A., *Multi-Stage Protection Coordination Optimization for Distribution Systems with Topology Changes*, in *2020 IEEE/PES Transmission and Distribution Conference and Exposition (T&D)*, 2020, 1–5. DOI: 10.1109/TD39804.2020.9300026.

[114] German Federal Ministry of Education and Research. Kopernikus-Projekte: ENSURE. (2023), [Online]. Available: https://www.kopernikus-projekte.de/projekte/neue-netzstrukturen (visited on 05/25/2023).

[115] Zafirov, B.: Generic data model for the evaluation of power system protection for electric power supply grids of the future, Chair of Electrical Energy Systems, Master thesis, Friedrich-Alexander Universität Erlangen-Nürnberg, Erlangen, 2013.

[116] International Electronical Commission, Ed.: Energy management system application program interface (EMS-API) - Part 301: Common information model (CIM) base, Geneva, Switzerland, 2020.

[117] Object Management Group, Unified Modeling Language, Version 2.5.1, [Online]. Available: https/www.omg.org/spec/UML/ (visited on 05/25/2023).

[118] Pradeep, Y.; Seshuraju, P.; Khaparde, S. A.; Joshi, R. K., CIM-Based Connectivity Model for Bus-Branch Topology Extraction and Exchange, *IEEE Transactions on Smart Grid*, 244–253, 2011, ISSN: 1949-3053. DOI: 10.1109/TSG.2011.2109016.

[119] Gruhn, V.; Pieper, D.; Röttgers, C., *MDA©, Effektives Software-Engineering mit UML2©und Eclipse$_{TM}$* (Xpert.press). Dordrecht: Springer, 2006, ISBN: 978-3-540-28746-9. DOI: 10.1007/3-540-28746-9.

[120] Booch, G.; Rumbaugh, J.; Jacobson, I., *Das UML Benutzerhandbuch, Aktuell zu Version 2.0* (Programmer's Choice Addison Wesley), ger. München: Addison Wesley in Pearson Education Deutschland, 2006, 543 pp., ISBN: 9783827325709.

[121] Liu, G.; Yuan, C.; Chen, X.; Wu, J.; Dai, R.; Wang, Z., A High-Performance Energy Management System Based on Evolving Graph, *IEEE Transactions on Circuits and Systems II: Express Briefs*, vol. 67, no. 2, 350–354, 2020, Feb, ISSN: 1558-3791. DOI: 10.1109/TCSII.2019.2910488.

[122] Power System Relaying and Control Committee of the IEEE Power and Energy Society, IEEE Guide for Synchronization, Calibration, Testing, and Installation of Phasor Measurement Units for Power System Protection and Control, *IEEE Std C37.242-2021 (Revision of IEEE Std C37.242-2013)*, 1–98, 2021. DOI: 10.1109/IEEESTD.2021.9574625.

[124] Cigre working group B 5.17: Relay software models for use with electromagnetic transient analysis program, Cigre, Ed., 2016.

[125] Kai Trunk: Schutzsimulation zur Berechnung der Netzsicherheit unter Berücksichtigung der Netzdynamik, Institute of Electrical Energy Systems, Diplomarbeit, Friedrich-Alexander Universität Erlangen-Nürnberg, Erlangen, 2009.

[126] Holbach, J., *New Out of Step Blocking Algorithm for Detecting Fast Power Swing Frequencies*, in *2006 Power Systems Conference: Advanced Metering, Protection, Control, Communication, and Distributed Resources*, 2006, 182–199. DOI: 10.1109/PSAMP.2006.285388.

[127] Siemens AG: Applications for SIPROTEC Protection Relays, Nürnberg, Germany: Siemens AG, 2005.

[128] Kotras, B.; Göttlinger, M.: PSS NETOMAC 19.0 Automation, Automation Functions for PSS NETOMAC, Siemens AG, Ed., 2022.

[129] Keil, T., *Schutzsysteme für elektrische Energieversorgungsnetze mit dezentralen Stromerzeugungsanlagen*, Zugl.: Erlangen, Nürnberg, Univ., Diss., 2011 (Berichte aus der Elektrotechnik). Aachen: Shaker, 2011, ISBN: 9783844000764.

[130] Heyde, C. O., *Dynamic voltage security assessment for on-line control room application*, Zugl.: Magdeburg, Univ., Fak. für Elektrotechnik und Informationstechnik, Diss., 2010 (Res electricae Magdeburgenses), 1. Aufl. Magdeburg: Univ, 2011, vol. 32, ISBN: 9783940961402.

[131] Rebizant, W.; Szafran, J.; Wiszniewski, A., *Digital Signal Processing in Power System Protection and Control* (Signals and Communication Technology), eng. London: Springer-Verlag London Limited, 2011, ISBN: 978-0-85729-801-0. DOI: 10.1007/978-0-85729-802-7.

[132] Kerzel, M.; Garzon-Real, J.; Zdrallek, M.; Wolter, D.; Schacherer, C., *Optimal Switch Configuration Algorithm for Dynamically Meshed Power Distribution Grids*, in *2020 International Conference on Smart Energy Systems and Technologies (SEST)*, 2020, 1–6. DOI: 10.1109/SEST48500.2020.9203089.

[133] Kerzel, M.; Garzon-Real, J.; Zdrallek, M.; Wolter, D.; Schacherer, C., *Effects of Static and Dynamically Meshed Topologies on Short-Circuit Currents and the Reliability of Medium Voltage Grids*, in *26th International Conference on Electricity Distribution (CIRED)*, vol. 2021, 2021, 2735–2739. DOI: 10.1049/icp.2021.1624.

[134] Ospina, L. D. P.; Correa, A. F.; Lammert, G., *Implementation and validation of the Nordic test system in DIgSILENT PowerFactory*, in *2017 IEEE Manchester PowerTech*, 2017, 1–6. DOI: 10.1109/PTC.2017.7980933.

[135] van Cutsem, T.; Glavic, M.; Rosehart, W., *et al.*, Test Systems for Voltage Stability Studies, *IEEE Transactions on Power Systems*, vol. 35, no. 5, 4078–4087, 2020, ISSN: 0885-8950. DOI: 10.1109/TPWRS.2020.2976834.

[136] Heusinger, E.; Porst, J.; Raab, A.; Luther, M.; Samaan, S., *Impact of Inverter-Based Generation on Voltage Stability in a Modified Nordic Test System*, in *2021 IEEE Kansas Power and Energy Conference (KPEC)*, 2021, 1–5. DOI: 10.1109/KPEC51835.2021.9446224.

Own Publications

[P37] Dauer, M.; Meyer, G. J.; Jaeger, J.; Bopp, T.; Krebs, R., *EPSODE algorithm for system-wide protection coordination*, in *19th Power Systems Computation Conference (PSCC)*, 2016. DOI: 10.1109/PSCC.2016.7541000.

[P70] Meyer, G. J.; Jaeger, J.; Dauer, M.; Krebs, R.: Flexible Schutzbewertung für multivariate Netze anhand fuzziverzierter Einstellparameter des Distanzschutzes, Berlin: ETG-CIRED-Workshop 2018 (D-A-CH) powered by VDE Tec Summit, 2018.

[P71] Meyer, G. J.; Lorz, T.; Wehner, R.; Jaeger, J.; Dauer, M.; Krebs, R., Hybrid Fuzzy Evaluation Algorithm for Power System Protection Security Assessment, *Electric Power Systems Research*, vol. 189, 2020, ISSN: 0378-7796. DOI: 10.1016/j.epsr.2020.106555.

[P76] Meyer, G. J.; Romeis, C.; Jaeger, J.: Automatisierte Bewertung der Schutzsicherheit unter Berücksichtigung elektromechanischer Ausgleichsvorgänge in Hochspannungsnetzen, Berlin: 10. FNN-/ETG-Tutorial Schutz- und Leittechnik, 2018.

[P77] Meyer, G. J.: Protection Security Assessment during Fault and Post-Fault Period, Portland, OR, USA: 2018 IEEE Power & Energy Society General Meeting (PESGM), Panel Session, 2018.

[P78] Meyer, G. J.; Jaeger, J., *Protection Security Assessment with Guiding Optimization Criteria based on Stability Indices*, in *2022 IEEE PES Innovative Smart Grid Technologies Europe (ISGT Europe)*, 2022. DOI: 10.1109/ISGT-Europe54678.2022.9960547.

[P79] Meyer, G. J.; Jaeger, J.: Window Evaluation – A new Technic for Stability Security Assessment in Dynamic Protection Simulations, Jeju, Republic of Korea: 9th International Conference on Advanced Power System Automation & Protection, 2021.

[P109] Meyer, G. J.; Biller, M.; Romeis, C., *et al.*, Digital System Protection Design – A new Toolchain for Protection System Automation, in *25th International Conference on Electricity (CIRED)*, Madrid, Spain, 2019. DOI: 10.34890/906.

[P110] Meyer, G. J.; Jaeger, J.; Romeis, C.; Shang-Jäger, L.; Dauer, M.; Krebs, R.: Protection Toolchain, Automatisierte Erstellung netzintegrierter und adaptiver Schutzkonzepte, Online: VDE ETG Kongress, 2021.

[P111] Meyer, G. J.; Jaeger, J.; Romeis, C.; Shang-Jäger, L.; Dauer, M.; Krebs, R.: Protection Toolchain, Automated Generation of Adaptive Grid Protection Concepts, Online: 2021 IEEE Power & Energy Society General Meeting (PESGM), Panel Session, 2021.

[P112] Meyer, G. J.; Jaeger, J.; Romeis, C.; Shang-Jaeger, L.; Dauer, M.; Krebs, R.: Von der Planung bis zum Schutzgerät im Feld, Automatisierte Schutzkonzepterstellung, Parametrierung und Systemkoordination, Berlin: VDE FNN / ETG Tutorial Schutz - und Leittechnik, 2022.

[P113] Meyer, G. J.: Data Lake Based Approach for a Predictive Review and Optimization of Protection Settings, Denver, CO, USA: 2022 IEEE Power & Energy Society General Meeting (PESGM), Panel Session, 2022.

[P123] Ganjavi, R.; Scoble, C.; Dantas, R., *et al.*, *On-line and Adaptive Load Blinding Protection Scheme to Resolve Protection Limits in Networks with Highly Integrated DERs*, in *27th International Conference on Electricity Distribution (CIRED)*, Rom, Italy, 2023.

[P137] Knothe, D.; Meyer, G. J.; Lorz, T.; Jaeger, J.: Adaptiver Netzschutz mit IEC 61850 Client und Hardware-in-the-Loop Echtzeitsimulation, Online: Tutorial Schutz- und Leittechnik - Online Preview, 2022.

[P138] Meyer, G. J.; Jaeger, J.: Systemweite Fehlerortbestimmung basierend auf einem Mustererkennungsansatz, Berlin: 11. ETG/FNN-Tutorial Schutz- und Leittechnik, 2020.

[P139] G. J. Meyer; I. Dimopoulos; J. Jaeger, *System-based Fault Locator Based on a Pattern Recognition Approach*, in *2020 IEEE Power & Energy Society General Meeting (PESGM)*, 2020. DOI: 10.1109/PESGM41954.2020.9281758.

List of Symbols and Abbreviations

List of Abbreviations

Abbreviation	Description
ACO	Ant Colony Optimization
ADI	Angle Deviation Index
AHP	Analytical Hierarchy Process
AI	Artificial Intelligence
ANN	Artificial Neural Networks
AQI	Angle Quality Index
AR	Automatic Reclosing
BMBF	Federal Ministry of Education and Research
BPSO	Binary Particle Swarm Optimization
$BPSO_{DE}$	Binary PSO with Differential Evolution
CEC	IEEE Congress on Evolutionary Computation
CIM	Common Information Model
COM	Component Object Model
CT	Current Transformer
DE	Differential Evolution
DEEPSO	Differential Evolutionary Particle Swarm Optimization
DER	Distributed Energy Resource
DL	Deep Learning
DPSA	Dynamic Protection Security Assessment
DSA	Dynamic Security Assessment
DSI	Dynamic Stability Index
DTOC	Definite-Time Overcurrent
EA	Evolutionary Algorithm
$EBPSO_{DE}$	Evolutionary Binary PSO with Differential Evolution
EC	Evolutionary Computation
EC	Electrical Center
EES	Institute of Electrical Energy Systems
EMT	Electromagnetic Transients
EPSO	Evolutionary Particle Swarm Optimization
$EPSO_{DE}$	Evolutionary PSO with Differential Evolution
ES	Evolutionary Strategy
FACTS	Flexible AC Transmission Systems
FAU	Friedrich-Alexander-Universität Erlangen-Nürnberg
FCI	Fault Current Index

Abbreviation	Description
FDI	Frequency Deviation Index
FES	Function Evaluations
FGI	Frequency Gradient Index
FIR	Finite Impulse Response
VQI	Frequency Quality Index
FV	Fitness Value
GDM	Generic Data Model
GLI	Grid Loading Index
GPI	Guiding Penalty Index
HVDC	High Voltage Direct Current
IC	Impedance Center
IEC	International Electrotechnical Commission
IED	Intelligent Electronic Device
IOC	Instantaneous Overcurrent
IP	Integer Programming
IPCC	Intergovernmental Panel on Climate Change
ISGA	Integral Square Generator Angle Index
ITOC	Inverse-Time Overcurrent
JSON	JavaScript Objective Notation
LLI	Load Loss Index
MCT	Monte Carlo-Tree Search
MIP	Mixed Integer Programming
ML	Machine Learning
NFL	No Free Lunch
NTS	Nordic Test System
OOS	Out-of-Step
ProToc	Protection Toolchain
PSA	Protection Security Assessment
PSB	Power-Swing Blocking
PSI	Protection Security Index
PSO	Particle Swarm Optimization
QoS	Quality of Supply
RES	Renewable Energy Sources
RL	Reinforcement Learning
RMS	Root Mean Square
ROCOF	Rate of Change of Frequency
ROI	Rotor Oscillation Index
RoS	Reliability of Supply
RTDS	Real Time Digital Simulator

Abbreviation	Description
SI	Swarm Intelligence
SoS	Security of Supply
SRI	Supply Reliability Index
STFT	Short-Time Fourier Transform
TSI	Transient Stability Index
TSP	Traveling Salesman Problem
UML	Unified Model Language
VFI	Voltage Funnel Index
VQI	Voltage Quality Index
VT	Voltage Transformer
WE	Window Evaluation
WT	Wavelet Transform

List of Symbols

Symbol	Unit	Description
δ_i	°	Rotor angle of i-th unit
δ_{COI}	°	Center of inertia
$\vec{gb}$		Position vector of global best particle
$\vec{lb}$		Position vector of local best position
K		Trajectory constant
M_i	kgm²	Moment of inertia of i-th unit
M_{total}	kgm²	Total moment of inertia
$nAAF$		Number of all aditional available protection functions
nAF		Number of aditional activated protection functions
n_b		Bit length required to represent a number in the binary system
nF		Number of all faults of a fault package
$nGGR$		Number of all generators within a generator group
nGN		Number of all generator nodes
nGR		Number of all generators
nL		Number of all lines
nLO		Number of all loads

Symbol	Unit	Description
nN		Number of all nodes
nVN		Number of all load and generation nodes as well as all nodes with more than two connections to other nodes
nW		Number of all evaluation windows
p		Communication factor
$\vec{P}$		Communication vector
r_1		Uniformly distributed random variable
r_2		Uniformly distributed random variable
r		Replication rate
$S_{\mathrm{th,1s}}$	A/m²	1 s short-time current density
$S_{\mathrm{th,1s,r}}$	A/m²	1 s rated short-time current density
τ		Learning rate
t_{e}	s	End time
t_{s}	s	Start time
$\vec{v}$		Velocity vector of a particle
$V_{\max}$		Maximum particle velocity
$V_{\min}$		Minimum particle velocity
w_1		Inertia weighting factor
$\vec{w}_1$		Inertia weighting vector
w_2		Memory weighting factor
$\vec{w}_2$		Memory weighting vector
w_3		Social weighting factor
$\vec{w}_3$		Social weighting vector
$\vec{w}_4$		Noise vector
$\vec{x}$		Position vector of a particle
x^*		Optimal point

Electric power systems are pioneers and drivers of prosperity in modern societies. In this respect, they play a key role worldwide in achieving climate goals, electrifying sectors and connecting renewable energies. The entire energy system landscape is facing major challenges and is confronted with increasing changes, variable infeed and integration of new technologies. Operating and fault conditions are thus becoming more diverse as well as more difficult to predict and distinguish. Protection systems have the task of preventing power systems from the consequences and impacts of faults. However, protection concepts are still created by experts today and are rarely reviewed and adapted after changes. The goal must therefore be to digitize and fully automate the generation, parameterization, assessment and optimization of protection concepts. Protection systems shall be adjusted prior to system changes or when security vulnerabilities occur.

The approach presented in this book consists of six sequential steps and is called Protection Toolchain. The workflow relies on a comprehensive database and a generic data model to process, compute and analyze protection and simulation data. A hybrid binary particle swarm optimization algorithm is proposed to set different protection functions of multiple protective devices of a system-wide power system section in a coordinated manner. Together with a specially designed dynamic evaluation method, applicable and trustworthy protection settings can be generated.

ISBN 978-3-96147-709-8

FAU UNIVERSITY PRESS 2023